TABLE DES MATIÈRES

LISTE DES FIGURES

LISTE DES TABLEAUX

LISTE DES ABRÉVIATIONS, SIGLES ET ACRONYMES

DBH	Diameters at the Breast Height
DEM	Digital Elevation Model
DTM	Digital Terrain Model
EC	Electrical Conductivity
ECO	Épaisseur de la Couche Organique
EM	Electromagnetic
g	Gramme
GHz	Gigahertz
GPR	Ground Penetrating Radar
GPR	Géoradar ou Radar-sol
GNSS	Global Navigation Satellite System
GPS	Global Positioning System
ha	Hectare
IQS	Indice de Qualité de Station
K	Dielectric constant
kg	Kilogramme
LiDAR	Light Detection And Ranging
m	Mètre
m^2	Mètre carré
m^3	Mètre cube
m asl	Metres Above Sea Level
MHz	Megahertz
MS	Mineral Soil
MNT	Modèle Numérique du Terrain

MS-DEM	Digital Elevation Model at the Mineral Soil
n	Nombre d'observations effectuées à l'intérieur de l'échantillon
Of	Fibric horizon
Oh	Humic horizon
OL	Organic Layer
OLT	Organic Layer Thickness
Om	Mesic horizon
P-value	Seuil de la signification statistique
r	Coefficient de corrélation de Pearson
r_s	Coefficient de corrélation de Spearman
R^2	coefficient de détermination
SI	Site Index
T	Tonne
z	Altitude

RÉSUMÉ

La forêt boréale canadienne a une importance écologique et économique considérable. Toutefois, les forêts d'épinettes noires situées dans la ceinture d'argile, une région boréale de l'est de l'Amérique du Nord, sont sujettes à la paludification. Ce phénomène est un processus naturel par lequel une couche organique s'accumule sur le sol forestier conduisant à une diminution importante de la productivité de ces forêts. Théoriquement, il existe deux types de paludification, à savoir la paludification permanente et réversible. La paludification permanente se produit dans des endroits où les conditions d'humidité du sol sont élevées (ex., reliefs plats, dépressions topographiques); alors que la paludification réversible intervient dans des sites à pente faible ou moyennement forte au fil du temps en réponse à une perturbation telle qu'un feu peu sévère. L'épaisseur de la couche organique (ECO) et la topographie constituent des paramètres clefs de la présence de la paludification dans cette région et y affectent négativement la productivité. La recherche proposée dans cette thèse consiste à approfondir la compréhension et la détection du phénomène de paludification dans les forêts d'épinette noire dans une perspective de maintien ou d'accroissement de la productivité des arbres. Cette thèse a pour objectif principal de déterminer et de sélectionner les variables permanentes des site permettant d'expliquer les écarts de productivité de la pessière à épinette noire observés dans la ceinture d'argile à l'aide des méthodes à haute résolution et des données recueillies sur le terrain. L'expression de ces variables a été ensuite utilisée pour prédire la productivité actuelle et potentielle des sites soumis à la paludification. Les objectifs spécifiques de cette thèse étaient de (1) détecter et identifier d'une manière continue l'interface sol minéral/couche organique afin de cartographier la topographie du sol minéral à l'échelle des sites paludifiés; (2) étudier d'une façon quantitative les relations entre l'ECO et la topographie (au niveau du sol minéral et de la surface) afin de caractériser ces relations à l'échelle du paysage, notamment la distribution et la variabilité spatiale de l'ECO; (3) identifier les variables topographiques permettant de distinguer et de cartographier la paludification réversible et la paludification permanente à l'échelle du paysage; et (4) évaluer l'effet de l'ECO et des variables topographiques, exprimées à différentes résolutions spatiales, sur la productivité forestière des forêts paludifiées de la ceinture d'argile. Le but ultime est d'améliorer notre compréhension de la façon dont ces variables ainsi que leurs résolutions influencent la productivité des arbres dans les forêts d'épinette noire.

Les résultats du premier chapitre de la thèse ont démontré que la méthode géophysique géoradar, ayant une bonne corrélation de ses résultats avec les données du terrain ($r = 0{,}93$; $P < 0{,}001$), a permis d'obtenir une cartographie précise, continue et fiable de l'interface couche organique/sol minéral dans des sites faiblement à modérément paludifiés. Cependant, en dépit de son incapacité à cartographier l'interface couche organique/sol minéral dans les sites hautement paludifiés, le recours au géoradar s'est révélé pertinent dans la mise en évidence de l'interface horizon fibrique/couche organique et de sa continuité spatiale. Cela rend le géoradar particulièrement intéressant dans la détection des niveaux d'entourbement constituant ainsi une méthode de détection indirecte prometteuse pour l'aménagement des forêts paludifiées.

Le deuxième objectif a été abordé dans deux différents chapitres (II et III) à l'aide d'une approche quantitative de modélisation de l'ECO par arbre de régression. Différentes variables topographiques (élévation, pente, exposition, indice topographique d'humidité (TWI), courbure totale, courbure transversale, et courbure horizontale) ont été utilisées dans les modèles sélectionnés des deux chapitres. D'une façon générale, nous avons démontré que les topographies de surface et du sol minéral influencent l'accumulation de la couche organique à l'échelle du paysage dans la ceinture d'argile. Les résultats du deuxième chapitre ont permis de délimiter les principaux patrons de l'ECO et d'élucider trois relations spatiales entre l'ECO et les variables explicatives: (i) les zones avec une couche organique épaisse (62 cm) avaient des pentes douces ($\leq$ 1,8%); (ii) les zones avec pentes plus raides ($>$ 3,2 %) ont été associées à une couche organique peu profonde (27 cm); et (iii) les résultats les plus significatifs ont été obtenus avec des résolutions 10 et 20 m en comparaison au 1 et 5 m. Le troisième chapitre a permis de mettre en évidence les différentes relations entre la topographie du sol minéral et l'ECO à l'échelle du paysage. La construction d'un modèle numérique d'élévation au niveau du sol minéral à l'échelle du paysage est un élément central de notre démarche. Les modelés développés nous permettent d'affirmer que : (i) la pente du sol minéral, la composition du sol minéral (argile, till et régolithe), le TWI et l'exposition sont les quatre principales variables influençant l'accumulation de la couche organique; (ii) les valeurs seuils de pente du sol minéral $>$ 3,5% et $\leq$ 2% permettent respectivement de distinguer les zones les plus prometteuses et les plus vulnérables pour l'aménagement forestier; (iii) les zones avec une exposition nord et est étaient associées à une couche organique plus profonde par rapport à celles exposées vers le sud et l'ouest; et (iv) la distinction entre les zones paludifiées et non paludifiées sur la base d'une valeur seuil de la pente du sol minéral de l'ordre de 3,5% constitue un des apports majeurs de cette étude.

Afin de répondre au troisième objectif, une approche semi-automatique de subdivision sous SIG du territoire à l'étude en des entités du paysage distinctes a été réalisée en combinant des données topographiques, notamment l'indice topographique de position (TPI), l'indice topographique d'humidité (TWI) ainsi que la pente de surface. Cette approche s'est révélée efficace, car elle a permis de délimiter des entités possédant des caractéristiques géomorphologiques semblables, notamment en terme de susceptibilité à l'accumulation de la couche organique, et par conséquent ont été assignées à l'un ou l'autre type de paludification, soit réversible ou permanente. Un apport majeur de cette approche semi-automatisée est la mise en évidence de deux sous-entités statistiquement différentes (le test *HSD de Tukey*, $P <$ 0,001), à savoir des dépressions ouvertes préférentiellement drainées (paludification réversible) et des dépressions fermées potentiellement engorgées (paludification permanente) du fait de leurs positions topographiques et conditions d'humidité. Cela rend l'outil développé particulièrement utile pour la mise en œuvre des stratégies d'aménagement durable dans les forêts paludifiées.

Pour atteindre le quatrième objectif, deux modèles ont été explorés pour la modélisation de la productivité (exprimée par l'indice de qualité de station (IQS) dans notre cas) en utilisant une approche par arbre de régression. Le premier modèle contient les variables topographiques et l'ECO, alors que le deuxième modèle inclut seulement les variables topographiques issues des données LiDAR. Les résultats de cette modélisation ont démontré que l'ECO, l'exposition et la pente sont les trois variables les plus importantes pour expliquer la productivité forestière à l'échelle du paysage; et pour déterminer des seuils d'ECO et des

variables topographiques qui permettent de caractériser, à la fois, des zones productives et improductives. En effet, les zones avec une productivité élevée étaient associées à une couche organique peu profonde (< 35 cm) et à des pentes orientées sud-ouest et dont la valeur est supérieure à 2,2%, favorisant ainsi une plus forte croissance des arbres; en revanche, les zones avec une faible productivité avaient une couche organique très profonde (> 85 cm), favorisant l'invasion de mousses et de sphaignes. Du point de vue de l'échelle (résolutions), le premier modèle semble relativement indépendant de l'échelle, alors que la réponse du deuxième modèle augmentait significativement avec la taille du pixel. Ces résultats pourraient donc être appliqués à des échelles opérationnelles et là où des informations sur l'ECO sont disponibles afin de prédire la productivité. Des cartes thématiques prédictives de la distribution spatiale de la productivité ont été réalisées avec nos deux modèles.

Les résultats de cette thèse ont permis d'approfondir les connaissances sur les variables permettant d'expliquer les écarts de productivité dans la pessière à épinette noire ainsi que sur l'importance des variables topographiques dans la modélisation de l'ECO et la productivité à l'échelle du paysage. De plus, cette étude a permis de caractériser la distribution spatiale des deux types de paludification (permanente et réversible) à l'échelle du paysage. Quoique cette étude s'intéresse plus particulièrement à la pessière à épinette noire, les connaissances acquises pourraient être applicables à d'autres territoires paludifiés de la forêt boréale.

MOTS-CLÉS : Paludification; Productivité forestière; GPR; LiDAR; Épaisseur de la couche organique; Sol minéral; Topographie; Ceinture d'argile «*Clay Belt*»; Pessière à épinette noire; Forêts d'épinette noire; Forêt boréale.

A. INTRODUCTION GÉNÉRALE

A.1. MISE EN CONTEXTE ET PROBLÉMATIQUE

La forêt boréale est le deuxième plus grand biome terrestre et elle couvre la majorité de la partie nord de l'Eurasie et de l'Amérique. Au Canada, la forêt boréale couvre environ trois cent neuf millions d'hectares du territoire canadien (Price *et al.*, 2013), soit le tiers des forêts boréales encore existantes dans le monde. Au Québec, la forêt boréale est présente dans les régions de la Côte-Nord, le Saguenay-Lac-Saint-Jean, l'Abitibi-Témiscamingue ainsi que le Nord-du-Québec et s'étend sur différentes zones bioclimatiques : la sapinière à bouleau blanc, la pessière à lichen, la toundra forestière, et les pessières à mousse de l'Est et de l'Ouest. Dans cette dernière zone, la forêt boréale est principalement caractérisée par la dominance de l'épinette noire (*Picea mariana* (Mill.) BSP). Ces forêts nordiques d'épinette occupent une grande partie de la forêt boréale en Amérique du Nord (Hollingsworth *et al.*, 2006). Elles revêtent une importance économique majeure, tout en soutenant d'une manière très considérable l'industrie forestière. Toutefois, ces forêts résineuses sont caractérisées par une faible productivité. La productivité forestière réfère à la quantité de matière ligneuse qu'un peuplement est capable de produire en un temps donné. Elle dépend essentiellement de la combinaison entre les variables climatiques et les variables physiques du milieu (Skovsgaard et Vanclay, 2008). La productivité peut être évaluée à l'échelle locale, pour chaque site, et aussi à l'échelle du paysage en considérant l'ensemble des sites que l'on y trouve (Anyomi *et al.*, 2013). Dans la littérature, il existe deux types de productivité : la productivité actuelle des peuplements déjà sur pied et la productivité potentielle. On entend par la productivité potentielle d'un site, la quantité de matière ligneuse que le site par ses caractéristiques intrinsèques (par exemple : le drainage, le type de dépôts, étages bioclimatiques) est capable de produire (Pokharel et Froese, 2009).

Plusieurs compagnies forestières s'approvisionnent du bois dans les forêts d'épinettes noires de la ceinture d'argile, une région boréale qui s'étend sur environ 125 000 km^2 dans le Nord-Est ontarien et le Nord-Ouest québécois (Figure 1.1). Elles doivent composer avec un territoire présentant souvent une faible productivité. Une meilleure compréhension des facteurs qui affectent négativement cette productivité, notamment la topographie et

l'accumulation d'horizons organiques épais sur le sol forestier (aussi appelé paludification) faciliterait la gestion du territoire. La paludification n'est pas propre aux régions canadiennes nordiques (p. ex., la région des basses terres de la Baie James et le Labrador), mais touche également d'autres régions boréales du monde telles que les régions de l'intérieur de l'Alaska et de la plaine de Sibérie occidentale. Toutefois, les mécanismes de paludification peuvent différer d'une région à une autre. Par exemple, en Alaska, la paludification est reliée principalement au pergélisol. Dans la région de la pessière à épinette noire de l'Ouest, située sur la ceinture d'argile (Figure 1.1), ce phénomène de paludification est souvent associé à la présence de dépôts de surface très fins, à un mauvais drainage (Lavoie *et al.*, 2005) et à la prolifération de sphaigne (Fenton *et al.*, 2005; Fenton et Bergeron 2007). Il cause une diminution importante de la température du sol et une augmentation du niveau de la nappe phréatique (Fenton *et al.*, 2006). Ce phénomène naturel contribue, d'une part, à une diminution importante de la productivité des arbres (Simard *et al.*, 2007) et, d'autre part, à la conversion des peuplements forestiers productifs (secs et denses) en des peuplements ouverts et humides de faible productivité (Lavoie *et al.*, 2005). La paludification est influencée par le temps écoulé depuis le dernier feu. Par exemple, Simard *et al.*, (2007) ont démontré qu'en absence de feu prolongé, la paludification conduit à une diminution importante de la productivité (biomasse en kg/m^2) de la pessière noire allant de 50 à 80%.

Outre le temps écoulé depuis le dernier feu, la topographie de surface est aussi considérée comme un facteur déterminant dans le processus de paludification en forêt boréale (Grant 2004; Lavoie *et al.*, 2007) et dans le degré de paludification d'un site (Simard *et al.*, 2009). En effet, les sites avec des fortes pentes montrent des degrés de paludification moins élevés que ceux avec des pentes faibles (Simard *et al.*, 2009). On reconnaît actuellement, l'existence de deux types de paludification: permanente et réversible (aussi appelés édaphique et successionelle respectivement). La paludification permanente se produit dans des endroits où les conditions d'humidité du sol sont élevées et les reliefs plats ou dans des dépressions topographiques. Par contre, la paludification réversible intervient dans des sites à pente faible ou moyennement forte en réponse à une perturbation telle qu'un feu. Alors que la paludification réversible peut être inversée par un feu sévère ou une combinaison de pratiques sylvicoles et de préparation du site, telle que décrite par Fenton *et al.*, (2009), la paludification permanente est considéré comme un état irréversible. De nombreuses études

ont porté sur divers aspects de l'un ou l'autre des deux types de paludification dans les forêts d'épinettes noires de la ceinture d'argile (Fenton *et al.*, 2005; Lavoie *et al.*, 2005; Simard *et al.*, 2009; Thiffault *et al.*, 2013). Cependant, très peu de recherches ont été concernées par la distribution spatiale de ces deux types de paludification à l'échelle du paysage (p. ex., Laamrani *et al.*, 2014b; Lavoie *et al.*, 2007). La cartographie de ces zones de paludification (réversible et permanente) à l'échelle du paysage est d'une importance majeure pour les gestionnaires forestiers, en particulier, s'ils sont appelés à mettre en œuvre des pratiques de gestion appropriées. Pour une gestion efficace des forêts d'épinettes noires dans la ceinture d'argile, il nous a semblé primordial de mieux comprendre la distribution de ce phénomène tout en identifiant les variables qui le contrôlent. Pour des études de spatialisation de la paludification, le recours aux données d'élévation et au système d'information géographique (SIG) comme outils d'analyse deviennent essentiels. Cependant, toute la difficulté d'une telle démarche réside dans l'identification des importantes variables permanentes du site nécessaires pour la caractérisation de la paludification. À notre connaissance, c'est la première fois qu'une telle approche est expérimentée dans un contexte d'un terrain avec un relief peu prononcé en utilisant des outils d'analyse avec des variables exprimés à une haute résolution spatiale. C'est dans ce contexte, qu'une méthode de classification basée sur des données topographique a été réalisée sous un SIG dans le cadre de cette thèse et dont les détails sont fournis dans la section méthodologie ci-dessous.

En plus de la topographie de surface, plusieurs études semblent suggérer un rôle important de la topographie du sol minéral (sous la couche organique) dans l'accumulation de la couche organique (p. ex., Lavoie *et al.*, 2005). Malgré son association présumée au phénomène de paludification, la topographie du sol minéral est difficile à cartographier dans les régions boréales en raison de l'épaisse couche organique qui couvre le sol minéral. C'est probablement pourquoi peu d'études ont examiné la manière dont la topographie (macro et micro) du sol minéral affecte la productivité de la pressière noire. D'après Lavoie *et al.*, (2005), une meilleure connaissance de la topographie au niveau du sol minéral et de l'épaisseur de la couche organique (ECO) faciliterait la localisation des zones de paludification permanentes ainsi que leurs expansions latérales. Une cartographie plus précise à haute résolution du niveau d'entourbement de la pessière à épinette noire et des variations des pentes du sol minéral est désormais nécessaire pour la localisation des zones de

paludification permanentes (dépressions) par rapport à celles réversibles. Une telle cartographie permettrait de mieux cibler les secteurs pouvant être aménagés en identifiant a priori les contraintes liées à la future remise en production et à la productivité potentielle des forêts. Dans ce contexte, l'utilisation des méthodes de télédétection et de géophysique à haute résolution et précision constituent une avenue prometteuse dans la quantification de la topographie, de l'ECO ainsi que de leurs interactions.

A.2. OBJECTIFS DE LA THÈSE

La recherche proposée dans cette thèse consiste à approfondir la compréhension et la détection de la paludification dans la pessière à épinette noire afin de maintenir ou d'augmenter la productivité des forêts. Le but de ce projet est d'identifier et de sélectionner les variables permanentes des sites permettant d'expliquer les écarts de productivité actuelle dans la forêt boréale du Nord-Ouest du Québec et plus particulièrement dans la pessière à épinette noire. L'expression de ces variables permettra ensuite de prédire la productivité potentielle des sites soumis aux processus de paludification dans notre zone d'étude. Les objectifs spécifiques de cette thèse sont donc de : (1) détecter et identifier d'une manière continue l'interface sol minéral/couche organique afin de cartographier la topographie du sol minéral à l'échelle des sites paludifiés; (2) étudier d'une façon quantitative les relations entre l'ECO et la topographie (au niveau du sol minéral et de la surface) afin de caractériser ces relations à l'échelle du paysage, notamment la distribution et la variabilité spatiale de l'ECO; (3) identifier les variables topographiques permettant de distinguer et de cartographier la paludification réversible et permanente à l'échelle du paysage; et (4) évaluer l'effet de l'ECO et des variables topographiques exprimées à différentes résolutions spatiales sur la productivité forestière afin d'améliorer notre compréhension de la façon dont ces variables ainsi que leurs résolutions influencent la productivité des forêts paludifiées de la ceinture d'argile.

A.3. MÉTHODE ET MATÉRIEL

A.3.1. Présentation de la zone d'étude

La zone d'étude est localisée dans la ceinture d'argile, une région du nord-ouest du Québec et du nord-est de l'Ontario (Figure 1.1). La ceinture d'argile consiste en une unité

physiographique composée principalement de dépôts d'argile laissés par le lac glaciaire Ojibway. Par la suite, la réavancée glaciaire de Cochrane de la dernière glaciation a généralement aplani le relief, compacté les argiles lacustres déjà en place tout en les rendant plus imperméables (Veillette, 1994). La zone d'étude est située dans la partie nordique de la ceinture d'argile et plus précisément dans la marge distale de la dernière crue de Cochrane. Elle chevauche deux cartes du quaternaire de la commission géologique du Canada: la première carte, partie sud, représente la Rivière Wawagosic (Veillette et Thibaudeau 2007) et la deuxième carte, partie nord, represente la Rivière Harricana (Veillette 2007). Selon ces cartes, la zone d'étude est caractérisée par (i) d'importantes perturbations (p. ex., rainures résultant du glissement des glaces sur l'argile lors des crues de Cochrane) et (ii) une couche d'argile relativement mince dont la couche supérieure a été modifiée par le passage des glaces (Till de Cochrane). De plus, la zone d'étude présente une micro-topographie accidentée et elle est ponctuée d'affleurements rocheux et de till sableux en surface. Une description détaillée des différentes zones formant la ceinture d'argile ainsi que de leurs impacts respectifs sur la productivité forestière est donnée dans l'annexe en fin de cette thèse.

La zone d'étude fait partie du domaine bioclimatique de la pessière à mousse de l'Ouest (Saucier *et al.*, 2003) et le feu y est le principal type de perturbation naturelle (Bergeron *et al.*, 2004). Les forêts de la ceinture d'argile sont dominées par l'épinette noire (*Picea mariana* (Mill.) BSP) où la paludification est présente principalement en raison du mauvais drainage du sol, du faible relief topographique ainsi que du climat froid et modérément humide (Lavoie *et al.*, 2005). La station météorologique la plus proche du territoire à l'étude est située dans la ville de Matagami et enregistre des précipitations totales annuelles de l'ordre de 890 mm et des températures moyennes annuelles de -0,7 (Environment Canada, 2011).

Plus spécifiquement, notre zone d'étude est située à environ 70 km au sud-ouest de la ville de Matagami, à proximité du Lac Mistaouac, centré sur 49° 27' 30" N, 78° 31' 5" W et couvre un territoire d'environ 100 km^2 (Figure 5.1). Nous avons utilisé des cartes écoforestières (3e programme d'inventaire décennal), une image Landsat-TM (Path/Row : 19/26, date d'acquisition : 30 juin 2005), et des visites de terrain (printemps et été 2009) pour planifier le dispositif expérimental de notre étude. La zone faisant l'objet d'étude a été choisie de façon à représenter la variabilité topographique de cette région et les différents

gradients de paludification exprimés par une forte variabilité d'ECO, tout en étant à l'intérieur du plan quinquennal de récolte de la compagnie forestière Tembec.

A.3.2. Dispositif expérimental et collecte des données

Un dispositif expérimental composé de treize transects quasi parallèles totalisant 15 km et distancés de 20 m au minimum les uns des autres et de 80 placettes d'échantillonnage circulaires de 400 m^2 a été mis en place pour les fins de cette étude (Figure 3.1). Les placettes ont été disposées aléatoirement entre les transects de façon que les centres de deux placettes voisines soient distancés de 20 m au minimum. Deux campagnes de terrain de six mois au total ont été menées en 2009 et en 2010 pour collecter des données pédologiques et forestières sur le terrain. L'épaisseur de la couche organique (ECO) a été mesurée de façon systématique à un intervalle de 10 m le long de l'ensemble des transects, ainsi qu'au centre et aux quatre coins cardinaux de chaque placette à l'aide d'une sonde manuelle. En plus de l'ECO, la composition du sous-bois (% mousse, sphaigne, lichens, arbustes etc.), le diamètre à la hauteur de la poitrine (DHP, 1,3 m) des arbres > 9 cm ainsi que le pourcentage de la cime vivante ont été mesurés dans chacune des 80 placettes. Par la suite, des carottes y ont été prélevées à 1 m de hauteur à l'aide d'une sonde de Pressler afin de déterminer l'âge des arbres sélectionnés (trois à six arbres) dans chacune des 80 placettes. Ce dispositif expérimental fait partie d'un projet multidisciplinaire qui vise à mieux caractériser l'effet des conditions avant et après des pratiques sylvicoles (récolte et préparation de terrain par la compagnie forestière Tembec) sur le phénomène de paludification. Des travaux de recherche sur le régime hydrique, la productivité forestière, l'efficacité de la préparation de terrain, la caractérisation des microsites et l'identification des bryophytes y ont également été effectuées. Par conséquent, des données provenant de certains de ces travaux (p. ex., les données sur la végétation et l'ECO dans les placettes et les transects), issues des mêmes campagnes de terrain, ont aussi été utilisées à l'occasion dans cette thèse en raison de leur proximité de notre dispositif ou pour des fins de validation.

A.3.3. Évaluation de la productivité

En Amérique du Nord, l'indice de qualité de station (IQS, aussi appelé indice de site) est la mesure quantitative la plus souvent utilisée pour exprimer et évaluer le potentiel de

croissance d'un peuplement forestier (Anyomi *et al.*, 2013; Hamel *et al.*, 2004; Ung *et al.*, 2001). L'IQS est représenté par la hauteur moyenne des arbres dominants et co-dominants à un âge de référence de 50 ans, et par conséquent, il utilise des données dendrométriques et tient compte de l'évolution verticale du peuplement, car il exprime une relation âge-hauteur. L'IQS a largement été utilisé pour déterminer la productivité potentielle de différents sites dans la forêt boréale de la ceinture d'argile du Québec et plus spécifiquement dans la pessière à épinette noire (p. ex., Hamel *et al.*, 2004; Simard *et al.*, 2007). Lors de cette thèse, j'ai aussi utilisé l'IQS comme indicateur de productivité qui a été calculé à l'échelle de la placette à l'aide des équations de Pothier et Savard (1998). Une explication détaillée sur le calcul et l'utilisation de l'IQS dans le cadre de cette thèse est présentée dans le cinquième chapitre.

A.3.4. Méthodes de télédétection à haute résolution et précision spatiales

Aux fins de cette thèse, nous proposons deux méthodes à haute résolution et précision qui semblent bien adaptées pour détecter les différentes caractéristiques de la paludification dans la zone d'étude. Il s'agit de la méthode géoradar aussi appelée GPR «*Ground Penetrating Radar*» ou radar-sol et de la technique de télémétrie laser, ou LiDAR «*Light Detection And Ranging*».

A.3.4.1. Méthode Géoradar

Le géoradar est une méthode géophysique utilisant des impulsions électromagnétiques (EM). Les ondes EM sont envoyées dans le sol à l'aide d'une antenne émettrice; quand elles rencontrent un contact entre deux milieux de nature différente (p. ex., tourbe/argile ou argile/socle rocheux), elles seront réfléchies, renvoyées vers la surface et recueillies par une antenne réceptrice. Cette dernière mesurera le temps d'arrivée et l'intensité des signaux réfléchis. L'atténuation du signal de radar dépend fortement de la constante diélectrique totale du milieu et de la fréquence utilisée. Cette méthode géophysique permet à partir de mesures effectuées en surface de tomographier des structures sous-jacentes. En dépit de sa faible profondeur de pénétration allant de centimètres à plusieurs dizaines de mètres dans des conditions optimales, le géoradar est considéré comme une méthode utile pour l'estimation de l'ECO. À titre d'exemple, Slater et Reeve (2002) ont utilisé cette méthode pour cartographier et examiner les différentes caractéristiques du sous-sol dans les tourbières en milieu forestier. Ces auteurs ont démontré le potentiel de la méthode géoradar pour

cartographier le contact tourbe/sol minéral jusqu'à 8 m de profondeur ainsi que l'épaisseur des couches d'argiles dans des tourbières situées dans les forêts du Maine aux États-Unis. Le géoradar a été utilisé dans d'autres études en forêt boréale canadienne pour estimer la topographie du sol minéral ainsi que l'ECO (Emili *et al.*, 2006; Lapen *et al.*, 1996). Les résultats de ces études ont montré une forte relation entre les ECO acquises par le géoradar et celles collectées manuellement sur le terrain dans une tourbière en Colombie-Britannique et en Ontario (r = 0.99, Lapen *et al.*, 1996; r = 0.91, Emili *et al.*, 2006). D'autres études ont démontré le potentiel du géoradar pour fournir des informations utiles sur la nature de la distribution de sphaigne dans les tourbières boréales (Comas *et al.*, 2005a) ainsi que la morphologie et la stratigraphie des milieux humides forestiers (Comas *et al.*, 2004). Le GPR a aussi été utilisé avec succès pour étudier la discontinuité du pergélisol (interface sol gelé/non gelé) dans les Territoires du Nord-Ouest (Kettles et Robinson, 1997).

Dans le cadre de cette thèse, nous avons utilisé le système pulse EKKO PRO (Sensors & Software inc., Mississauga, Ont.) dans deux sites forestiers paludifiés couvrants une superficie de 800 m^2 (40 m x 20 m) chaque (Figure 1.2). Ces deux sites représentent différents types de sol et d'ECO, associés à différents degrés de paludification, soit faible à moyennement paludifié ou fortement paludifié. Sur chacun des sites, trois profils géoradar parallèles d'une longueur de 40 m chacun ont été acquis selon un pas d'échantillonnage de 20 cm et une fréquence de 200 MHz (Figure 1.2). Une fois les données géoradar acquises, il était nécessaire d'appliquer plusieurs traitements aux profils pour leur interprétation. À cet effet, nous avons principalement utilisé le logiciel EKKO View Deluxe (Sensors & Software inc.). L'interprétation des données géoradar a été comparée avec l'ECO mesurée d'une façon systématique à un intervalle de 1 m le long de l'ensemble des profils à l'aide d'une sonde manuelle. De plus, un profil géoradar CMP (Commun Middle Point) a été effectué au centre de chacun site afin d'obtenir une estimation précise de la vitesse des ondes électromagnétiques dans le sous-sol. Un explicatif de la méthode CMP est fournie dans le premier chapitre.

A.3.4.2. Technique LIDAR

Le LiDAR est une technique de télédétection active qui utilise un télémètre laser permettant une acquisition précise, rapide et fiable de nuages de points en 3D géoréférencés.

Le principe de fonctionnement du LiDAR aéroporté consiste en l'émission d'une série d'impulsions qui sont enregistrées par le capteur une fois qu'elles rencontrent des objets au niveau de la surface. En connaissant avec précision l'altitude de l'avion, il est alors possible de déterminer l'altimétrie de chaque point ou objet. Les applications du LiDAR dans le domaine de l'estimation de paramètres forestiers et topographiques en milieu boréal sont désormais de plus en plus nombreuses (p. ex., Bolton *et al.*, 2013; Southee *et al.*, 2012; St-Onge *et al.*, 2008; Webster *et al.*, 2011).

Des variables topographiques telles que le degré et la direction de la pente de surface, la position sur la pente, les réseaux de paléo-drainage, les indices topographiques de position et d'humidité ainsi que la courbure du terrain semblent importants dans l'explication de la distribution spatiale de l'ECO et de la productivité de la pressière noire. C'est dans ce contexte qu'un relevé LiDAR a été réalisé le 28 mai 2010 afin d'extraire les indicateurs associés à ces variables. La densité moyenne de points obtenus était de 2,8 points par mètre carré. Le relevé considéré couvre une zone forestière d'une superficie d'environ 100 km^2 (~ 9 km x 11 km). Nous avons effectué plusieurs tests de précision des données en x, y et z en les comparant à des données issues de relevés GPS à l'aide du système GNSS (Global Navigation R8 Satellite System, précision centimétrique). Les résultats de ces tests sont en accord avec la précision fournie en z (z ± 6,5 cm) par le fournisseur des données LiDAR, la compagnie GÉOLOCATION (http://www.geolocation.ca).

Dans un premier temps, le relevé LiDAR a été utilisé dans le but de fournir un modèle numérique du terrain (MNT) à la surface. Ce MNT nous a permis par la suite de réaliser une cartographie continue des différentes variables topographiques de la surface à l'échelle du paysage. Ensuite, les valeurs des variables topographiques ont été générées à partir des cartes résultantes avec différentes résolutions au niveau des points d'échantillonnages acquis sur le terrain (placettes et transects). Dans un deuxième temps, les données d'altitude extraites des MNT ont été combinées aux mesures d'ECO acquises sur le terrain afin de générer un modèle numérique d'élévation (DEM) au niveau du sol minéral. En effet, ce DEM a été généré en mode raster à une résolution optimale de 15 m à l'aide des algorithmes disponibles dans le SIG (ESRI, 2011). Pour ce faire, nous avons soustrait les valeurs d'ECO à la valeur d'altitude (z) extraite du MNT au niveau des points du terrain tout en interpolant entre les

différents points de mesures le long et entre les 13 transects de la zone à l'étude. Le DEM généré a permis ainsi de générer une autre série de variables topographiques, mais cette fois-ci au niveau du sol minéral l'élévation, la pente, l'exposition, la courbure totale, la courbure transversale, la courbure horizontale, et l'indice topographique d'humidité (TWI).

Par la suite, nous avons établi des relations quantitatives entre l'ECO et les topographies au niveau de la surface (chapitre II) et du sol minéral (chapitre III), via des approches de modélisation par arbre de régression ainsi que par simples corrélations entre chaque variable topographique et l'ECO. Ces relations ont servi à extrapoler l'ECO et la productivité au-delà de la zone couverte par notre dispositif expérimental, soit sur un territoire plus grand correspondant à la totalité de la zone couverte par le relevé LiDAR (~10 000 hectares) (Figure 5.1). Les chapitres II, III, IV et V décrivent d'une manière détaillée les caractéristiques du relevé LiDAR ainsi que les variables topographiques qui y ont été dérivées à différentes résolutions.

A.3.5. Cartographie et délimitation spatiales de la paludification réversible vs permanente

La cartographie et la délimitation spatiales de la paludification réversible vs permanente constituent l'élément central du quatrième chapitre. Peu de recherches auparavant se sont penchées sur cette question, malgré son grand intérêt pour les études écologiques et l'aménagement forestier. Bien qu'il existe un grand nombre de méthodes et algorithmes qui ont été mis au point pour subdiviser le paysage en entités morphologiques (p.ex., Clark *et al.*, 2009; Creed et Beall , 2009), la plupart de ces méthodes ont été développées pour des applications non forestières (p. ex., l'hydrologie) et ne permettaient pas la caractérisation des dépressions, supposément associées à la paludification permanente. Dans les rares cas où des études visaient à distinguer les dépressions des autres formes du paysage (p. ex., terrains plats vs dépressions; Lindsay et Creed, 2005), les approches et les algorithmes utilisés étaient compliqués et leur mise en œuvre et interprétation souvent nécessitaient des connaissances approfondies en statistique et beaucoup d'investissements en temps. Afin d'éviter ces problèmes, nous avons opté pour une méthode semi-automatisée basée sur des variables topographiques pouvant être facilement applicable à d'autres zones d'étude dans la forêt boréale, et en plus d'être exécutable dans un SIG (p. ex., ArcGIS 10). À cet effet, nous avons

choisi une méthode qui combine la pente de surface et deux indices : l'indice de position topographique (TPI, Weiss, 2001) et l'indice topographique d'humidité (TWI, Moore *et al.*, 1993).

Le TPI caractérise l'entourage d'un pixel cible en tenant compte de sa position par rapport à son voisinage. Il mesure la position topographique relative du pixel central comme la différence entre l'altitude de ce pixel et l'élévation moyenne dans un voisinage prédéterminé (50 m dans le cas de notre étude). Son utilisation conjointe avec la pente de surface a permis d'assigner chaque pixel du MNT à différentes classes comme les dépressions, les plateaux, les crêtes, les milieux de pente, les hauts de pente ou les hauts de collines en utilisant une méthode automatisée sous SIG développée par Jenness *et al.*, (2001). Dans le cadre de cette thèse, nous avons opté pour une version raffinée de la méthode initialement proposée par Weiss (2001), tout en y fixant de nouvelles classes et de nouveaux seuils plus adaptés à notre zone d'étude. Une présentation détaillée de la méthode de classification et des variables topographiques qui y sont utilisées est fournie dans le quatrième chapitre.

Le TWI est considéré comme un indice de saturation dont la valeur reflète le potentiel de saturation du sol, les zones saturées étant celles avec de fortes valeurs de TWI et vice versa. Le TWI, à cet effet, a fréquemment été utilisé dans des approches de modélisations hydrologiques permettant de discriminer les zones bien drainées de celles potentiellement saturées du fait de leurs positions topographiques. Un descriptif de l'équation utilisée pour le calcul du TWI est fourni dans le chapitre IV. Dans le cadre du quatrième chapitre, les valeurs du TWI ont été utilisées pour distinguer des zones présentant des conditions d'humidité relativement homogènes. À cet effet, trois catégories de conditions d'humidité (sec, modéré et humide) ont été déterminées. La combinaison des valeurs des deux indices (TPI et TWI) et de la pente ont permis de produire plusieurs catégories (p. ex., sec-plateau, humide-dépression, etc.) et chacune d'elles s'est vue assigner un type de paludification déterminé. Cette assignation a été réalisée en se basant sur des valeurs seuils des trois variables topographiques: TPI, TWI et pente. Une explication détaillée sur les valeurs seuils sélectionnées et utilisées dans le cadre de cette étude est fournie dans le quatrième chapitre. Les résultats de la classification ont été ensuite corroborés en utilisant des données

ponctuelles sur le sol et la végétation acquises sur le terrain. Il est à noter que quoique certaines études ont démontré l'utilité de ces deux indices (conjointement ou séparément) pour la classification du paysage en forêt boréale (Emili *et al.*, 2006; Pierce *et al.*, 2012; Tchir *et al.*, 2004), à notre connaissance, aucune étude n'a auparavant utilisé ces indices pour la cartographie et la délimitation spatiales de la paludification réversible vs permanente, notamment dans les forêts paludifiées de la pessière à épinette noire.

A.3.6. Analyse des données

Des modèles de distribution spatiale de l'ECO (chapitres II et III) et de la productivité (chapitre V) ont été construits en utilisant la procédure de traitement de données par arbres de régression d'après Hothorn *et al.*, (2006). L'idée principale de ces arbres de régression était de subdiviser récursivement et le plus efficacement possible les jeux de données disponibles jusqu'à obtenir des unités paysagères homogènes. Dans chacune des entités qui en résulte, des règles définissant la manière dont les données devaient être partitionnées ont été sélectionnées sur la base d'un test d'indépendance entre les variables explicatives et la variable réponse et une division des données a été créée lorsque la valeur de P était inférieure à $\alpha = 0,05$. La procédure des arbres de régression était bien adaptée aux jeux des données de trois chapitres de cette thèse (chapitres II, III et V) pour différentes raisons : elle était immédiatement interprétable, elle a permis de manipuler, à la fois, des variables catégoriques et continues et elle a permis d'en déduire des règles de classification. Ces règles ont été utilisées par la suite pour cartographier l'ECO et la productivité forestière.

Des corrélations de Spearman et de Pearson ont aussi été utilisées afin d'analyser certaines des relations établies dans le cadre de cette thèse (p. ex., ECO vs variables topographiques), alors que des coefficients de corrélation ont été utilisés pour mesurer l'intensité de la relation entre les variables étudiées. Le seuil de signification (P) a été fixé à $\alpha = 0,05$. Des tests de comparaisons multiples tels que le test *HSD de Tukey* et le test de *Scheffe* ont été utilisés dans le cadre de cette thèse afin de produire des moyennes pondérées et pour déterminer les différences significatives entre les moyennes de groupes dans une analyse de variance (chapitres II et IV).

Toutes les analyses statistiques de cette thèse ont été effectuées à l'aide du logiciel R (R Development Core Team. 2011) et notamment les arbres de régression qui ont été réalisés en utilisant la fonction ctree du package party d'après Hothorn *et al.*, (2006).

A.5. PRÉSENTATION DE L'ORGANISATION DE LA THÈSE

Cette thèse comporte cinq chapitres sous forme d'articles scientifiques rédigés en anglais. Chacun des cinq chapitres de cette thèse situe les différentes caractéristiques de la zone étudiée, résume la physiographie de la ceinture d'argile et de la zone d'étude et décrit les caractéristiques générales de la couche organique, le sol minéral, le socle rocheux et les différentes espèces du couvert végétal et du sous-bois. Le design expérimental, la collecte des données utilisées et les analyses réalisées y sont décrits en détail. Chacun des chapitres présente l'analyse et l'interprétation des résultats, une discussion à propos des choix des méthodes utilisées, de leurs limites, des améliorations possibles et de leurs applications à l'échelle du paysage ainsi que de la contribution des résultats à un aménagement durable des forêts paludifiés. La dernière section de la thèse consiste en une conclusion globale faisant ressortir les principales contributions, conclusions et recommandations qui se dégagent de la présente étude.

En tant que premier auteur pour chaque article de la thèse, j'ai planifié les études, préparé les protocoles d'échantillonnage, mis en place les dispositifs expérimentaux, recueillis les données, produit, analysé et interprété toutes les données et les résultats, rédigé les manuscrits et géré le processus de publication. En plus d'avoir supervisé les travaux de recherches de cette thèse et orienté les grands axes de travail, mon directeur (Dr Valeria) et mes codirecteurs (Dr Bergeron et Dre Cheng) ont contribué aux différents manuscrits de cette thèse dont ils sont coauteurs. Ils ont contribué à la réflexion sur les analyses et les résultats et à la révision critique des cinq chapitres impliquant une contribution au contenu intellectuel. Cela a permis d'améliorer la qualité et la compréhension des différents chapitres. Le traitement et l'analyse des données géophysiques du premier chapitre I se sont déroulés dans le laboratoire du groupe de recherche de géophysique appliquée à l'Université Pierre et Marie Curie-Paris 6 dans le cadre de mon stage de cinq mois sous la direction du professeur Dr Camerlynck. Il est coauteur sur le premier chapitre car il a révisé en contribuant notamment sur le plan intellectuel. Dre Nicole Fenton, chercheur à l'UQAT, est coauteure sur quatre des

chapitres de cette thèse, car ses études doctorales et ses travaux de recherche en cours sont en lien direct avec les travaux de cette thèse. Elle a révisé les quatre derniers chapitres de cette thèse notamment en contribuant au contenu sur le plan intellectuel. Dr Anyomi, stagiaire postdoctoral à l'Université de Colombie-Britannique, est coauteur sur le cinquième chapitre car il m'a guidé et aidé sur l'utilisation de l'indice de qualité de station et il a révisé ce dernier chapitre de la thèse en contribuant au contenu sur le plan intellectuel.

CHAPITRE I

THE USE OF GROUND PENETRATING RADAR FOR REMOTE SENSING THE ORGANIC LAYER-MINERAL SOIL INTERFACE IN PALUDIFIED BOREAL FORESTS

Ahmed Laamrani[1], Osvaldo Valeria[1], Li Zhen Cheng[2], Yves Bergeron[1], and Christian Camerlynck[3]

[1] Chaire industrielle CRSNG-UQAT-UQAM en aménagement forestier durable, Institut de recherche sur les forêts et Centre d'étude sur la forêt.
Université du Québec en Abitibi-Témiscamingue. 445 boul. de l'Université, Rouyn-Noranda, Québec J9X 5E4, Canada.

[2] Institut de recherche en mines et environnement (IRME), Université du Québec en Abitibi-Témiscamingue. 445 boul. de l'Université, Rouyn-Noranda, Québec J9X 5E4, Canada.

[3] Unité Mixte de Recherche 7619-Sisyphe, Université Pierre et Marie Curie-Paris 6, Tour 46-56 3ème étage, 4 Place Jussieu - 75252 PARIS CEDEX 05, France.

Article publié en 2013 dans

Canadian Journal of Remote Sensing.

Volume 39, No 1, pages74-88. Doi:10.5589/m13-009

ABSTRACT

Black spruce forests that are located in the Clay Belt, within the boreal region of eastern North America, are prone to paludification. Paludification is a natural process where organic layer accumulates on the forest floor, leading to substantial decreases in forest productivity. This study assessed the ability of using ground penetrating radar (GPR) to remotely sense the organic layer-mineral soil (OL-MS) interface (representing organic layer thickness «OLT»), which has a major influence on the occurrence of paludification in this region. The two chosen sites for this study represented different types of soil and organic layer thicknesses that are linked to different degrees of paludification: low to moderately paludified (site A) and highly paludified (site B). At each site, GPR measurements were collected along three 40 m parallel transects at 20 cm intervals with 200 MHz antenna. GPR interpretations were compared with field manual probing measurements. Detection of this continuous interface was successful at site A (r = 0.93, $P < 0.001$), but mesic and humic horizon clay content limited radar depth penetration, rendering the OL-MS undetectable at site B. However, we found that GPR data, coupled with ground truth information, were effective in mapping the thickness of the organic fibric horizon (r = 0.79, $P < 0.001$) at site B, which could be considered as an indicator of the OLT in highly paludified areas. Overall, GPR appeared effective for mapping the OL-MS interface in the low to moderately paludified site, which is attractive for implementing forest management strategies that will help to stop the advance of paludification.

RÉSUMÉ

Les forêts d'épinettes noires situées dans la ceinture d'argile, une région boréale de l'est de l'Amérique du Nord, sont sujettes à la paludification. Ce phénomène est un processus naturel par lequel une couche organique s'accumule sur le sol forestier, conduisant à une diminution importante de la productivité de ces forêts. Cette étude a évalué l'aptitude du radar-sol (géoradar, ou GPR « Ground Penetrating Radar ») à cartographier l'interface «OL-MS» constituée entre la couche organique et le sol minéral (la profondeur de cette interface correspond de fait à l'épaisseur de la couche organique (OLT « Organic Layer Thickness »), paramètre clef de la compréhension de la paludification dans cette région. Deux sites ont été choisis pour cette étude; ils représentent différents types de sol et d'OLT, associés à différents degrés de paludification, soit faiblement à moyennement paludifié (site A) ou fortement paludifié (site B). Trois profils radar-sol parallèles d'une longueur de 40 m chacun ont été acquis sur chaque site selon un pas d'échantillonnage de 20 cm et une fréquence de 200 MHz. L'interprétation des données GPR a été comparée avec les sondages manuels de l'OLT effectués sur le terrain. La détection de cette interface continue a été faite avec succès sur le site A (r = 0,93; P < 0,001); sur le site B, la forte teneur en argile des horizons mésiques et humiques a limité la pénétration en profondeur des ondes radar, en rendant le sol minéral indétectable. Cependant, nous avons découvert que l'utilisation des données de radar-sol combinée à des mesures de l'OLT sur le terrain du site B, a permis de cartographier l'épaisseur de l'horizon fibrique (r = 0,79; $P < 0,001$), ce qui pourrait être considéré comme un indicateur de l'OLT dans les zones fortement paludifiées. Cette étude montre que le radar-sol apparaît l'instrument efficace pour cartographier l'interface OL-MS dans un site faiblement à modérément paludifié. Ce résultat apparaît prometteur pour la mise en œuvre de stratégies de gestion forestière qui permettront de stopper la progression de la paludification.

1.1. INTRODUCTION

The black spruce forests of the Clay Belt cover about 125 000 km^2 and are considered as a potential source of wood fibre. However, a considerable volume of timber in this region is located in areas that are prone to paludification (Fenton *et al.*, 2005; Lavoie *et al.*, 2005). Paludification is a natural process that is characterized by gradual accumulation of surface organic matter deposits over time (Payette and Rochefort 2001), which can lead to losses of forest productivity (Simard *et al.*, 2007, 2009). The depth to the top of the mineral soil beneath the thick organic layer can determine where and to what extent paludification will occur in the Clay Belt (Lavoie *et al.*, 2005). Thus, accurate estimates of organic layer thickness (OLT) are important for forest management, as predictions of this parameter will help guide appropriate management practices to control and improve forest productivity and prevent the advance of paludification into the lowland black spruce forests of the region. Yet, determining the organic layer-mineral soil (OL-MS) interface (representing OLT) over such a large area is complicated by the presence of the relatively thick and dense organic layer. OLT estimation at spatially disconnected locations (i.e., plots) throughout the landscape are time consuming, labour intensive, and cannot provide continuous data at either landscape or regional scales. In addition, information regarding the interface between the organic layer and underlying mineral soil and its spatial variability over large areas cannot be measured directly by traditional remote sensing techniques (i.e., multispectral imaging, photogrammetry), despite demonstrable advantages of the latter in covering very large surfaces (Valeria *et al.*, 2012). In contrast, ground penetrating radar (GPR), a remote sensing technology, can be a viable alternative for delimiting the OL-MS interface and its spatial continuity through a shallow organic layer in paludified sites of the Clay Belt.

The interest in the use of GPR for characterizing forest ecosystems has expanded rapidly over the last decade in conjunction with changes in technology as well as increases in computing and software capacity. GPR operates by transmitting short pulses of high frequency (25 MHz to2.5 GHz) electromagnetic (EM) energy into the ground from an antenna. When the emitted EM wave reaches an interface between materials with contrasting dielectric (K) properties (i.e., peat and saturated clay with K values of 50-70 and 10, respectively), part of the energy is reflected back to a surface receiving antenna and

registered as a single radar trace. Juxtaposition of the recorded traces can be used to display a 2-D image of the surveyed subsurface. By knowing the propagation velocity of the pulse through the substrate and the time it takes for a pulse to travel from the transmitter to the reflector and back to the receiver, it is possible to determine the location, depth, presence, and spatial continuity of underground features (Davis and Annan, 1989; Annan, 1999). The velocity of the radar signal is mainly controlled by the relative dielectric constant (K), which in turn closely depends upon substrate water content. GPR works well in forested peatlands because the low electrical conductivity of the peat in these environments allows large penetration depths (Lowry *et al.*, 2009), and the moisture content changes that occur at various interfaces (i.e., within the organic layer and between the organic layer and mineral soil) cause strong GPR reflections (Slater and Reeve, 2002). For instance, GPR has permitted successful measurement of the OL-MS interface to depths ranging from a few decimetres (i.e., 25 cm; Lapen *et al.*, 1996) to 10 m or deeper, with resolutions of 10 to 15 cm (Lowe, 1985; Theimer *et al.*, 1994; Comas *et al.*, 2005b). Numerous studies have used GPR to characterize and estimate OLT and the depth of underlying mineral subsoils (Hänninen, 1992; Lapen *et al.*, 1996; Slater and Reeve, 2002; Comas *et al.*, 2004, 2005a; Emili *et al.*, 2006; Lowry *et al.*, 2009; Rosa *et al.*, 2009). Few studies, however, have used GPR to investigate thin internal organic layer structures (a few centimetres in thickness), such as ash and wood layers (Theimer *et al.*, 1994), or the interfaces between poorly and highly decomposed organic horizons (Lowe, 1985; Warner *et al.*, 1990; Kettridge *et al.*, 2008), which represent the degree of peat humification. Other forest applications of GPR surveys include mapping tree root systems at the stand and plantation level (Hruska *et al.*, 1999; Butnor *et al.*, 2001, 2003; Stover *et al.*, 2007; Amato *et al.*, 2008; Zenone *et al.*, 2008; Hirano *et al.*, 2009), estimating soil depths in mountainous forest soils (Sucre *et al.*, 2011), and defining lithologic contacts (Jol and Smith, 1991). Despite the increased interest in using GPR in different forestry applications, no research has examined its practical application in characterizing paludified black spruce forest soils of the Clay Belt. This study is the first attempt to use GPR in remotely sensing the OL-MS interface in paludified forests of the Clay Belt region and to link GPR data to different degrees of organic accumulation. This is considered as a completely promising approach in the field of GPR applications. Prior to exploring the use of GPR over larger areas (i.e., landscape scale) we initially tested its applicability at the site scale. The

objectives of this research were to investigate whether or not the GPR method is sufficiently sensitive to continuously map the OL-MS interface in boreal paludified stands and to quantify the accuracy of the GPR method by comparing its results with OLT measurements determined by manual probing. To achieve these objectives, we made two hypotheses. First, the OL-MS interface should be identifiable as the dielectric constant (K) is different between the organic layer and underlying mineral soil. Second, the measurements of OLT that were obtained by GPR should be well correlated with those determined by manual probing, as demonstrated in studies conducted in the Canadian boreal forest (i.e., r = 0.99, Lapen *et al.*, 1996; r = 0.91, Emili *et al.*, 2006).

1.2. MATERIALS AND METHODS

1.2.1. Study area and field sites

The study area is situated in the James Bay Lowlands physiographic region of Quebec and more specifically in the Clay Belt region that spans the border between Ontario and Quebec (Figure 1.1a). The Clay Belt region of Quebec (Figure 1.1b) is part of the western black spruce-feather moss bioclimatic domain (Robitaille and Saucier, 1996). This region has low relief, which was determined by flat-laying clay deposits of glaciolacustrine origin that were left behind by the pro-glacial Lake Ojibway (Veillette, 1994). Mean annual temperature and precipitation are -0.7 °C and 906 mm, respectively (Environment Canada, 2011), as measured at the Matagami weather station located at about 60 km northeast of our study sites.

Two sites at two different locations within the Quebec Clay Belt were selected for this study. They will be referred to in this study as site A and site B (Figure 1.1c), and were chosen on the basis of their accessibility to roads and their potential for contrasting responses. These sites differ in OLT, degree of paludification, drainage, vegetation cover, and substrate moisture conditions. Site A (78°3'52"W, 49°27'46"N) is located in imperfectly drained terrain, whereas site B (78°30'12"W, 49°27'06"N) is located in a poorly drained area. Soil drainage classes are based on Landscape of Canada Units according to Baldwin *et al.*, (2000). Both sites are characterized by nearly flat topography. The two sites are covered mostly with coniferous forest, which is dominated by black spruce (*Picea mariana* (Miller) BSP), jack pine (*Pinus banksiana* Lambert), and tamarack or eastern larch (*Larix laricina* (Du Roi) K.

Koch). The canopy of the 75-year-old site A is less open than that of the 135-year-old site B, where the shrub layer is well developed and tree height averages 20.6 m (Table 1.1 and Figure 1.2). On site A, mean tree height is 16.1 m. At both sites, the forest floor is composed of *Sphagnum* mosses, feather mosses, and shrubs (mainly dwarf ericaceous shrubs) in varying amounts (Table 1.1). Feather mosses consist principally of *Pleurozium schreberi* (Brid.) Mitten. *Sphagnum* coverage was higher on site B (80%) than on site A (20%).

The 75-year-old site A has an average OLT of 40 cm, while the organic layer is also well developed in site B, with an average thickness of 95 cm. The underlying mineral soil is clay rich (47-62%) at both sites, containing various amounts of sand and silt. The thickness of the clayey mineral layer over bedrock was within 1 m of the surface in site A but unknown in site B. However, in an area located about 50 km northwest of our study area, Veillette *et al.*, (2005) obtained mineral deposit thicknesses ranging from 6 m to 60 m. At site A, the water table level is most likely located beneath the shallow OL-MS interface, as no water was present when we excavated through the organic layer to the top of the mineral soil. Field observations showed that the water table in site B was often within 75 cm of the surface. Site details and photographs are shown in Table 1.1 and Figure 1.2.

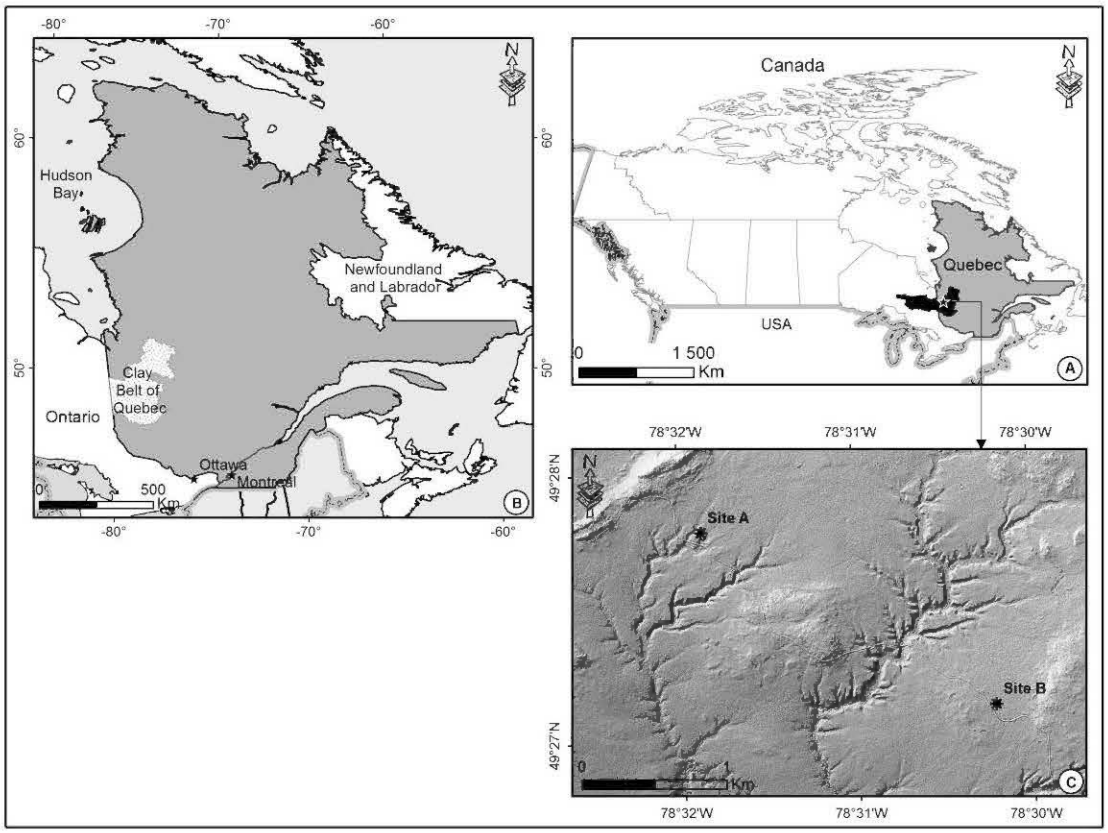

Figure 1.1. Regional view of the Clay Belt spanning the Ontario-Quebec border and the location of study area (white star) (A). View of the Clay Belt located in the western part of the Quebec province (B). LiDAR-derived DTM image showing the location of the two representative study sites (C).

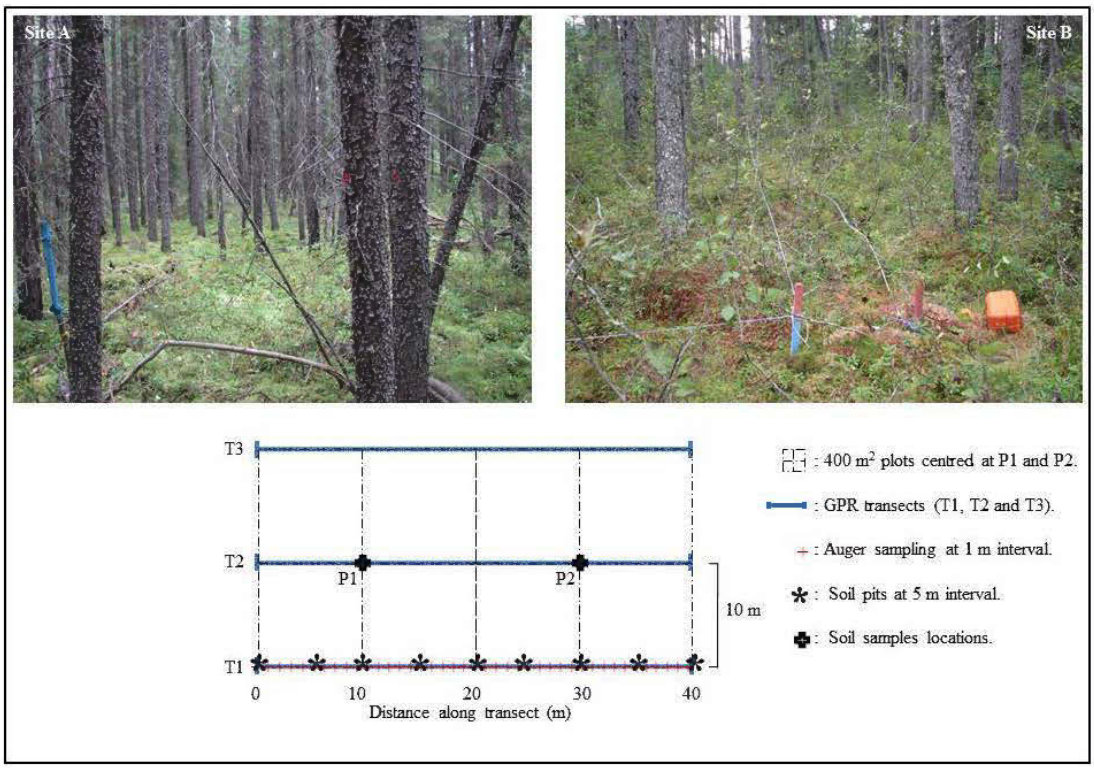

Figure 1.2. Photographs from sites A and B showing their main characteristics cited in Table 1.1 (top). Schematic presentation of the three GPR surveyed transects (T1, T2, and T3) at both sites as well as the location of the different sampling points and plots (bottom). Soil pits and augering measurements were done along each of the three transects and are shown here only for transect 1 for purposes of illustration.

Table 1.1. Summary of site conditions and stand characteristics at sites A and B.

Condition	Site A	Site B
Stand age (yr)	75	135
Mean OLT (cm)	40 (*2.5*)	95 (*3*)
Mean DBH (cm)	14.6 (*3.8*)	21.1 (*6.4*)
Mean tree height (m)	16.1 (*2.2*)	20.6 (*1.1*)
Density (steams/ha)	2375	475
Drainage class	Imperfect	Poor
Understory cover		
Feathermosses (%)	75	5
Sphagnum (%)	20	80
Shrubs (%)	5	15
Tree species cover		
Black spruce (%)	85%	90
Jack pine (%)	15%	0
Tamarack (%)	0%	10
Debris (coarse dead wood) cover (%)	< 3	20-25
Mineral soil composition	Glaciolacustrine clay	Glaciolacustrine clay

Note: Values shown in italics within parentheses indicate standard deviations of the means. OLT: organic layer thickness; DBH: diameter at breast height (1.3 m).

1.2.2. GPR measurements, processing, and interpretation

1.2.2.1. GPR measurements

In the summer of 2009, GPR surveys were conducted at each site (A and B) using the pulse EKKO PRO (Sensors & Software Inc., Mississauga, Ont.), to determine spatial variability in OLT. GPR measurements were performed at 20 cm intervals along three parallel 40 m transects on each site; at each site the transects were spaced 10 m apart. The antenna was carried by hand and moved along the transect to be surveyed. The antenna centre frequency that was used was 200 MHz, which is appropriate as the expected depth of the mineral soil was generally B1.5 m. Each collected trace was the result of 32 stacks to improve the signal-to-noise ratio. Figure 1.3 shows a schematic representation of GPR reflected and propagated EM energy travelling through the organic and mineral soil layers.

1.2.2.2. GPR data processing

Standard data post-processing was performed on the raw data to enhance them for easier interpretation. EKKO View Deluxe software (Sensors & Software Inc.) was used for data processing. The processing steps included correction for background noise (Dewow filtering) by removing low frequency interferences, zero-time static correction, and the application of spherical and exponential compensation (SEC) gain and automatic gain control (AGC) to enhance weaker reflectors and smoothing across traces. The AGC was suitable for increasing the continuity of reflections within the targeted investigation depth, but it erases all amplitude information (Jol and Bristow, 2003). This was of less importance because amplitude information was not used in the present study.

Using common mid-point (CMP) surveys, two velocities of 0.065 m/ns and 0.042 m/nswere calculated for the mineral soil and organic layer, respectively, along the central transects at sites A and B. These CMP surveys consisted of the collection of traces with increasing antenna spacing while keeping the common mid-point position between the antennae constant (Moorman *et al.*, 2003). These velocities were quite similar to those reported by Emili *et al.,* (2006) for organic layers (0.038 m/ns) and mineral soil (0.06 m/ns) in the western Canadian boreal forest. We used these velocities of 0.065 m/ns and 0.042 m/ns

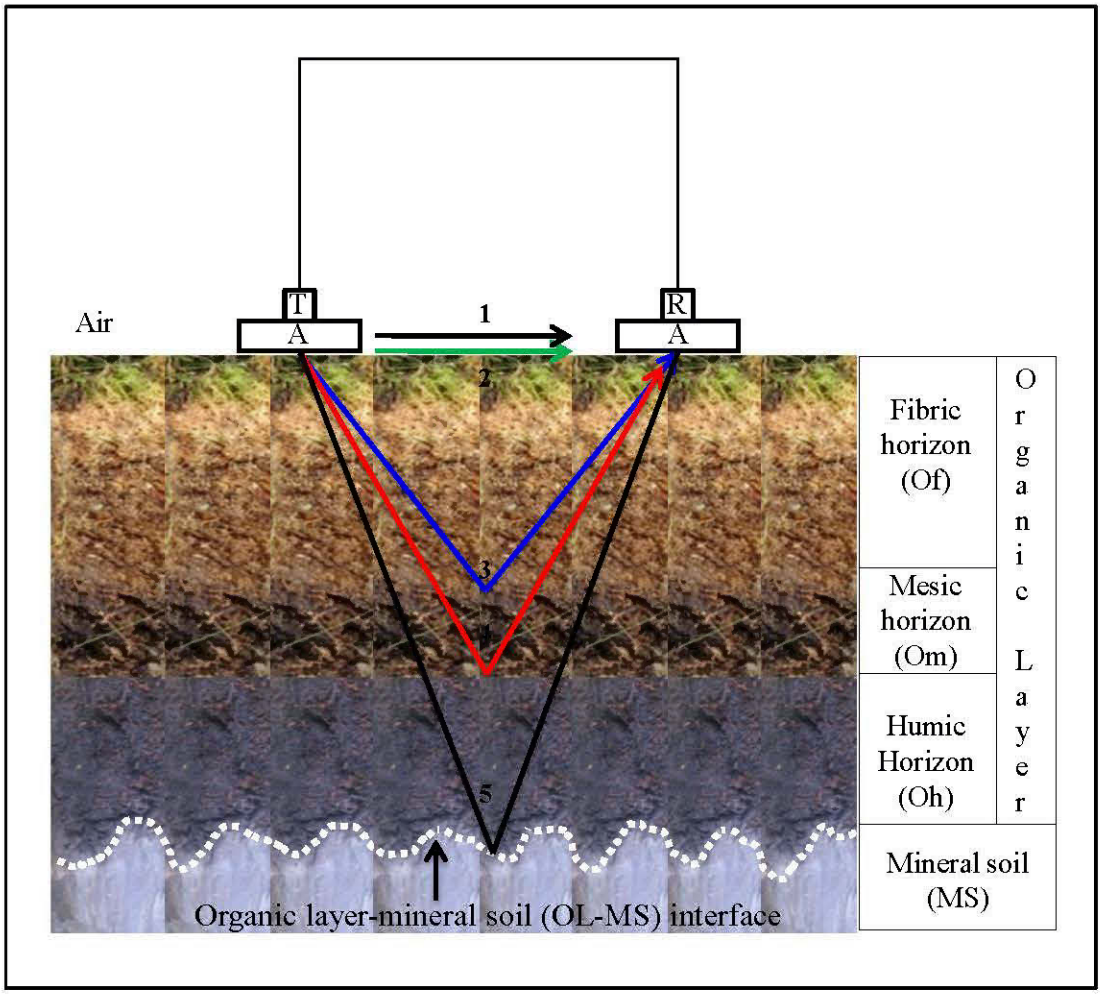

Figure 1.3. Schematic illustrating GPR reflected and propagated EM energy within the organic horizons (Of + Om + Oh) and mineral soil layers. The GPR system consists of a 200 MHz antenna (A), transmitter (T), and receiver (R). GPR signal travel paths are, in order of arrival: 1) direct air wave; 2) direct ground wave; 3) reflection from the Of-Om interface; 4) reflection from the Om-Oh interface; and 5) reflection from the OL-MS interface (white dashed line).

to convert the time scale in a depth scale, to display the real depth of the resulting underground features at each site, and to interpret the different organic horizons (fibric (Of), mesic (Om), and humic (Oh), and their respective interfaces) and the OL-MS interface location at both sites.

All profiles were geo-referenced and LiDAR elevation data were incorporated into each GPR line. LIDAR-derived surface elevations showed that both sites exhibit near flat topography, with negligible changes in elevation. For example, changes in elevation range from 299.29 to 299.93 m above sea level (asl) at site A (i.e., 64 cm), whereas the difference between the highest (303.63 m asl) and lowest (303.02 m asl) points on site B is about 61 cm. In this study, GPR profiles were displayed without topographic correction because its incorporation introduces image artifacts into GPR measurements.

1.2.2.3. Identification of soil layers and horizon interfaces

In general, the identification and interpretation of interfaces from the GPR profiles depend on how much knowledge the interpreters have about underground structures. Before undertaking the interpretation of GPR profiles, it was important to precisely identify the ground wave that represents the top of the surveyed ground surface. We determined the ground wave as the second wave to arrive (after the air wave), as described in Jol and Bristow (2003).

Based on the characteristic reflection pattern of the radar returns, delineation criteria were defined as follows. (*i*) We applied SEC gain to enhance the spatial pattern of major reflections and to improve visual discrimination of the different reflectors on each GPR profile; (*ii*) Major reflections were visually identified and marked manually on GPR profiles after application of AGC; (*iii*) We assume that such major reflections will occur where there is variation in the dielectric constant, which is linked to the water content, as is the case for the OLT-MS interface; therefore, the continuity of reflectors was another criterion that was used to pick out interfaces; (*iv*) Further, because of the homogenous soil conditions that were found within each site and that were confirmed by field observations, continuous reflectors had to be present on three profiles of the same site to be considered as real changes in the subsurface; and (*v*) We used the largest peak on signal traces to pick up an interface, as

illustrated in Gerber *et al.*, (2007). Together, these visual patterns allowed us to delineate different reflectors that could be interpreted as interfaces within the organic layer and at the OL-MS interface based on our knowledge of ground information as determined from soil pit-augering measurements. Once depth to the mineral soil was estimated along each transect from GPR profiles, these were correlated with manual probing measurements that were made at the same locations.

1.2.3. Field soil sampling and statistical analyses

Soils were described and classified as organic layer or mineral soil according to the Canadian system of soil classification (Soil Classification Working Group, 1998). This scheme separates the organic layer into three different horizons (Of, Om, and Oh) that are based on the von Post scale (von Post and Granlund, 1926) and that reflect the degree of decomposition of peat. OLT was measured manually using a hand probe to validate the GPR interpretations. Those manual measurements were done at 1 m increments along each transect, for a total of 123 measurements at each site. At each sampling point, the hand probe bored through the organic layer until the mineral soil was encountered (Figure 1.4). As those measurements did not provide the thickness of each individual organic horizon, nine soil pits (30 cm 30 cm depth to the mineral soil contact) were dug every 5 m along each transect for a total of 27 pits per site (Figure 1.4). For each soil pit, the total OLT was measured; the OL-MS interface was located, as was each organic horizon. Details of these horizons, together with typical physical properties of the Of, Om, and Oh materials, are provided in Table 1.2.

At both sites, samples were taken from the organic layer and mineral soil at 10 m and 30 m distances along the central transect for physical and chemical analyses. Electrical conductivity (EC) and organic and mineral matter contents were determined by the Forest Resources and Soil Testing Laboratory of the Lakehead University Centre for Analytical Services, Thunder Bay, Ont. (http://lucas.lakeheadu.ca/forest). The EC of soil samples was determined in1:2 (soil: water) solution using an Accumet Research AR20pH/mV/Conductivity meter. The percentage of water in each soil sample was calculated by drying the sample (at 105 °C) to constant mass, after which gravimetric water content (moisture content) was expressed as the percentage of the dry sample. Samples used

for soil analyses were taken at about 1-2 cm from interfaces. Physical and electrical properties of the organic layer are summarized in Table 1.3.

Pearson product-moment correlations (r) explored the strength of the relationship between OLT that was measured by manual probing versus that estimated by GPR. Significance was fixed at $\alpha = 0.05$ and all statistical analyses were conducted in R (http://www.r-project.org/).

Figure 1.4. Photographs from the study sites. At each sampling point, the auger was bored through the organic layer until the mineral soil was encountered (upper left), then the OL-MS interface was clearly identified and measured (upper right). Pictures showing an example of pits excavated at site A (lower left) and site B (lower right).

1.3. RESULTS

1.3.1. Direct soil pit-augering information

Thickness of each horizon, and the total organic layer and OL-MS interface were manually measured along each transect at sites A and B. Our results (Figure 1.5) showed that, between sites A and B, a great degree of variability characterized the depth of the OL-MS interface and the different organic horizons thicknesses and their respective interfaces. Organic layer thicknesses were greater in site B than those in site A. Most Of horizons (93%) in site A were 10-15 cm thick, whereas most Of horizon thicknesses in site B were > 20 cm (96%). The Om and Oh horizons were present in all soil pits in varying amounts (Figure 1.5). Measured EC is higher in the Oh horizon (208-287 µS/cm) than at the OL-MS interface (70-178 µS/cm) (Table 1.3). Such values are characteristic of nonsaline soils and are considered low. The low EC was confirmed by a background EM31 conductivity survey that was conducted over the three transects of each site prior to GPR survey. The apparent EC values from this EM31 survey ranged from 13 to 18 µS/m for the 1 m horizontal dipole mode and from 19 to 26 µS/m for the 1 m vertical dipole mode (unpublished results).

At both sites, the OL-MS transition is characterized by large decreases in water content and organic matter content (Table 1.3). For instance, the OL-MS transition is characterized by a large water content decrease from 65% in the Oh horizon to about 23% in the MS, as well as a large decrease in organic matter content from about 50% in the Oh horizon to about 1% in the MS. Mineral soil sand content is higher on site A (20%-27%) than on B (8%-9%), whereas silt content is slightly higher on site B (30%-33%) compared with A (23%-33%). Both sites have clay-rich mineral soils with a total clay percentage (0.0011-0.002 mm and < 0.001 mm fractions) ranging from 47%-50% (site A) to 58%-68% (site B). The presence of high silt and clay content in the Om and Oh horizons indicated that the organic matter probably has undergone a high degree of mineralization.

Table 1.2. Details of organic soil horizons present at both sites and some of their important features and typical physical properties.*

Soil Horizons	Important Features	Bulk density (Kg/m^3)	Total porosity (% vol)	Water content† (%)
Fibric (Of)	Consists largely of amorphous material, mostly roots and moss detritus, which are easily identifiable.	< 75	> 90	< 48
Mesic (Om)	Made of partly altered material both biochemically and physically. Plant structure are clear but becoming indistinct.	75-195	85-90	48-70
Humic (Oh)	Consists of highly decomposed organics that are almost unrecognizable.	> 195	< 85	> 70

* According to Soil Classification Working Group (1998) and Boelter (1969).
†Refers to volumetric water.

Table 1.3. Comparison of particle distribution results and soil analyses of different samples (Om, Oh, and MS) extracted along the central transect (T2) at sites A and B.

Site ID	Position T2 (m)	Soil Material	Depth (cm)*	Sand (%)	Silt (%)	Clay (%)	Fine clay (%)	EC (µS/cm)	Organic matter (%)	Moisture Content (%)
A	10	MS	35	20	33	10	37	178	0	23
	30	MS	41	27	23	9	41	110	1	20
	10	Oh	33	7	24	0	69	275	48	62
	30	Oh	39	7	26	0	67	287	53	65
B	10	MS	91	9	33	17	41	110	1	26
	30	MS	99	8	30	16	46	70	1	21
	10	Oh	89	10	16	0	74	208	51	78
	30	Oh + MS	98	3	10	9	78	169	11	42
	30	Om†	35	50	50	0	0	234	92	72

* Indicates the depths to which soil samples were taken.
†Insufficient sample after organic removal (about 2 g). This may make the accuracy of the particle distribution results of this sample questionable and was not dealt with in this study.
Note: The grain size distribution of our samples was on standard particle size classification, Sand ≥ 0.05 mm; Silt: 0.0021-0.049 mm; Clay, 0.0011-0.002 mm; fine clay ≤ 0.001mm.

1.3.2. GPR analysis and interpretation

GPR produced different reflection patterns at the ground surface and belowground on both sites (Figures 1.6a and 1.6b). An effect of ground coupling is evident near surface. This coupling is caused by the interaction between the EM wave that is radiated from the antennae and the ground, which leads to continuous reflections at the top of each profile. These reflections are not representative of the true signal amplitude, because the GPR receiver antenna is saturated with that signal. The first 0.20 m depth at site A and about the first 0.15 m at site B correspond to ground coupling (Figures 1.6a and 1.6b). Therefore, they were not considered for retrieving the organic layering information. Below these zones, profiles of each site are characterized by distinctly different patterns of reflections, which were enhanced by the application of gain (Figure 1.6).

1.3.3. Organic layer thickness estimation from the GPR data at site A

A continuous reflection in all of the GPR profiles occurs at about 40 cm below the surface at position 0 m along the transect (Figure 1.7). Ground truth data from soil pit-augering measurements suggest that this reflection coincides with location of the OL-MS interface. At this interface, substantial decreases in substrate water content are found (Table 1.3) and the abrupt changes in dielectric constant likely lead to this distinct reflection. The mineral-organic interface is nearly continuous and located at about same depth along the three parallel transects, indicating that its position is likely spatially constant over the investigated site. OLT estimates that were obtained with GPR and manual probing were well correlated (Figure 1.8; $r = 0.93$, $P < 0.001$). Overall, depths to the OL-MS interface that were obtained from GPR and manual measurements were very similar and differed only by ± 2 cm.

In addition to the OL-MS interface reflection, another reflection was estimated to be about 90 cm below the surface at the 0-m position (Figure 1.7b). Although, there is no reflector on the CMP survey that could be associated with the bedrock, this reflection is believed to delineate the transition between the thin MS layer (15-45 cm) and bedrock. Augering data that were collected from around the site showed that bedrock is close to the surface (i.e., positions between 5- and 10-m along transect 2 in Figure 1.6a). The lack of

distinctly different patterns of reflections below 90 cm supports our contention that this contact is the mineral soil-bedrock (MS-Bedrock) interface.

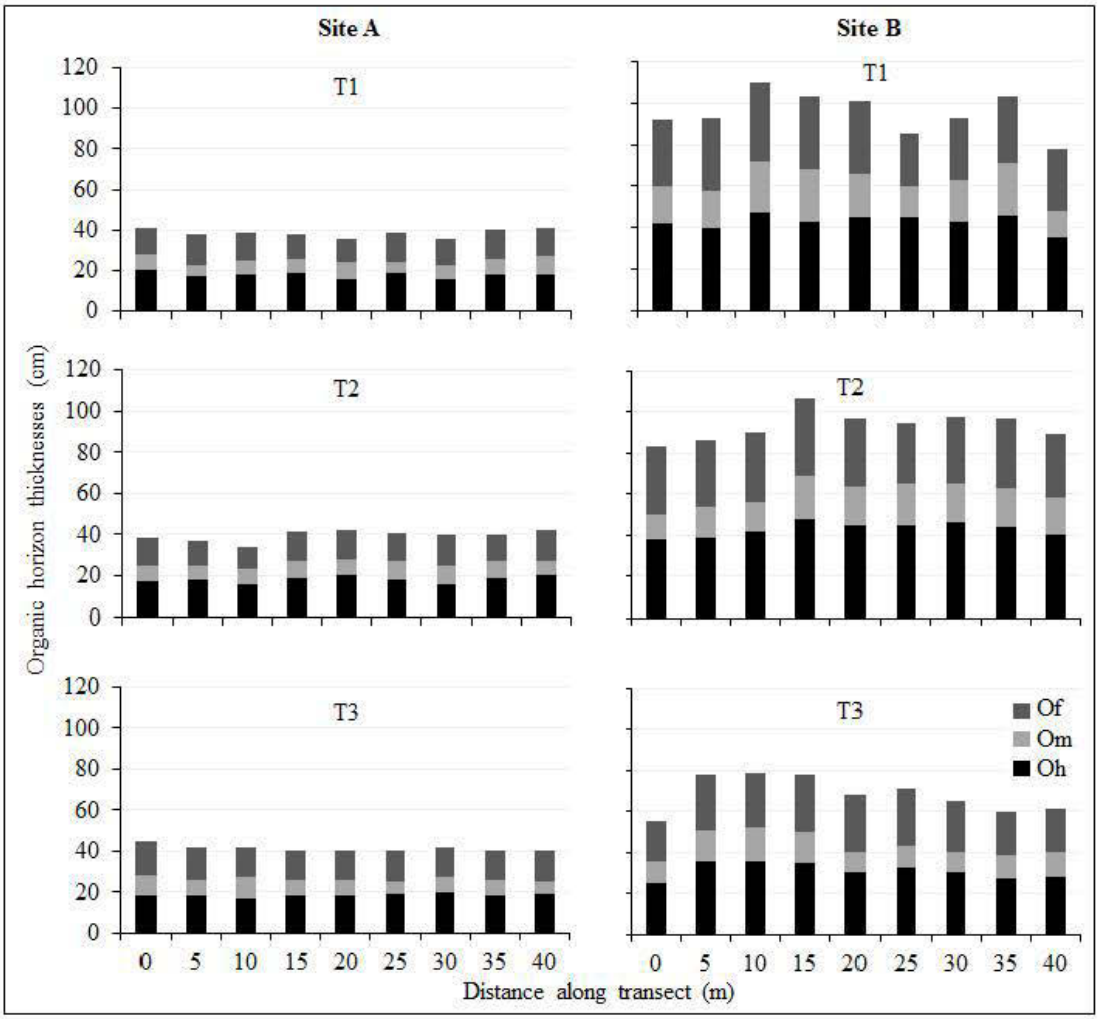

Figure 1.5. Results of organic horizon (Of + Om + Oh) delineation from soil pits obtained along the three transects (T1, T2, and T3) at both sites (pit localization is referred to in Figure 1.2)

The top bedrock reflection is relatively weak, which is most likely due to significant attenuation of the signal as it is being propagated through the clayey mineral layer. The MS-Bedrock contact is characterized by an irregular contour, which features small depressions in the underlying bedrock (Figure 1.7; the area between positions 18 m and 30 m along transect 1, for example). GPR measurements and soil augering data showed that the organic layer is thickest where these depressions occur and that the occurrence of these depressions coincides with the formation of sphagnum hummocks. Internal reflections are also visible within these depressions (Figure 1.7) and most likely attributed to small internal variations in moisture content of the mineral soil contained therein. The absence of reflector on the CMP survey associated with bedrock can be explained because the CMP survey was done at a location where the bedrock was locally deeper (position at about 25 m) and where the clayey mineral layer was thicker, which caused the wave to attenuate before reaching the top of the bedrock.

1.3.4. Organic layer thickness estimation from the GPR data at site B

GPR profiles that were obtained along the three transects at site B show multiple reflections from the surface because of the ground coupling effect (Figure 1.9). Beyond this zone, a number of nearly continuous high resolution reflections are easily identifiable within the upper 15-60 cm of the GPR profiles. Based on the analysis of soil-pit samples taken from site B, some of these nearly continuous reflectors can be attributed to the interface between the Of horizon and the underlying Om/Oh horizon (Figure 1.9). At this interface, abrupt changes in the dielectric constant can be assumed. Such a contrast in dielectric constants between these two layers is most likely the result of their different water contents (Table 1.3). Statistical analysis shows that GPR derived Of horizon thicknesses were significantly correlated with the soil pit-derived measurements (Figure 1.10; $r = 0.79$, $P < 0.001$). It is interesting to note that the interface between the Of horizon and the underlying Om/Oh horizon is locally discontinuous in the GPR profiles (Figure 1.9). These breaks could be caused by the presence of buried dead wood beneath the organic layer. Indeed, site B was characterized by a high dead wood surface cover, which was most likely attributable to stand characteristics such as formation of canopy openings and tree death (Table 1.1). In addition to the interface between the Of horizon and the Om/Oh horizon, there are several other reflectors that could be attributed to near-surface buried features such as roots and dead wood,

the interpretation of which is not dealt with in this study. Beyond 60 cm depth, the GPR signals are strongly attenuated and, consequently, the OL-MS interface is not detectable. Soil at site B had low EC suggesting that the limited EM wave penetration beyond a depth of 60 cm is most likely due to the high clay contents of the Oh and Om horizons (Table 1.3).

At the time of the GPR survey, the top of the water table was located at about 75 cm below the surface, as confirmed by in situ observations. This is consistent with Fenton *et al.*, (2006), who found that water tables in black spruce stands of the Clay Belt of Quebec were often within 1 m of the surface. Reflections from the water table are not detectable by GPR at this shallow depth because of strong EM wave attenuation.

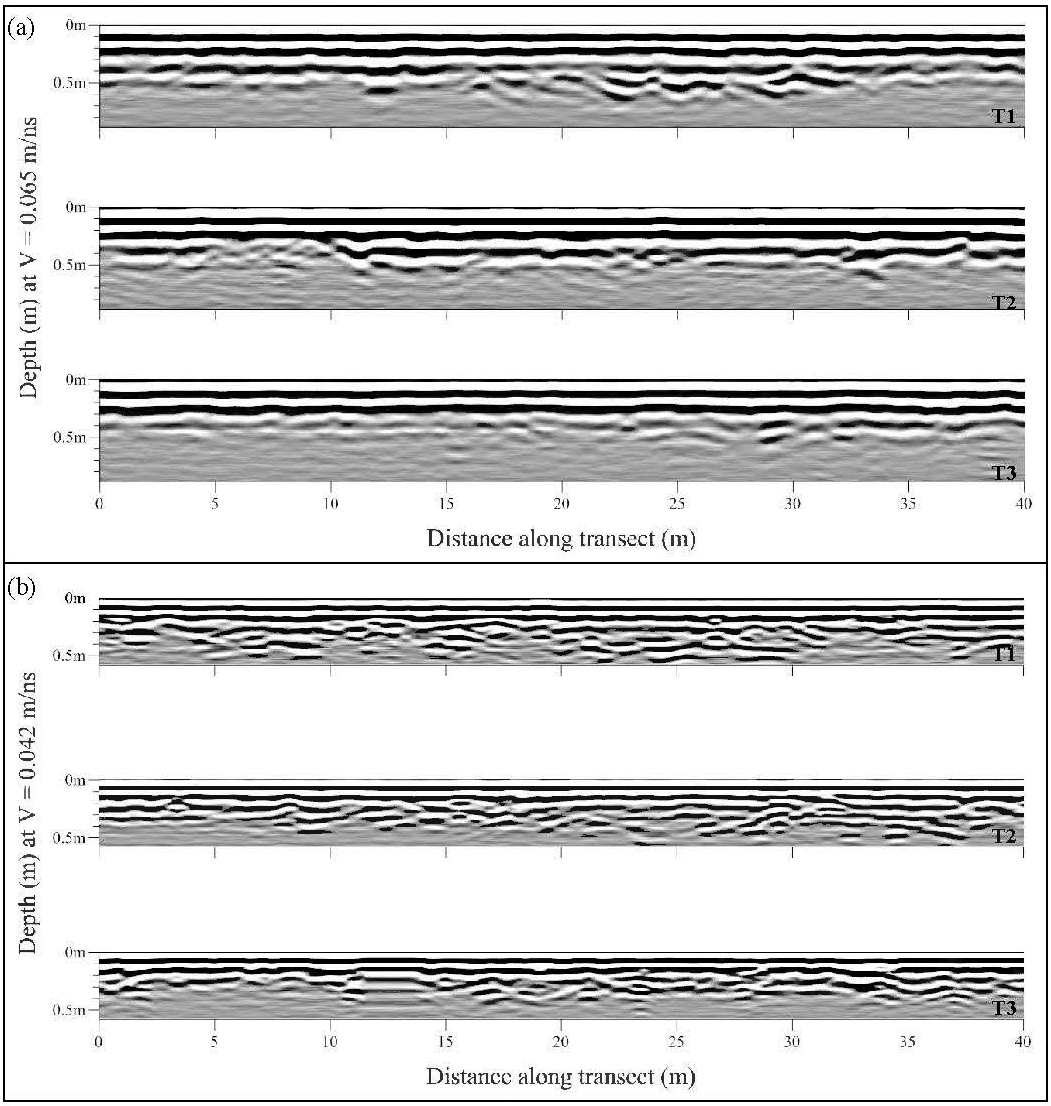

Figure 1.6. Processed GPR profiles obtained along the three transects (T1, T2, and T3) at site A (a) and site B (b) using an AGC gain of 200. The Y axis represents the depth that was obtained by converting the time it takes for the wave to travel to the reflector.

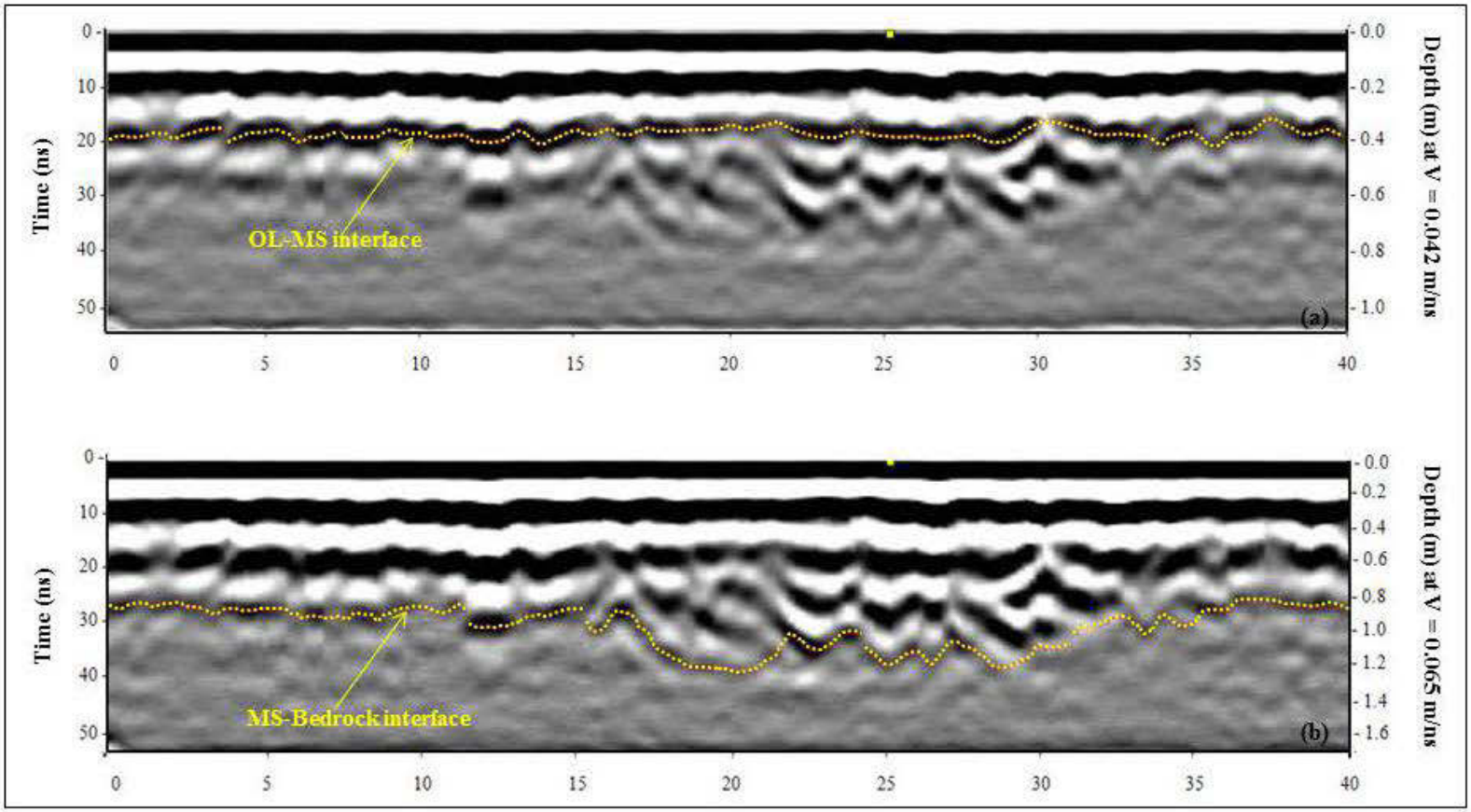

Figure 1.7. Results of delineating the OL-MS (a) and MS-Bedrock (b) interfaces along transect 1 of site A using 0.042 m/ns and 0,065 m/ns, respectively, and an AGC gain of 200. As the use of different velocities is not allowed in EKKO View Deluxe Software, GPR profiles were plotted twice using two different velocity scales.

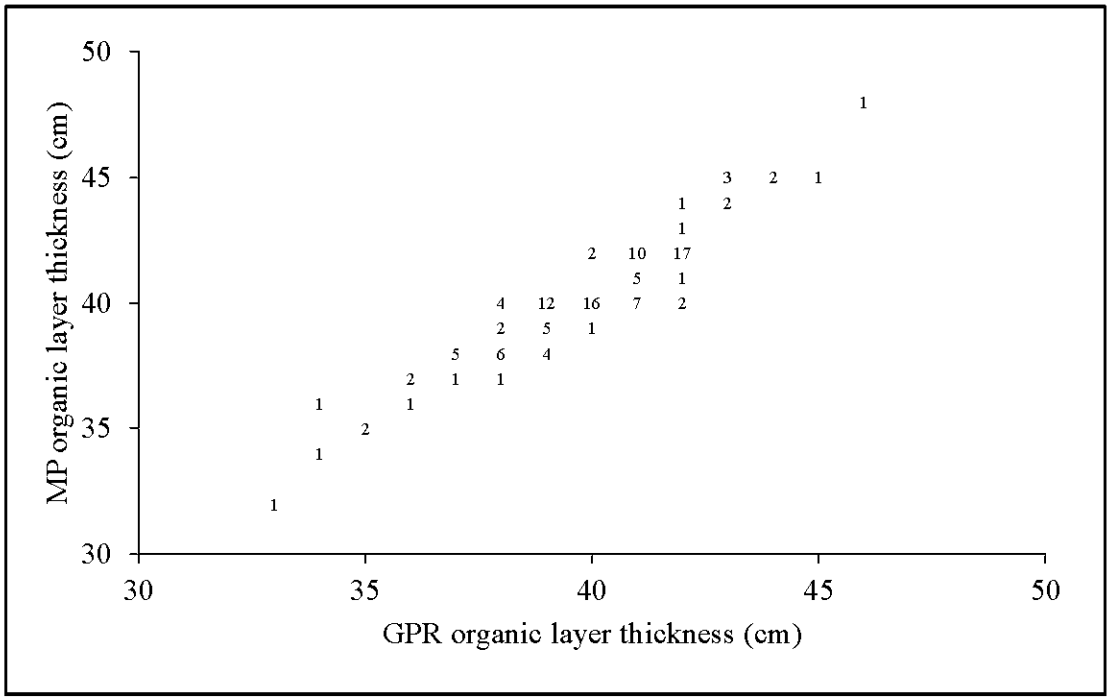

Figure 1.8. Relationship between organic layer thickness as determined by manual probing and GPR in site A (r = 0.93, P < 0.05, R^2 = 0.87, and n = 120). Arabic numbers were used as data markers and where each number referred to how many times similar pairs of observations (xy) were repeatedly measured (The sum of all of the numbers on the plot corresponds to n).

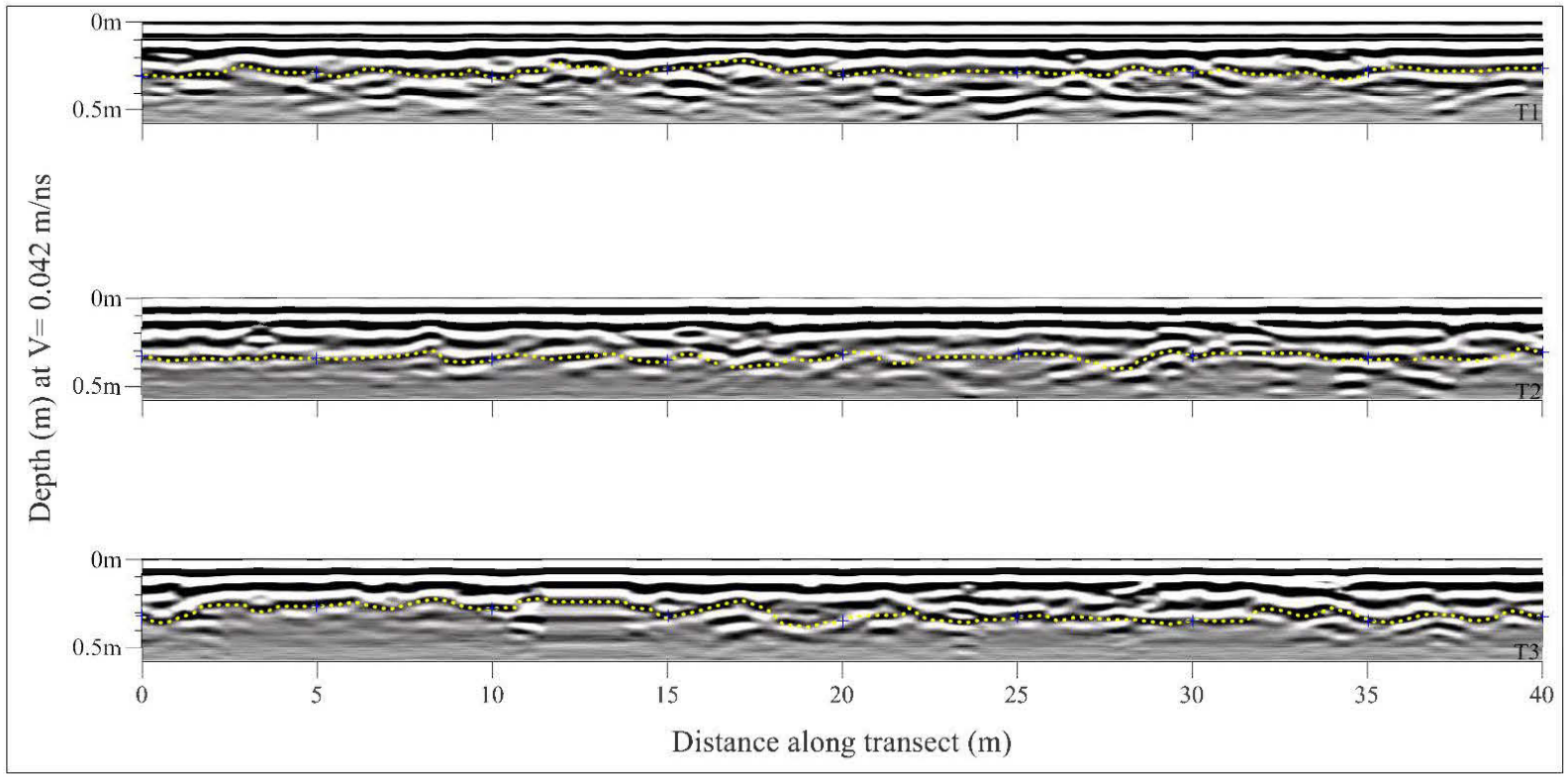

Figure 1.9. GPR profiles obtained at site B along the three transects (T1, T2, and T3). The yellow dotted lines indicate the lower limit of the fibric horizon, as determined from the soil pits, whereas plus sign (+) indicates the sampling positions.

1.4. DISCUSSION

Obviously, interpretation of GPR profiles is subjective, but with a little experience and some corroborative field measurements, it was possible to identify the OLT (as determined from the depth of the OL-MS interface) in site A as well as the Of horizon thickness in site B from the processed profiles. As previously mentioned, part of the upper organic layer was covered by multiple reflections (ground coupling) from the surface at both sites and could not be used. At the same time, more information below this depth appeared to be realistically usable for interpretation (site A, 0.20-1.0 m; site B, 0.15-0.60 cm).

1.4.1. Utility and limitations of GPR

1.4.1.1. Estimating the OL-MS interface at site A

This study demonstrated the potential for GPR to accurately identify the continuous interface between organic layers and mineral soil horizons in a site with a low to moderate degree of paludification (site A). The clarity with which this interface was identified has also been highlighted by other researchers (i.e., Emili *et al.*, 2006; $r = 0.91$; Lapen *et al.*, 1996; $r = 0.99$) through shallow organic layers within a boreal forest environment. Although reflections were discontinuous at some locations, the resulting GPR profiles provided more information about spatial continuity of the OL-MS interface than did manual probing measurements. This was previously highlighted by Hänninen (1992) as an important advantage of GPR over manual probing. The fact that GPR had the ability to detect and map local depressions in bedrock topography was another important finding of this study. Most likely, these depressions in the bedrock created wetter soil conditions that probably favored local organic layer build up, which may potentially accelerate the advance of paludification. This is consistent with Giroux *et al.*, (2001), who found that depressions in the mineral soil in some areas of the Clay Belt favored the accumulation of water and the establishment of *Sphagnum*. More research is needed to explore how shallow bedrock topography influences the occurrence and spread of paludification. Until now, no efficient method has been devised that can rapidly and economically meet the aforementioned goal. For instance, the OL-MS interface has been estimated within the Clay Belt from manually measured 400 m^2 plots (Simard *et al.*, 2007, 2009). Simard *et al.*, (2007, 2009) had to carefully choose their plots to satisfactorily represent variation in OLT over the larger study area. Unfortunately, this

sampling method could not provide spatially continuous data at either landscape or regional scales, as organic soil thickness was estimated only at spatially disconnected locations throughout the landscape. In this context, measuring OLT with GPR is a viable alternative to manual measurements in low to moderately paludified sites of the Clay Belt. For site A, GPR provided demarcation of the OL-MS interface, allowing us to distinguish greater spatial continuity within OLT than was possible with manual measurements. This result is of great interest, as site A represents very attractive conditions for forest managers and predictions of the OLT will help guide appropriate management practices and permit optimization of future forest management practices that would control and improve forest productivity.

1.4.1.2. Estimating the OL-MS interface at site B

The detection of the OL-MS interface within the highly paludified B site was not feasible, mainly because of signal attenuation. Butnor *et al.*, (2001) reported that soils with high EC rapidly restrict radar penetration depths. Given the low EC of our soil samples, it is clear that high clay content of the Om and Oh horizons limited radar penetration, rendering the mineral soil undetectable. This response was consistent with previous studies that have reported maximum attenuation being observed where the MS is clay rich (Theimer *et al.*, 1994; Slater and Reeve, 2002; Gómez-Ortiz *et al.*, 2010).

Under hypothetical conditions where silt and clay content is low in highly paludified areas, the proximity of the water table to the surface (within the organic layer) may affect GPR interpretation. Under such conditions, the water table interface should result in a very strong reflection in the GPR profiles and, therefore, may interfere with interpretations. This means that the OL-MS interface will not be detectable because of the strong reflection caused by the water table. Most highly paludified areas within the Clay Belt are considered to be moisture-saturated sites (Fenton *et al.*, 2005; Lavoie *et al.*, 2005), with large quantities of silt and clay and, therefore, GPR would be less useful in estimating the thickness of the entire organic layer. The high mineralization of the organic horizons is another factor that may affect the EC in peat throughout the Clay Belt, but few quantitative relationships have been established (Theimer *et al.*, 1994).

Salt concentrations and the calcareous content of the soils would have been other factors explaining rapid attenuation of GPR signals (Simeoni *et al.*, 2009; Grant and Schultz, 1994) at site B by increasing the EC of soil. However, our low EC values indicated that all of our soil samples were nonsaline and that carbonate likely did not contribute to radar signal attenuation in either of our sites.

1.4.1.3. Identifying the Of and Om horizons

While not the focus of this work, GPR measurement and corroborative soil pit data allowed us to map the thickness of the upper unit of the organic layer (Of horizon) at site B. The fact that GPR-derived Of horizon thicknesses were significantly correlated with soil pit-derived measurements was of great importance because a recent study reported that the low productivity of black spruce stands within the Clay Belt is mainly related to the thickness of the Of, as the Om and Oh are considered a good growth medium (Lafleur *et al.*, 2010). In this context, GPR can supply useful information about the thickness of the Of horizon in highly paludified areas. Because no research has been conducted regarding the relationship between Of horizon thickness and whole organic layer thickness within the Clay Belt, the benefit of using this variable to characterize sites with high paludification rates is largely unknown.

We estimated neither Of horizon thickness nor Om horizon thickness at site A because the antenna that was used (200 MHz) could only resolve horizons with a minimum thickness of about 5 cm; this latter value represents the estimated theoretical vertical resolution ($\lambda/4$). In many locations, the thickness of the two horizons was below this threshold. Furthermore, the uppermost 20 cm depth of the GPR profile simply multiplies reflections (ground coupling effect) of the organic layer surface that are difficult to remove from the GPR (Holden *et al.*, 2002) without altering the quality of underlying information. Therefore, it was difficult to assess the real potential of GPR for characterizing these two horizons in low to moderately paludified sites. It is important to reiterate that the use of GPR to map the Of horizon within the context of a paludified boreal forest soil has not been previously tested. However, higher frequency antennas (i.e., 500, 800, 1000 MHz) could be used to increase resolution and decrease the ground coupling effect. This will also likely improve Of horizon delineation while reducing the ability to delineate the OL-MS. An alternative approach for further

investigations regarding the organic layer horizons and the OL-MS is the use of the 200 MHz antenna in conjunction with an antenna of higher frequency.

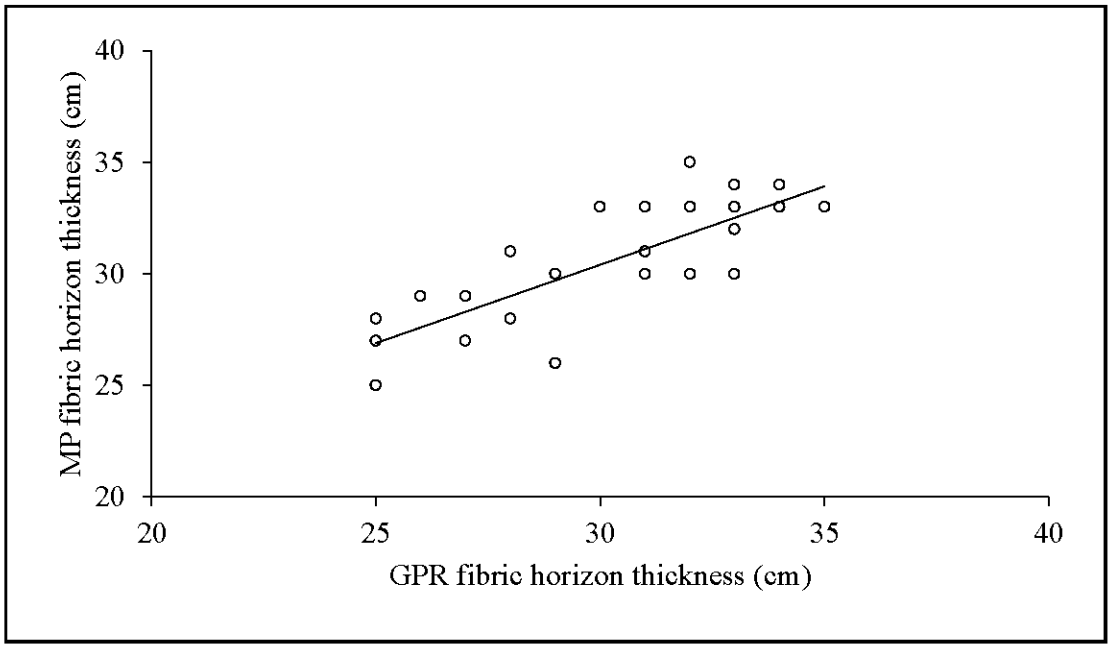

Figure 1.10. Relation between fibric horizon thickness as determined by manual probing and GPR in the highly paludified site B (r = 0.79, P < 0.001, R^2 = 0.63, and n = 27).

1.4.1.4. Potential use of GPR data at the landscape and regional scale within the Clay Belt

Because of its ability to cover large regions over short time periods with high vertical and horizontal resolution, GPR can be considered as a good method for mapping continuous spatial variability of the mineral soil contour at the landscape scale. However, for this method to be applicable at the landscape scale, some modifications must be taken in consideration. Among these modifications, the presence of snow cover is required to ease such acquisition, as GPR surveys have proven to be extremely difficult to perform at the landscape scale when extensive forest debris covers the ground surface. The use of GPR in frozen landscapes to map soil depths has provided better results than conventional techniques such as manual probing (Gerber *et al.*, 2010), and the maximum depth observed with GPR can be extended to greater depths than those in unfrozen environments. Future work will focus on the application of GPR during late winter with appropriate frequencies to quantify the effects of topographic variables (both at the surface and MS) on organic layer accumulation at the landscape scale within the black spruce forests of the Clay Belt.

Also, the possibility of operating a GPR system from an airborne platform (Marchand *et al.*, 2003; Catapano *et al.*, 2012) or being towed behind a snowmobile could cover larger areas, which would be much faster and cheaper and would allow the acquisition of continuous spatial measurements, compared to traditional manual measurements. In a comparison with manual measurements, Doolittle and Collins (1995) found that the use of GPR reduced field time and costs, thereby increasing their respective efficiencies by 70% and 200%, respectively. However, appropriate ground truthing will still be required to guide interpretations of the GPR profiles. Moreover, without the direct information provided by pit-augering sampling, GPR interpretations for this study could be uncertain.

At the regional scale, C- and L-band space borne Synthetic Aperture Radar (SAR) imagery is being employed by researchers from the Canadian Forest Service-Laurentian Forestry Centre to determine OLT and soil moisture parameters in the Clay Belt, but it has not been used much in combination with GPR measurements. We believe that the combination of SAR imagery with local GPR measurements will prove invaluable in this on-going regional paludification mapping campaign (Beaudoin *et al.*, 2012; unpublished) by providing stronger validation of equivalent OLT data as maps are derived from SAR imagery.

1.5. CONCLUSIONS

To our knowledge, this study was the first to use GPR to remotely sense the OL-MS within the paludified forest soils of the Clay Belt. The research conducted in this study has shown that the application of GPR to determine the OL-MS at the site with shallow organic accumulations was successful (site A), but signal attenuation at the deeper site (site B) prevented the identification of the mineral soil interface. It is well known that GPR interpretation requires ground truthing measurements and, thus, GPR interpretations at both sites would remain uncertain without appropriate soil pit-augering information.

Mapping the OL-MS interface in the low to moderately paludified site A using GPR produced promising results, thereby paving the way for future use at the landscape scale. Our results suggest a strong linear relationship between OLT that was estimated with GPR and that determined by manual probing (r = 0.93) at site A. Thus, GPR is effective in detecting OLT and its horizontal continuity under conditions that would seem more attractive or amenable to forest management strategies.

At site B, the high clay contents of the Oh and MS strata limited radar EM wave penetration, rendering the mineral soil undetectable. Therefore, GPR did not appear useful for gathering OLT information within highly paludified black spruce forest soils of the Quebec Clay Belt. Nevertheless, we found that, when coupled with ground truth information, GPR data were effective in mapping the thickness of the upper unit of the Of horizon (r = 0.79, $P <$ 0.001), which could be considered as an indicator of the OLT in highly paludified areas. Further, the use of high-frequency antennas (i.e., 500s, 800s, 1000s MHz) that provide higher vertical resolution could increase the delineation of such interfaces.

CHAPITRE II

LANDSCAPE-SCALE INFLUENCE OF TOPOGRAPHY ON ORGANIC LAYER ACCUMULATION IN PALUDIFIED BOREAL FORESTS

Ahmed Laamrani[1], Osvaldo Valeria[1], Nicole Fenton[1], and Yves Bergeron[1]

[1] Chaire industrielle CRSNG-UQAT-UQAM en aménagement forestier durable, Institut de recherche sur les forêts et Centre d'étude sur la forêt.
Université du Québec en Abitibi-Témiscamingue. 445 boul. de l'Université, Rouyn-Noranda, Québec J9X 5E4, Canada.

Article publié en 2014 dans Forest Science (en ligne : 19 Septembre 2013).
Volume 60, No. x, pages 1–12. Doi:10.5849/forsci.13–025;

ABSTRACT

The aim of this study was to quantitatively investigate the relationship between topographic variables and organic layer thickness (OLT) and to use these relationships for mapping OLT distributions at the landscape scale within the paludified boreal forests of eastern Canada. Topography was quantified by a set of predictor variables (slope, elevation, aspect, mean curvature, plan curvature, and profile curvature) that were extracted from a LiDAR-derived digital terrain model (DTM) with four resolutions (1, 5, 10, and 20 m). OLT was collected from field measurement (n = 1600) across the landscape and varied from 5 to 150 cm. Weak correlations between OLT and individual topographic variables were obtained at the landscape scale. Stratification by aspect did not significantly improve these correlations. Consequently, regression tree analysis divided the data into six different landscape units, based on slope, aspect, and mean curvature. The resulting landscape units delimited the major patterns of OLT and elucidated three spatial relationships between OLT and topographic variables: greater OLTs (mean = 62 cm) were confined to gentle slopes ($\leq$ 1.8%), whereas lower OLTs (mean = 27 cm) were found in steeper slopes (> 3.2%); OLTs were deeper on south- and west-facing than on north- and east-facing slopes; and the most accurate results were obtained by the LiDAR-derived DTM at 10 and 20 m resolutions. A thematic productive map of the distribution of the resulting six landscape units showed good matching (71%) with both vulnerable and promising areas for forest management. This study confirmed the fact that topographic variables influence OLT at the landscape scale, which had been previously reported at the plot scale within the Clay Belt.

Keywords: paludification, topography, Clay belt, regression tree, LiDAR -derived digital terrain model

RÉSUMÉ

Le but de cette étude était d'examiner quantitativement la relation entre les variables topographiques et l'épaisseur de la couche organique (ECO) et d'utiliser ces relations pour caractériser la distribution spatiale d'ECO à l'échelle du paysage dans les forêts boréales paludifiées de de la ceinture d'argile. La topographie a été quantifiée par un ensemble de variables prédictives (pente, altitude, exposition, courbure totale, courbure transversale, et courbure longitudinale) qui ont été extraites d'un modèle numérique de terrain-LiDAR (DTM) avec quatre résolutions (1, 5, 10 et 20 m). Mille six cents mesures d'ECO ont été obtenues à l'aide de sondages manuels effectués sur le terrain et varient de 5 à 150 cm. De faibles corrélations ont été obtenues à l'échelle du paysage entre les variables topographiques individuelles et l'ECO. Une stratification par exposition n'a pas permis d'améliorer de manière significative ces corrélations. Par conséquent, l'analyse de l'arbre de régression a permis de subdiviser les données en six différentes unités, en fonction de la pente, l'exposition, et la courbure totale. Les six unités résultantes ont permis de délimiter les principaux patrons de l'ECO et d'élucider trois relations spatiales entre l'ECO et les variables topographiques : les zones avec une couche organique épaisse (62 cm) avaient des pentes douces ($\leq$ 1,8%) , tandis que les zones avec pentes plus raides (pente $>$ 3,2%) ont été associées à des couches organiques plus faibles (27 cm); les zones avec une exposition vers le sud et l'ouest étaient associées à une couche organique plus profonde par rapport à celles exposées vers le nord et l'est et les meilleurs résultats ont été obtenus avec des résolutions de 10 et 20 m. Une carte thématique productive de la distribution spatiale des six unités résultante a été réalisée. La précision globale entre les six unités et les zones à la fois vulnérables et les plus prometteurs pour la gestion des forêts a été de 71%. Cette étude a démontré que la topographie de surface influence l'accumulation de la couche organique à l'échelle du paysage dans la ceinture d'Argile, ce qui avait déjà été démontré auparavant à l'échelle de la parcelle.

2.1. INTRODUCTION

Boreal northern black spruce forests are characterized by the development of thick organic layers in regions prone to paludification such as the interior of Alaska, the Canadian Hudson Bay-James Bay lowlands, and the western Siberian plain. Paludification is a natural process in which organic material accumulates on the forest floor over time and is generally thought to be caused by increasing soil moisture (Crawford *et al.*, 2003; Vygodskaya *et al.*, 2007). This process creates wetter conditions that lead over time to a reduction in soil temperature, decomposition rates, microbial activity, and nutrient availability (Lavoie *et al.*, 2005). This promotes the growth of sphagnum mosses (Fenton *et al.*, 2005; Fenton and Bergeron 2007) and the conversion of potentially forested areas to large bog landscapes, largely resistant to forest establishment and growth (Crawford *et al.*, 2003), consequently, leading to a marked decrease in forest productivity (Simard *et al.*, 2007, 2009). In addition to these factors, time since last fire and topography play important roles in the occurrence of paludification in these regions.

Although the effect of topography on organic layer thickness (OLT) has been well studied at the plot scale, there is no research, to our knowledge, documenting the effect of topography at the landscape scale. In the Clay Belt, a region of the Hudson Bay-James Bay lowlands of boreal eastern Canada, OLT usually displays high spatial variability both at the landscape and plot scale. This variability in OLT within Clay Belt black spruce forests is largely influenced by time since last fire and topography. Moreover, an understanding of the causes of this variability is important for accurately predicting the locations of highly paludified areas as well as their impacts on forest management. Consequently, there is an increasing practical demand for maps that contain information concerning variation in OLT and topography in paludified areas. The end users of this information are involved mainly in forest management (i.e., forest planning and productivity assessment).

Within paludified forests, there have been few studies that describe or analyze topographic factors that influence the spatial distribution and accumulation of organic layers at larger scales (i.e., Emili *et al.*, 2006; Seibert *et al.*, 2007). Other studies have been conducted at larger scales to characterize the influence of topography on soil properties; however, these studies have been largely restricted to well-drained hardwood in the south of

the boreal forest (i.e., Johnson *et al.*, 2009; Martin and Timmer 2006). Previous studies that have tried to relate OLT to topography in the Clay Belt region have been limited to either the plot scale or to only slope estimates as the controlling variable (Giroux *et al.*, 2001; Fenton *et al.*, 2005; Lavoie *et al.*, 2005; Lecomte *et al.*, 2005; Simard *et al.*, 2007, 2009). As yet, no research has tested whether the plot-scale relationship between slope and OLT can be observed at larger scales (i.e., landscape scale) or whether other topographic variables could influence OLT individually or in combination with slope. Until recently, the availability of accurate topographic information regarding the organic layer at larger scales (landscape or regional) was a limiting factor for both land management and modeling of spatial OLT variability.

Recent advances in remote sensing now permit the generation of appropriate data for determining these relationships. Consequently, there is much interest in relating different OLT information to high-resolution topographic data. These data, in turn, can be used to generate topographic variables such as slope, aspect, elevation, or curvature. In this context, high-resolution airborne laser scanning (also known as LiDAR [light detection and ranging]) is becoming one of the most effective and reliable remote-sensing technologies for assessing topography at both the plot and landscape scales in boreal forested environments (i.e., Hodgson *et al.*, 2003, 2005; Hyde *et al.*, 2005; Southee *et al.*, 2012; Webster *et al.*, 2011; Work *et al.*, 2011).

The objective of this study was to quantitatively investigate the relationship between topographic variables and OLT and to use these relationships for mapping OLT distributions at the landscape scale within the black spruce forests of the Clay Belt. To do so, we correlated field OLT measurements (response variable) obtained by manual probing with topographic variables (predictor variables) derived from LiDAR digital terrain models (DTMs).

2.2. MATERIALS AND METHODS

2.2.1. Study area

The study sites were located within an area of approximately 72 ha of boreal forest in the southwestern James Bay Lowlands physiographic region of Quebec and, more precisely, in the Clay Belt region that spans 125,000 km^2 across the Ontario-Quebec border (Figure 2.1A). This study is part of a larger project that deals with the effects of environmental variables and forest harvesting on paludification. The dominant landforms in the area are gently sloping plains, which were generated by extensive and thick glaciolacustrine clay deposits left behind by the proglacial Lake Ojibway (Veillette, 1994). Bedrock outcrops and gentle hills are also found in the area. Elevation ranges between 289 and 315 m, with an average of 304 m above sea level. Within the study area, ground surface slope ranged from 0.1 to 14.9%; about 45% of the area had a slope $\leq$ 2%. Many drainage courses run locally in a southwestern direction through the study area to produce a relatively complex topographic pattern in this hilly landscape relief (Figure 2.1B).

Black spruce (*Picea mariana* (Mill.) BSP) and jack pine (*Pinus banksiana* Lamb.) dominate stands in the study area, constituting 79 and 16% of the canopy, respectively. These species are followed by trembling aspen (*Populus tremuloides* Michx), which occupies about 4% of the study area. The remaining 1% of the area is covered by tamarack or eastern larch (*Larix laricina* [Du Roi] K. Koch), balsam fir (*Abies balsamea* [L.] Miller), and paper birch (*Betula papyrifera* Marshall). The forest floor is composed of *Sphagnum* spp., feather mosses (principally *Pleurozium schreberi* [Brid.] Mitten), and shrubs, (mainly dwarf ericaceous species), with variable coverage across the landscape. The mean annual temperature is -0.7 °C, and the mean annual precipitation is 906 mm (Environment Canada 2011; Matagami weather station, approximately 60 km northeast of the study area).

2.2.2. Sampling design and field data collection

The study goals were addressed by establishing transects over representative forest stands at the landscape scale. We used provincial Forest Inventory Maps from the Quebec Ministry of Natural Resources (MRNQ) within a geographic information system (GIS) and

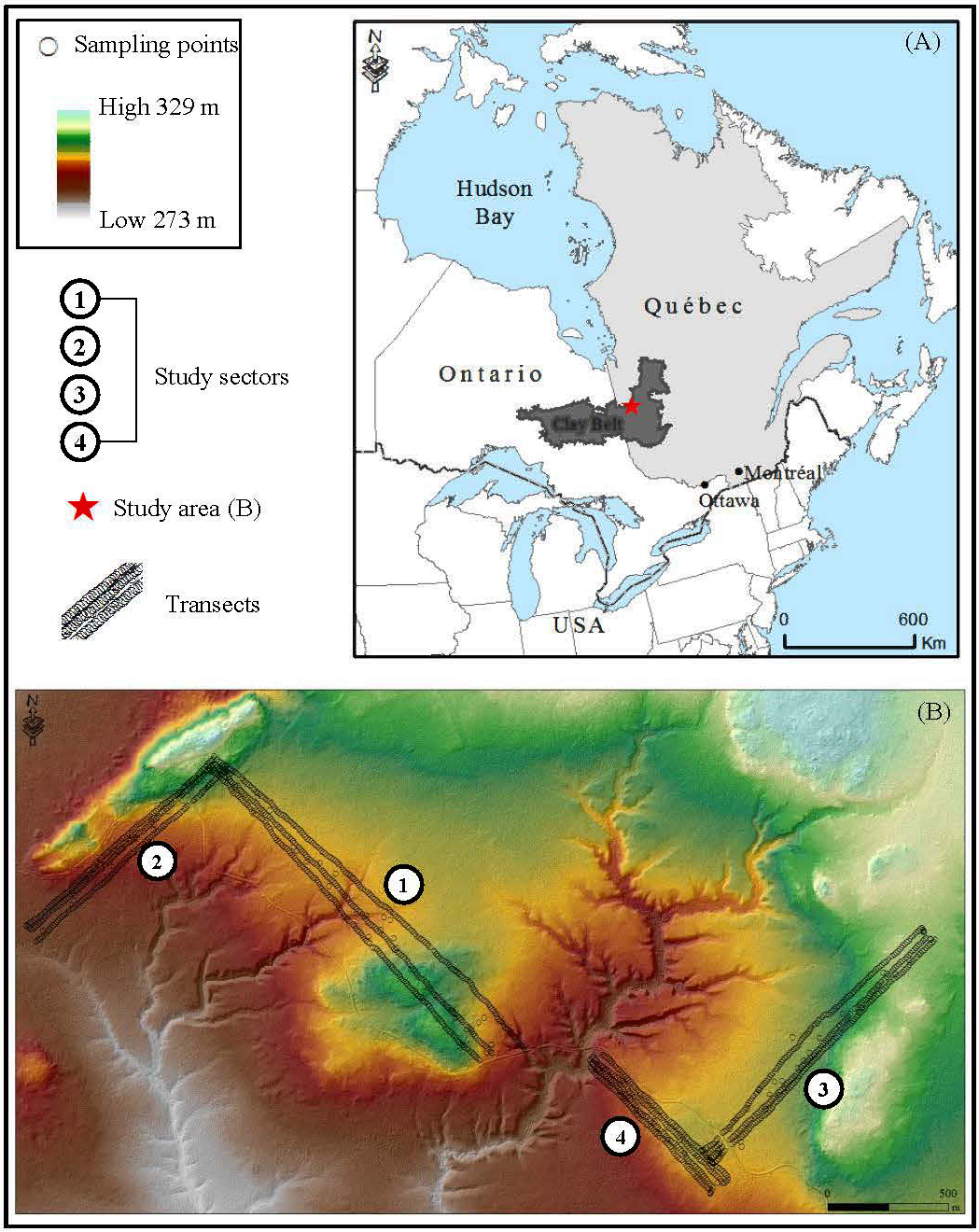

Figure 2.1. Study area located in the Clay Belt region (A) with a DTM derived from LiDAR data (B) and sampling point locations along 13 transects that were established across four sectors (1, 2, 3, and 4).

information collected during field visits to select stands representing a broad range of OLT, slope inclinations, and stand productivities. Such attributes were obtained from the interpretation of data available from the Forest Inventory Maps of the MRNQ (i.e., cover density classes, age classes, species, height classes, and slope classes). For the purposes of providing a spatially continuous cross-sectional profile of OLT at the landscape scale, field data were acquired along and between continuous transects. Thirteen transects, totalling 15 km in length, were established across four different sectors, running from northeast to southwest (sectors 2 and 3) and northwest to southeast (sectors 1 and 4) (Figure 2.1B). Within each sector, a minimum of 20 m was maintained between transects, and OLT was measured manually using a standard auger at intervals of 10 m along each transect. At each sampling point, the auger bored through the organic layer until the mineral soil was encountered. The auger was then removed, and the marked depth to mineral soil was accurately measured (OLT ranging from 5 to 125 cm) (Figure 2.2). The thickness of the organic material was taken as the distance between the organic layer surface and the mineral soil interface. In nearly all cases, the transition between the organic layer and mineral soil was clearly marked by an obvious change in color and texture (Figure 2.2). When the full length of the auger (= 125 cm) was inserted into the organic layer without contacting the mineral soil, the corresponding point was marked as deeper than 125 cm. These sites were excluded because it was technically impossible to measure depths greater than 125 cm while measuring so many points. There are only 17 sites (about 1% of the entire data) that were excluded from the analysis, which should not affect the result. An additional 85 circular plots of 400 m^2 were randomly distributed between transects over the study area and sampled for forest canopy measurements, soil samples (not included in this article), and organic layer information. A 30 × 30-cm pit was dug in each of the 85 plots and depth to mineral soil (total OLT, ranging from 7 to 150 cm) was recorded, together with an accurate measurement of the thickness of each individual soil organic horizon (cm). For the entire data set (n = 1600; sampling points along transects and plots), the nature of the underlying mineral deposits was recorded in the field as clay, till, or bedrock; however, their effects, together with those of time-since-last fire, on OLT were not examined in this study, because they will be dealt with in a future study.

Figure 2.2. Photographs from the study area. At each sampling point, the anger was bored through the organic layer until the mineral soil was encountered (A and B) and then the depth to mineral soil (represents the OLT) was clearly identified (pointer finger on C) and measured (distance between flag mark and pointer finger on D).

2.2.3. LiDAR processing and topographic variable measurements

LiDAR data were collected over the study area in late May 2010 using a Multipulse Leica ALS50 phase II airborne laser scanner. LiDAR acquisition was conducted with an average sampling of 2.8 points/m^2 and an absolute vertical accuracy of 0.065 m (root mean square error). All collected LiDAR data were preprocessed by separating canopy pulse returns from ground pulse returns. Inverse distance weighting was used as the grid interpolating model and for predicting z values within the study area. The latter data were used to produce a DTM with a basic cell resolution (cell size) of 0.5 m using ArcGIS 10.0 (Environmental Systems Research Institute [ESRI] 2011). Spatial Analyst tools (ArcGIS) were used to generate different DTMs of the selected topographic variables at four cell resolutions (1, 5, 10, and 20 m). A detailed description of each selected topographic variable (elevation, slope, aspect, mean curvature, plan curvature, and profile curvature) is provided in Table 2.1. The DTM cell corresponding to each field sampling point was determined and the values of its topographic variables were calculated at the four cell resolutions. These data were used for two purposes: to determine how the extracted values of topographic variables are sensitive to DTM resolutions and to evaluate the correlations between the OLT and individual topographic variables.

2.2.4. Statistical analysis

Preliminary statistical analysis was done using backward stepwise linear regression to investigate which topographic variables significantly influence OLT at the landscape scale. All topographic variables that were used in the stepwise regression analysis were tested for multicollinearity and their coefficients of variation (CVs), which were calculated as their SDs divided by the respective means, were used to evaluate the distribution of the data and the interactions between different topographic variables and OLT. Two nonparametric methods, Spearman's rank correlation and regression tree analysis, were also used. Because many of the topographic variables were highly intercorrelated (Pearson's $r \geq 0.7$) and had highly skewed distributions, we used Spearman's rank correlation (rs) instead the usual parametric product-moment correlation coefficient (r). Spearman's coefficient has been used in similar studies with larger data sets that are characterized by a high degree of heterogeneity (e.g.,Seibert *et al.*, 2007; n = 1300–4000 points). The high CVs (> 0.56) for OLT also

suggested that the data had a strongly skewed distribution. For these reasons, no attempt was made to explore the relationships between OLT and topographic variables using multiple regression or linear mixed-effects models.

A common way of spatially segmenting the landscape is to divide it into internally homogeneous and mutually contrasting units (Mulder *et al.*, 2011). Landscape segmentation involves grouping similar topographic variables into distinct spatial units, which can then be used as treatments for spatial analysis (Pennock and Corre, 2001). Therefore, we used regression tree analysis as an automated landscape segmentation method to identify spatial units that could empirically model the complex interactions among topographic variables in controlling OLT distribution. The regression tree approach was well suited to the analysis of our data sets for several reasons: (i) its potential to successfully predict soil organic matter distribution and to analyze ecological data has been demonstrated (i.e., De'Ath and Fabricius, 2000; Häring *et al.*, 2012; Johnson *et al.*, 2009); (ii) it is capable of handling both categorical and quantitative data (Johnson *et al.*, 2009); (iii) it allows complex interactions among predictor variables with no assumptions of linearity (Rothwell *et al.*, 2008); (iv) the regression tree method repeatedly splits the response data (in our case, OLT) into more homogeneous groups, based on the predictor variables and predictor values (or identifiers, if categorical, i.e., aspect variable), which results in a tree diagram that is easy to read and interpret (Johnson *et al.*, 2009); and (v) recursive partitioning of the data set into more homogeneous groups allows the identification of potential relationships between the response variable and the environmental predictors, while also identifying interactions among these latter independent variables (Rothwell *et al.*, 2008). In each resulting spatial unit, rules defining how the data were to be partitioned were selected based on a significance test of independence between covariates and the response variable, and a split was established when the P value was smaller than $\alpha = 0.05$ (Hothorn *et al.*, 2006). In this study, the resulting spatial units were named "landscape units" that refer to relatively homogeneous areas in term of OLT distribution. All statistical analyses were performed in R (R Development Core Team 2011). Regression trees were implemented using the *ctree* function in the *party* package (Hothorn *et al.*, 2006).

Table 2.1. Topographic variables measured from LiDAR-derived DTMs of the study area.

Topographic variables	Description
Slope	Gradient or rate of maximum change in z value from each cell of a raster surface (%).
Elevation	Refers to how high above sea level a particular location in the study area is; also known as z value (m).
Aspect	Direction of the maximum rate of change in the z value from each cell to its neighbors. The value of each cell in an aspect data set (0° up to 360°) indicates the direction the cell's slope faces (N, NE, E, SE, S, SW, or NW). Each of these directions represents an interval of 22.5°.
Mean curvature†	Represents the roughness of the terrain and corresponds to the second derivative of the surface or the slope of the slope. A positive curvature indicates that the surface is upwardly convex at that cell, whereas a negative curvature indicates the surface is upwardly concave at that cell. Profile and plan are two output curvature types.
Plan curvature	Perpendicular to the direction of the maximum slope. Sidewardly convex surfaces have a positive value, sidewardly concave surfaces have a negative plan, and linear areas have a value of zero. Profile curvature relates to the convergence and divergence of flow across a surface.
Profile curvature	Parallel to the direction of the maximum slope. Upwardly convex surfaces have a negative value, upwardly convex surfaces have a positive plan, and flat areas have a value of zero. Profile curvature affects the acceleration or deceleration of flow across the surface.

†The reasonably expected values of curvature rasters (curvature, plan, and profile) for a hilly area (moderate relief) can vary from -0.5 to 0.5, whereas for steep, rugged mountains (extreme relief), the values can vary between -4 and 4 (ESRI 2011).

2.3. RESULTS

2.3.1. Effect of different LiDAR-derived DTM resolutions on the values of topographic variables

Figure 2.3 shows that both elevation and aspect are invariant with changes in resolution, whereas variation strongly decreased as spatial resolution decreased for the mean curvature, plan curvature, and profile curvature. Median and range estimates of elevation did not indicate significant bias (Figure 2.3A), whereas those of slope decreased markedly with decreasing resolution (Figure 2.3B). Aspect did not show any obvious trends across the different resolutions (Figure 2.3C). The range of values of all curvature variables (curvature, plan, and profile) decreased clearly with decreasing resolution, whereas the medians did not vary with changes in resolution (Figure 2.3D-F).

2.3.2. Correlations between OLT and topographic variables based on different DTM resolutions

Extracted values of topographic variables at each sampling point were used to graphically illustrate and evaluate the effect of resolution on OLT (Figure 2.4; Table 2.2). Even though Spearman's rank correlations were considered weak ($r_s \leq 0.56$) (Table 2.2), most were statistically significant and provided some insight into which factors influenced the spatial distribution and accumulation of the organic layer at the landscape scale. Of the topographic variables examined, slope had the strongest correlation with OLT across the 5- to 20-m DTM resolutions. Across all DTMs resolutions, slope was consistently and negatively related to OLT ($P < 0.001$). Figure 2.4A illustrates the tendency of OLT to generally decrease with increasing slope over the landscape.

Elevation and OLT were significantly positively correlated ($r_s = 0.12$, $P < 0.001$) at all resolutions. However, the correlation is weak ($r_s = 0.12$) as illustrated by the marked scatter of the data (Figure 2.4B), and no clear trend could be seen when the whole data set was used ($n = 1600$).

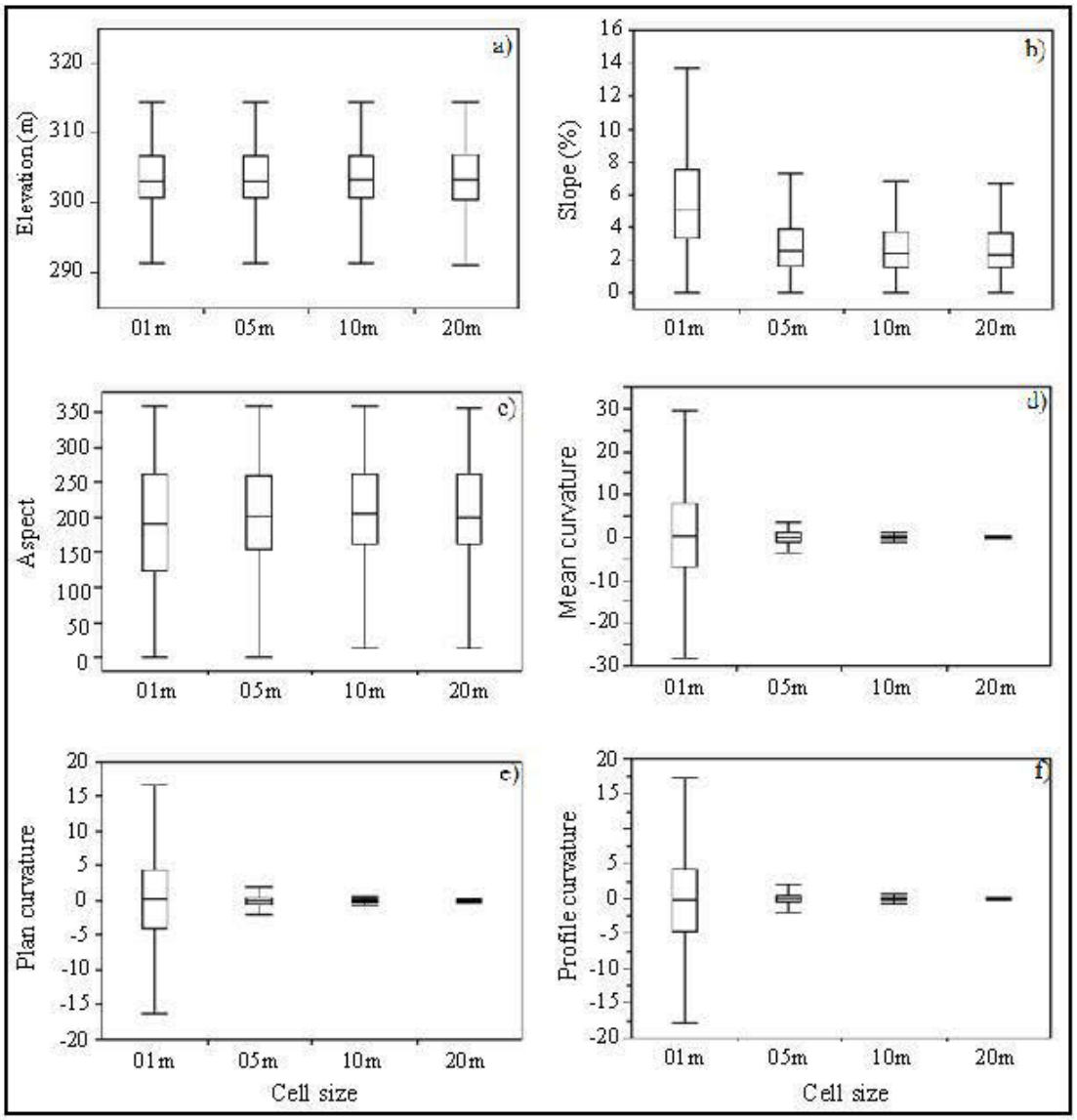

Figure 2.3. Box plots of topographic variables for four DTM resolutions. (A) Elevation (m). (B) Slope (%). (C) Aspect. (D) Mean curvature. (E) Plan curvature. (F) Profile curvature. The lower and upper edges of the box represent the 25th and 75th percentiles, and the median is represented by the band in the middle of the box. Whiskers represent the lower and upper extremes (lowest and highest values, respectively).

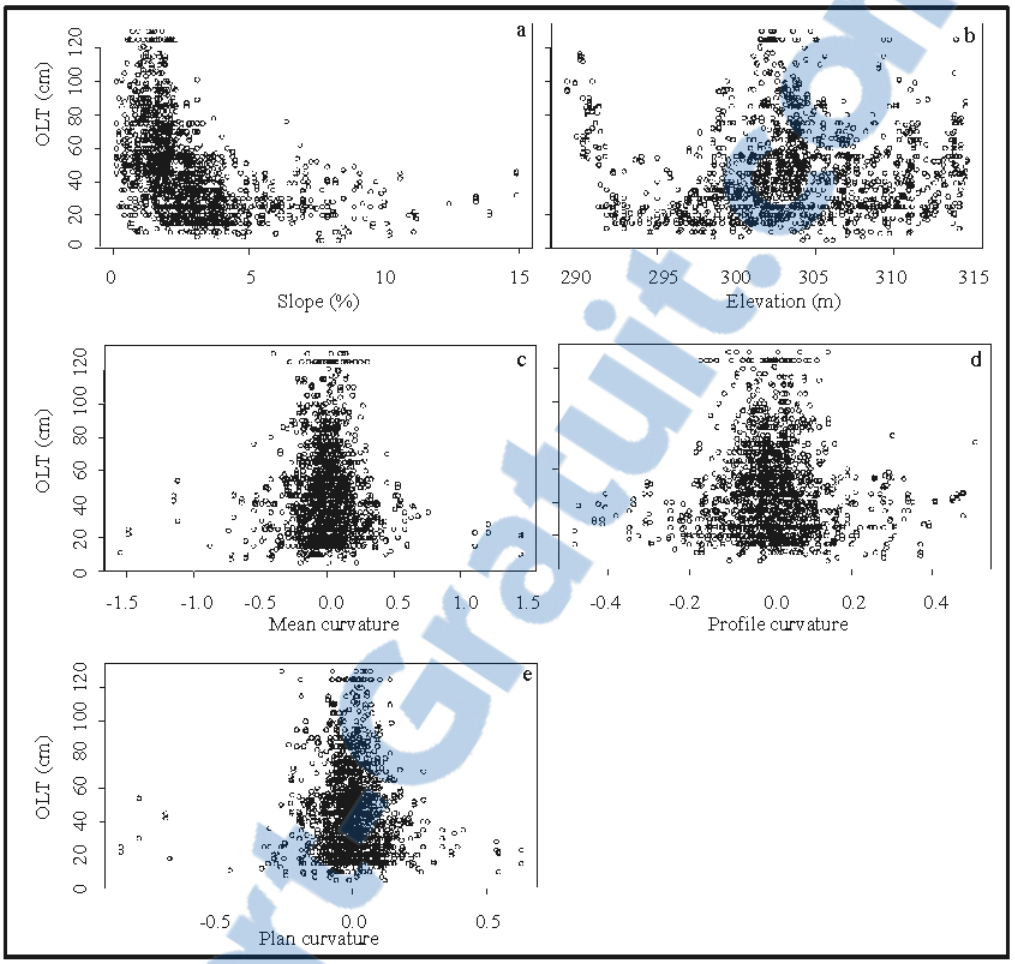

Figure 2.4. Relationships Between OLT and topographic variables at 20-m DTM resolution (n = 1600). (A) Slope. (B) Elevation. (C) Mean curvature. (D) Profile curvature. (E) Plan curvature.

Table 2.2. Spearman rank correlations between OLT and topographic variables at different DTM resolutions.

Topographic Variables	r_s at DTM resolutions of			
	01 m	05 m	10 m	20 m
Slope	-0.13*	-0.46*	-0.53*	-0.56*
Elevation	0.12*	0.12*	0.12*	0.12 *
Mean curvature $_{[Convex]}$	-0.01	0.01	-0.15*	-0.25*
Mean curvature $_{[Concave]}$	-0.00	-0.08†	0.06	0.14*
Plan curvature $_{[Convex]}$	-0.01	-0.02	-0.12*	-0.22*
Plan curvature $_{[Concave]}$	-0.06	-0.09‡	0	0.08†
Profile curvature $_{[Convex]}$	-0.00	0.01	0.15*	0.27*
Profile curvature $_{[Concave]}$	-0.02	0.08†	-0.07	-0.16*

n = 1600; * $P < 0.001$; † $P < 0.01$; ‡ $P < 0.05$.

The reasonably expected values of plan and profile curvatures variables (extracted from LiDAR-derived DTM) for our study area (moderate relief) should vary from -0.5 to 0.5 (ESRI 2011). However, 72 to 97% of plan and profile curvatures values at 1- and 5-m resolutions were outside this expected range and consequently were excluded from the analysis. At the 10- and 20-m resolutions, the correlation between OLT and all curvature variables indicated that OLT tended to decrease with convexity. This result is in accord with landscape observations for which thinner organic layers are habitually associated with areas having convex slopes. At the 10- and 20-m resolutions, coefficients of correlations were significantly higher for convex curvatures (mean, plan, and profile) than those for the concave curvatures. All correlations between concave curvatures (mean, plan, and profile) and OLT were very small and not significant at the 1- and 10-m resolutions (Table 2.2).

Because aspect was not measured on a linear scale (circularly disturbed), it was excluded from the correlation analysis (Table 2.2). To determine whether correlations between OLT and other topographic variables improved with aspect stratification, correlations between OLT and topographic variables were calculated for main aspect classes, which are summarized in Tables 3 and 4 (20-m resolution data only). From Table 3, we can deduce that 81% of sampling points had an aspect ranging from southeast (southeast [SE], south [S], or southwest [SW]) to west (W), whereas only 19% had a northern (northwest [NW], north [N], or northeast [NE]) or eastern (E) exposure. Average OLT in areas with southern and western aspects (SE S SW W) was higher than that in areas with northern or eastern aspects (NW□N□NE□E). In addition, CVs for OLT were relatively high (≥ 0.35), suggesting that aspect stratification did not notably reduce the variability within most of the aspect classes and the existence of interactions between different landscape topographic variables and OLT.

Table 2.3. OLT data for major aspect classes for the study area.

Variable	*n*	OLT		
		Mean (cm)	SD (cm)	CV
North	57	45	19	0.42
Northeast	32	43	15	0.35
East	82	35	16	0.46
Southeast	224	39	25	0.64
South	459	43	28	0.65
Southwest	231	53	28	0.53
West	386	48	22	0.46
Northwest	129	44	19	0.43
All data	1600	45	25	0.56

n represents number of sampling points.

Results of Spearman's rank correlations between OLT and individual topographic variables for each major aspect class, as well as their improvement or diminution with regard to all the data, are shown in Table 2. 4. Δr_s values were calculated as the absolute r_s for the aspect class minus the absolute r_s of all the data (n = 1600) listed in Table 2.3. After aspect stratification, most coefficients were still very small or not significant, even though some strong relationships existed between the S, SE, W, and N classes and OLT, especially for 10- and 20-m resolutions.

The correlation between slope and OLT for the S aspect class was significantly improved with respect to the collective data set (r_s = -0.70, $P < 0.001$, and $\Delta r_s = 0.14$). This relation, in which OLT increased as slope decreased in the S aspect, is illustrated in Figure 2.5A. To test the significance of Δr_s, we performed an omnibus test of homogeneity among the eight aspect classes (k=8) in terms of their Spearman's rank correlations, which takes the form of a X^2-distributed test. For example, at the 20-m resolution, estimates of slope correlations with OLT indicated very strong differences among the eight aspect classes in Table 4 (overall $X^2 = 92.85$, df = 7, $P < 0.001$).

The correlation with elevation in the W aspect class was potentially improved with regard to the collective data set (r_s = 0.49, $P < 0.001$, and Δr_s = 0.37) at the 20-m resolution, suggesting that organic layer accumulation was more pronounced at higher, rather than at lower elevations (Figure 2.5B). An important increase in the correlation coefficient was also found in the west aspect class at the 1-, 5-, and 10-m resolutions with Δr_s values of 0.09, 0.24, and 0.33, respectively.

For all curvature variables (mean, plan, and profile), the correlation coefficient was generally higher than that for the collective data set, primarily at the 20-m resolution (Table 4). A significant increase in the correlation coefficient of convex-mean curvature (r_s = -0.38, $P < 0.01$, and Δr_s = 0.13) and convex-plan curvature (r_s = -0.52, $P < 0.01$, and Δr_s = 0.30) was found in the SE aspect class (Table 2.4) compared with that in the collective data set. These negative correlations suggest that shallow organic layers were, in large part, confined to convex areas (Figure 2.5C). Correlations for some plan curvature and profile curvature variables were substantially improved in the N aspect class (Table 2.4), but these were not included in the interpretation because of the lower sample size. For example, the correlation of the OLT and the north-facing concave profile curvature had r_s = -0.50, $P < 0.01$, Δr_s = 0.34, and n = 28 (second column and last row of N aspect class in Table 2.4).

Table 2.4. Spearman's rank correlation between OLT and topographic variables for each major aspect class.

	N		NE		E		NW		SE		S		SW		W	
Cell size and variable	r_s	Δr_s	r_s	Δr_s	r_s	Δr_s	r_s	Δr_s	r_s	Δr_s	r_s	Δr_s	r_s	Δr_s	r_s	Δr_s
1 m																
Slope	−0.14	0.01	−0.07	−0.06	−0.13	0.00	0.01	−0.12	−0.16†	0.03	−0.27[a,*]	0.14	−0.10	−0.03	−0.08	−0.05
Elevation	0.05	−0.07	0.16	0.04	−0.02	−0.10	0.25[a,*]	0.13	0.00	−0.12	0.04	−0.08	0.22*	0.10	0.21*	0.09
Curvature [Convex]	−0.21	0.20	−0.17	0.16	−0.12	0.11	0.15	0.14	−0.04	0.03	0.06	0.05	0.12	0.11	−0.04	0.03
Curvature [Concave]	0.10	0.10	−0.07	0.07	0.03	0.03	0.10	0.10	0.04	0.04	−0.06	0.06	0.02	0.02	−0.02	0.02
Plan [Convex]	−0.12	0.11	−0.16	0.15	−0.12	0.11	0.06	0.05	0.02	0.01	0.00	−0.01	0.22[a,†]	0.21	−0.04	0.03
Plan [Concave]	−0.09	0.03	−0.04	−0.02	−0.01	−0.05	0.09	0.03	−0.03	−0.03	−0.14	0.08	−0.04	−0.02	−0.05	−0.01
Profile [Convex]	0.22[b,†]	0.22[b]	0.03	0.03	0.23[b,†]	0.23	−0.03	0.03	−0.02	0.02	−0.08	0.08	−0.03	0.03	−0.12	0.12
Profile [Concave]	0.08	0.06	0.00	−0.02	0.11	0.09	0.00	−0.02	−0.05	0.03	−0.10	0.08	−0.10	0.08	0.04	0.02
5 m																
Slope	−0.27*	−0.19	−0.40*	−0.06	−0.24†	−0.22	−0.44*	−0.02	−0.51*	0.05	−0.53[a,*]	0.07	−0.41*	−0.05	−0.40*	−0.06
Elevation	0.20	0.08	−0.10	−0.02	−0.03	−0.09	0.18†	0.06	0.05	−0.07	0.02	−0.10	0.20*	0.08	0.36[a,*]	0.24
Curvature [Convex]	−0.23	0.22	−0.08	0.07	0.16	0.15	0.03	0.02	−0.10	0.09	0.02	0.01	0.02	0.01	0.13	0.12
Curvature [Concave]	−0.15	0.07	−0.28	0.20	−0.07	−0.01	0.05	−0.03	−0.03	−0.05	−0.04	−0.04	−0.29[a,*]	0.21	0.08	0.00
Plan [Convex]	−0.26[b,*]	0.24[b]	−0.16	0.14	−0.02	0.00	−0.08	0.06	−0.02	0.00	−0.03	0.01	0.03	0.01	−0.01	−0.01
Plan [Concave]	−0.17	0.08	−0.08	−0.01	−0.10	0.01	−0.06	−0.03	−0.05	−0.04	−0.12	0.03	−0.22[a,*]	0.13	−0.01	−0.08
Profile [Convex]	0.21	0.20	−0.28	0.27	−0.15	0.14	0.06	0.05	0.02	0.01	0.09	0.08	−0.07	0.06	−0.04	0.03
Profile [Concave]	0.00	−0.08	0.10	0.02	0.29	0.21	−0.04	−0.04	0.01	−0.07	−0.01	−0.07	0.20[a,*]	0.12	0.09	0.01
10 m																
Slope	−0.38*	−0.15	−0.45*	−0.08	−0.45*	−0.08	−0.45*	−0.08	−0.48*	−0.05	−0.65[a,*]	0.12	−0.35*	−0.18	−0.54*	0.01
Elevation	0.04	−0.08	0.08	−0.04	0.15	0.03	0.20†	0.08	0.16†	0.04	−0.06	−0.06	0.08	−0.04	0.45[a,*]	0.33
Curvature [Convex]	−0.33	0.18	0.24	0.09	−0.08	−0.07	−0.16	0.01	−0.12	−0.03	−0.23[a,*]	0.08	−0.08	−0.07	−0.15†	0.00
Curvature [Concave]	−0.15	0.09	0.24	0.18	0.29	0.23	0.14	0.08	−0.02	−0.04	0.01	−0.05	0.01	−0.05	0.15[a,†]	0.09
Plan [Convex]	−0.59[b,*]	0.47[b]	−0.02	−0.10	−0.18	0.06	−0.17	0.05	0.02	−0.10	−0.09	−0.03	−0.13	0.01	−0.08	−0.04
Plan [Concave]	−0.24	0.24	−0.36	0.36	0.17	0.17	−0.06	0.06	0.10	0.10	−0.09	0.09	0.04	0.04	0.13	0.13
Profile [Convex]	0.24	0.09	0.17	0.02	−0.06	−0.09	0.30[a,*]	0.15	0.10	−0.05	0.22*	0.07	−0.02	−0.13	0.21*	0.06
Profile [Concave]	0.22	0.15	−0.09	0.02	−0.07	0.00	−0.09	0.02	0.03	−0.04	−0.15†	0.08	−0.07	0.00	0.04	−0.03
20 m																
Slope	−0.41*	−0.15	−0.01	−0.55	−0.05	−0.51	−0.35*	−0.21	−0.56*	0.00	−0.70[a,*]	0.14	−0.31*	−0.25	−0.56*	0.00
Elevation	−0.14	0.02	0.01	−0.11	0.27†	0.15	0.28*	0.16	0.20*	0.08	−0.12†	0.00	0.06	−0.06	0.49[a,*]	0.37
Curvature [Convex]	0.11	−0.14	−0.24	−0.01	−0.44[b]	0.19[b,*]	−0.01	−0.24	−0.38[a,*]	0.13	−0.20*	−0.05	−0.11	−0.14	−0.34*	0.09
Curvature [Concave]	0.13	−0.01	−0.43	0.29	0.00	−0.14	0.19	0.05	0.12	−0.02	0.15†	0.01	0.20[a,†]	0.06	0.10	−0.04
Plan [Convex]	0.07	−0.15	−0.34	0.12	−0.23	0.01	−0.15	−0.07	−0.52[a,*]	0.30	−0.23*	0.01	−0.21†	−0.01	−0.13	−0.09
Plan [Concave]	0.32	0.24	−0.38	0.30	0.05	−0.03	0.02	−0.06	0.02	−0.06	0.11	0.03	0.10	0.02	0.13	0.05
Profile [Convex]	−0.32	0.05	0.11	−0.16	0.28	0.01	0.17	−0.10	0.33[a,*]	0.06	0.29*	0.02	0.21†	−0.06	0.24*	−0.03
Profile [Concave]	−0.50[b,*]	0.34[b]	0.21	0.05	0.00	−0.16	0.14	−0.02	−0.10	−0.06	−0.19[a,*]	0.03	−0.04	−0.12	−0.11	−0.05

A positive value of Δr_s indicates that the associated r_s increased with aspect stratification, where as a negative value of Δr_s indicates a decrease in associated r_s. $\Delta r_s = |r_{s2}| - |r_{s1}|$ where r_{s1} refers to the collective data (in Table 2) and r_{s2} to individual topographic variable data for a specific class aspect.

[a] The strongest r_s increase for each significant topographic variable under the same cell size with their Δr_s.

[b] Significant correlations that were not included in the interpretation because of lower n.

* $P < 0.01$.

† $P < 0.05$.

2.3.3. Regression Tree-Based Landscape Segmentation

In this study, the landscape was segmented with the 20-m resolution data because this scale showed a distinct advantage over the other DTMs (1, 5, and 10 m) in explaining accumulation and distribution of the organic layer across the landscape (Table 2.4). The landscape segmentation is illustrated in Figure 2.6 and in Table 2.5. At the landscape scale, regression tree analysis resulted in six landscape units with the topographic variables slope, aspect, and mean curvature classes, which were highly correlated with OLT ($P < 0.05$) (Figure 2.6A). Slope represented the best descriptor of the variability within OLT. The landscape was initially subdivided into two units with slope < 2.3% and slope > 2.3% (Figure 2.6A). Under slope conditions > 2.3%, aspect was an important variable, but, in contrast, mean curvature was a more important variable for areas with slope ≤ 2.3%. Regression tree analysis showed higher OLT in areas with slopes ≤ 2.3% (landscape units A, B, and C) and lower OLT in areas with slopes > 2.3% (landscape units D, E, and F, with mean depths of 29, 43, and 27 cm, respectively) (Table 2.5; Figure 2.6B). CVs for each group (Table 2.5) were lower than that for the collective data set (CV = 0.56), demonstrating that the landscape segmentation process markedly reduced the range of variability within each of the six landscape units.

2.3.3.1. Areas with Slope ≤ 2.3%

Areas with slopes ≤ 2.3% were further subdivided on the basis of slope (≤ 1.8% and > 1.8%) and mean curvature (concave and convex), resulting in three landscape units (A, B, and C, with mean OLTs of 62, 56, and 48 cm, respectively). Field observations indicated that the deposit material type underlying each of the landscape units A, B, and C was composed of clay (86, 89, and 68%, respectively), till (13, 10, and 29%, respectively), and bedrock (1, 2, and 4%, respectively).

2.3.3.2. Areas with Slope > 2.3%

Under conditions for which slopes were > 2.3%, the data were most effectively split on the basis of slope (≤ 3.2% and > 3.2%) and aspect class (N to S versus SW to NW) into three landscape units (D, E, and F). Regression tree analysis indicated that under slope conditions ≤3.2%, OLT was lower in southwest- to northwest-facing areas (landscape unit D) compared

with those having north- to south-facing slopes (landscape unit E). Landscape units D and F had the lowest OLT of any units (Table 2.5). For landscape unit F, the nine highest values of OLT (up to 78 cm) are indicated as outliers in Figure 2.6B. Quantitative evidence from the field observations indicated that these values occurred where higher organic accumulations were observed on sloping terrain and were found in local depressions in the underlying bedrock. Indeed, landscape unit F had the second highest number of sampling points lying on bedrock (15% after landscape unit D with 57%).

Table 2.5. Summary statistics for OLT by landscape unit for the study area.

Landscape units	*n*	Mean (cm)	SD (cm)	CV	Median (cm)
A	543	62	25	0.40	60
B	122	56	25	0.45	55
C	140	48	21	0.44	46
D	117	29	14	0.48	25
E	158	43	16	0.37	41
F	520	27	11	0.42	25

The landscape units correspond to those obtained by regression tree analysis and depicted in Figure 6. *n* represents number of sites.

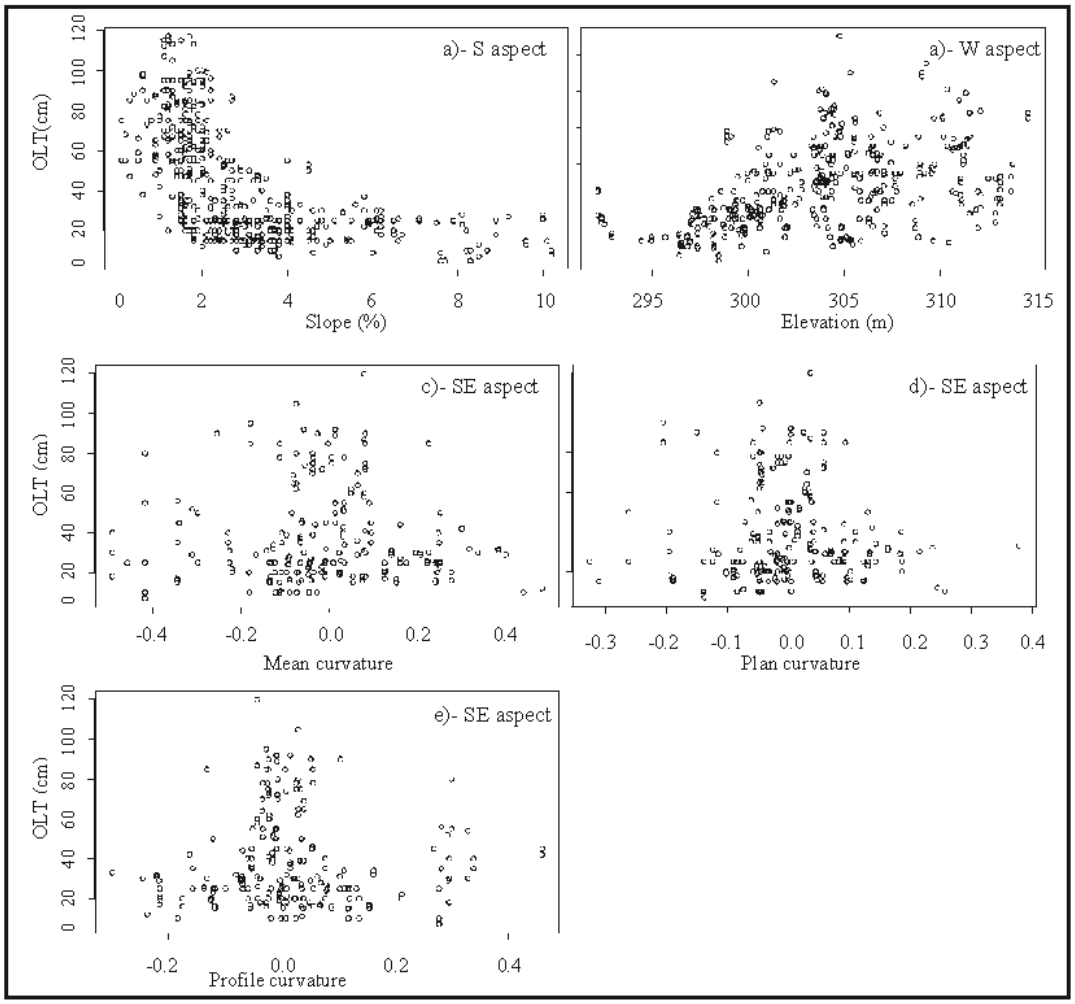

Figure 2.5. Relationships between selected topographic variables and OLT for areas with different aspects at 20-m resolution. (A) Slope. (B) Elevation. (C) Mean curvature. (D) Plan curvature. (E) Profile curvature.

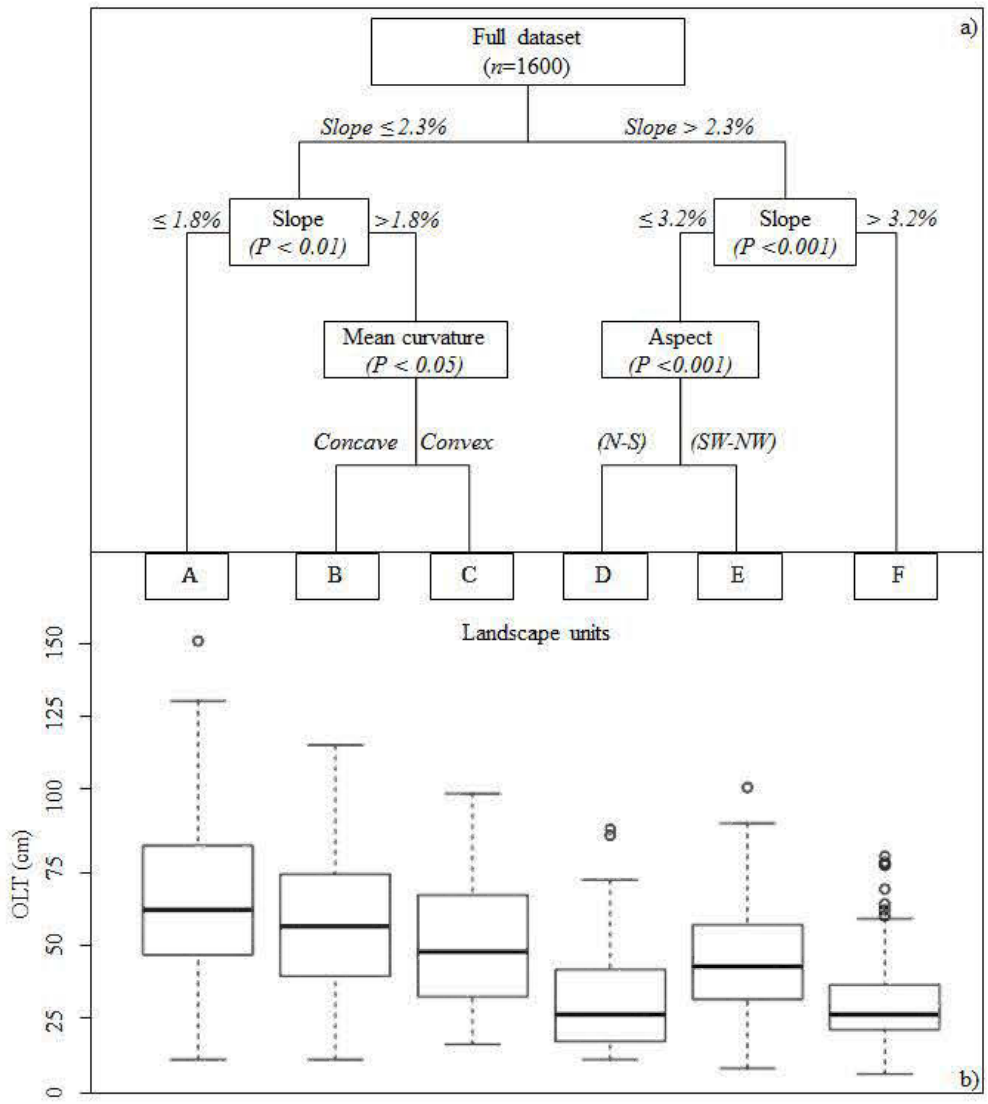

Figure 2.6. Regression tree hierarchical landscape unit segmentation based on 20-m DTM (a). Each box corresponds to a final landscape unit (A-F), with the topographic variable on which the unit was subdivided listed and the range (value or identifier) for the topographic variable by which the unit was defined listed above. Box plots of the OLT variability within each final landscape unit (b). A description of each component of the box and whiskers plot is given in Figure 2.3.

2.4. DISCUSSION

2.4.1. Relationships between OLT and topographic variables at different DTM resolutions

Except for elevation, for which the correlation was consistently weak (r_s = 0.12) across all resolutions, correlation strength of topographic variables increased with decreasing resolution. In other words, lowering resolution caused details (i.e., shorter slopes) to be lost as resolution decreased and consequently tightened the variability range within the topographic variables studied. Of the four resolutions that were examined, the 20-m LiDAR-derived DTM showed the strongest correlations between topographic variables and OLT. This can be mainly attributed to topographic smoothing at the landscape scale that results from decreased resolution of DTMs. This finding was consistent with other studies that have found that small-scale topographic variation was lost with the use of a coarser digital elevation model (Grant, 2004; Potter *et al.*, 1999; Seibert *et al.*, 2007; Wu *et al.*, 2008).

Poor correlation between elevation and OLT indicated that elevation is a minor influence on OLT. When the collective data were used, elevation could not be used to discriminate between areas of higher and lower organic thicknesses over the entire study area. However, stratification of the data based on aspect classes revealed that elevation was positively correlated with OLT for areas having a west-facing slope, which was consistent with other studies, in which higher rates of paludification were found on plateaus (Lavoie *et al.*, 2005; Gorozhankina, 1997).

Not surprisingly, among all of the topographic variables that were studied, slope was the most important single control on OLT within the study area. Despite the observation of some strong relationships for some aspect classes (i.e., areas on south- and southeast-facing slopes), no major improvement in the strength of correlation coefficients was achieved with aspect stratification. Overall, it was apparent that the spatial distribution of OLT in our study area cannot be explained by simple bivariate relationships between OLT and individual topographic variables. In addition, the correlation analysis suggested a complex interrelationship between OLT and topographic variables, and, therefore, the use of a method that could split the study area into more homogeneous spatial units was justified.

2.4.2. Landscape Segmentation

Regression tree segmentation produced some landscape units with high variability that could be explained by local scale features. For example, depressions in the rock were locally observed on sloping terrain within landscape unit F. These topographic depressions, which were filled mostly with fibric and mesic materials, are scattered across the landscape and were probably created by episodic freeze-thaw events in the bedrock or by glacial erosion or may simply represent the surface roughness of the bedrock (Laamrani *et al.*, 2013). This finding is consistent with earlier studies (Payette, 2001; Simard *et al.*, 2009), which found that paludification can occur on sloping well-drained terrain (up to 16%-20%) directly on bedrock where the humic material is almost inexistent and the fibric material is dominant (about 97%; Larocque *et al.*, 2003).

In addition to confirming the importance of slope effects on OLT at the landscape, which had been reported previously for the surface layers within the Clay Belt (i.e., Giroux *et al.*, 2001, Simard *et al.*, 2009), this study quantified the threshold (1.8%) at which slope could be used to discriminate units with the deepest organic layers (landscape unit A). Slope ≤1.8% could be used as a predictor for zones of soil saturation where a thick organic layer often accumulates. Furthermore, a slope threshold of 3.2% seemed to represent a cutpoint for discriminating between paludified and non paludified areas. This study illustrated that even very small differences in slope, on the order of 1.4%, can significantly contribute to the estimation of paludified landscapes. This finding is consistent with those of previous researchers (Giroux *et al.*, 2001; Lavoie *et al.*, 2005; Simard *et al.*, 2009), who calculated in the field differences in slope on the order of 0%-7% within the Clay Belt where slope is frequently less than 0.1% (Lavoie *et al.*, 2007).

Contrary to our expectation, this study showed that overall, areas with slopes > 2.3% and □≤ 3.2% exposed to the south and west (landscape unit E) were more prone to organic layer accumulation than those exposed to the north and east (landscape D). The higher OLT on west- and south-facing slopes may be tentatively explained by higher sphagnum moss growth stimulated by more radiation from the sun combined with higher moisture storage capacity. On the other hand, on areas with slopes exposed to the north and east (landscape unit D), dry soil conditions seems to prevail as a result of water movement causing a decrease in OLT.

Seibert *et al.*, (2007) found that the influence of aspect is largest at latitude 40°-60°, which corresponds to the location of our investigated region.

Beside slope and aspect, mean curvature had the greatest influence on organic layer accumulation and contributed to the separation of units with varying OLT. Concave-mean curvature (landscape unit B) can be an indicator of areas of soil saturation, and organic layers often accumulate in lowlands. On the other hand, plan curvature and profile curvature variables were not selected by the regression tree analysis, and their effect was probably masked by the large number of almost flat areas on the landscape, because these two topographic variables represent flow dynamics across the surface (Table 2.1).

Despite various significant trends, the data exhibited obvious variability (expressed as data scattering). This kind of scattering is expected when one is working with a large data set that covers a range of different site conditions (Seibert *et al.*, 2007). Another issue when one is working with large data sets is that even weak correlations are often statistically significant. In contrast, because of the large variability in site conditions, high correlation coefficients are not expected, and the correlations found may still have a physical meaning.

2.4.3. Management implications and future research

The results of this study are important for landscape management for several reasons. (1) Understanding how surface topography is related to OLT is an important first step in predicting and mapping productivity across landscapes. This information will aid forest managers in predicting potential zones of saturation where organic layer often accumulates and will help them to adopt the appropriate forest management practices (i.e., field preparations, treatments, and replanting). For example, slope can be used to better manage forest resources where high soil moisture limits productivity. (2) To maintain or improve forest productivity in the Clay Belt region, management strategies should focus on sloping sites (i.e., > 2.3%) rather than on almost flat sites (≤ 1.8%). The latter are associated with a deep organic layer that is often not suitable for tree plantations (Lafleur *et al.*, 2010) and provide few ecological or economic motives to manage soils with low slopes (Simard *et al.*, 2009). (3) We expect that the use of LiDAR-derived topographic variables as sources of information in environmental management will increase in the future, especially as the

availability of precise digital data increases. The potential of LiDAR data to provide spatial detail for planning and the optimization of forest management activities in boreal forests has been demonstrated in a previous study (Woods *et al.*, 2011). (4) This study is part of a larger project that deals with the effects of environmental variables and forest harvesting on paludification and was conducted before implementation of recent forest management. Therefore, results from this study could be used to determine the long-term impact of forest management practices (i.e., forest harvesting, field preparation treatments, and replanting) on the original organic layer proprieties.

Our segmentation of the landscape illustrated that areas with higher slopes were associated with thinner organic layers, as did that of Simard *et al.*, (2009), who found that rates of organic layer accumulation at the plot scale were highest on flatter sites and diminished with increasing slope on the Clay Belt. This result supported our hypothesis that topography has a significant influence on the spatial distribution of OLT and that these relationships can be used for partitioning the landscape and, therefore, can help in future planning of landscape management.

The combination of topographic information (from remotely sensed LiDAR data) with field measurement has the potential to be useful for defining both promising and vulnerable areas for forest management. For instance, landscape units A and B seem to represent areas with conditions that may be less favorable for tree growth because the presence of a thick organic layer combined with wet conditions on flat terrain is expected to limit the use of equipment for mechanical site preparation and harvesting within the highly paludified areas (Lavoie *et al.*, 2007). This was supported by ongoing studies that deal with the effect of OLT and slope on forest productivity (A. Laamrani and N. Fenton, UQAT, unpublished. observations, 2013), which found that on average, landscape units A and B showed the lowest stand volumes (estimated for trees with dbh > 9 cm) with 104 and 125 m^3/ha, respectively. On the other hand, landscape units D and F with estimated stand volumes of 204 and 207 m^3/ha, respectively, seem to represent very attractive conditions for forest managers.

Once the regression trees were completed, they provided a set of decision rules that defined the range of conditions, i.e., values of the predictor variables, which are best used to predict each landscape unit. We used these rules to create a thematic map of the spatial

distribution of the resulting landscape units across the study area (Figure 2.7). When forest inventory maps from the MRNQ were superimposed on the regression tree-derived thematic map using ArcGIS 10.0 (ESRI 2011), there was good statistical matching (71%; validating data set $n = 97$; Figure 7) between the landscape unit distribution and forest management area status (suitable or not). Thus, regression tree and the derived thematic map might be useful for identifying and predicting spatial differences in terms of OLT on the landscape, which would be of interest to facilitate forest management in areas of limited data availability within the Clay Belt region. In addition, the regression tree breakdown of the data into the six landscape units was statistically and visually related to the distribution of three landscape topographic variables (slope aspect and mean curvature; maps of each of these variables are not shown in this study).

Finally, our study illustrated not only the potential of some topography variables to explain the occurrence of highly paludified areas but also the need for further studies. Our future work will focus on the importance of mineral soil topography on the spatial distribution of the organic layer over the same landscape, especially if topographic variables could be used to discriminate between the two common types of paludification (successional and edaphic) (for an overview of paludification types, see Fenton *et al.*, 2009).

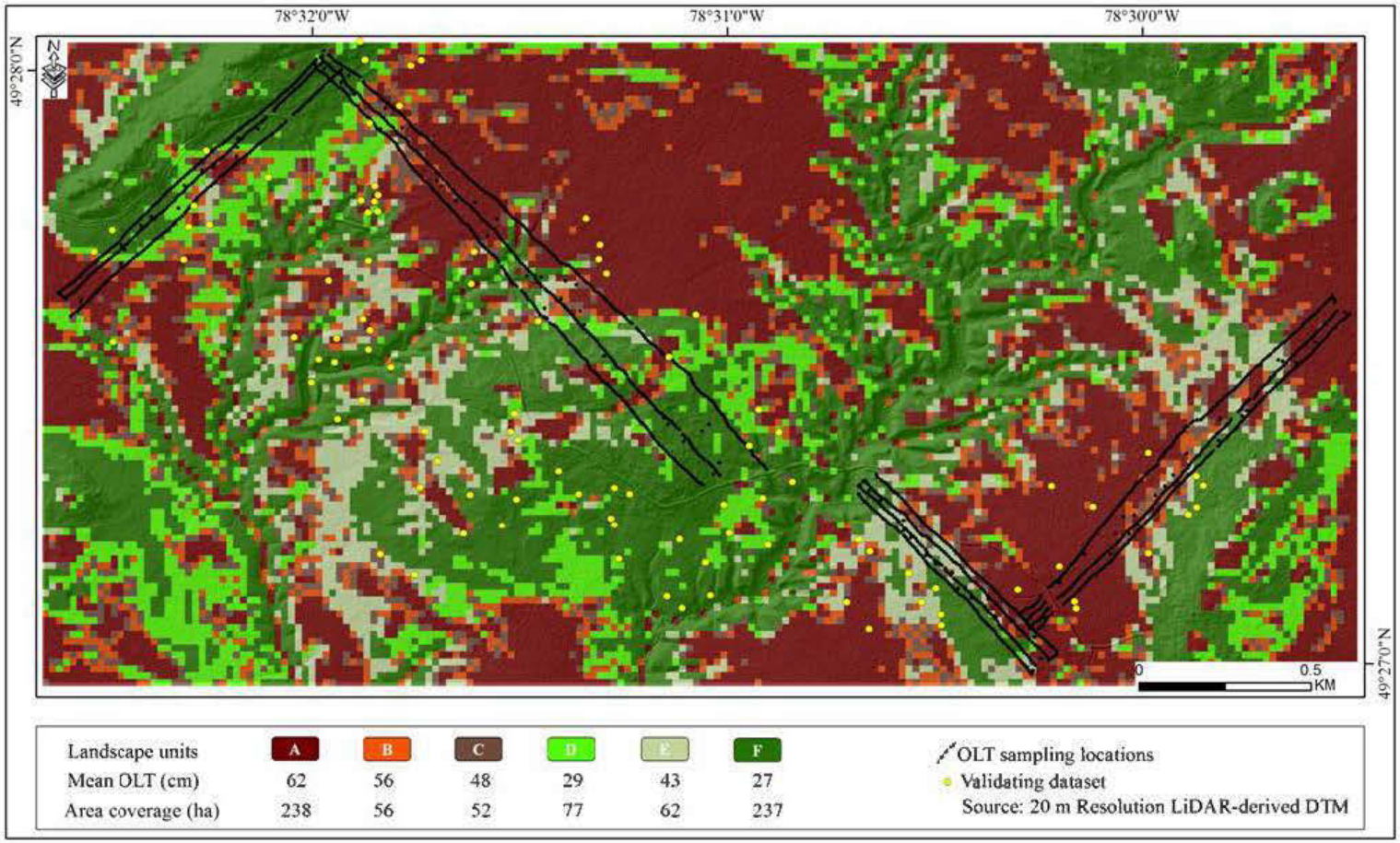

Figure 2.7. Thematic map showing the spatial distribution of the six resulting landscape units (A-F) across the study area. This map was produced using the regression tree rules based on the combination of slope, aspect, and mean curvature.

2.5. CONCLUSIONS

This study demonstrated that the relationship between OLT and most individual topographic variables (obtained from LiDARderived DTMs) is consistently weak. Slope was found to have a significant role in the spatial distribution of OLT at the landscape scale. A regression tree analysis partitioned landscape data into six statistically different landscape units. Further, the mean OLT of each landscape unit was either significantly different from that of all other units or the lack of differences could be explained by meaningful field observations. Landscape segmentation served to discriminate between areas of greater and lesser OLT based on slope, aspect, and mean curvature variables. Indeed, higher OLT was confined to gentle sloping areas ($\leq$ 1.8%). For areas with relatively higher slopes ($>$ 2.3% and $\leq$ 3.2%), organic layers were also found to be deeper for south-facing slopes than north-facing slopes. A thematic productive map of the distribution of the resulting six landscape unit was generated using the regression tree based on the combination of slope, aspect, and mean curvature. This thematic map was useful for recognizing both vulnerable and promising areas (overall matching of 71%) for forest management. To summarize, relationships between OLT and topographic variables at the landscape scale confirmed the importance of topography on OLT, which was previously noted at the plot scale within the Clay Belt. Finally, the most accurate results were obtained from the 10- and 20-m resolution LiDAR-derived data rather than from that of higher resolution (1 and 5 m).

CHAPITRE III

THE ROLE OF MINERAL SOIL TOPOGRAPHY ON THE SPATIAL DISTRIBUTION OF ORGANIC LAYER THICKNESS IN A PALUDIFIED BOREAL LANDSCAPE

Ahmed Laamrani[1], Osvaldo Valeria[1], Nicole Fenton[1], Yves Bergeron[1], and Li Zhen Cheng[2]

[1] Chaire industrielle CRSNG-UQAT-UQAM en aménagement forestier durable, Institut de recherche sur les forêts et Centre d'étude sur la forêt.
Université du Québec en Abitibi-Témiscamingue. 445 boul. de l'Université, Rouyn-Noranda, Québec J9X 5E4, Canada.

[2] Institut de recherche en mines et environnement (IRME), Université du Québec en Abitibi-Témiscamingue. 445 boul. de l'Université, Rouyn-Noranda, Québec J9X 5E4, Canada.

Article publié en 2014 dans Geoderma (En line, 28 janvier 2014)
http://dx.doi.org/10.1016/j.geoderma.2014.01.003

ABSTRACT

Mineral soil topography is difficult to describe in boreal regions because of the thick overlying organic layer despite its presumed importance in determining where and at what rate an organic layer will accumulate (paludification). The overall purpose of this study was to examine the relationship between mineral soil topography and OLT at the landscape scale. More specifically, these relationships can be used to map the distribution and spatial variability of paludification across the landscape, thereby exploring the potential to discriminate between the two commonly known paludification types (permanent and reversible). Seven topographic variables (elevation, slope, aspect, mean curvature, plan curvature, profile curvature and topographic wetness index) were generated from a digital elevation model that we developed for the mineral soil surface (MS-DEM). OLT data were collected from field measurements across the landscape by manual probing and values varied from 5 to 150 cm. The MS-DEM was generated by subtracting OLT field values from the corresponding LiDAR-derived elevation values. Most correlations between OLT and individual predictor variables were weak and illustrated that OLT and its landscape-scale distribution cannot be explained by simple bivariate relationships. Consequently, two regression tree-based models were developed using: only the seven mineral soil topographic variables (model 1), and all predictor variables (mineral soil topography and surficial deposits; model 2). Mineral soil slope was the most important variable for both models and corresponded to the first level of splitting the dataset into homogenous landscape units in terms of organic layer thickness. Surficial deposit, topographic wetness index (TWI) and aspect were also related to OLT and proved to be contributing to the development of the two models. Model 1 explained 0.34 of the OLT variability and offer simple models with few landscape units that are easy to interpret. Model 1 splitting rules allowed the combination of different maps (slope, TWI and aspect) for producing a landscape units map, on which OLT was determined and related to increasing paludification categories. A good overall accuracy of 74% was achieved for this map. Model 2 was the best model in terms of estimate quality (R^2_{adj} = 0.52). Both models were successful in discriminating highly paludified landscape units. Except for one landscape unit that was assigned to permanent paludification type, both models were unable to further subdivide more landscape units into reversible and permanent paludification, suggesting that both of these types interact within the same landscape unit. This study demonstrated that the combination of topographic information from remotely sensed LiDAR data and field OLT measurement data has the potential to be useful for defining both promising and vulnerable areas for forest management.

Keywords: Paludification; Soil organic layer depth; Boreal forest soil; Mineral soil topography; Clay-Belt region; Regression tree; LIDAR-derived DTM.

RÉSUMÉ

En raison de la couche organique relativement épaisse qui caractérise les forêts boréales, la topographie du sol minéral est difficile à déterminer, malgré son importance présumée dans l'accumulation des couches organiques. L'objectif général de cette étude était d'examiner la relation entre la topographie du sol minéral et l'épaisseur de la couche organique (ECO) à l'échelle du paysage. Plus précisément, les relations établies pourront être utilisées pour cartographier la distribution et la variabilité spatiale de l'entourbement à travers le paysage, tout en explorant leurs potentiels de discriminer entre les deux types de paludification: permanente et réversible. Des données d'ECO ont été recueillies à partir de mesures de terrain dans le site à l'étude à l'aide d'une sonde manuelle et dont les valeurs varient de 5 à 150 cm. Sept variables topographiques (élévation, pente, exposition, indice topographique d'humidité (TWI), courbure totale, courbure transversale, et courbure horizontale) ont été générées à partir d'un modèle numérique d'élévation que nous avons développé pour la surface du sol minéral (MS-DEM). Le MS-DEM a été généré en soustrayant les valeurs d'ECO à la valeur d'altitude (z) extraite du MNT-LIDAR au niveau des points du terrain. Nous avons établi différentes relations quantitatives entre l'ECO et chacune des sept variables topographiques. La plupart de ces corrélations étaient faibles, suggérant que la variation de l'ECO et sa distribution spatiale ne pouvaient pas être expliquées par de simples corrélations. Par conséquent, deux modèles basés sur une approche de modélisation par arbre de régression ont été développés en utilisant: un premier modèle qui contient uniquement les variables topographiques et un deuxième modèle qui intègre aussi le type de dépôt de surface en plus des variables topographiques. Les modèles développés nous permettent de tirer plusieurs conclusions quantitatives. La pente du sol minéral, le type de dépôt de surface (argile, till et régolithe), le TWI et l'exposition sont les quatre principales variables influençant l'accumulation de la couche organique. Les valeurs de pente du sol minéral $> 3,5\%$ et $\leq 2\%$ constituent des seuils permettant de distinguer, respectivement, les zones les plus prometteuses et les zones plus vulnérables pour l'aménagement forestier. Les zones avec une exposition nord sont associées à une couche organique plus profonde par rapport à celles exposées vers le sud et l'ouest. La qualité de prédiction du modèle utilisant uniquement les variables topographiques était moins élevée ($R^2_{adj} = 0,34$) en comparaison à celle du modèle qui intègrait aussi le type de dépôt de surface en plus des variables topographiques ($R^2_{adj} = 0,52$). Un autre apport majeur de cette étude est le fait que nous avons été en mesure d'établir un seuil de la pente du sol minéral de l'ordre de 3,5% permettant de distinguer les zones paludifiées de celles non paludifiées. Les règles de fractionnement du modèle 1 ont permis l'utilisation de différents rasters (pente, TWI et exposition) pour produire une carte d'entités paysagères correspondant à différentes catégories de paludification. La carte résultante a une précision globale de l'ordre de 74%. Les modèles utilisés ont réussi à discriminer les entités de paysage hautement paludifiées, sans pour autant être capables de clairement distinguer les deux types de paludification, permanente vs réversible. Cette étude a démontré l'utilité de l'utilisation de données conjointes recueillies sur le terrain et à partir de produit de télédétection (LiDAR) pour l'identification respective les zones les plus prometteuses et les plus vulnérables pour l'aménagement forestier.

3.1. INTRODUCTION

Paludification is a natural process where organic material accumulates on the ground surface over time, resulting in higher soil moisture levels and elevated water tables (Crawford *et al.*, 2003; Vygodskaya *et al.,* 2007). These conditions alter dynamic succession and favour the invasion of *Sphagnum* moss species (Fenton *et al.*, 2005; Fenton and Bergeron 2006, 2007), which can lead to the development of forested peatlands and substantial decreases in forest productivity (Simard *et al.*, 2007, 2009). While essentially a regional process, many parts of the world, including interior Alaska, the western Siberian plain, and the Hudson Bay-James Bay Lowlands of Canada, are prone to paludification. In the black spruce forests of the Clay Belt, a region in the southern portion of the Hudson Bay-James Bay Lowlands (Figure 1A), time-since-last fire and ground surface topography have been reported as the two main factors that cause paludification. Consequently, two types of paludification can be identified: permanent and reversible, respectively (Fenton *et al.*, 2009; Lavoie *et al.*, 2007; Simard *et al.*, 2007). Within the landscape, permanent paludification dominates in natural depressions, which have wetter soil conditions that favour organic layer build-up. Reversible paludification occurs on flat or sloping terrain, where a feather moss-dominated bryophyte layer is replaced over time by Sphagnum species, starting about 100 years following fire (Fenton and Bergeron 2006; Simard *et al.*, 2007).

Numerous studies have been conducted to characterise the influence of topography on the accumulation and spatial variability of the organic layer across the Clay Belt (i.e., Giroux *et al.,* 2001, Lavoie *et al.*, 2005, 2007; Simard *et al.*, 2009); however, these studies have largely been restricted to investigations of the ground surface topography at the plot scale. In a recent extensive study at the landscape scale, Laamrani *et al.*, (2014a) found weak correlations between organic layer thickness (OLT) and topographic surface variables, suggesting that OLT may also be controlled by other factors, such as the mineral soil topography, i.e., the contours of the surface beneath the organic layer.

Mineral soil topography affects the accumulation of organic layer mainly through its control of water movement at the landscape scale (Emili *et al.*, 2006). This topography has been difficult to describe in boreal regions because it is masked by the thick overlying organic material. Despite the presumed importance of mineral soil topography in determining

where and to what degree paludification will occur in the Clay Belt, no attempt has been made in this region until now to measure and link mineral soil topography to OLT and to the two paludification types (permanent and reversible) at the landscape scale. In this context, the overall purpose of this study was to examine the relationship between mineral soil topography and OLT at the landscape scale. More specifically, these relationships can be used to map the distribution and spatial variability of paludification across the landscape, thereby exploring the potential to discriminate between permanent and reversible paludification. To do so, we correlated field organic layer measurements that were obtained by manual probing with topographic variables that were derived from a digital elevation model (DEM), which was generated at the mineral soil surface. The mineral soil DEM was generated using LiDAR (*Li*ght *D*etection *A*nd *R*anging) data together with field OLT measurements.

3.2. METHODS AND MATERIALS

3.2.1. Study area

The study was located in the James Bay Lowlands physiographic region of Quebec, Canada (Figure 1A). It was centred (49°27'30" N, 78°31'5" W) on a 72 ha site within the Clay Belt region, which is dominated by black spruce (*Picea mariana* [Mill.] BSP) forest (Figure 3.1B). The forest floor was composed of *Sphagnum* spp., feather mosses (principally *Pleurozium schreberi* (Brid.) Mitten), and shrubs, (mainly dwarf ericaceous species), with variable coverage across the landscape. This region has low topographic relief, as the Canadian Shield was overlain by extensive clay deposits by pro-glacial Lakes Barlow-Ojibway (Veillette, 1994). Within the study area, ground surface slope ranged from 0.3 to 15.7%; about 60% of the area has a slope greater than 2%. Elevation ranged from 290 m to 314 m above sea level (mean = 303 m).

OLT varied from 5 to 150 cm across the landscape. The underlying mineral soil is variable, ranging in composition from clay to till. The thickness of the mineral layer over bedrock is variable across the landscape, ranging from 1 m (Laamrani *et al.*, 2013a) to up to 60 m (Veillette *et al.*, 2005). A detailed description of mineral deposits present in an area located about 50 km northwest of our study area has been provided in Veillette *et al.*, (2005).

The study area is underlain by bedrock, which is a complex mixture of Precambrian granitic rock types that occasionally appear at the ground surface and which form scattered gentle hills across the landscape. Many streams run locally in a southwestern direction through the area, which produced a relatively complex topographic pattern within the landscape (Figure 3.1C). At the La Sarre weather station, located at about 85 km southwest of the site, mean annual temperature is 0.7 °C and total annual precipitation is 890 mm (Environment Canada, 2011).

3.2.2. Sampling design and field data collection

The objectives of this study were addressed by establishing thirteen sub-parallel transects through forest stands within the study area (Figure 3.1B). The thirteen transects, totalling 15 km in length, were established across four different sectors (1, 2, 3, and 4; Figure 3.1B), which covered a variety of sites that differed in OLT, degree of paludification, drainage, vegetation cover, and substrate moisture conditions. This transect configuration took a long time to complete but provided an extra dimension that was important for interpreting the mineral soil topography. This also permitted us to generate a spatially continuous cross-sectional profile of the mineral soil topography. A minimum distance of 20 m was maintained between transects in order to optimise lateral interpolation between transects.

Field organic layer measurements (response variable) were collected at 10-m intervals along each transect by probing with a manual auger (n = 1550). At each sampling point, the auger bored through the organic layer until the mineral soil was encountered. The auger was then removed and the marked depth to mineral soil was accurately measured. The thickness of the organic material was taken as the distance between the organic layer surface and the mineral soil interface. In nearly all cases, the transition between organic layer and mineral soil was clearly marked by an obvious change in colour and texture. An additional 172 OLT measurements were also collected over the study area and used for validation purposes (Fig 1C). These 172 sampling points were randomly disturbed between transects (n = 85) and along the central transect (n = 87). Each organic layer measurement along the central transect was located halfway between two sampling points established at 10-m intervals. Two locations along the central transects had to be excluded, as it was technically impossible to

measure OLT because they were located in deep depressions; consequently, the exclusion of two sites, which should not affect the results, reduced the validation dataset to 170 sampling points.

At every sampling point, the presence of each organic horizon(Of, Om, Oh) and the nature of the underlying mineral material (clay, till, bedrock) were recorded in the field. The spatial distribution, stratigraphy and origin of the surficial deposits were highly variable across the study area. It should be mentioned that surficial deposits nomenclature (clay, till, bedrock) used in this study referred to the mineral material underlying the organic layer. In the present study, "bedrock" referred to unconsolidated material (also called regolith) overlying solid rock. To correlate each type of surficial deposits (clay, till, bedrock) with organic layer thickness, surficial deposits were considered as a factor, taking nominal values of 0 for till, 1 for clay, and 2 for bedrock.

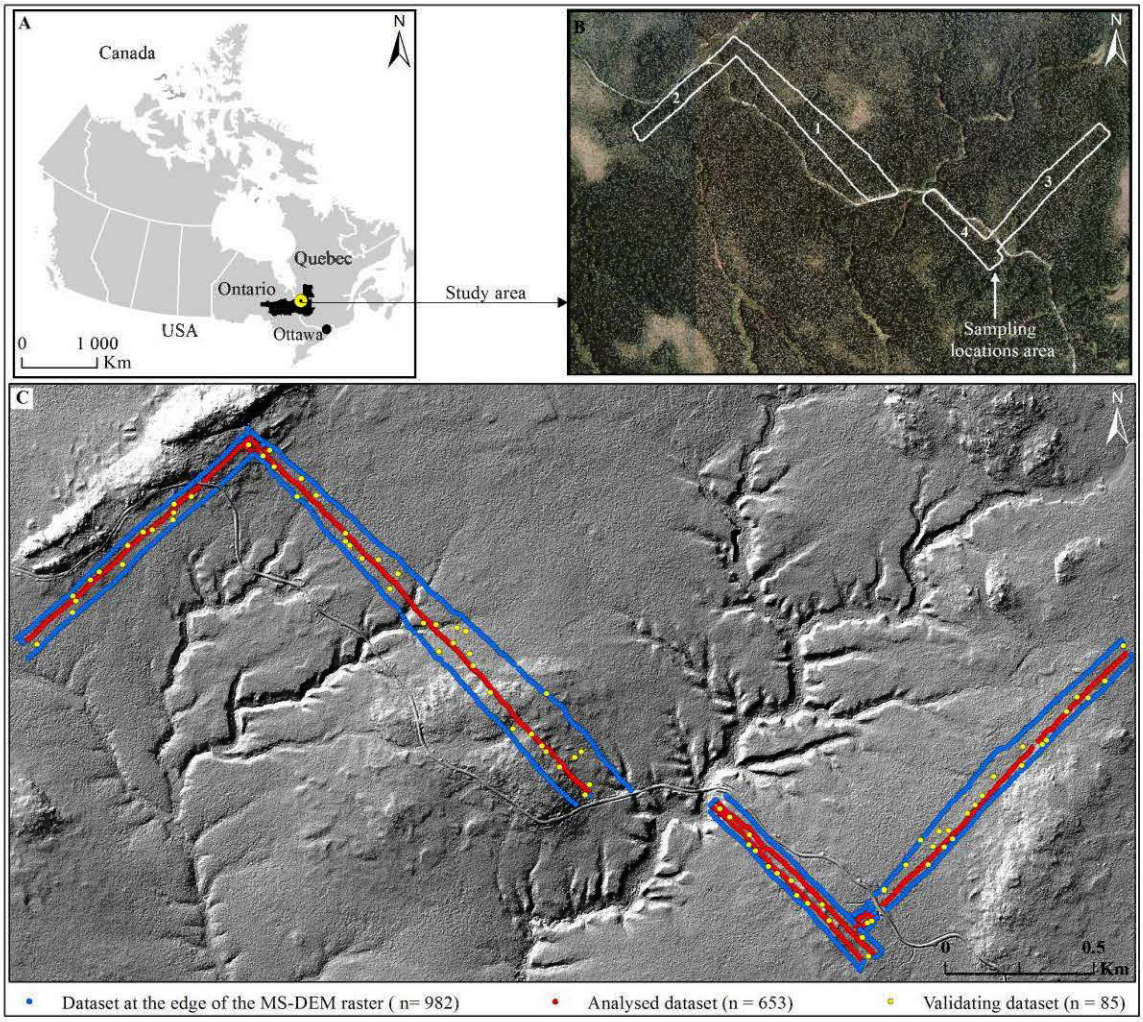

Figure 3.1. Study area within the Clay Belt of Ontario and Quebec (A). Sampling locations along transects within four sectors (1, 2, 3, and 4) and delimitation of the mineral soil digital elevation model area (B). Landscape map of the study area showing the field organic layer thickness sampling points locations (C). The analysed dataset (n= 653) was formed by summing the original dataset along the central transects (n= 568) and independent validation datasets along the same transects (n= 85).

3.2.3. Mineral soil topography

3.2.3.1. Generation of mineral soil digital elevation model

Prior to the creation of a mineral soil digital elevation model (MS-DEM), a digital terrain model (DTM) was generated based on LiDAR data (with ± 0.065 m vertical accuracy and 15-m resolution). The latter is becoming one of the most effective and reliable remote sensing technologies for assessing topography at both the plot- and landscape-scales in boreal forested environments (i.e., Laamrani *et al.*, 2014a; Southee *et al.*, 2012; Webster *et al.*, 2011, Work *et al.*, 2011). Laamrani *et al.*, (2014a) and Vepakomma *et al.*, (2011) described in detail the processing and creation of the LiDAR-derived DTM.

Positions of all field sampling measurements (along transects and plots) were recorded using a Trimble GeoXT handheld GPS to provide 50 cm-level positioning accuracy and to allow direct comparison with the DTM. The field OLT dataset was then superimposed upon the DTM and surface topography elevations were extracted for each sampling location. By subtracting the OLT values from the corresponding DTM values at each field point, a new dataset of mineral soil elevations was obtained for the study area. This new dataset was first used to create a digital representation of the three-dimensional surface using (TIN) procedure (Triangulated Irregular Networks; Peucker *et al.*, 1978). A digital elevation of the mineral soil surface model was then created by converting the TIN to a raster format with an optimal resolution of 15 m (cell size). The resulting mineral soil digital elevation model (MS-DEM) was validated with a set of field-measured points (n = 170; 85 sampling points along the central transects and another 85 points between transects; Figure 3.1C). This raster validation dataset was not part of the original dataset (n = 1550) that was used to produce the MS-DEM (Figure 3.1C).

3.2.3.2. Topographic variable calculation

Mineral soil surface topographic variables (predictor variables), which were derived from the MS-DEM, included elevation, slope, aspect, mean curvature, plan curvature, profile curvature, and a compound topographic wetness index. A detailed description of each of these topographic variables is provided in Table 3.1. The chosen topographic variables may aid spatial estimation of paludified areas, because the topography is presumed to have a great

influence on organic layer accumulation whereby topographic lows/depressions would be associated with an accumulation of organic matter and a concomitant rise in the water table. The topographic wetness index (TWI) has been found to play a significant role in estimating different soil features that are related to paludified areas such as local soil moisture (Blyth *et al.*, 2004; Güntner *et al.*, 2004), horizon depth (Moore *et al.*, 1993; Gessler *et al.*, 1995; Seibert *et al.*, 2007), vascular plant species richness in boreal forests (Zinko *et al.*, 2005; Sørensen *et al.*, 2006), and the spatial distribution of groundwater flow along forest-peatland complexes within the boreal forest (Emili *et al.*, 2006).

Values of each of the topographic variables were calculated for each cell of the MS-DEM using ArcGIS 10 (ESRI 2011). Conceptually, the topographic variable tool (i.e., slope, aspect) fits a plane to the z-values of a 3 x 3 cell neighbourhood around the central cell. When a cell location within this nine-cell neighbourhood with a "NoData" z-value, the z-value of the central cell was assigned to the location, after which the topographic variable was then computed. At the edge of the MS-DEM raster, at least three cells (outside the raster's extent) contained NoData as their z-values. For mineral soil slope calculation, for instance, this problem resulted in a flattening of the 3 × 3 plane fitted to these edge cells, which leads to a decrease in the slope (ESRI 2011), and thus to a biased value of this topographic variable. To avoid including biased values from cells next to the physical edge of the MS-DEM raster, OLT measurement corresponding to cells that had at least one NoData cell as a neighbour was excluded from the analysed dataset. These excluded data were located mainly along transects at the edge of the MS-DEM raster (Figure 3.1C). In addition, simple correlations between OLT and the topographic variables showed that when data from cells next to the physical edge of the MS-DEM raster were excluded, relationships were improved for most topographic variables. For instance, TWI, slope and elevation correlations were improved by 17%, 9% and 4%, respectively; this rationalises our use of a reduced dataset (n = 653) for subsequent analyses, rather than the entire dataset, which was used to generate the MS-DEM (n = 1550). The reduced dataset is referred to in this study as the "analysed dataset" and consisted of the sum of central transect sampling points (n = 568) and the validation dataset sampling points along the central transect (n = 85), for a total of 653 sampling points.

Table 3.1. Description of the topographic variables that were derived from the mineral soil digital elevation model (MS-DEM).

Topographic variables	Description
Elevation	Height above sea-level of a particular mineral soil location. Mineral soil *z*-value was calculated for each sampling location as the difference between the LiDAR DTM and the organic layer thickness at that location.
Slope	Calculated for each grid cell as the maximum rate of change in *z*-value from that cell to its neighbours. Slope affects the overall rate of movement downslope.
Aspect	Direction of the maximum rate of change in the z-value from each cell to its neighbours. Aspect defines the direction of flow and was classified into four major classes, viz., North, East, South and West.
Mean curvature	A general measure of the convexity of the landscape, where sinks and valleys are considered concave (negative values), and peaks and highs are considered convex (positive values).
Plan curvature	Curvature of the surface perpendicular to the slope direction. (+) values indicate that water flow would diverge (convex surface), whereas (-) values indicate that water flow would converge (concave surface).
Profile curvature	Curvature of the surface in the direction of slope. (+) values indicate that water flow would decelerate (concave surface), whereas a (-) values will indicate that water flow would accelerate (convex surface).
Topographic wetness index	$TWI = \ln (A_s / \tan \beta)$ (Moore *et al.*, 1993). A_s is the local upslope contributing area and β is the local slope. The higher the value of the TWI in a cell, the higher the soil moisture and water accumulation that can be found on it.

3.2.4. Relating topography variables and OLT

To investigate relationships between predictor variables (topographic variables and surficial deposits) and the response variable (field-measured organic layer thickness), we used Spearman's rank correlation and regression tree modelling, which are both non-parametric methods. Spearman rank correlation (r_s) was used instead of the usual parametric Pearson product-moment correlation. In the latter variables are presumed to have a linear relationship, which was not the case of the entire dataset used in this study. For these reasons, no attempt was made to explore the relationships between predictor and response variables using linear mixed-effects models.

Regression trees are well-suited to the analysis of our datasets because of their (i) capability in modelling both complex and non-linear relationships (Greve *et al.*, 2012a; Rothwell *et al.*, 2008) between covariates and response variables, which can be easily interpreted and discussed (Bou Kheir *et al.*, 2010); (ii) ability of handling both categorical (i.e., surficial deposits) and quantitative (i.e., elevation and slope) data (Greve *et al.*, 2012b; Johnson *et al.*, 2009); further, (iii) recursive partitioning of the dataset into more homogeneous groups allows the identification of potential relationships between the response variable (in our case, organic layer thickness) and the environmental predictors, while also identifying interactions among these latter independent variables (Rothwell *et al.*, 2008).

In the present study, regression trees were used to split the landscape OLT data into different homogeneous spatial units (also known as terminal nodes). In this study, the terminal nodes were named as "landscape units" that refer to relatively homogeneous areas in term of OLT distribution. Splits or rules defining how the data were to be partitioned were selected based on a significance test of independence between covariates and the response variable. A split was established when the *P*-value was smaller than $\alpha = 0.05$. In other words, the split was established when the global null hypothesis of independence between the response variable and any of the predictors could not be rejected at $\alpha = 0.05$ (Hothorn *et al.*, 2006). Unlike other decision tree methods (e.g., CARTs), there was no need for the regression tree modelling approach used in this study for using post hoc pruning to prevent overfitting since *P*-values were used as the stopping criterion (Everitt and Hothorn, 2009).

In this study, individual predictor variables that were significantly correlated with organic layer (Table 3.2) and surficial deposits were used to develop two regression tree-based models. Model 1 was developed using only the mineral soil topographic variables (slope, aspect, mean curvature, plan curvature, profile curvature, and TWI) that had been directly derived from the MS-DEM. Model 2 was developed using all of the predictor variables (mineral soil topography and surficial deposits). Once the regression trees were completed, they provided a set of decision rules that defined the range of conditions, i.e., values of the predictor variables, which are best used to predict each landscape unit. Predictive maps of OLT could then be created through the application of the subsequent splitting rules using ArcGIS 10.0 (ESRI 2011). Mean values of OLT in the resulting landscape units were then used to classify them into one of four categories of increasing paludification: null (0-25 cm); low (26-40 cm); moderate (41-60 cm); and high (> 60 cm). This classification scheme was inspired by previous studies from the same region (Beaudoin *et al.*, *unpublished results*; Laamrani *et al.*, 2014a; Simard *et al.*, 2009). The resulting predictive paludification categories were verified against OLT field measurements (n = 85) using datasets that were randomly selected between the transects sampling locations (Figure 3.1C) and were not used in regression tree development. The validation procedure, of the resulting map and paludification categories, was based on conventional confusion matrix procedure, using overall accuracy and producer accuracy following Congalton (1991).

Assumptions regarding the lack of multicollinearity (Variance inflation factors), normality of the data (Shapiro-Wilk test), and equal error variance (homoscedasticity, Levene's test) of the regression models were satisfied. Significance was declared at a level of $\alpha = 0.05$, with all statistical analyses were performed in R (R Development Core Team 2011). Regression trees were realised using the *ctree* function in the *party* package (Hothorn *et al.*, 2006).

3.3. RESULTS

3.3.1. Importance of individual predictor variables

Analyses revealed that among all of the mineral soil surface topographic variables, the highest correlations with OLT were exhibited by slope (r_s = -0.54, $P < 0.001$) and TWI (r_s = 0.40, $P < 0.001$). When the data were stratified according to aspect, these coefficients were even higher, especially for south-facing areas (Slope, r_s = -0.66, $P < 0.001$; TWI, r_s = 0.56, $P < 0.001$; Table 3.2 and Figure 3.2). Elevation had a weak relationship with OLT measurements (r_s = 0.15, $P < 0.001$), and shallow and thick organic layers occurred at both high and low elevations in the study area (Figure 3.2). When stratified by aspect, the correlation between elevation and OLT was only significant for west-facing sites (r_s = 0.36, $P < 0.001$). The positive relationship between elevation and OLT could be attributable to thick organic layers accumulating over mineral soil on plateaus (flat areas at higher elevation). Because of this local pattern and the narrow range of elevations (290-314 m) over the study area, we chose to exclude elevation from subsequent analyses.

All curvature variables (mean, plan and profile) were not correlated to field measurements of OLT (Table 3.1), however these correlations were significant when we split each of the surface curvature topographic variables into two classes, viz., concave and convex (Figure 3.3). Although the correlations were not strong ($r_s \leq 0.26$), overall OLT tended to increase with concavity.

Table 3.2. Relationships between organic layer thickness and topographic variables, where the latter values were extracted from the mineral soil digital elevation model (MS-DEM).

Topographic Variables	All data [a]					r_s [b]				r_s [c]		
	Min	Mean	Max	SD	r_s	North	East	South	West	Till	Clay	Bedrock
Elevation	290	303	314	5	0.15**	0.04	0.04	0.06	0.36**	0.22*	-0.07**	-0.33*
Slope	0.2	2.9	14.7	1.9	-0.54**	-0.20	-0.27†	-0.66**	-0.44**	-0.15*	-0.34**	0.03
Mean curvature	-1.7	0.02	2.4	0.4	0.01	0.01	0.08	0.06	-0.07	-0.10	0.03	-0.10
Plan curvature	-0.7	0.01	1.4	0.2	0.02	-0.05	0.01	0.03	0.02	-0.07	0.04	-0.07
Profile curvature	-1	-0.01	1.6	0.2	-0.03	0.00	-0.13	-0.08	0.08	-0.11	-0.03	0.08
TWI	6	8	11	1	0.40**	0.23	0.34*	0.56**	0.11	0.26**	0.13†	0.38*

**, * and † statistically significant at $P < 0.001$, < 0.01 and < 0.05, respectively. r_s refers to Spearman's rank correlation coefficient.
[a] Analysed dataset: $n = 653$.
[b] Dataset stratified by aspect with $n_{[North]} = 51$; $n_{[East]} = 64$; $n_{[South]} = 281$; and $n_{[West]} = 257$.
[c] Dataset stratified by surficial deposit types with $n_{[Till]} = 236$; $n_{[Clay]} = 363$; and $n_{[Bedrock]} = 54$.

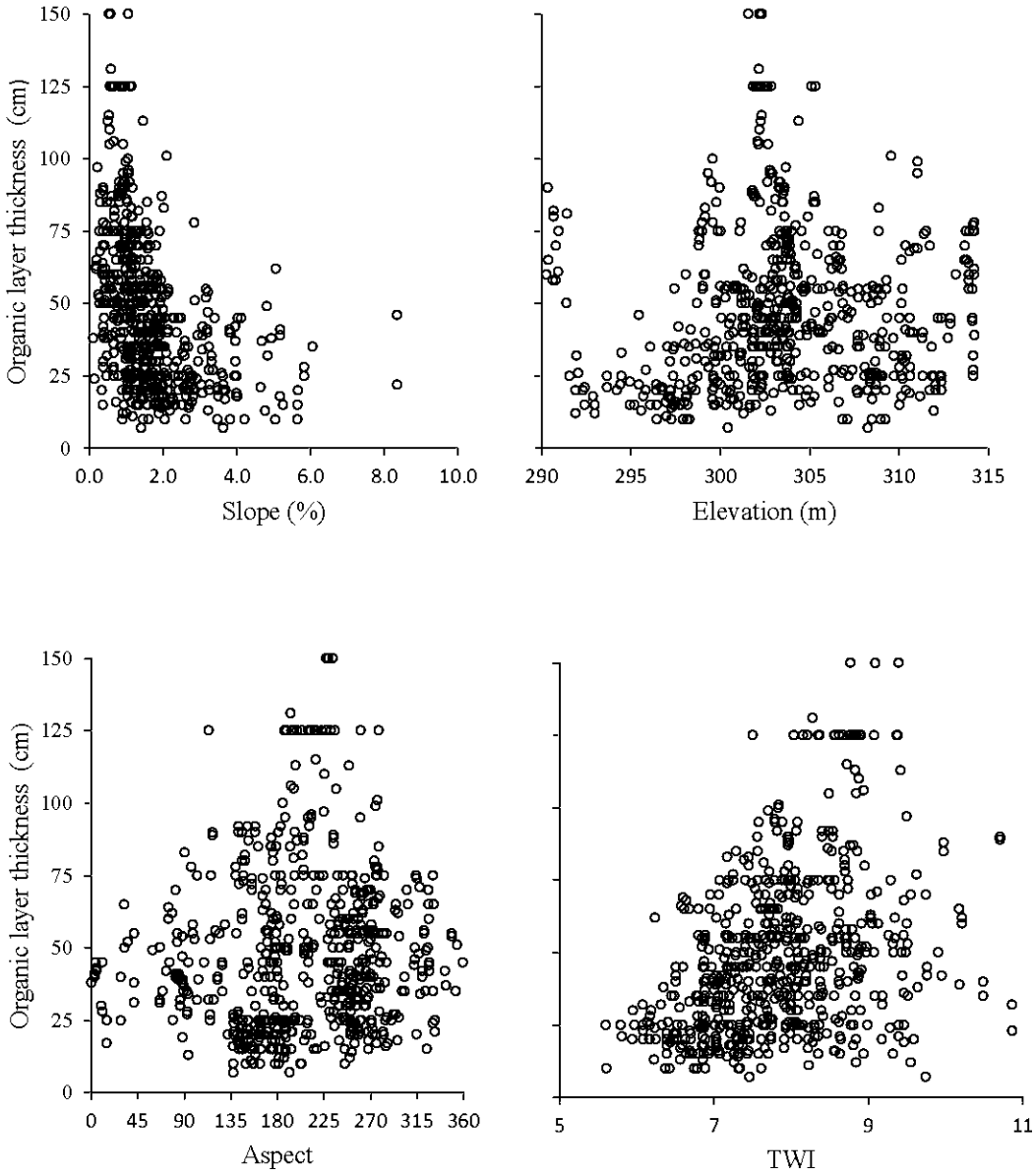

Figure 3.2. Field measured organic layer thickness versus mineral soil surface topographic variables.

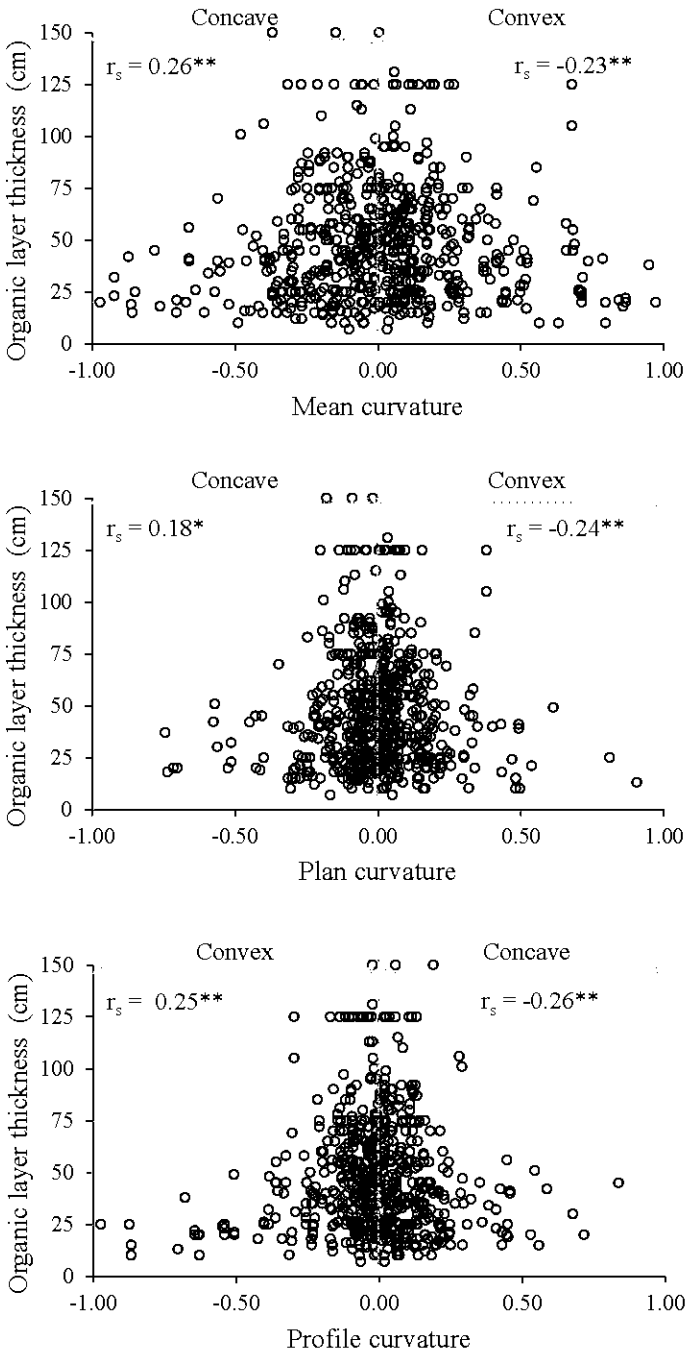

Figure 3.3. Relationship between organic layer thickness and mineral soil curvature variables (mean, plan and profile). ** *P-value* < 0.001; **P-value* < 0.01.

Mean OLT overlaying the three types of surficial deposits differed significantly (Post hoc Tukey's HSD, $P < 0.0001$: clay-till, clay-bedrock and till-bedrock). Surficial deposits were significantly correlated with OLT ($r_s = 0.58$, $P < 0.001$, $n = 653$). Correlations between OLT and topographic variables were also calculated for each of the surficial deposits (clay, till, bedrock) to determine whether or not they improved with stratification by surficial deposits. Most coefficients were smaller than or not significant compared to the coefficients that had been calculated for the entire dataset. Of all the topographic variables that were examined, only TWI was significantly correlated with the three types of surficial deposits (Table 3.2). Correlations were weak but significant between OLT and clay- ($r_s = -0.34$, $P < 0.001$, $n = 363$) and till-slope ($r_s = -0.15$, $P < 0.001$, $n = 236$), whereas the organic layer thickness-bedrock slope correlation did not significantly differ from zero ($r_s = 0.03$, $P = 0.82$, $n = 54$; Table 3.2). A scatter plot of these relationships showed that deep organic layers (mean = 64 cm) were largely confined to clayey mineral soil, whereas shallower organic layers (mean = 25 cm) were typically located on till (Figure 3.4). TWI was correlated with the presence of clay ($r_s = 0.13$, $P < 0.05$), till ($r_s = 0.26$, $P < 0.001$) and bedrock parent materials ($r_s = 0.38$, $P < 0.01$). Higher values of TWI (≥ 9) are mainly associated with areas having clayey mineral soils (Figure 3.4). Stratification of the whole dataset by surficial deposits slightly reduced OLT variability within the clay, till and bedrock. Coefficients of variation are 0.42, 0.40, and 0.30, respectively, but stratification was less successful in improving correlation coefficients between individual topographic variables and organic layer thickness. In fact, OLT distribution at the landscape scale could obviously not be explained by simple bivariate relationships between OLT and individual predictor variables. In addition, the higher coefficient of variation for the whole OLT dataset (CV = 0.58) suggested a strong interaction between the different predictor variables and the spatial distribution of organic layer thickness. To reduce this variability in the whole dataset, a quantitative subdivision of the landscape into new datasets covering smaller and more homogeneous areas was undertaken.

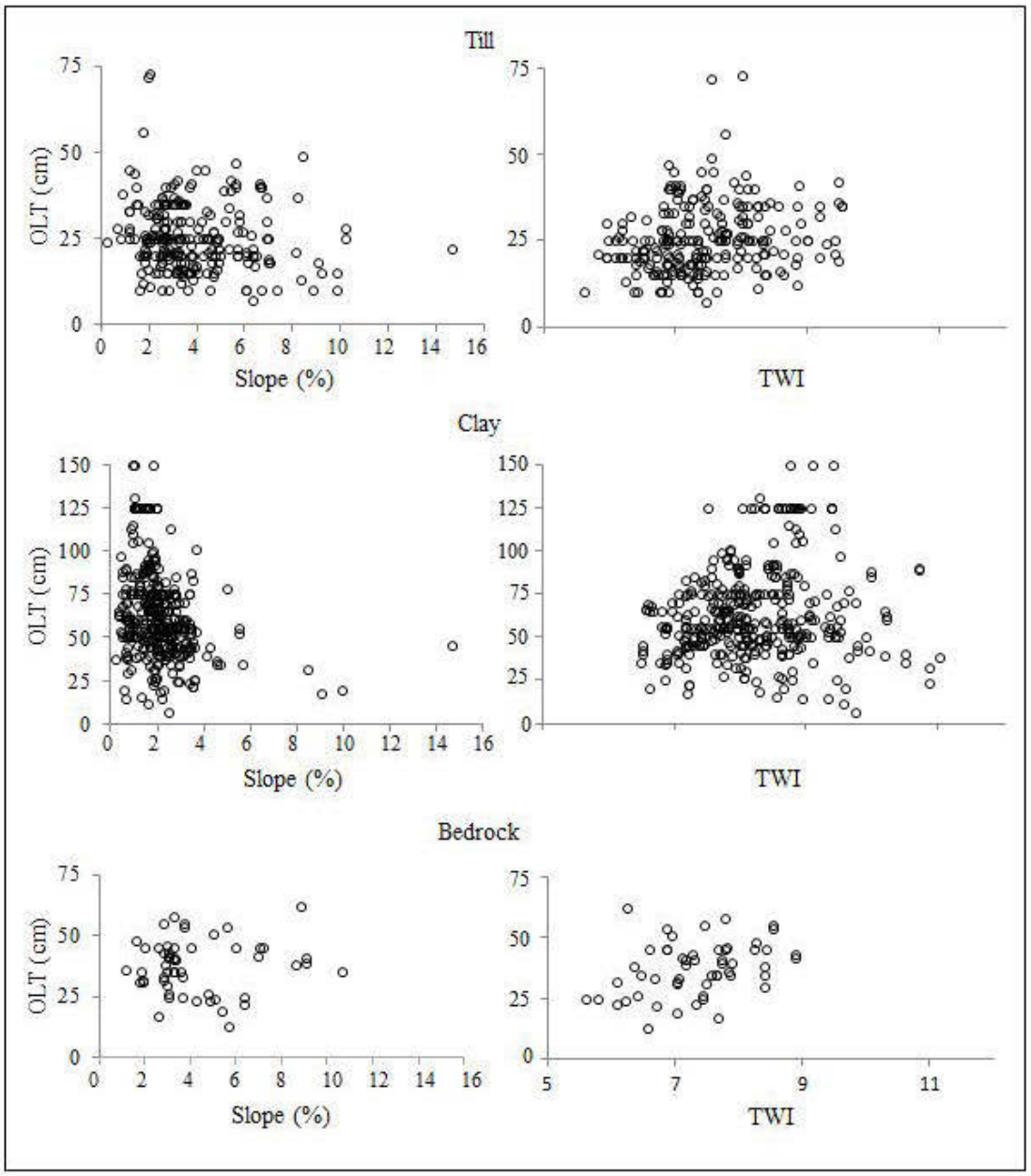

Figure 3.4. Relationship between organic layer thickness and selected topographic variables for the three different surficial deposits (Till, Clay and Bedrock).

3.3.2. Regression tree-based model evaluations

Results for the regression tree-based models that we developed using only mineral soil topographic variables (Model 1) and all the predictor variables (mineral soil topography and surficial deposits; Model 2) are illustrated in Table 3.3 and Figures 3.5 and 3.7. Table 3.3 summarises the statistics obtained during model building and the regression tree criteria used in predicting OLT for regression tree-based models 1 and 2. Each of the 653 sampling locations were assigned to one of the resulting landscape units (A to F for model 1; A to J for model 2). In both models, the predictor variables that were used to generate the splits were mineral soil slope, surficial deposits, TWI and aspect. These four variables alone were important in predicting OLT over the landscape (Figures 3.5, 3.7 and Table 3.3). Mineral soil curvature variables (mean curvature, plan curvature and profile curvature) were not found to contribute to the development of either regression tree-based model, suggesting that they did not play a role in controlling OLT at the landscape scale.

3.3.2.1. Regression tree-based model 1

Model 1, based on topographic variables only, resulted in six landscape units and had a prediction quality of R^2_{adj} = 0.34, r = 0.58 and $RMSE$ = 23 (Table 3.3). In model 1, the first node at which the entire dataset was initially subdivided into two groups, was based on slope $\leq$ 2% versus slope > 2%. This resulted in areas of higher and lower organic layer thickness, respectively. Areas with slopes $\leq$ 2% were further subdivided at a second node into two landscape units (A and B, with mean organic layer depths of 43 cm and 68 cm, respectively), based on a TWI threshold value of 7 (Table 3.3). Within areas with slopes > 3.5%, organic layers were deeper on north- and east-facing slopes (landscape unit D) compared to south- and west-facing areas (landscape units E and F) (Figure 3.5, Table 3.3). Moderate OLT were found for areas with slopes > 2% and $\leq$ 3.5% (Landscape unit C; mean OLT = 41 cm). These results supported our hypothesis that mineral soil topography has a significant influence on the spatial distribution of OLT. The predictive thematic map of landscape units (Figure 3.6), indicated that 46.8% (33.6 ha) of the investigated area correspond to the high paludification category (landscape unit B), 43.4% (31.2 ha) to the moderate ones (landscape units A, C and D), and 9.8% (5.7 ha) to the non-paludified category (landscape units E and F) (Table 3.4). The confusion matrix between the measured paludification categories and the modelled ones

showed a good overall accuracy of 74% of the sites (Table 3.4). The highly paludified category had the highest producer's accuracy (83%) followed by moderate and null categories with 74% and 57%, respectively (Table 3.4).

Table 3.3. Regression tree-based models that were used in this study to explain organic layer thickness and their statistics.

Model	Terminal Landscape unit splits	*n*	Mean (cm)	*r*	R^2_{adj}	RMSE
Model 1				0.58	0.34	23
	A) Slope ≤ [2%]**, TWI ≤ [7]*	32	43			
	B) Slope ≤ [2%]**, TWI > [7]*	234	68			
	C) Slope>[2%]**, Slope ≤ [3.5%]**	240	41			
	D) Slope > [3.5%]**, Aspect [N&E]**	46	41			
	E) Slope > [3.5%]**, Aspect [S] †	78	21			
	F) Slope > [3.5%]**, Aspect [W] †	23	25			
Model 2				0.72	0.52	19
	A) Slope ≤ [2%]**, SurfDep [Till]**	39	26			
	B) Slope ≤ [2%]**, SurfDep [Clay]*	220	71			
	C) Slope ≤ [2%]**, SurfDep [Bedrock]*	7	37			
	D) Slope > [2%]**, SurfDep [Till]**, TWI ≤ [7]**, Aspect [N&E]**	18	35			
	E) Slope > [2%]**, SurfDep [Till]**, TWI ≤ [7]**, Aspect [S&W]**	102	20			
	F) Slope > [2%]**, SurfDep [Till]**, TWI > [7]**	77	28			
	G) Slope > [2%]**, SurfDep [Clay]**, Slope ≤ [3.7%]†	130	53			
	H) Slope > [2%]**, SurfDep [Clay]**, Slope > [3.7%]†	13	39			
	I) Slope > [2%]**, SurfDep [Bedrock]**, TWI ≤ [7] †	27	34			
	J) Slope > [2%]**, SurfDep [Bedrock]**, TWI > [7] †	20	43			

**, * and † statistically significant at $P < 0.001$, $P < 0.01$ and $P < 0.05$, respectively. *r* refers to correlation between measured and predicted values. Mean refer to mean organic layer thickness. RMSE = root mean square error. SurfDep refers to surficial deposit. N, E, S and W indicate north, east, south and west aspect directions, respectively.

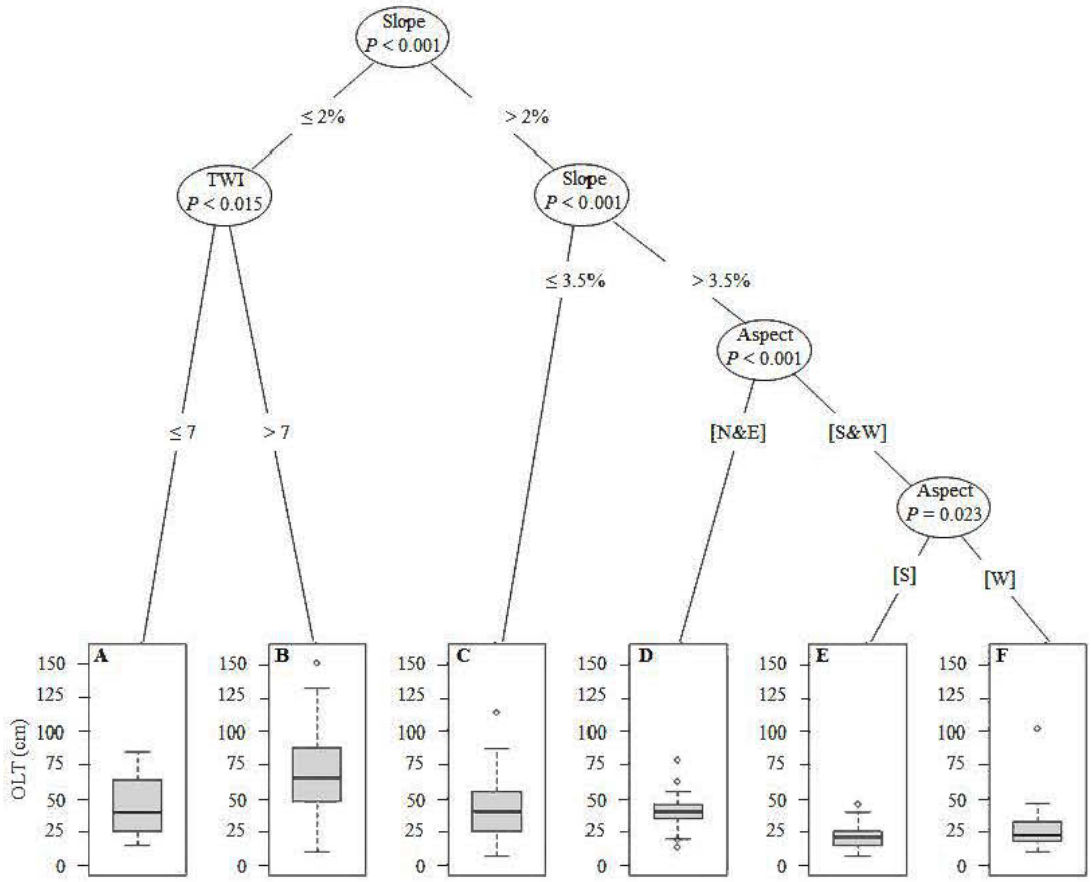

Figure 3.5. Graphical representation of the regression tree model 1 in Table 3.3. The distribution of OLT in the resulting landscape units nodes (A to F) is visualised via box and whisker plots. The lower and upper edges of the box represent the 25th and 75th percentiles, and the median is represented by the bar in the middle of the box. The whiskers showed the largest and smallest values, and outliers are represented by individual points.

Table 3.4. Accuracy assessment and related statistics of map prediction of the landscape units, based on regression tree model 1.

Landscape units	Area		OLT (cm)	Paludification Category	Area		Producer's accuracy	Overall accuracy
	%	ha			%	ha		
A	46.8	33.6	68	High	46.8	33.6	83%	
B	2.5	1.8	43	Moderate				
C	29.5	21.2	41	Moderate	43.4	31.2	74%	
D	11.4	8.2	41	Moderate				74%
E	8.0	5.7	21	Null	9.8	7.0	57%	
F	1.8	1.3	25	Null				

OLT: mean organic layer thickness. Overall accuracy is computed by dividing the total correctly classified sites on the map by the total number of sites in the confusion matrix. Producer's accuracy indicates the probability of a field measurement site being correctly classified on the map (measure of class accuracy).

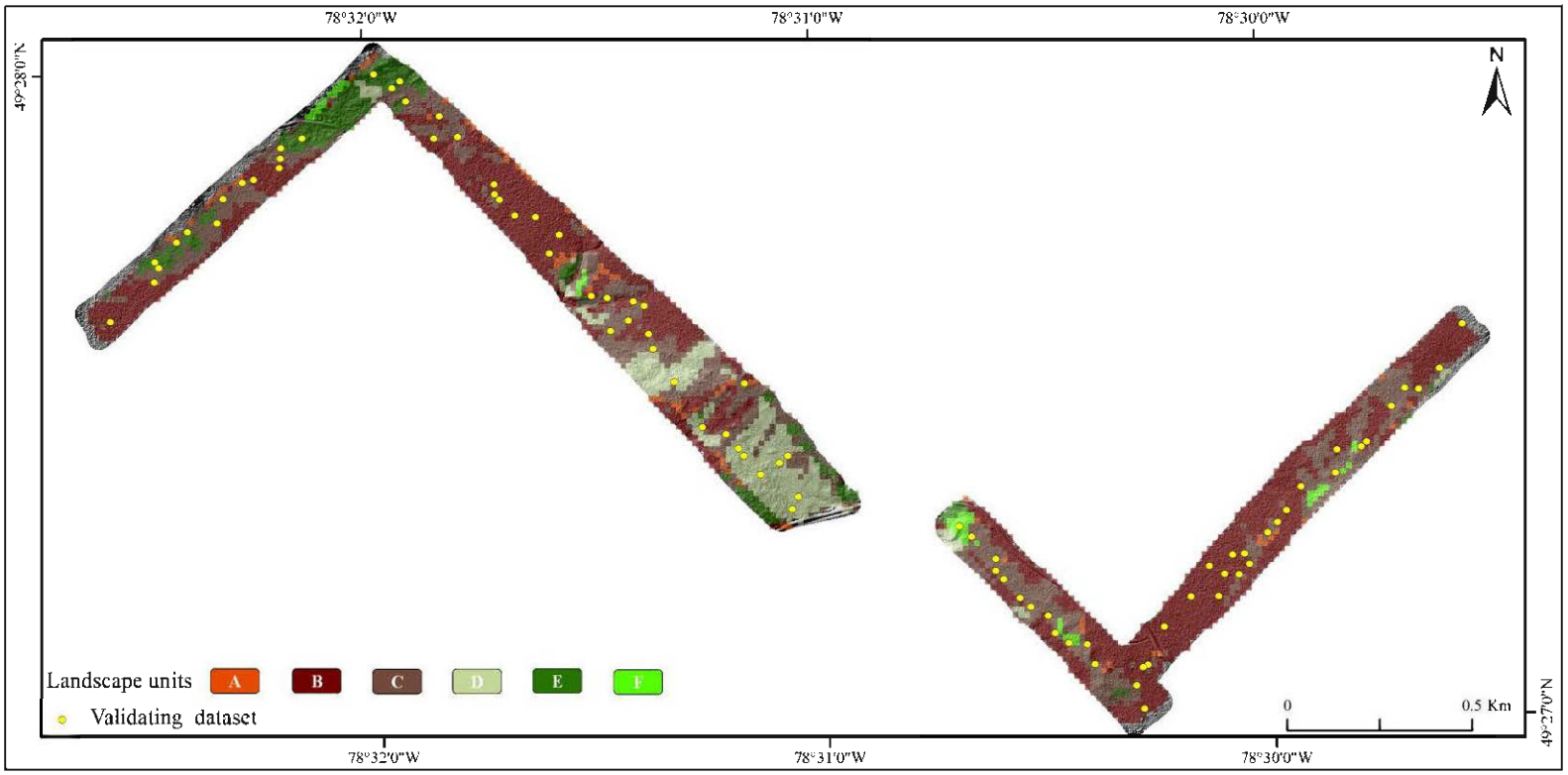

Figure 3.6. Map showing the distribution of the landscape units in the study area based on regression tree model 1 in Table 3.3.

3.3.2.2. Regression tree-based model 2

Model 2, based on all predictor variables, showed a substantial improvement in prediction quality (R^2_{adj} = 0.52, r = 0.72 and *RMSE* = 19; Table 3.3). The number of resulting landscape units was higher compared to model 1 and, consequently, some landscape units had few observations (i.e., Landscape units C and H in Table 3.3 and Figure 3.7). The highest OLT was found on clayey surficial deposit with slopes between 2 and 3.7% (landscape units B and G with mean organic layer thicknesses of 71 cm and 53 cm, respectively), whereas shallow OLT (non-paludified) was associated with south- and west-facing areas situated on till, with slopes > 2% and TWI ≤ 7 (landscape unit E with mean OLT of 20 cm). Lower OLT was found on bedrock with slope ≤ 2% and slope > 2% (Landscape units C and I with a mean OLT of 34 cm and 37 cm, respectively) and on till (Landscape units A, F and H with a mean OLT of 26 cm, 28 cm and 39 cm, respectively). Areas on bedrock with slope > 2% were most effectively subdivided on the basis of the TWI into lower and moderate OLT landscape units (I and J, respectively) (Table 3.3 and Figure 3.7). The moderate OLT unit was associated with a higher TWI (> 7) suggesting that landscape unit J represents zones of soil water saturation.

3.4. DISCUSSION

3.4.1. Individual relationship trends

The negative correlation between OLT and mineral soil slope indicated that the organic layer tended to be shallower in areas with high slopes and deeper in areas with low slopes. Similar results were found in other studies on ground surface slopes (i.e. Laamrani *et al.*, 2013b; Simard *et al.*, 2009).

Higher values of TWI are mainly associated with clayey mineral soil areas, which are the best candidates for high soil moisture content and water accumulation. These results are similar to those of other studies that found moisture-saturated sites were the most highly paludified areas (Fenton *et al.*, 2005; Lavoie *et al.*, 2005). When compared to a previous study that was conducted at the surface by Laamrani *et al.*, (2014a), relationships between mineral soil aspect and OLT had similar trends. In contrast to the previous study, convex and concave mineral soil curvature variables (mean curvature, plan curvature and profile

curvature) were found to be greater and more statistically significant compared to those computed at the ground surface, presumably because of depressional features that were revealed in the mineral soil topography.

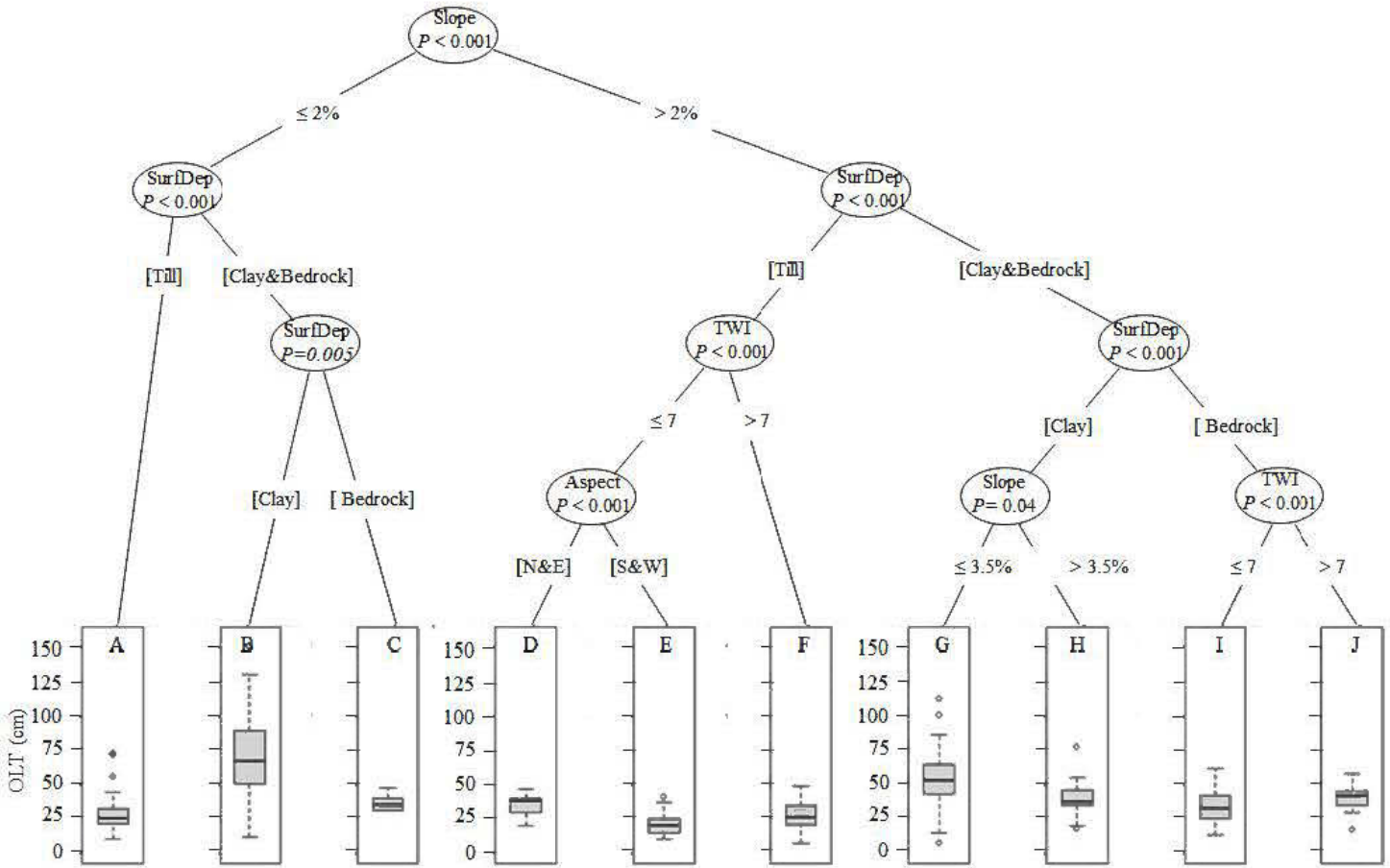

Figure 3.7. Graphical representation of regression tree model 2 with the distribution of organic layer thickness in terminal nodes (A to J) visualised via box plots. Description of each component of the box and whiskers plot is given in Figure 3.5.

3.4.2 Regression tree-based modelling approach

Mineral soil slope was involved in all landscape unit subdivisions in both models (1 and 2) and was the first level of splitting (Fig 5 and 7), suggesting that OLT was largely controlled by the mineral soil slope at the landscape level. Alone, mineral soil slope explained 28% of the variation in the whole dataset (not shown). In addition to confirming the importance of mineral soil slope effects on OLT at the landscape scale, which had been previously reported for the surface layers within the Clay Belt (i.e., Giroux *et al.*, 2001; Laamrani *et al.*, 2013b; Simard *et al.*, 2009), our study also quantified the threshold (2%) at which mineral soil slope could be used to discriminate units with deeper versus moderately shallow organic layers. Furthermore, for model 1, a slope threshold 3.5% seemed to represent a cutpoint for discriminating between paludified and non-paludified areas.

This study showed that higher OLT was found on north- and east-facing slopes (lower exposure to solar radiation). The higher OLT might be explained by the fact that north- and east-facing areas are colder and allow more *Sphagnum* moss to accumulate. This finding was similar to what was reported for the ground surface by Johnson et al (2009). In contrast to our results, Laamrani *et al.*, (2013b) found higher organic layer to accumulate on southwest-, west- and northwest facing slopes (see map of OLT, Figure 7 in Laamrani *et al.*, 2014a).

Despite the significant correlations found between OLT and individual stratified curvature variables, the latter were not involved in any prediction of the OLT distribution through either regression model. One possible reason that could explain why curvature variables effect was masked is that the variation in the mineral soil curvature, at the local scale, was too small to be captured by the 15 m-resolution digital model.

Surficial deposits and TWI also contributed to the landscape unit partitioning for both regression tree models. Therefore, under conditions where slopes were $\leq 2\%$, clayey surficial deposit and TWI > 7, models 1 and 2 resulted in a homogeneous unit (B), representative of high paludification conditions. Landscape units B for both models seem to represent areas with conditions that may be less favourable for tree growth since the presence of thick organic layer combined with wet conditions on flat terrain is expected to limit tree establishment and productivity (Lavoie *et al.*, 2007); this was supported by an on-going study

that deals with the effect of organic layer thickness and slope on forest productivity (Laamrani *et al.*; under review). They found that in average, landscape unit B showed the lowest stand volumes, estimated for trees with diameters at breast height (dbh) greater than nine cm, with 83 m^3/ha and 80 m^3/ha for models 1 and 2, respectively. In addition, evidence from field observations, together with Figure 3.6 and aerial photos, indicated that landscape unit B most likely occur in both permanently and non-permanently paludified areas.

The TWI threshold of 7 was also used as splitting rule in model 2 to discriminate between low (landscape unit I) and moderately (landscape unit J) paludified bedrock with slopes > 2%. Our field observations and Figure 3.6 indicated that most of the sampling points in landscape unit J (higher TWI values) were located in topographic depressions at mid-slope (i.e., concave bedrock irregularities). This was consistent with other studies, which found that TWI describes the distribution and extent of soil moisture zones; the largest values were predicted in topographic hollows at higher elevation (Bou Kheir *et al.*, 2010); and therefore, TWI could be used as a means of delineating and classifying landforms (Burrough *et al.*, 2000; MacMillan *et al.*, 2000). In addition, the lack of correlation between bedrock slope and OLT (r_s = 0.03, P = 0.82, Table 3.3) was presumably related to these bedrock irregularities. These topographic conditions favour high moisture resulting in organic layer accumulation, the development of a deeper organic layer (paludification) that is mainly composed of a thick Of horizon (Laamrani *et al.*, 2013; Lafleur *et al.*, 2010; Lavoie *et al.*, 2007), and are most likely specific to permanent paludification sites. We expected that these depressions would affect many of measured surface properties such as water movement in the near surface organic soil horizon, water infiltration, tree establishment and productivity.

Overall, the model that was based only on mineral soil topography explained 34% of the variation in the dataset. The model that was based on mineral soil topography, together with surficial deposits, had the greatest predictive power (R^2_{adj} = 0.52). For most spatial models, coefficients of determination (R^2) $\leq$ 0.5 are common, whereas R^2 values that are greater than 0.7 are unusual (Dahlke *et al.*, 2009). For both of our models, TWI made a significant contribution to estimating moderate to highly paludified landscapes, since it is a predictor of zones of saturation, and thick organic layers often accumulate in lowlands. Except for landscape unit J, which was assigned to the permanent paludification type in this study, both

models were unable to further subdivide landscape units (i.e., landscape unit B) into reversible and permanent types. This suggested that both factors (time and topography) interact together. Both models (i) produced simpler models that were easier to understand, (ii) represented landscape units that were meaningful in terms of the physical processes of OLT variability and distribution, and (iii) consisted of a small number of rules. Model 1 could be easily and quickly implemented for making predictions whenever a DEM is available with OLT measurements (Figure 3.6), but model 2 can only be used in situations where spatial information on surficial deposits (clay, till, bedrock) exist, which is not the case in most of the Forest inventory maps.

3.4.3. Management implications

The results of this study are important for landscape management for several reasons:

(1) Understanding how surface topography is related to OLT is an important first step in predicting and mapping forest productivity across landscapes. This information will aid the forest managers in predicting potential saturation zones, where an organic layer often accumulates and will help them to adopt the appropriate forest management practices (i.e., field preparation treatments and replanting). For example, TWI is simple in concept, easily defined, and provides an intuitive notion of wetness. Consequently, it can be used to better manage forest resources where high soil moisture limits productivity.

(2) In order to maintain or improve forest productivity in the Clay Belt region, management strategies should focus on sloping sites (i.e., > 2.3%) rather than on almost flat sites (≤ 2%) that are associated with deep organic layer. The latter are often not suitable for tree plantations (Lafleur *et al.*, 2010), provide few ecological or economic motives to manage soils with low slopes (Simard *et al.*, 2009), and are expected to limit the use of equipment that would be required for mechanical site preparation and harvesting within the highly paludified areas (Lavoie *et al.*, 2007).

(3) This study is part of a larger project that deals with the effects of environmental variables and forest harvesting on paludification and was conducted prior to implementation of recent forest management prescriptions (harvesting, site preparation, and planting). Therefore, the results and data from this study could be used to determine the long-term

impact of forest management practices (i.e., forest harvesting, field preparation treatments, and replanting) on the original organic layer properties.

(4) Results from this study have demonstrated that mineral soil topography has a significant influence on the spatial distribution of OLT and that these relationships can be used for partitioning the landscape and, therefore, can help in future planning of landscape management. For instance, they can be used for defining (i) promising areas where efforts and investments should be made to obtain higher productivity after logging and planting and (ii) vulnerable areas where structure and biodiversity of paludified forest can be preserved.

3.5. CONCLUSIONS

To our knowledge, this study was the first to link topographic variables that were extracted at the surface of the mineral soil to different degrees (representing organic layer thickness) and types of paludification at the landscape-scale. The analysis of topography at the mineral soil surface within the Clay Belt region demonstrated correlations between individual topographic variables (slope, aspect, TWI), surficial deposits and organic layer thickness. These correlations were found to be relatively weak, and indicated that, at the landscape scale, OLT and its distribution cannot be adequately explained by simple bivariate relationships. Consequently, two regression tree-based models (models 1 and 2) were developed in this study and provided insight into set of predictor variables that are most important for OLT distribution. Mineral soil slope, TWI and aspect proved to be highly correlated with OLT for both models. Model 1 based on mineral soil surface topography explained 34% of the variation in organic layer thickness, whereas model 2 based on mineral soil surface topography and surficial deposits explained 52%.

Regression tree Model 1 allowed the combination of different maps (slope, TWI and aspect) for producing a landscape unit map, upon which OLT was determined and related to increasing paludification categories. A good overall accuracy of 74% was achieved for the resulting model 1 map. One of the most important finding that was revealed by model 2 indicated that bedrock irregularities (i.e., depressions) modified topographic control of wetness and promoted the advancement of permanent paludification. Except for landscape unit J, which was assigned to the permanent paludification type, both models were unable to

further subdivide the resulting landscape units (i.e., landscape unit B) into reversible and permanent types. Future work will focus on the use of additional topographic variables (i.e., topographic slope position) and other remote sensing techniques (i.e., automated classification) to discriminate between the two categories of paludification (reversible and permanent) within a larger LiDAR covered area (100 km^2).

CHAPITRE IV

MAPPING PERMANENT AND REVERSIBLE PALUDIFICATION IN BLACK SPRUCE FORESTS, CANADA USING REMOTE SENSING AND GIS-BASED AUTOMATED CLASSIFICATION.

Ahmed Laamrani[1], Osvaldo Valeria[1], Yves Bergeron[1], Nicole Fenton[1], and Li Zhen Cheng[2]

[1] Chaire industrielle CRSNG-UQAT-UQAM en aménagement forestier durable, Institut de recherche sur les forêts et Centre d'étude sur la forêt.
Université du Québec en Abitibi-Témiscamingue. 445 boul. de l'Université, Rouyn-Noranda, Québec J9X 5E4, Canada.

[2] Institut de recherche en mines et environnement (IRME), Université du Québec en Abitibi-Témiscamingue. 445 boul. de l'Université, Rouyn-Noranda, Québec J9X 5E4, Canada.

Article soumis à Geoderma

ABSTRACT

Northern Canadian boreal forest is characterised by accumulation of a thick organic layer (paludification). Two types of paludification are recognised on the basis of topography and time since the last fire, viz., permanent paludification that dominates in natural depressions within the landscape, and reversible paludification that occurs on flat or sloping terrain over time following fire or mechanical site preparation. Accurate information about the occurrence of permanent or reversible paludification is required for land resource management. Such information is useful for the identification of locations of existing paludified areas where investment after harvesting should help to achieve greater productivity. This study investigated the potential for using a semi-automated method that was based on geomorphological analysis to map and differentiate between the two paludification types at the landscape scale within the Canadian Clay Belt region. Slope, topographic position index (TPI), and topographic wetness index (TWI) were generated from a LiDAR digital terrain model. TPI and TWI are predictors of surface morphology (i.e., depressions vs flat areas) and moisture conditions (i.e., wet vs dry) respectively, and were used to explain paludification processes. A semi-automated classification method based on TPI and slope was firstly used to create six initial topographic position classes: deep depressions, lower slope depressions, flat surfaces, mid-slopes, upper slopes, and hilltops. Each of these six classes was then combined with TWI classes (representing moisture conditions, wet, moderately wet, and dry) and this combination assisted in assigning each resulting class to one of the two paludification types. Slope and TWI values also assisted in subdividing the lower slope depression class was split, based on slope, into significantly different sub-classes, namely open and closed depressions (Tukey's HSD, $P < 0.001$). The distribution of field data (e.g. tree basal area, organic layer and fibric horizon thicknesses) within each position class provided additional information to corroborate the assignment of each class to a defined paludification type. The proposed semi-automated classification provided a relatively simple and practical tool for distinguishing and mapping permanent and reversible paludification types with an overall accuracy of 74%. The tool would be particularly useful for implementing strategies of sustainable management in boreal remote areas where field survey information is limited.

Keywords: Paludification; Black spruce forests; Topographic wetness index; Topographic position index; LiDAR; Clay-Belt.

RÉSUMÉ

La forêt boréale nordique du Canada est caractérisée par l'accumulation d'une couche organique épaisse (paludification). On reconnaît actuellement l'existence de deux types de paludification sur la base de la topographie et du temps depuis le dernier feu, à savoir la paludification permanente et réversible. Théoriquement, les deux types de paludification se produisent dans différents endroits à l'échelle du paysage. La paludification permanente se produit dans des endroits où les conditions d'humidité du sol sont élevées et les reliefs plats ou dans des dépressions topographiques, alors que la paludification réversible intervient dans des sites à pente faible ou moyennement forte au fil du temps en réponse à une perturbation telle qu'un feu peu sévère ou une préparation mécanique du site. Des informations précises sur la distribution spatiale des deux types de paludification (permanente et réversible) à l'échelle du paysage sont nécessaires pour l'aménagement des ressources forestières dans des zones paludifiées dans le but d'obtenir une plus grande productivité après des travaux sylvicoles. Le but de cette étude est d'identifier les variables topographiques permettant de distinguer et de cartographier la paludification réversible et permanente à l'échelle du paysage dans la région canadienne de la ceinture d'argile. Pour atteindre cet objectif, nous avons utilisé une approche semi-automatique de subdivision du territoire à l'étude en des entités du paysage distinctes en combinant des données topographiques, notamment l'indice topographique de position (TPI), l'indice topographique d'humidité (TWI) ainsi que la pente de surface extraits de données LiDAR (MNT). Cette méthode semi-automatisée de classification sous SIG a permis de créer six classes avec différentes positions topographiques : (1) les dépressions profondes, (2) les dépressions dans les bas de pentes, (3) les surfaces planes, (4) les mi-pentes, (5) les hauts de pentes, et (6) les hauts des collines. Cette approche s'est révélée efficace, car elle a permis de délimiter des entités possédant des caractéristiques géomorphologiques semblables, notamment en terme de susceptibilité à l'accumulation de la couche organique, et par conséquent ont été assignées à l'un ou l'autre type de paludification, soit réversible ou permanente. Un autre apport majeur de ce méthode est la mise en évidence de deux nouvelles sous-entités statistiquement différentes (le test *HSD de Tukey*, $P < 0,001$), à savoir des dépressions ouvertes préférentiellement drainées (paludification réversible) et des dépressions fermées potentiellement engorgées (paludification permanente) du fait de leurs positions topographiques (pente et TPI) et conditions d'humidité (TWI). Cela rend l'outil développé particulièrement utile pour la mise en œuvre des stratégies d'aménagement durable dans les forêts paludifiées.

4.1. INTRODUCTION

Accumulation of a thick organic layer over time is a characteristic of the northern boreal forest regions such as the interior of Alaska, the Canadian Hudson Bay- James Bay lowlands, and the western Siberian plain. This accumulation is mainly attributed to the natural process of paludification, which is generally thought to create wetter conditions that lead over time to a reduction in soil temperature, decomposition rates, microbial activity, nutrient availability, and canopy openings (Crawford *et al.*, 2003; Lavoie *et al.*, 2005; Vygodskaya *et al.*, 2007). Paludification can be regarded as an important factor that causes substantial losses in productivity in the boreal forest and, consequently, potential sources of wood fiber. Paludification is particularly problematic in the forested landscape of the Clay Belt, a region of the Canadian Hudson Bay- James Bay lowlands, where this process has contributed to the transformation of many productive forested areas into non-productive forested peatlands. Within the Clay Belt region, ground surface topography and time-since-last fire have been considered as the two major drivers of paludification (Fenton *et al.*, 2009). Consequently, permanent (also called edaphic or paludification of wet depressions in Payette and Rochefort 2001) and reversible paludification (or successional in Simard *et al.*, 2009) are two types of paludification that can be recognised. Within the landscape, permanent paludification dominates in natural depressions, which have wetter soil conditions that favour organic layer build-up. Reversible paludification occurs on flat or sloping terrain, where a feather moss-dominated bryophyte layer is replaced over time by *Sphagnum* species (Boudreault *et al.*, 2002; Fenton and Bergeron 2006), starting at approximately 100 years after fire (Fenton and Bergeron 2006; Simard *et al.*, 2007). On one hand, reversible paludification may be reversed through natural severe fire or a combination of silvicultural practices and site preparation, as detailed by Fenton *et al.*, (2009). On the other hand, permanent paludification can be considered as an irreversible condition.

A number of studies have dealt with various aspects of either one or the other type of paludification within the black spruce forests of the Clay Belt (Fenton *et al.*, 2005; Lavoie *et al.*, 2005; Simard *et al.*, 2009; Thiffault *et al.*, 2013). Yet very little research has been concerned with the spatial distribution of these two paludification types across larger areas (Laamrani *et al.*, 2014b; Lavoie *et al.*, 2007). Mapping the occurrence of these areas

(reversible and permanent) at the landscape scale is critically important for land managers and decision makers, if they are to implement appropriate management practices. For effective management of the black spruce forests in the Clay Belt, accurate spatial maps that can identify the two paludification types are needed. Such maps could be used to identify promising areas where efforts and investments should be made to obtain higher productivity after logging or identify retention areas to maintain structural attributes and habitats. However, the challenge of landscape classification is to find the terrain attribute that can potentially most easily differentiate between both paludification types.

Remote sensing systems have become an important source of elevation data, Light Detection And Ranging (LiDAR) data in particular. LiDAR is an active remote sensing technique that can capture topographic features with high vertical and horizontal precision, making it a practical technology for landscape analysis (Southee *et al.*, 2012). In other words, LiDAR data has the potential to provide information on surface morphology (e.g., flat areas vs depressions) and wetness conditions (e.g., wet vs dry), which are intuitively important for discriminating between reversible and permanent paludification types (Laamrani *et al.*, 2014a). Topographic position and topographic wetness indices, generated from LiDAR, were used in this study, as we presume that they are closely related to both permanent and reversible paludification process. Many studies have found that the use of these indices is a powerful approach for landscape classification forested environments (Emili *et al.*, 2006; Laamrani *et al.*, 2014a; MacMillan *et al.*, 2007; Pierce *et al.*, 2012; Tchir *et al.*, 2004; Weber 2011). While there are a large number of methods and algorithms that have been devised to classify the landscape into morphological classes (e.g., Clark *et al.*, 2009; Creed and Beall, 2009; Lindsay and Creed, 2005), most of these methods have been developed largely for non-forestry applications (e.g., hydrology) and, in almost all cases, did not address the characterization of depressions. In the few studies that aimed to distinguish depressions from other landscape classes (i.e. flats areas vs depressions; Lindsay and Creed, 2005), the approaches and algorithms that were used were complicated and very time-consuming; moreover, their implementation and interpretation often required a solid statistical background. To avoid these problems and allow this work to be ultimately used by resource managers, the method that was to be selected for this study had to be relatively simple to implement, automated or semi-automated, feasible in a GIS environment and applicable to

other areas. The objective of this research was to investigate the potential of using a semi-automated landscape classification method based on the chosen topographic indices to distinguish and map reversible and permanent paludification in the black spruce forests of the Clay Belt. This distinction was corroborated by field data.

4.2. STUDY AREA

The study area is located within the western black spruce feathermoss bioclimatic domain (Robitaille and Saucier 1998). More precisely, our site was situated in the Clay Belt region, which is a vast conifer-dominated area that spans the Ontario-Quebec border (Figure 4.1a). The dominant landforms in the area are flat plains, which were generated by extensive and thick glaciolacustrine clay deposits that were left behind by pro-glacial Lake Ojibway (Veillette, 1994). Bedrock outcrops and gentle hills are also found within the Clay Belt region. The site being studied covered 720 ha of boreal forest land in which elevation ranges from 278 m to 315 m, averaging 304 m above sea level. Ground surface slope ranges from 0.0 to 34.3%; about 65% of the area has a slope $\leq$ 3.2%, whereas slopes $\geq$ 16.3% represent about 1% of the area. Many drainage courses run locally in a southwestern direction through the study area to produce a relatively complex topographic pattern (Figure 4.1b). Mean annual temperature is -0.7° C, and total annual precipitation is 906 mm (Environment Canada 2011; Matagami weather station, about 60 km NE of the study area).

Black spruce (*Picea Mariana* [Mill.] BSP) and jack pine (*Pinus banksiana* Lamb.) dominate stands in the study area, making up 79% and 16% of the canopy respectively. These species are followed by trembling aspen (*Populus tremuloides* Michx), which covers about 4% of the study area. The remaining 1% is covered by tamarack or eastern larch (*Larix laricina* (Du Roi) K. Koch), balsam fir (*Abies balsamea* (L.) Miller) and paper or white birch (*Betula papyrifera* Marsh). The forest floor is composed of *Sphagnum* spp., feather mosses (principally *Pleurozium schreberi* (Brid.) Mitten), and shrubs, (mainly dwarf ericaceous species), with variable coverage across the landscape.

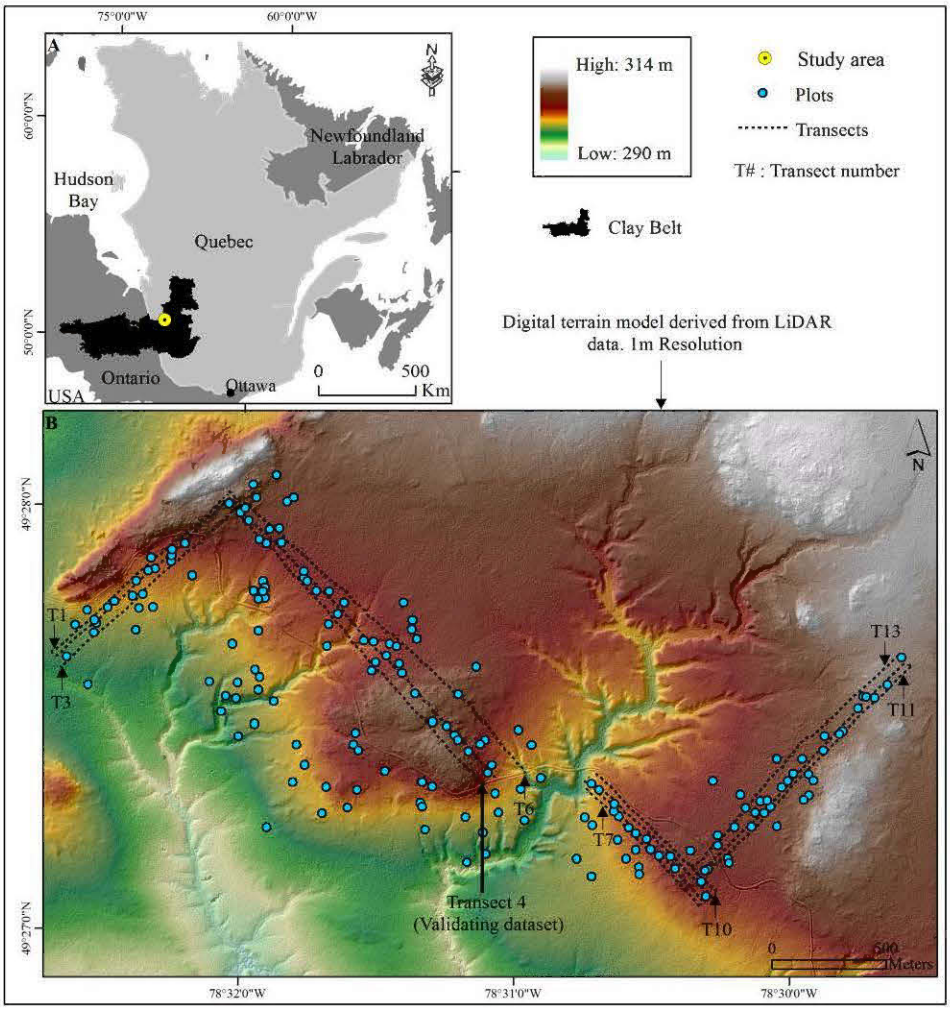

Figure 4.1. Study area location within the Clay Belt of Ontario and Quebec (A). Topographic overview of the study area showing field sampling points along transects and plots (B). This figure is available in color online.

4.3. MATERIALS AND METHODS

4.3.1. Digital terrain model and derived topographic variables

The study area was surveyed on 28 May 2010 using a multipulse ALS50-II Airborne Laser Scanner (Leica Geosystems, Aarau, Switzerland). LiDAR data was collected over an area of about 100 km^2 with a high precision (2.8 points/m^2) and vertical accuracy (RMSE of 0.065 cm). LiDAR raw data, which were provided in LAS format, were pre-processed by separating canopy pulse returns from ground pulse returns. The last returns that were classified as ground surface were interpolated with 0.5 m resolution and gridded at a 10 m resolution to produce a digital terrain model (DTM). Since the major aim of the DTM was to identify topographic features at the landscape scale, we considered an interpolated grid resolution of 10 m as adequate to represent those features. Laamrani *et al.*, (2014a) have found that DTMs with 10- and 20-m resolution are of a suitable size to capture the topography at the area being studied and in the context of characterizing a paludified area. For the purposes of this study, slope, elevation, topographic position index, and topographic wetness index grids were created from DTM using standard procedures in ArcGIS 10 (ESRI, 2011) (Table 4.1). These resulting grids were then intersected with a field samples' layer information (point locations) and corresponding parameters (topographic variables and field datat information) were extracted for each sampling location. Positions of all field sampling locations were recorded using GPSs with mm/cm-level positioning accuracy to allow for direct comparison with the DTM.

4.3.2. Field datasets collection

Field data were collected during the summer 2010 along a series of transects and within plots (Figure 4.1b). Thirteen sub-parallel transects, totaling 15 km in length, with nested sampling points were established across the landscape, with a minimum distance of 20 m between transects. Sampling points were established at 10-m intervals along each transect. At every sampling point, the organic layer thickness was measured by probing with an auger following Laamrani *et al.*, (2014a,b). Additionally, 178 circular plots of 400 m^2 were randomly distributed between and outside of transects; these encompassed different forest types and topographic positions. In each of the 178 plots, a pit was dug and depth to mineral

soil (representing total organic layer thickness) and the thickness of each individual soil horizon (fibric, mesic and humic) was recorded. In each plot, forest composition and structure data, such as species composition, diameter at breast height (dbh, 1.3 m) and tree height (m), were recorded and used to calculate basal area (m^2/ha) as a productivity indicator. Overall, the field dataset consisted of three groups, one group for topography/organic layer-terrain relationships (1380 points; corresponding to sampling points at 10-m interval along transects, the second group for the vegetation/soil–terrain relationships (178 points; corresponding to plots) and the third group for validation of the produced maps (170 points; transect #4 in Figure 4.1b).

Table 4.1.Topographic variables created from 10-m-resolution LiDAR- derived digital terrain model.

Topographic variables	Description
Elevation (m)	Refers to the altitude above sea level and was derived from the digital terrain model (DTM)
Slope (degree)	Identifies the slope (gradient, or rate of maximum change in z-value) from each cell of used the DTM
Topographic Wetness Index (TWI)	Accounts for the propensity of a site to be wet or dry. The higher the value of the TWI in a cell, the higher the soil moisture and water accumulation that can be found on it.
Topographic Position index (TPI)	TPI measure is the difference between a cell's elevation and the average elevation of surrounding cells within a specific radius distance. Positive and negative values tend towards hilltops and depressions respectively, whereas zero or near-zero values tend toward flat and mid-slopes areas.

4.3.3. Topographic position index and classification

The topographic position index (TPI) is the difference between a central cell elevation value and the average elevation of the neighbourhood around that cell. Neighbourhood refers to all grid cells whose cell centers lie within a defined radius distance of the central cell. Negative TPI values indicate that the central cell is lower than its surroundings, whereas positive TPI values mean that it is higher than its average surroundings. TPI values of zero and near-zero indicate that the central cell is close to the mean elevation of the neighbourhood (Jenness *et al.*, 2011; Weiss 2001). Since TPI represents a measure of surface morphology (Tagil and Jenness (2008), its values have the potential to provide a simple and powerful means to classify the landscape into topographic position classes.

In this study we applied the semi-automated method of Weiss (2001) that classifies the landscape into discrete topographic position classes using the standard deviation of TPI and slope. Following this classification scheme, logically the high TPI values would be found in higher terrain positions (e.g., hilltops) while low TPI values would be found in lower terrain positions (e.g., depressions). As for many other studies, the choice of a neighbourhood size for this study was based on an iterative process in which several neighbourhood sizes were tried until the generated output that best corresponded with the study area topographic reality was found (50 m in our case; Figure 4.2a). Therefore, in this study, the TPI grid with a neighbourhood size of 50 m was used to generate six topographic position classes named deep depressions, lower slope depressions, flat surfaces, mid-slopes, upper slopes, and hilltops. The six classes were generated using the Weiss's classification criterion and the *Land Facet Corridor Tools* ArcGIS extension (Jenness *et al.*, 2011).

4.3.4. Topographic wetness index and classification

The topographic wetness index (TWI) is a relative measure of soil moisture for a specific cell. It can be regarded as an indicator of topographically-driven soil moisture conditions (Wilson and Gallant 2000) and a guide to water and sediment movement in a particular landscape (McKenzie and Ryan 1999). The TWI at a specific point on the landscape is the ratio between the catchment area contributing to that point and the slope at that point (Wilson and Gallant 2000). TWI values were calculated for each cell (10 m x 10 m)

using the formula TWI = ln (As / tan β) (Moore *et al.*, 1993), where As is the specific catchment area and β is the local slope angle (degrees). In other words, TWI corresponds to the amount of water that should enter a given cell divided by the rate at which the water should flow out of that cell, or the propensity for the soil to be saturated. The highest values of TWI are associated with wet areas while the lowest TWI values are found in dry areas (Bou Kheir *et al.*, 2010; Sørensen *et al.*, 2006).

In this study, continuous TWI values and their variation within each of the six classes were firstly assessed. Soil wetness classes were then created by classifying TWI values into three categories of wetness (wet, moderately wet, and dry; representing moisture conditions,) based on TWI thresholds found by our previous study (Laamrani *et al.*, 2014b). These TWI thresholds were similar to values reported in other studies to delineate wet areas (i.e., a TWI threshold of 6.9 was reported in Creed and Sass, (2011) vs TWI threshold of 7.0 in our case). The resulting TWI classification is shown in Figure 4.2b.

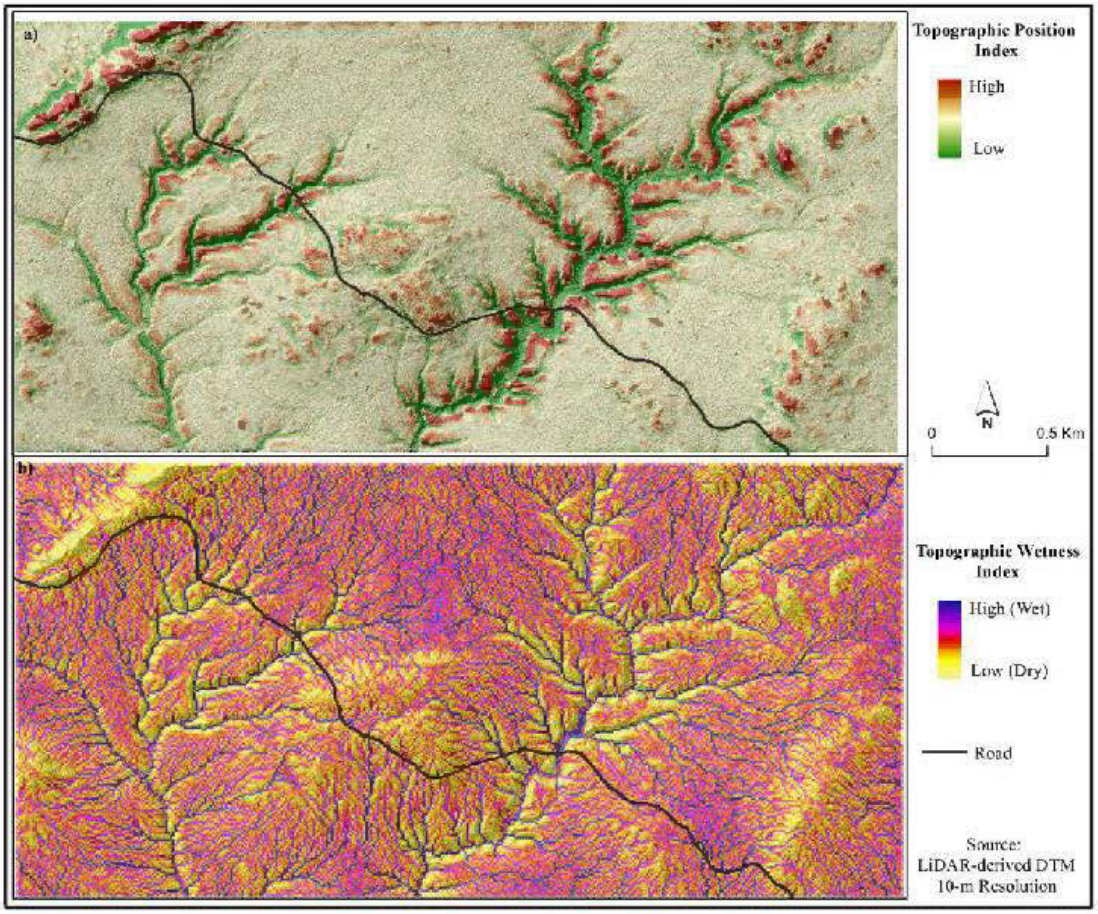

Figure 4.2. Topographic indices grids used in this study. a) Topographic position index (TPI) grid derived using a 50-m neighbour: the highest and lowest TPI values occur in higher and lower terrain positions respectively. b) Topographic wetness index (TWI) grid: the lowest, moderate, and highest TWI values are found in dry, moderately wet, and wet areas respectively. This figure is available in color online.

4.3.5. Assignment of paludification types to topographic position classes and theirs validations

The assignment of paludification types to one or another topographic position classes was based on the relation between the soil wetness classes and the six resulting position classes and was realized in several steps. TPI values and slope were firstly used to classify landscape into six topographic classes (Figure 4.2b); then the distribution of TWI classes within each topographic position class was analysed. The combination of TWI classes and topographic position classes produced a set of new classes (e.g., dry/flat surfaces, wet/flat surfaces, dry/upper, and so on). Each of these new classes was then assigned to a defined paludification type based on the relation between the soil wetness classes, slope and the six resulting topographic position classes. For example, an area on the landscape with the dry/upper combination may reasonably be assigned to the reversible paludification type. Field data information (vegetation and soil) was also used to determine (i) whether or not the assignment of topographic position class to one or the other paludification type was plausible and (ii) the ease with which a paludified area can be reversed. For example, paludified areas with lower organic layer thickness and dry conditions could be much easier to reverse than those with higher organic layer thickness and wet conditions.

Overall, the assignment approach provided a set of decision rules that were applied in the ArcGIS environment to create a thematic map of the spatial distribution of the resulting paludification types across the study area as well as for the whole LiDAR covered area (~100 km^2). The produced thematic map was then validated based on field surveys using the independent dataset of transect 4 (Figure 4.1b) consisting of 170 sites and chosen randomly. The validation was performed by comparing the thematic map results with the classification that had been obtained based on manual interpretation. This was done by extracting elevation values along transect 4 and using them to generate a spatially continuous cross-sectional profile section of the surface topography. Each sampling location along the profile section was then assigned to one of the six resulting topographic classes (according to Weiss 2001) and compared to its corresponding class over the thematic map using a confusion matrix (matched-unmatched decision). Because guidelines for selecting permanent vs reversible

paludification types on the field were lacking, only validation of topographic position classes was done and used to infer to paludification types.

4.3.6. Statistical analyses

Slope, elevation, TWI and field data statistics were computed within each of the resulting six topographic position classes. One-way analysis of variance (ANOVA) was used to test the equality of the variable means among the resulting classes. Post hoc Tukey's HSD tests were performed to determine whether topographic indices and field data for pairs of landscape classes significantly differed from one another. Significance was declared at a level of $\alpha = 0.05$, with all statistical analyses being performed in R (R Development Core Team, 2011).

4.4. RESULTS AND DISCUSSION

4.4.1. Topographic position classification

The results of topographic position classification based on Weiss's criterion are summarised in Table 4.2 and the spatial distributions of each of the resulting six topographic position classes is shown in Figure 4.3. More than 53% of the area was classified as flat surface, 6% as deep depressions, 10 % as lower slope depressions, 12% as mid-slope, 13% as upper-slope and 5% as hilltops. As shown in Table 4.2, flat surfaces and mid-slope areas had the same TPI thresholds and a slope values were used to distinguish between these two possibilities. In this study, we used a slope threshold of 1.8% based on our recent work where we have found that a slope of 1.8% is an appropriate threshold for distinguishing between areas with lower and higher slopes on our study site (Laamrani *et al.*, 2014a). In applying Weiss's method, the use of different slope thresholds value to distinguish between flat and mid-slope areas was done in other studies (e.g., De Reu *et al.*, 2013; Deumlich *et al.*, 2010).

Table 4.2. Description of the resulting six topographic position classes based on standardised topographic position index (TPI) and slope.

Topographic position classes		Criteria		Area [b]	
Class [a]	Description [b]	TPI [a]	Slope [b]	ha	(%)
1	Deep depressions	TPI ≤ -1 SD		43	6
2	Lower slope depressions	-1 SD < TPI ≤ -0.5 SD		74	10
3	Flat surfaces	-0.5 SD < TPI < 0.5 SD	≤ 1.8%	385	53
4	Mid-Slopes	-0.5 SD < TPI < 0.5 SD	> 1.8%	88	12
5	Upper-Slopes	0.5 < SD TPI ≤ 1		92	13
6	Hilltops	TPI > 1 SD		39	5

Note: TPI and slope criteria are after Weiss (2001) and Laamrani *et al.*, (2014a) respectively.
[a] Designation according to Weiss (2001) classification scheme.
[b] Designation according to this study.
SD = Standard Deviation.

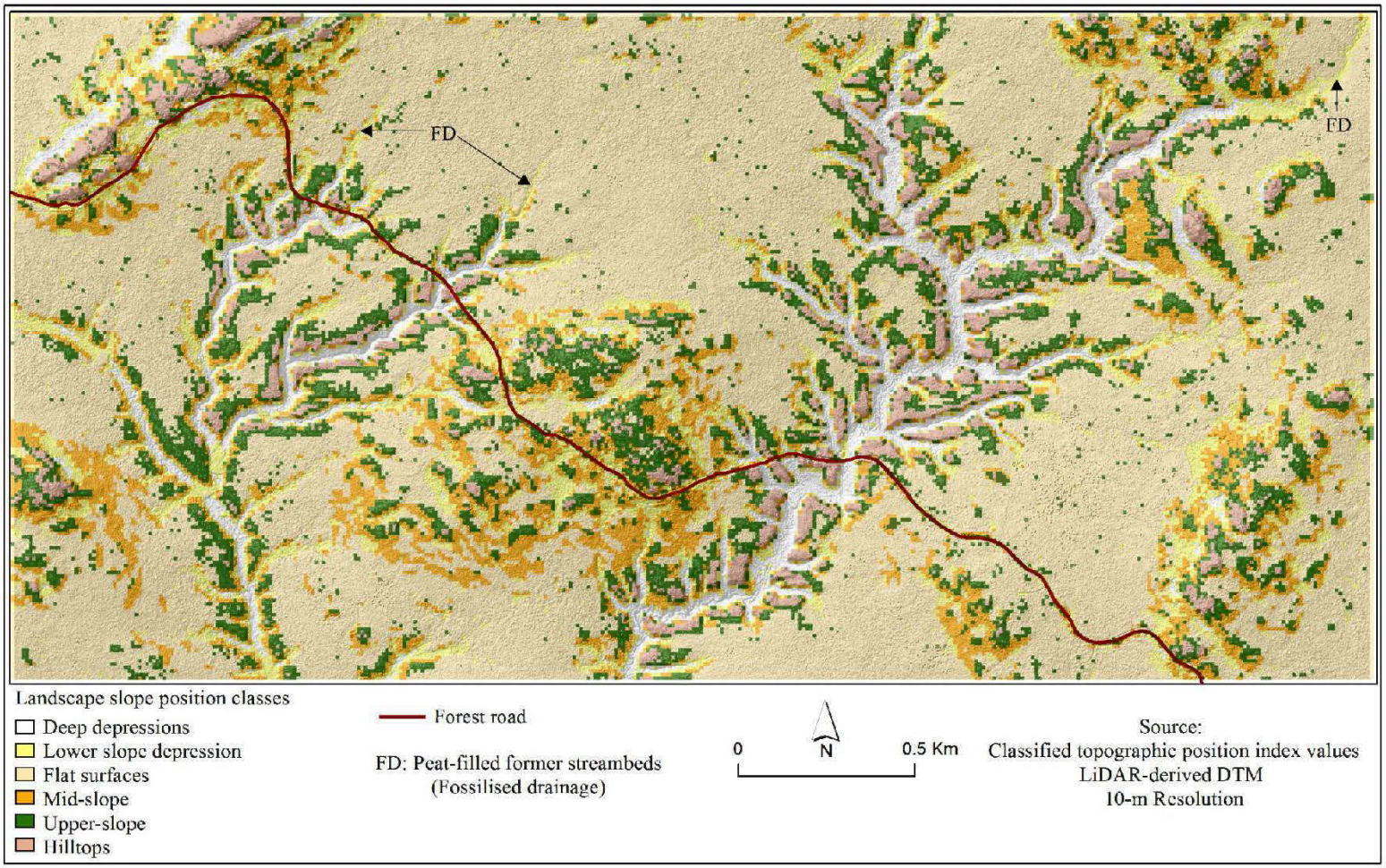

Figure 4.3. Thematic landscape map based on Topographic Position Index (TPI) values. Descriptions of each class are in Table 4.2.

4.4.2. Relationship between topographic position classes and individual topographic variables

Figure 4.4 shows the relation between the cell-derived mean values of individual topographic variables used in this study and the six resulting topographic position classes. As was confirmed by field survey, the largest (i.e., high wetness) values were found in depressions (i.e., channels), in flatted terrains and topographic hollows at higher elevation (i.e., in local depressions in bedrock). Mean TWI values decreased with increasing local topographic relief from deep depression (9.7 ± 0.64; mean ± SE) through flat surfaces (8.7 ± 0.05) to hilltops (6.6 ± 0.16). Mean TWI values were significantly different between the six classes (ANOVA, $P < 0.001$; Figure 4.4) suggesting that TWI could be used as a complementary tool to quantify the position of a site in the landscape. Figure 4.4 also showed that mean ground surface slopes and elevations varied significantly between topographic position classes. Slope was lowest on flat surfaces (1.9 ± 0.03%), intermediate on lower slope depressions (4.8 ± 0.20%) and highest in hilltop (6.0 ± 0.58%). Except for upper-slope and hilltops classes, which did not differ from one another (Tukey's HSD test, $P > 0.05$), the other classes significantly differed from one another (Tukey's HSD test, $P < 0.05$; Figure 4.4).

4.4.3. Assigning topographic position classes to paludification types

Assigning topographic position classes to one of the paludification types was based on the association of TPI classes (topographic position classes), slope and TWI classes (dry, moderately wet and wet). Result of the assignment approach was corroborated by field data survey and is shown in Table 4.3.

4.4.3.1. Deep depression class

Deep depressions (class 1) were often associated with deeper active streams and treeless depressions and were accurately recognized by the Weiss's classification (75% of site matching). Figure 4.5 shows that about 67% of class 1 was dominated by wet/moderately wet soils. As class 1 represented mostly permanently saturated or inundated areas, they were not considered important from a forest management perspective and were deliberately excluded from our field survey and subsequent analyses.

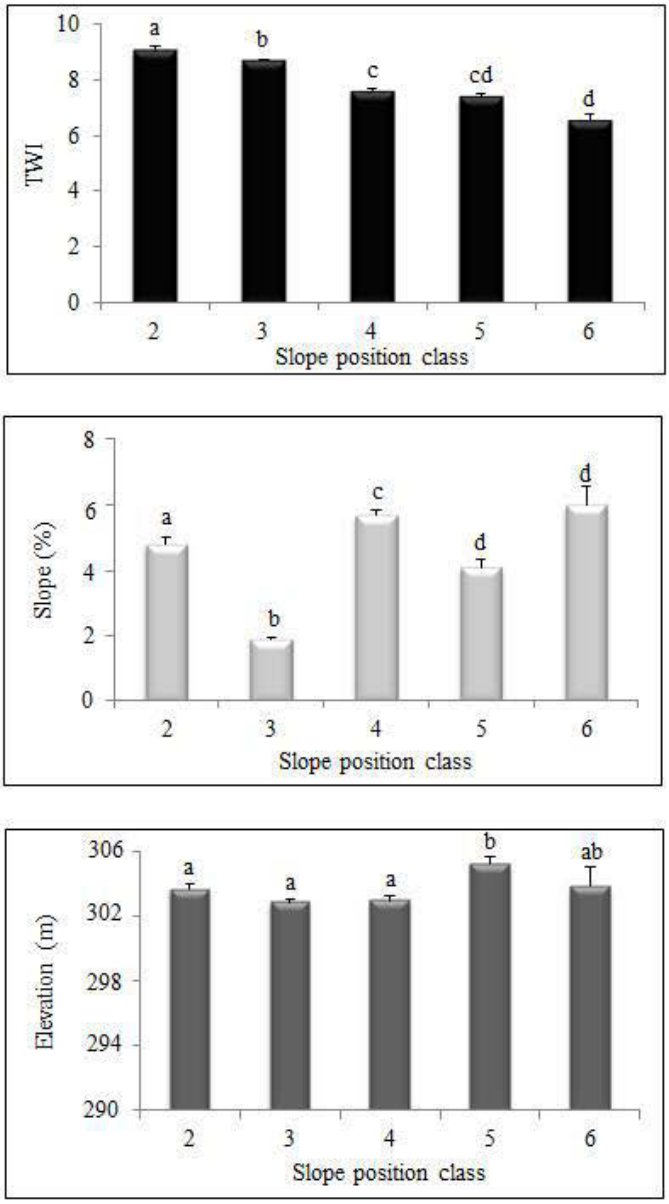

Figure 4.4. Variation in TWI, slope, and elevation values within the topographic position classes. Classes 2 to 6 (x-axis) refer to lower-slope depressions, flat surfaces, mid-slopes, upper slopes, and hilltops respectively. As explained in section 4.4.3.1, class 1 (deep depressions) was excluded. Error bars indicate SE of the mean; different letters designate statistically significant ($P < 0.05$) differences, according to pairwise Tukey tests.

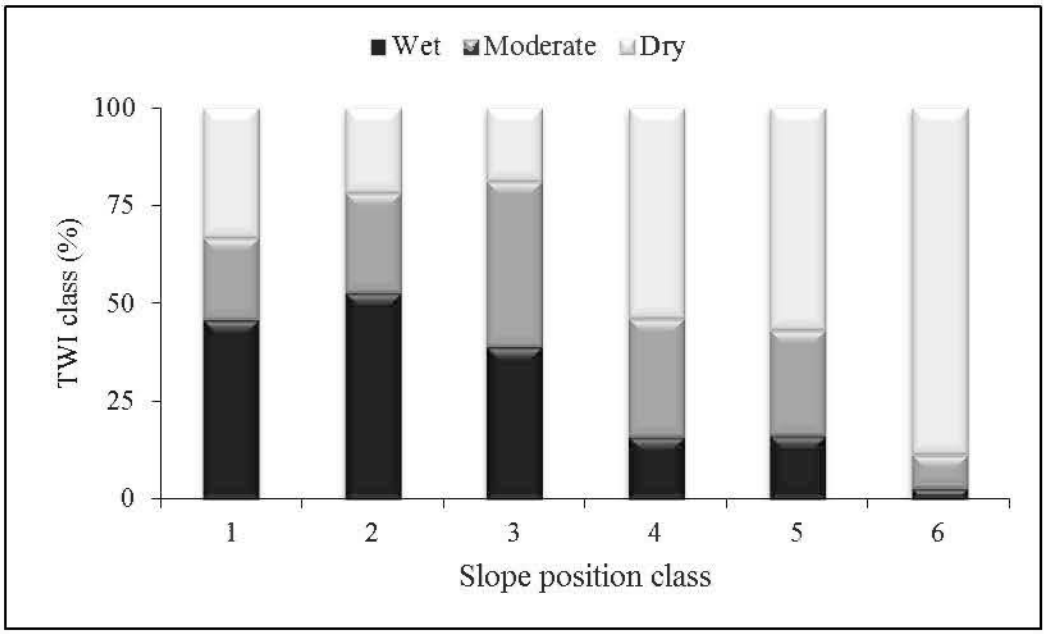

Figure 4.5. Distribution of TWI classes within each of the six topographic position classes. Class numbers 1 to 6 refer to Deep depressions, lower slope depressions, flat surfaces, mid-slopes, upper slopes, and hilltops respectively.

4.4.3.2. Lower slope depressions class

Lower slope depressions (class 2) was frequently identified in shallow depressions (negative TPI), where it can be associated with elongated peat-filled former streambeds (fossilised drainage system) and within depressions in the underlying bedrock (Figure 4.6; the area between positions 320 m and 360 m; 1200 m and 1300 m along transect 4, for example). To our knowledge, this type of paludified depressions has never been reported in the Canadian boreal forest and very rarely mentioned in the literature in other parts of the world (e.g., Gorozhankina 1997). As for class 1, wet and moderately wet soil was predominant in lower slope class (79%; Figure 4.5).

Class 2 had a mean organic layer thickness of 38 ± 1.8 cm, mean tree basal area of 28 ± 3.1 m^2/ha (low productivity) and mean fibric horizon thickness of 14 ± 2.5 cm (Table 4.3). For most of the used variables (topographic and field data), class 2 displayed high standard

error (SE) suggesting that there was a notable variability and that a subdivision of the initially defined class 2 may be required. Indeed, to reduce this variability within class 2, we considered splitting the lower slope depressions into two sub-classes (closed and opened depressions) based principally on a slope threshold of 2° following aforementioned work by Laamrani *et al.*, (2014a). Once this split was done, on one hand open depressions exhibited greater mean tree basal area (39 ± 2.2 m^2/ha), lower organic layer thickness (29 ± 1.4 cm), and more decomposed fibric horizon (thickness of 10 ± 1.9 cm) (Table 4.3). On the other hand closed depressions had lower tree basal area, higher organic layer thickness and higher fibric horizon thickness with 18 ± 2.3 m^2/ha, 53 ± 3.5 cm and 17 ± 5.0 cm respectively. Opened and the closed depressions sub-classes also significantly differed from one another (Tukey's HSD test, $P < 0.001$) with respect to tree basal area, organic layer and fibric horizon thicknesses.

The closed depression class is likely to represent locations within the landscape with wetter soil conditions that favor organic layer accumulation and where surface runoff is impeded or slowed down, whereas the open depression class is likely to represent areas within the landscape with shallow organic layer that do not impede downslope water movement and more favorable for tree growth. Consequently, opened and closed depressions may reasonably be assigned to reversible and permanent paludification types respectively. The distinction between open and closed depressions was not captured by the initial Weiss' classification but could be easily added to using a new slope criteria (open depressions with slope > 1.8% and closed depressions with slope ≤ 1.8%).

4.4.3.3. Flat surfaces class

It was not surprising that the majority of the area being studied was classified as flat surfaces (class 3) because the area is predominantly flat (Veillette, 1994). As seen in Figure 4.5, about 81% of class 3 sites had moderately wet (39%) to wet (42%) soils. Among the initially defined classes, the greatest organic layer thickness (55 ± 0.9 cm) and the lowest tree basal areas (25 ± 1.3 m^2/ha) were encountered in class 3 (Table 4.3). It should be noted that trees in class 3 displayed a broad range of basal area values (0.59-50.59 m^2/ha), suggesting local sources of variation that were not taken into consideration during landscape classification (e.g., the shape of the underlying material, time-since-last-fire, etc). Similar to

class 2, most of the variables (topographic, vegetation, and soil) exhibited a relatively high SE, suggesting a high variability within the dataset and that flat surfaces may be split into different sub-classes. Indeed, field measurements showed that locations on the landscape corresponding to depressions in the mineral soil occurred mostly within flat bogs (Figure 4.6; e.g., the area between positions 400 and 650 m along transect #4) and had very low mean tree basal area (4.4 ± 1.1 m^2/ha) and very thick organic layers (86 ± 2.4 cm) and fibric horizons (35 ± 3.2 cm). Such conditions seemed to be representative of permanent paludified areas that are not suited for forest management. While the distinction between the two sub-classes was mainly based on field survey data, it could also have been done using forest inventory maps, where flat bogs areas are clearly recognised. When flat samples that coincided with depressions in mineral soil or bedrock were excluded from the initial dataset (unsplit data), mean tree basal area slightly increased (27 ± 1.2 m^2/ha) and mean organic layer thickness (49 ± 2.7 cm) and fibric horizon decreased (13 ± 1 cm; Table 4.3).

It is clear that the reduction in variability obtained by separating class 3 into two sub-classes using the shape of the underlying material was only slightly less than that provided using the Weiss's classification and suggesting that it was extremely difficult to discriminate more sub-classes based mainly on topographic indices (TPI) because class 3 is located in flat areas where no slope variability in terrain exists. Therefore, a further subdivision based on TWI classes (dry, moderately wet and wet) was applied to class 3 data set (excluding bogs) and resulted into two new subclasses, viz., flat moderate/wet surfaces and flat dry surfaces (Table 4.3; sub-classes 3.2 and 3.3 respectively). These two new classes differed significantly in terms of organic layer thickness (52 ± 1.3 cm and 37 ± 2.0 cm respectively, Tukey's HSD $P < 0.001$) but did not differ in terms of tree basal area (26 ± 2.8 m^2/ha and 25 ± 1.2 m^2/ha respectively; Tukey's HSD $P = 0.95$). Regarding the effect of time-since-fire on reduction of variability within the data set, our field observations showed that stands in the area under study belonged to two age classes (75- and 125-years-old), and that the first class was over-represented relative to the second one with 89% and 11% of the sampling points, respectively. Consequently, the effect of time-since-fire in reducing data set variability was not assessed, given the insufficient number of sampling points within the 125-year-old class. Paludified flat dry surfaces were very likely associated with shallow to moderate organic layers and could be possibly easily reversed. In contrast, paludified flat moderate/wet surfaces represent an

advanced stage of paludification and may be reversed through a combination of costly mechanical silvicultural practices and site preparation that would have the benefit of removing the thick fibric layer (e.g. the use of powered disc trenching, T26 when the soil is not frozen).

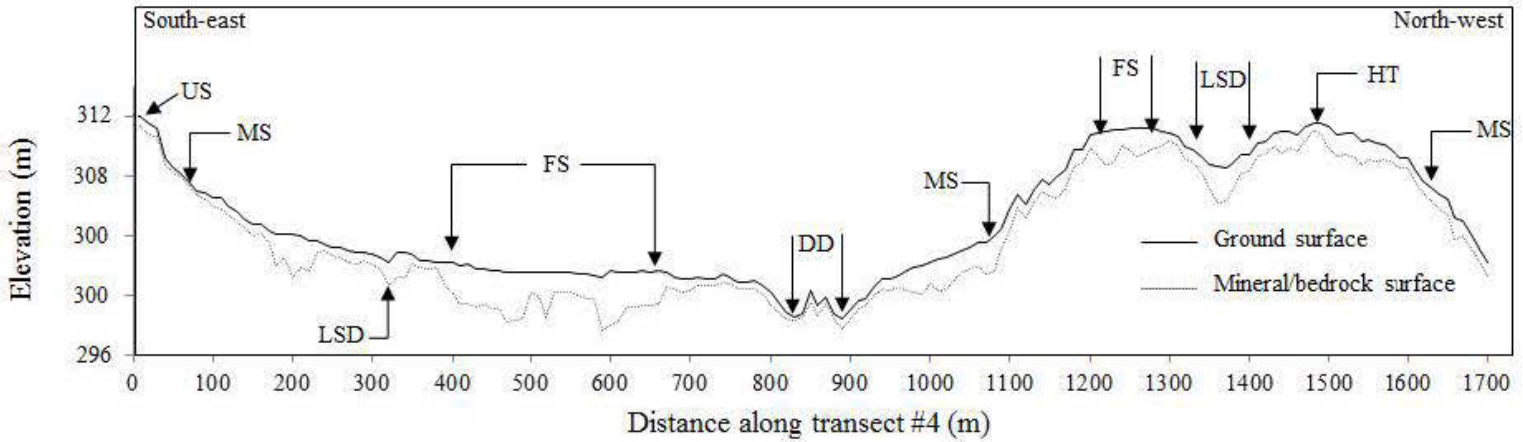

Figure 4.6. Landscape profile section of the surface topography along transect 4. Field sampling points were established at 10 m intervals along transect # 4 and theirs elevations were obtained using a mm/cm-level positioning accuracy GPS (validating dataset; n = 170). Deep depression (DD), lower slope depression (LSD), flat surfaces (FS), mid-slope (MS), upper slope (US) and hilltops (HT) refer to the six classes in Weiss's (2001) classification. The distance between the two curves (continuous and dashed) represents the total organic layer thickness or depth to mineral soil (measured in the field) with vertical exaggeration of 3x.

4.4.3.4. Mid-slope, upper slope and hilltop classes

Mid-slope (class 4), upper slope (class 5) and hilltop (class 6) classes were generally associated with upper terrain positions. The three classes exhibited a high percentage of dry sites with 54%, 57% and 89% respectively (Figure 4.5). As expected, these sloping surfaces (class 4, 5, and 6) exhibited relatively high tree basal area (31 ± 1.5 m^2/ha, 36 ± 2.3 m^2/ha, and 35 ± 2.7 m^2/ha respectively) and low/moderate organic layers thickness (29 ± 1.0 cm, 36 ± 1.3 cm and 26 ± 1.3 cm respectively) (Table 4.3), which was most likely a result of their prevailing dry conditions which were mainly caused by downslope water movement.

The combination of higher positions, shallow-moderate organic layer depth and low soil moisture are conditions that may be more favorable for tree growth and thus, these three classes are likely to be representative in general of reversible paludified areas. However, field data survey showed that depressions in the bedrock were locally observed on these sloping surfaces (Figure 4.6; the area at positions at 170 m to 240 m, 960 m to 990 m, and 1200 m to 1240 m along transect 4, for example). The occurrence of these depressions in the bedrock created local wetter soil conditions that probably favored local organic layer build up (paludification). This finding is consistent with earlier studies that found that paludification can occur on sloping well-drained terrain directly on bedrock (Laamrani *et al.*, 2013, 2014a; Payette 2001; Simard *et al.*, 2009) where the humic material is almost inexistent and the fibric material is dominant (Larocque *et al.*, 2003). In most cases, these depressions in the bedrock were identified on the basis of the surface roughness of the bedrock, obtained from field data, and not on the basis of topographic position classification because they did not correspond to depressions in the ground surface. To our knowledge, topographic maps of bedrock are not available; however, we recently demonstrated the feasibility of using ground penetrating radar as a method to detect and map local depressions in bedrock beneath the organic layer thickness (Laamrani *et al.*, 2013).

Table 4.3. Assignment of topographic position classes and sub-classes to paludification types and summary of field data (organic layer thickness «OLT» and basal area) that were used to corroborate this assignment.

Topographic position class			OLT (Mean ± SE cm)		Basal area (Mean ± SE m^2/ha)	Paludification type assignment	Producer's Accuracy
#	Sub-class[a]	Description	Total	Fibric			
2		Lower Slope depressions	38 ± 1.8	14 ± 2.5	28 ± 3.1		86%
	2.1	Closed depressions	53 ± 3.5	17 ± 5.0	18 ± 2.3	Permanent	80%
	2.2	Open depressions	29 ± 1.4	10 ± 1.9	39 ± 2.2	Reversible+++	91%
3		Flat surfaces	55 ± 0.9	15 ± 1.4	25 ± 1.3		87%
	3.1	Flat bogs	86 ± 2.4	35 ± 3.2	4.4 ± 1.1	Permanent	96%
	3.2	Flat moderate/wet surfaces	52 ± 1.3	14 ± 1.4	26 ± 2.8	Reversible+	N/A
	3.3	Flat dry surfaces	37 ± 2.0	10 ± 2.4	25 ± 1.2	Reversible++	N/A
4		Mid-slopes	29 ± 1.0	8 ± 1.0	31 ± 1.5	Reversible++++	62%
5		Upper-slopes	36 ± 1.3	8 ± 1.7	36 ± 2.3	Reversible+++	59%
6		Hilltops	26 ± 1.3	8 ± 1.9	35 ± 2.7	Reversible++++	57%
						Overall accuracy:	74%

[a] Identified according to this study. SE = Standard Error. Plus (+) sign gradient refers to the ease with which a paludified area can be reversed (e.g., ++++ is easier than +++ and much easier than +).

N/A: accuracy not assessed because this sub-class division was based on soil wetness; no such field data were available.

Note: Overall accuracy is a ratio between correctly allocated number of field sites and the overall number of classified sites. Producer's accuracy measures classification accuracy for individual classes.

4.4.4. Topographic position classification performance

In our study, TPI values were used to semi-automatically derive topographic position classes (according to the criterion of Weiss, 2001) from the LiDAR-derived DTM. To our knowledge, we have used quantitative landscape classification for the first time to differentiate between permanently and reversibly paludified forest soils, in the current example, those of the Clay Belt. In this study, we demonstrated that Weiss's classification method was a useful tool for classifying landscape within flat to hilly areas of the Clay Belt. The initial classification segmented the DTM in six topographic position classes based on consideration of both local slope and landscape position as measured by TPI. In this study, we revised this classification to improve upon the recognition a number of sub-classes (based on slope and TWI information) that were assigned to one of the known paludification types. For example, lower slope depressions class was classified into closed and open depressions sub-classes that are representing permanent and reversible paludification types respectively. This allowed cells that are in closed depressions to be discriminated from cells that are not closed to downslope water movement. A suite of summary statistics describing the distribution of field data (e.g. organic layer thickness, fibric horizon thickness, tree basal area) within each topographic position class provides additional information to assist in assigning each class to a defined paludification type. This is in agreement with previous studies where factors other than morphological variables (e.g., vegetation, soil) are often important consideration in defining topographic positions classes and assigning them to ecological process (i.e., Bou Kheir *et al.*, 2010; MacMillan *et al.*, 2007; Martin and Timmer, 2006).

There were, however, occasionally some problems with the classification method: (i) the areas around streams were classified as hilltop due to their elevated position compared to the stream bottom and thus, the hilltops was most likely overrepresented and (ii) subtle topography within lower slope depressions and flat surfaces was not captured using the original classification. However, these problems might be dealt with using more sensitive criteria such as modifying the threshold breaking points of classes and/or assessing the combination of two neighbourhood sizes. The later was tested in this study (according to the criterion of Weiss, 2001) and provided no significant outcome. Despite these limitations, the classification used here recognized major terrain features and effectively delimited the major

paludification patterns for the study site. This was consistent with previous studies that found TPI values offered a powerful approach to classifying the landscape into topographic classes despite some restrictions (e.g., De Reu *et al.*, 2013; Tagil and Jenness, 2008).

4.4.5. Validation of the produced maps

The produced thematic map of the spatial distribution of both permanent and reversible paludified areas is illustrated in Figure 4.7. This map was validated based on spatially continuous cross-sectional profile section of the surface topography that was generated along transect 4 based on field surveys independent validating dataset, and consisting of 170 sampling points (Figure 4.6). An overall accuracy of 74% was achieved suggesting that about three-quarters of the permanent/reversible paludified sites were accurately mapped. Flat surfaces had the highest match (87%) followed by lower slope depression with 86%. Hilltop, upper slope and mid-slope had the lowest match (with 57%, 59%, and 62% respectively), which may be due to the prevalence of local depressions in the bedrock mentioned and discussed earlyer. Among sub-classes, flat bogs had the highest match (96%). Open depressions sites were accurately mapped (91% matching) compared to closed depressions sites (80% matching). Unfortunately, we were not able to compare our topographic position classification to another classification from boreal forest area because there is a lack of such studies.

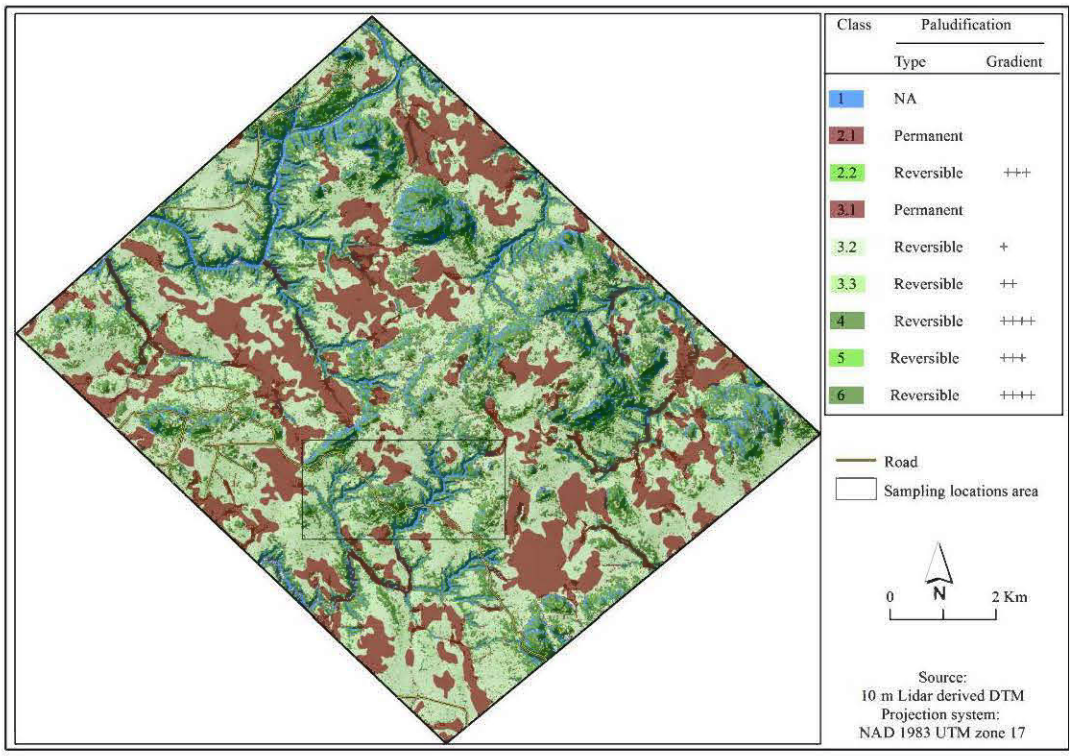

Figure 4.7. Map showing the distribution of permanent and reversible paludified areas in the study area as well as for the whole LiDAR-covered area (~100 km^2) within the Clay Belt region. Descriptions of each class are in Table 4.3.

4.4.6. Forest management implications

From a forest management perspective, we believe that understanding the spatial distribution of the resulting topographic position classes is an important first step in predicting and mapping productivity across landscapes. TPI and TWI derived from remotely sensed LiDAR data are simple in concept, easily defined, and provide an intuitive notion of surface morphology and wetness. They can be used by forest managers: (i) for defining both promising and vulnerable areas for forest management; (ii) to map zones of saturation where organic layers often accumulate; (iii) to better manage forest resources where high soil moisture limits productivity; (iv) to adopt appropriate management practices (e.g., field preparation treatments and replanting); and (v) to select sensitive areas where structure and biodiversity of paludified forest can be preserved.

The method that was used in the present study offered a reasonable first approximation of a useful stable framework for detecting and mapping permanent/reversible paludification types in the Clay Belt region. It has the potential to facilitate forest management decisions which in turn could improve forest productivity in the Clay Belt region. For example, in this study, we demonstrated that (i) flat sites that coincided with depressions in mineral soil or bedrock and closed depressions sites that are very likely associated with deep organic layers are often not suitable for tree plantations and provide no economic motives for managing them, (ii) Although flat moderate/wet surfaces represent an advanced stage of paludification, they might be reversed through a combination of silvicultural practices and mechanical site preparation (e.g. powered disc trenching, T26) that will have the benefit of removing the thick fibric layer, and (iii) Mid-slopes, upper-slopes and hilltops sites and open depressions sites represent an early to moderate stage of paludification and provide important economic motives for managing them. Their low to moderate organic layer thickness and low moisture are not expected to limit the use of equipment for mechanical site preparation and harvesting. It should be mentioned that the analytical approaches we used in this study provided only an actual portray of the paludified landscape, since paludification is a dynamic process that is changing with time.

4.5. CONCLUSIONS

The use of a classification method for identifying morphological classes at the landscape scale has proven to be a promising technique for forest management. In this study, slope, TPI, and TWI (all derived from LiDAR-DTM) were found to be the most useful variables that could be used to map paludified area at the landscape scale. TPI, slope, and TWI together identified continuous areas of the landscape that were linked to areas with varying wetness and morphological conditions, which were then used in explaining the paludification process. Slope and TPI were used in a semi-automated method to create six topographic position classes: deep depressions, lower slope depressions, flat surfaces, mid-slopes, upper slopes, and hilltops. Slope and TWI were used to further subdivide some of the six initial classes to sub-classes. Indeed, lower slope depression class was split into two sub-classes based on slope (open and closed depressions classes). Flat surfaces class was also split into three sub-classes based on TWI (flat moderate/wet surfaces and flat dry surfaces classes) and the shape of the underlying material (flat bogs). The resulting classes were then assigned to one of the paludification types, e.g., permanent (closed depression class) or reversible (open depression class).

Results showed that about 74% of the permanent/reversible paludified sites were accurately mapped highlighting the suitability of the semi-automated approach for data exploration, and the mapping and differentiation of permanent/reversible paludification types. This method was easily implemented in ArcGIS software, was easy to understand, and can be modified or adapted when necessary (e.g., thresholds modification or adaptation) and applied to other areas. It has the advantage of integrating topographic variables (e.g., slope) that were found, in previous studies, to be useful in explaining the paludification process. Our study also showed that splitting each of the lower slopes depression class and the flat surfaces class into two sub-classes explained more variation in the spatial distribution of permanent/reversible paludified landscapes and provided more realistic relationships between topographic position classes, topographic indices, and field survey data. Unlike the topographic position-based spatial classes defined by Weiss's classification, which is defined only on topographic criteria, our study benefited from the existence of field information data on vegetation and soil to create classes with comprehensive information on paludification.

Finally it is important to mention that LiDAR-derived DTM provide many potential for forest management other than simply a set of elevation values and yield a large variety of landscape morphological characteristics which may be important to forest managers and researchers in explaining processes such as paludification.

CHAPITRE V

EFFECTS OF TOPOGRAPHY AND THICKNESS OF ORGANIC LAYER ON PRODUCTIVITY OF BLACK SPRUCE BOREAL FORESTS OF NORTHWESTERN QUEBEC

Ahmed Laamrani[1], Osvaldo Valeria[1], Yves Bergeron[1], Nicole Fenton[1], Li Zhen Cheng[2] and Kenneth Anyomi[1]

[1] Chaire industrielle CRSNG-UQAT-UQAM en aménagement forestier durable, Institut de recherche sur les forêts et Centre d'étude sur la forêt.
Université du Québec en Abitibi-Témiscamingue. 445 boul. de l'Université, Rouyn-Noranda, Québec J9X 5E4, Canada.

[2] Institut de recherche en mines et environnement (IRME), Université du Québec en Abitibi-Témiscamingue. 445 boul. de l'Université, Rouyn-Noranda, Québec J9X 5E4, Canada.

Article soumis à:

Forest Ecology and Management- 2014

ABSTRACT

Northern Canadian boreal forest has a considerable ecological and economic importance, with the black spruce forest type occupying a large extent of this ecosystem. Organic layer thickness and its relationship to topography are two key factors affecting tree growth and forest productivity of northern Canadian boreal forests. This study linked multi-scale models of organic layer thickness and topography to improve our understanding of how these variables influence forest productivity and its distribution at different spatial scales within the Clay Belt region, northwestern Quebec. Field data were used to calculate site indices, which were used as estimators of forest productivity. Organic layer thickness was determined from field measurements obtained by manual probing, whereas topographic variables were extracted from multi-scale LiDAR-derived digital terrain models (DTM) at four resolutions, i.e., 5-, 10-, 15- and 20-m. Correlations between individual predictors and site index were found to be weak; few were significant. Regression tree-based models were fitted using two different sets of explanatory variables at the four scales: organic layer thickness and topography (model 1); and topographic variables only (model 2). Organic layer thickness, aspect, and slope were the most important variables explaining forest productivity (63% and 31% total variance explained for models 1 and 2, respectively). Model 1 was found to be scale-independent, since the total explained variance was similar under the four resolutions, whereas with model 2, effects of topography on productivity were greater for coarser scales (highest R^2 at 20-m resolution). Both models indicated higher forest productivity on southeast-facing slopes (i.e., > 2.2%) with shallow organic layers (< 35 cm), so then where organic horizons are the deepest the tree productivity is low. In contrast, lowest site indices (expressing productivity) were found in areas with very deep organic layers (> 85 cm). The resulting models could be applied at operational scales to predict site index at locations for which organic layer thickness information and DTM exist. Such information could be used to help forest managers in predicting how forest growth will respond to various harvesting activities.

Keywords: Site index; digital terrain model; Clay Belt; Paludification; Regression tree-based model.

RÉSUMÉ

Les forêts boréales nordiques du Canada ont une importance écologique et économique considérable, avec les forêts d'épinettes noires occupant une grande partie de cet écosystème. L'épaisseur de la couche organique (ECO) et sa relation à la topographie sont deux facteurs clés qui influent sur la croissance des arbres et la productivité de ces forêts. L'objectif de cette étude est d'évaluer l'effet de l'ECO et des variables topographiques exprimées à différentes résolutions spatiales sur la productivité forestière afin d'améliorer notre compréhension de la façon dont ces variables ainsi que leurs résolutions influencent la productivité des forêts paludifiées de la ceinture d'argile. Les données de terrain ont servi pour le calcul d'indicateurs de productivité potentielle (Indice de Qualité de Station, IQS) et actuelle (volume, surface terrière ou biomasse). Les mesures d'épaisseur de la couche organique ont été obtenues sur le terrain à l'aide une sonde manuelle, alors que les variables topographiques ont été extraites de modèles MNT-LiDAR multi-échelles à quatre résolutions (5, 10, 15 et 20 m). Les données de terrain et topographiques recueillies à différentes échelles ont été utilisées par la suite pour cartographier spatialement les effets des variables explicatives (l'ECO et variables topographiques) sur la productivité potentielle à l'échelle du paysage. Dans ce contexte, une démarche de modélisation basée sur l'application d'arbres de régression a été utilisée. Deux grands modèles ont été développés avec quatre résolutions: un premier utilisant toutes les variables explicatives exprimant l'ECO et la topographie (modèle 1), et un deuxième utilisant seulement les variables topographiques issues des différents MNT (modèle 2). Les résultats de cette étude ont mis en évidence plusieurs apports majeurs : (i) l'ECO, l'exposition et la pente sont les variables les plus importantes pour expliquer la productivité forestière (63% et 31% de variation expliquée pour les modèles 1 et 2, respectivement) à l'échelle du paysage; (ii) les zones avec un IQS élevé (synonyme de productivité élevée) étaient associées à une couche organique faible (< 35 cm) et à des pentes supérieures à 2,2 % orientées sud-ouest, favorisant une plus forte croissance des arbres; (iii) en revanche, les zones avec les plus petits IQS avaient une couche organique très profonde (> 85 cm). Ces conditions affectent la dynamique de la succession et favorisent l'invasion de mousses et de sphaignes ce qui favorise la progression de la paludification; (iv) le premier modèle semble relativement indépendant de l'échelle (résolutions), alors que la réponse du deuxième modèle augmentait significativement avec la taille du pixel. Les relations établies nous permettent ainsi de prédire et évaluer la productivité forestière à l'échelle du paysage; et les modèles qui résultent de cette étude pourraient être appliqués à des échelles opérationnelles et aux prédictions de la productivité là où des informations sur l'ECO en continu sont disponibles.

5.1. INTRODUCTION

The Canadian boreal forest has considerable ecological and economic importance. First, it provides habitat for diverse wildlife. Second, it acts as a reservoir for maintaining biological and genetic diversity. Third, it stores carbon, purifies air and water, and helps regulate regional and global climates. Last, it is the source of numerous resources for the industry in Canada. The forest type that is dominated by black spruce (*Picea mariana* [Miller] BSP) occupies a large extent of the northern Canadian boreal biome and is considered to be an important source of timber (Powers *et al.*, 2013). However, these northern boreal forests are characterized by extensive paludified areas with low forest productivity. Paludification is a natural process where organic material accumulates on the ground surface over time. These accumulations can lead to reductions in soil temperature, organic matter decomposition rates and nutrient availability that result in restricted tree growth, together with higher soil moisture levels and elevated water tables (Crawford *et al.*, 2003; Lavoie *et al.*, 2005; Vygodskaya *et al.*, 2007). These conditions alter dynamic succession and favour the invasion of Sphagnum moss species (Fenton *et al.*, 2005; Fenton and Bergeron 2006, 2007; Thiffault *et al.*, 2013), which can lead to the development of forested peatlands and substantial decreases in forest productivity (Simard *et al.*, 2007, 2009). Forest productivity refers to the quantity of timber that a stand is capable of producing within a given period of time (Skovsgaard and Vanclay, 2008), and depends mainly upon a combination of climatic and physical environmental variables. In boreal black spruce forests, time-since-last fire and topography are reported to be the two main factors causing paludification and, consequently, negatively affect forest productivity.

Many studies have investigated the effect of topography alone (i.e., Bonan and Shugart 1989; Grant 2004; Kljun *et al.*, 2006; McKenney and Pedlar 2003), or its effects in combination with paludification (i.e., Giroux *et al.*, 2001; Hollingsworth *et al.*, 2006; Laamrani *et al.*, 2014a,b; Lavoie *et al.*, 2005, 2007; Simard *et al.*, 2007, 2009), on forest productivity in boreal black spruce forests. To our knowledge, we are not aware of other studies that have examined the spatial scale at which topography and paludification will affect productivity, or which have quantified spatial variation in productivity of black spruce forests at the landscape scale, especially within the Clay Belt. The issue of spatial scale is important for productivity research because some factors are expected to act at local scales,

i.e., influencing productivity at sites within metres of one another, while the effect of other factors is not likely to be observed until sites are many hundreds of metres apart. Therefore, knowledge of the spatial scale at which these factors will affect forest productivity is of great importance to forest managers because it would allow them to make better cost-effective management decisions that optimize forest productivity and ensure sustainability of the forest.

Until recently, the availability of accurate topographic information at different spatial scales was a limiting factor for relating these data to forest productivity. Recent advances in remote sensing now permit the generation of appropriate data for determining these relationships at different spatial resolutions (scales). In fact, Light Detection And Ranging (LiDAR) is one of the most effective and reliable active remote sensing technologies that could be used directly or indirectly to assess forest productivity at different spatial scales in boreal forested environments (i.e., Bolton *et al.*, 2013; Laamrani *et al.*, 2014a,b; Magnussen and Wulder, 2012). Unlike previous studies that were conducted over a much more limited spatial extent and used simple topographic variables, such as slope, which were calculated in the field (e.g., Giroux *et al.*, 2001; Simard *et al.*, 2009), the current study has benefited from the application of LiDAR, which provided an opportunity (i) to investigate how forest productivity is related to both local- and landscape-scale topographic features across boreal forest areas, (ii) to derive more complex indices (i.e., topographic wetness and position indices), thereby obtaining information on morphological and wetness conditions, which are presumably linked to both more productive and less productive sites, and (iii) to document the effects of topography and paludification on black spruce forest productivity at the landscape scale, which has been done in only few studies.

The overall goal of the present study was to link productivity data (the response variable) with organic layer thickness and a set of topographic variables (predictor variables) at different spatial resolutions to improve our understanding of how these variables influence tree growth and productivity within the Clay Belt, a region in the southern portion of the Canadian Hudson Bay-James Bay Lowlands. The specific objectives of this study were (1) to investigate quantitatively the relationships between forest productivity and both organic layer thickness and topography; (2) to assess the effect of various resolutions (scale) on these relationships; (3) to predict forest productivity from soil and topographic data using a tree-

regression based model; and (3) to use these relationships to produce landscape-scale maps of productivity.

5.2. MATERIALS AND METHODS

5.2.1. Study area

This study was conducted within the western black spruce-feathermoss bioclimatic domain (Robitaille and Saucier, 1998). The study area was located in northwestern boreal Quebec (49°30' N, 78°30' W) within the Clay Belt region (Figure 5.1A). The topography is generally characterized by flat plains, which were generated by extensive and thick glaciolacustrine clay deposits that were left behind by pro-glacial Lake Ojibway (Veillette 1994). Elevation ranges between 290 m and 314 m, averaging 304 m above sea level (Figure 5.1B). Slope ranges from 0.0 to 34.3%. About 65% of the area has a slope $\leq$ 3.2%, whereas slopes $\geq$ 16.3% represent about 1% of the area.

Organic soils in the study area have developed over time on flat and gentle slopes with organic layer thicknesses ranging from 5 to 150 cm (Laamrani *et al.*, 2014b). The mineral soil beneath the organic layer is variable, ranging in composition from clay to till. The underlying bedrock is a complex mixture of Precambrian granitic rock types that occasionally appears at the ground surface and which form scattered gentle hills across the landscape.

The study area is characterized by open, extensive low productivity forest, which is found on flat, gentle slopes and forest bogs, whereas productive forests occur on mesic sloping areas. Figure 5.2 shows an example of site variability in forest productivity that was present across the area under investigation. Black spruce (*Picea mariana* [Mill.] BSP) was the most dominant species, followed by jack pine (*Pinus banksiana* Lamb.) and trembling aspen (*Populus tremuloides* Michx.). Other species such as eastern larch or tamarack (*Larix laricina* [Du Roi] K. Koch), balsam fir (*Abies balsamea* (L.) Miller), and paper or white birch (*Betula papyrifera* Marshall) covered a very small portion of the area (Laamrani *et al.*, 2014a). The understory was composed of *Sphagnum* spp., feather mosses (principally *Pleurozium schreberi* [Brid.] Mitten), and shrubs (mainly dwarf ericaceous species), with variable coverage across the landscape. Fire is the most natural important disturbance in the region (Bergeron *et al.*, 2001).

The climate is characterized by long cold winters (November to April) and short rainy summers. Mean annual temperature for the study area is -0.7 °C, with June, July and August as the warmest months, with a mean temperature of 14.4 °C; and December, January, February and March as the coldest months, with a mean temperature of -15.9 °C. Total annual precipitation is about 906 mm, of which more than one-third falls during the peak growing season, i.e., between June and early September (Environment Canada 2011; Matagami weather station, about 60 km NE of the study area).

5.2.2. Sampling design and field data collection

As part of a larger project that dealt with the effects of environmental variables and forest harvesting on paludification and productivity, our sampling design consisted of thirteen sub-parallel transects, totalling 15 km in length, and plots that had been established throughout the study area during summer 2010. One hundred circular sample plots of 400 m^2 were randomly distributed between and outside the transects (Figure 5.1C). Study plots and transects were located within stands that spanned the entire study area (about 720 ha; 1C), representing a large range of topography and organic layer thicknesses, together with a forest productivity gradient.

In each of the 100 sample plots, a set of vegetation variables were recorded following forest inventory guidelines of the Quebec Ministry of Natural Resources (MRNQ). The diameter at breast height (DBH, 1.3 m), status (alive or dead), live crown ratio, and species were recorded for each tree with a diameter > 9 cm. A subset of live dominant and co-dominant trees (three to six per plot) were selected for coring and total height measurement. Total height (m) was measured using a clinometer and tape measure; cores were taken at 1 m height using an increment borer. Cores were then used to determine the ages of each dominant and co-dominant tree and used as an estimate of time-since-last fire.

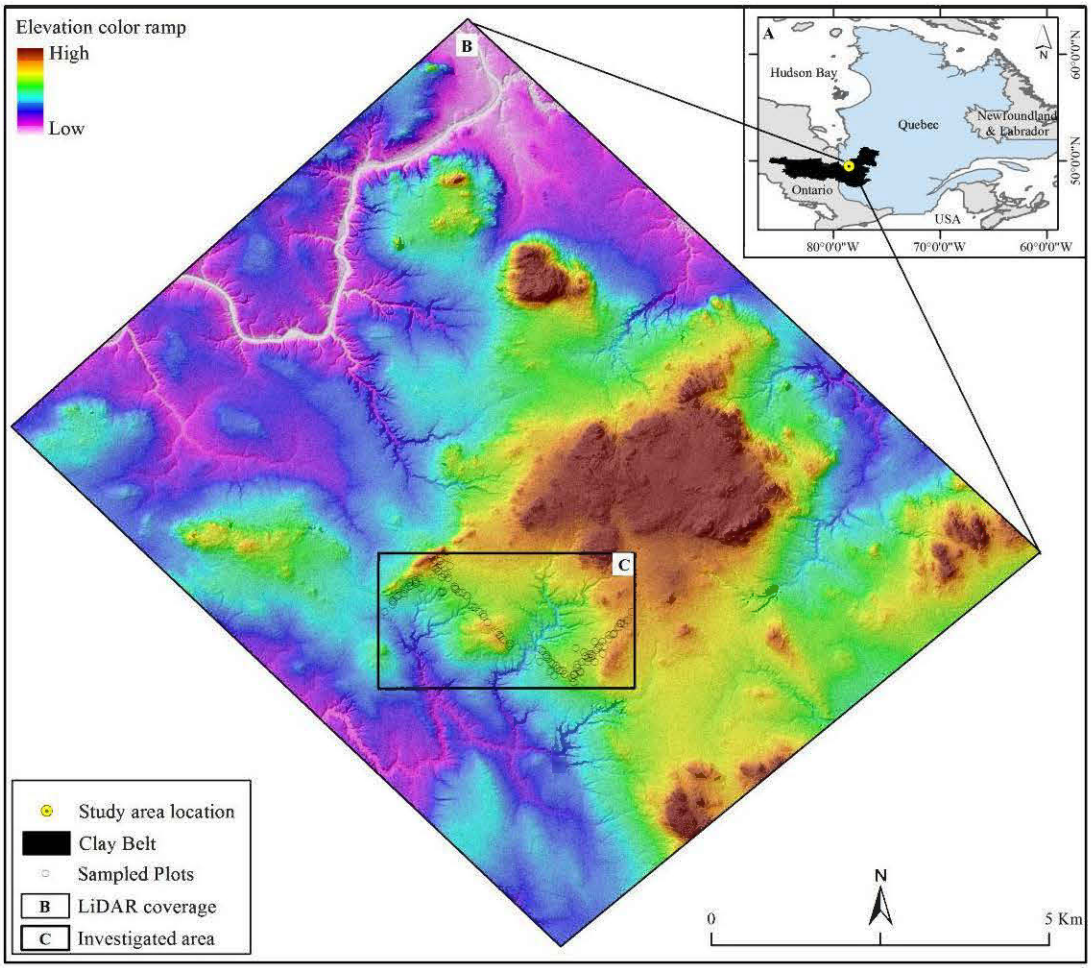

Figure 5.1. Location map of the study area in the northwestern boreal forest of the Clay Belt region, Quebec (A). LiDAR study area coverage represented by a 1-m resolution digital terrain model, which is overlain onto shaded relief (B). Area under investigation with sample plot locations (C) distributed along transects. The latter are not shown in (C) due to scale limitations, but can be seen in Laamrani et al. (2014b; Figure 1). The study was conducted and relationships were first developed within the area under investigation (C), and then extrapolated to produce spatial landscape-scale maps of productivity and its distribution across the whole region covered by LiDAR (B).

Figure 5.2. Photographs from the study area showing examples of variation in forest productivity within the study area: unproductive forest (A); low to moderately productive forest (B); area with substantial decline in forest productivity (C); and area with high forest productivity (D).

Other vegetation variables such as density, mean dominant height, basal area, volume and biomass were also calculated. Total basal area of each plot was calculated by adding the basal areas of all the trees and dividing by the plot area (400 m^2); the result was then converted to square metres per hectare (m^2/ha). Merchantable volume of each individual tree was calculated using its DBH and height values according to a local standardized merchantable volume that was found in Perron's (1983) tariff tables. Tree merchantable volumes from the same plot were summed and converted to provide an estimate of total merchantable wood volume per hectare (m^3/ha). Biomass was calculated using equations in Paré *et al.*, (2013). Data have been summarized for soil and vegetation variables in Table 5.1.

Ages that were calculated for the oldest trees were also used to confirm the dates of the two major fires that have been recognized in the study area, which were previously determined based on an existing map of the time-since-last fire (Bergeron et al., 2004). The most recent and oldest fires within the study area respectively dated back to the 1920's and the 1850's, with each representing about 85% and 15% of the investigated area.

5.2.3. Forest productivity assessment

Potential productivity refers to the quantity of timber that a site, given its intrinsic characteristics (i.e., drainage, topography and soil conditions), is capable of producing (Pokharel and Froese, 2009). It can be evaluated locally at site or plot scale, and also at the landscape scale by considering all the sites that are found on it (e.g., Anyomi *et al.*, 2013). In this study, we used the plot-level site index as a measure of potential forest productivity because it was well suited to the growth concept. Also, site index is one of the most widely used indicators of forest site productivity in North America (Anyomi *et al.*, 2013; Chen *et al.*, 2002; Hamel *et al.*, 2004; Mailly *et al.*, 2004; Pinno *et al.*, 2009; Pokharel and Froese, 2009), and also widely used in empirical growth and yield models to calculate the annual allowable cut of commercial species (e.g. Pothier and Savard, 1998). In this study, site index was estimated at a reference age of 50 years for each plot using site index equation s that were developed by Pothier and Savard (1998) for different species. For instance, the following equation is for predominantly black spruce plots:

[1] $$SI = b_1 H_d^{\,b_2} (1 - e^{-b_3 A})^{b_4 H_d^{\,-b_5}}$$

where SI is the site index; and b_1 = 0.9604, b_2 = 0.9412, b_3 = 0.03379, b_4 = -0.6970, and b_5 = -0.1046 are the coefficients for black spruce, parameter estimates for other species can be found in Potheir and Savard (1998). A is age at one metre height of selected dominant and codominant trees within each plot. H_d is the dominant height (m) and was calculated using Pothier and Savard's (1998) model, Eqn. (2).

$$[2]\quad H_d = 1.3 + \left[\frac{\overline{D}_4}{\left(\frac{\overline{D}}{\overline{H} - 1.3} \right) + \beta_2 \left(\overline{D}_4 - \overline{D} \right)} \right]$$

where $\overline{D}_4$ is the average DBH of the four largest trees per plot (cm), $\overline{D}$ and $\overline{H}$ are the respective average DBH (cm) and height (m) of dominant and codominant trees within each plot, and β_2 = 0.03490 is the regression coefficient for black spruce. Ninety-two of the sample plots were predominantly black spruce in terms of their basal area proportion (>75%), and for which the above equations were used. The remaining plots were predominantly aspen (5 plots) and jack pine (3 plots), for which different values were used of the same coefficients (i.e., b_1 to b_5 and β_2; values provided in Pothier and Savard, 1998).

Current productivity refers to established stand productivity and was estimated in this study by simple measures of merchantable volume, basal area, or biomass. These variables have been used in previous studies as proxies for forest productivity within the Clay Belt region (Giroux *et al.*, 2001; Simard *et al.*, 2007), and were well-correlated with site index in this study (Table 5.1).

Table 5.1. Summary statistics for measured and estimated variables within the study plots and their correlations with site index

Variables	Min	Max	Mean	SD	*r*
Volume (m^3/ha)	1.4	328.6	140.6	83.7	0.82**
Basal area (m^2/ha)	0.6	48.8	24.7	11.9	0.72**
Biomass (t/ha)	1.9	130.8	70.5	31.1	0.68**
Dominant height (m)	7.9	22.1	16.3	3.3	0.98**
Organic layer thickness (cm)	7	150	52	33	-0.48**
DBH (cm)	9.9	31.6	16.5	3.8	0.67**
Density (stems/ha)	75	2750	1385	662	0.23†
Tree Age (years)	62	159	84	23	-
Site Index (m at 50-yrs, age at 1m)	7.3	18.8	14.2	2.6	-

Note: DBH = diameter at the breast height. Density = the number of trees measured per plot times 25 (stems/ha). Calculation of the other variables is detailed in the Methods section. SD = Standard deviation.
r = Pearson product-moment correlation with site index. ***P-value* < *0.001*; †*P-value* < *0.05*; *n* = 100 plots.

5.2.5. Collection of predictor variables explaining forest productivity

The selection of topographic variables (Table 2) as terrain predictors was based on prior work that was performed under similar environmental conditions, where topography and paludification were important variables for predicting productivity (Giroux *et al.*, 2001; Grant 2004; Hollingsworth *et al.*, 2006; Laamrani *et al.*, 2014a,b; Simard *et al.*, 2007, 2009).

5.2.5.1. LiDAR derived topographic variables

A digital terrain model (DTM) was generated for the study area from terrain data that had been acquired using LiDAR technology on 28 May 2010. LiDAR data were collected over a 100 km^2 area (Figure 1B, including the area under the present study shown in Figure 1C), with a density of 2.8 points/m^2 and vertical accuracy of 0.065. The raw LiDAR data were pre-processed, interpolated with 0.5 m resolution, and gridded to produce a set of multi-scale DTMs. To assess the effect of spatial scale on forest productivity, a set of topographic variables was derived at four spatial scales corresponding to DTM resolutions of 5-, 10-, 15- and 20-m. Based on previous work done by Laamrani *et al.*, (2014a) within the same area, we believe that such a range of resolutions (5-m to 20-m) was adequate for capturing spatial variations in organic layer and topography, and consequently productivity variation within our study area.

A selection of nine topographic variables was then derived from each of the DTMs that we generated using standard procedures in ArcGIS 10 (ESRI, 2011). These ranged from simple topographic variables such as elevation, slope, aspect, mean curvature, plan curvature and profile curvature to more complex indices such as a topographic wetness index (TWI), topographic position index (TPI) and an aspect index. Descriptions of the topographic variables that were tested in this study are given in Table 2 and in Laamrani *et al.*, (2014a,b). Circular aspect was transformed to an aspect index following McCune's (2007) incident radiation model. This was accomplished by folding the aspect about the northeast-southwest line (30°), such that northeast becomes 0° and southwest becomes 180°, where Aspect index = 180 - |Aspect - 180|. Transformation rescales aspect so that lowest values are the coolest slope faces (northeast) and highest values are the warmest slope faces (southwest) (McCune and Keon, 2002). Topographic wetness index is usually used to characterize potential soil

moisture and its distribution across the landscape, such that higher values are associated with wet areas. Topographic wetness index was calculated using the Moore *et al.*,'s (1993) equation in Table 5.2. Topographic position index was given categorical values for low deep depressions, lower slope depressions, flat surfaces, mid-slopes, upper slopes, and hilltops, following the method originally proposed by Weiss (2001) and recently adapted to our study area by Laamrani *et al.*, under review. For each plot, values of the nine topographic variables were calculated using a moving three by three-cell window over the DTMs at the four spatial scales corresponding to the DTM resolutions of 5-, 10-, 15- and 20-m (representing 225, 900, 2025, and 3600 m^2 on the ground, respectively). Positions of each central plot location were recorded using GPS with mm/cm-level positioning accuracy to allow for direct comparison with the DTM.

5.2.5.2. Organic layer thickness measurements

A soil pit was dug at the centre of each of the 100 plots, in which depth to mineral soil (representing total organic layer thickness) was recorded. Total organic layer thickness was also measured by probing with an auger within a 1 m^2 quadrat located in each cardinal direction. Thickness of the organic material was taken as the distance between the organic layer surface and mineral soil interface. In most cases, the transition between organic layer and mineral soil was clearly marked by an obvious change in colour and texture, as shown in Figure 5.3.

The organic layer thickness was first measured at the plot-level, then these values were overlain upon DTMs that were created at the four spatial resolutions (5-, 10-, 15- and 20-m). When more than one plot was found within a three by three-cell window, their organic layer thickness values were averaged and the same mean value was assigned to each of these plots. As for topographic variables, the three by three-cell window was used for organic layer thickness; which would allow for efficient scale comparisons between organic layer thickness and topographic variables. Observed organic layer thickness mean values were then used as a measure of the degree of paludification.

Table 5.2. List of topographic variables created from LiDAR- derived digital terrain model and tested in the regression tree-based models.

Variables	Description	Source/Reference
Slope	Slope is defined as the gradient in the direction of maximum slope.	Horn's method (1981)
Aspect	Aspect is defined as the direction of maximum slope.	Horn's method (1981)
Mean curvature	A general descriptions of how curved the landscape is. It can be negative or positive and therefore does tell us whether the landscape is concave or convex.	Zevenbergen and Thorne's method (1987)
Plan curvature	Curvature of the surface perpendicular to the slope direction. It describes how water would diverge (- value) or converge (+ value) as it flows over a point.	Zevenbergen and Thorne's method (1987)
Profile curvature	Curvature of the surface in the direction of slope. It described how water would decelerate (- value) or accelerate (+ value) as it flows over a point.	Zevenbergen and Thorne's method (1987)
Aspect index	Aspect index = 180 – | Aspect – 180 | This aspect folding rescales aspect so that the lowest values being the coolest facing slope (northeast) and the highest values being the warmest facing slope (southwest)	McCune, (2007)
Topographic wetness index (TWI)	$TWI = \ln (A_s / \tan \beta)$. A_s is the local upslope contributing area and β is the local slope. Higher TWI values are representative of higher soil moisture and water accumulation areas.	Moore *et al.*,'s formula (1993)
Topographic position index (TPI)	TPI and slope were used to classify the landscape into discrete topographic position classes. (+) and (-) TPI values tend towards hilltops and depressions respectively, whereas zero or near-zero values tend toward flat and mid-slopes areas.	Jenness *et al.*, 2011; Laamrani *et al.*, under review

Figure 5.3. Photographs of organic layer measurements within each sample plot made by manual probing. In each plot, a soil pit was dug (centre; A) and an anger was bored throngh the organic layer until the mineral soil was encountered (four cardiual directions; B); then clearly identified (pointer finger on C); and measured as the distance between the organic layer surface and the mineral soil interface (distance between marker flag and index finger on D).

5.2.6. Statistical analyses

Prior to analysis, the dataset (n= 100 plots) was randomly split into two files. The first file consisted of 80% of the data (n= 80 plots), which were used to construct the models, while the second file with 20% of the data (n= 20 plots) was used for model validation. In a first stage of analysis, Pearson correlations (r) were calculated to assess whether plot soil and vegetation variables (volume, basal area, biomass, and organic layer thickness) and individual topographic variables at different resolutions were related to site index. In a second stage, we used regression trees to model site index as function of environmental variables that had been gathered at each plot and resolution, as estimated by the different resolutions that have been previously described. In this study, we used a conditional inference tree method following Hothorn *et al.*, (2006), which involved splitting the dataset into increasingly homogeneous subsets (also known as terminal nodes). This approach was well-suited for this study because of its capability in modelling both complex and non-linear relationships in a relatively simple way. Also, recursive partitioning of the dataset into more homogeneous groups allowed the identification of potential relationships between the response variable (i.e., forest productivity, expressed as site index) and environmental predictors (paludification and topographic variables), while also capturing interactions among these latter independent variables (Rothwell *et al.*, 2008). Splits or rules defining how the data were to be partitioned were selected based on a significance test of independence between covariates and the response variable. A split was established when the P-value was smaller than $\alpha = 0.05$, which meant that the global null hypothesis of independence between the response variable and any of the predictors could not be rejected at $\alpha = 0.05$. Unlike other decision tree methods (e.g., CART), our modelling approach did not require post-hoc pruning to prevent over-fitting of the regression trees, since P-values were used as stopping criteria (Hothorn *et al.*, 2006).

For each of the four resolutions, two sets of regression tree-based models were explored using (i) all of the aforementioned predictors (organic layer thickness + topography), and (ii) only topographic variables that had been derived from the DTM. These two models will be referred to as regression tree model 1 and regression tree model 2, respectively, in subsequent analyses. The efficiency of each regression tree-based model in predicting forest productivity

was assessed using the coefficient of determination (R^2) and root-mean-square error (RMSE), which measures the average squared difference between observed and predicted values. All statistical analyses were performed in R (R Development Core Team, 2011). Regression trees were created using the *ctree* function in the *party* package (Hothorn *et al.*, 2006).

5.2.7. Model validation

The creation of the regression trees provided a set of decision rules that defined the range of conditions, i.e., values of the predictor variables, which are best used to predict forest productivity. Predictive maps of the spatial distribution of productivity were created by applying the subsequent splitting rules in ArcGIS 10.0 (ESRI 2011) across Figure 5.1C and beyond the study area (Figure 5.1B) when data were available. The resulting productivity maps were validated based on field surveys using the independent, randomly chosen dataset (n = 20 plots), for which site index was calculated in the same manner as of the dataset used for constructing the regression tree-based models. The validation dataset was used for validating predictive forest productivity maps that we constructed, rather than in the regression tree models themselves. Accuracy assessment of the forest productivity maps was based on analysis of the confusion matrices described in section 3.4.

5.3. RESULTS

5.3.1. Vegetation characteristics and their relationships to site index at the plot-scale

Plot characteristics used in this study (n = 100) and their relationships with site index are summarized in Table 5.1. Merchantable mean volume, basal area, and biomass (stating current productivity) were all significantly ($P < 0.001$) correlated with site index, with respective Pearson coefficients (r) of 0.82, 0.72, and 0.68. Organic layer thickness was the only variable that was negatively correlated with site index (r = -0.48, $P < 0.001$; Figure 5.4a). As organic layer thickness increased, site index tended to decrease. This response was consistent with other studies that have been conducted across the Clay Belt, which have reported that organic layer thickness was highly and negatively correlated with productivity and that with increased paludification, black spruce productivity declined by 50-80% (Simard *et al.*, 2007, 2009). Dominant height was most strongly correlated with site index (r = 0.98, $P < 0.001$; Fig. 5.4b). This strong correlation can be tentatively explained by the low variability

of tree ages across the area that we investigated. This finding suggests that in the absence of dating core data, the dominant height that we calculated according to equation 2 could be used as an alternative to site index calculation in black forest plots for which aging data (i.e., cores) are missing.

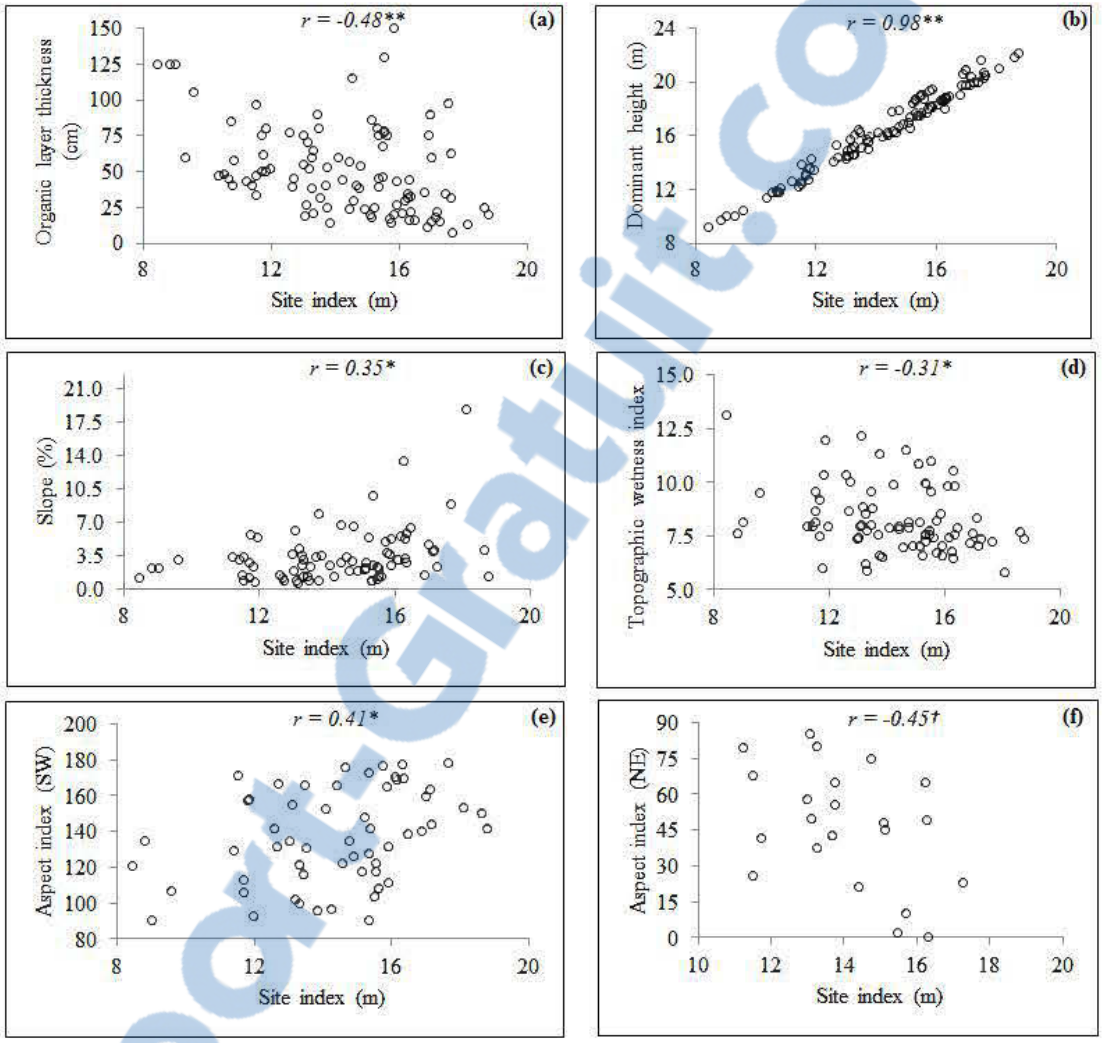

Figure 5.4. Relationships between selected individually measured variables and site index at different scales. Organic layer thickness and dominant height were measured at the plot-scale (Figs. 4a and 4b, respectively; n= 100). Slope and topographic wetness were extracted at 20-m resolution (Figs. 4c and 4d, respectively; n = 80 plots). Aspect index dataset was extracted at 5-m resolution and split into two classes, i.e., southwestern (Fig. 4e, n= 58) and northeastern (Fig. 4f, n= 22).

5.3.2. Correlations between site index and individual topographic variables

Derived topographic variables from each of the selected plots were used to evaluate resolution effects on site index (Table 5.3). Among the nine topographic variables that were tested, slope had the highest correlation with site index across 5- to 20-m resolutions (Table 5.3). Slope was consistently and positively related to site index over the landscape, with a correlation that increased from $r = 0.27$ to $r = 0.35$ as spatial resolution increased from 5- to 10-m (Table 5.3).

Topographic wetness index was significantly ($P < 0.05$) correlated with site index, ranging from -0.23 to -0.27 at 10-m and 15-m resolutions, respectively. At 20-m resolution, a more significant correlation was found between topographic wetness index and site index (r = -0.31, $P < 0.01$; Table 5.3), whereas no significant correlations were found at the 5-m resolution (r = -0.18, $P > 0.05$; Table 5.3). As was the case for slope, the correlation increased with increasing resolution for the topographic wetness index. At 10- to 20-m resolutions, the negative correlation between site index and topographic wetness index, which represents soil moisture variation caused by water accumulation, indicated that forest productivity tended to increase with dryer soil conditions (represented by low TWI values; Figure 5.4d). This result agrees with field observations for which productive forest was usually associated with areas having dryer conditions.

Across all resolutions, correlation between site index and aspect index were constantly very weak and not significant ($r \leq 0.16$, $P > 0.05$; Table 5.3). Nevertheless, this correlation increased for all resolutions when we divided the aspect index into two classes, viz., southwest and northeast (Table 5.3; Figures. 5.4e and 5.4f). For instance, at 5-m resolution, southwest-facing areas exhibited an improved significant correlation coefficient (r = -0.41, $P < 0.01$; Figure 5.4e). Across all resolutions, southwest-facing plots were all significantly correlated with site index (r ranging from $0.41_{[5m]}$ to $0.23_{[5m]}$, Table 5.3), whereas northeast-facing plots were only significantly correlated at 5-m resolution (r = -0.45, $P < 0.05$; Table 5.3).

Across all DTM resolutions, correlation between elevation and site index were also consistently very weak and not significant ($r = -0.12_{[5\text{-}, 10\text{-}, 15\text{-m}]}$ and $r = -0.11_{[20\text{-m}]}$, $P > 0.05$; Table 5.3). This weak correlation indicated that elevation had no influence on forest

productivity and could not be used to discriminate between areas of higher and lower forest productivity over the entire study area (Figure 5.4f). Topographic position index, which is simply the difference between a cell elevation value and the average elevation of the neighbourhood around that cell, was also found not to be significantly correlated with site index across the four resolutions ($r \leq 0.23$, $P > 0.05$).

All curvature variables (mean, profile and plan) were not correlated with site index for 5- to 15-m; however, correlation was weak but significant ($r \leq 0.23$, $P < 0.05$) at 20-m resolution. When we divided each of the curvature variables into two classes, viz., concave and convex, the correlation was not significant across all the resolutions (5- to 20-m), suggesting that curvature variables (mean, profile and plan) did not play a role in controlling forest productivity at any of the investigated resolutions.

Table 5.3. Pearson correlation, r, between topographic variables and site index based on different resolutions.

Topographic Variables	Resolutions			
	5-m	10-m	15-m	20-m
Elevation	-0.12	-0.12	-0.12	-0.11
Slope	0.35*	0.34*	0.32*	0.27†
Mean curvature	0.00	0.01	0.05	0.24†
Plan curvature	0.04	0.07	0.10	0.26†
Profile curvature	0.02	0.03	-0.07	-0.19
Aspect index [a]	0.16	0.16	0.14	0.11
Aspect index [NE] [b]	-0.45†	-0.08	-0.08	-0.01
Aspect index [SW] [b]	0.41*	0.33*	0.26*	0.22†
TPI	0.20	0.20	0.23	0.20
TWI	-0.18	-0.23†	-0.27†	-0.31*

Note: * $P < 0.01$; † $P < 0.01$.
[a] Entire data (n= 80);
[b] Stratified data by northeast- (NE, n = 22) and southwest- (SW, n = 58) facing slopes.

Table 5.4. Regression tree-based model rules that were used to explain site index.

Model $_{[Resolutions]}$	Terminal node splits
Model $1_{[5m, 10m, 15m, 20m]}$	
	A) OLT ≤ [85 cm]**, OLT ≤ [35 cm]**, Aspect index [NE]*
	B) OLT ≤ [85cm]**, OLT ≤ [35 cm]**, Aspect index [SW]*
	C) OLT ≤ [85cm]**, OLT > [35 cm]**
	D) OLT > [85 cm]**
Model $2_{[5m]}$	
	A) Slope ≤ [3.7%]*
	B) Slope > [3.7%]*, Aspect index [NE]†
	C) Slope > [3.7%]*, Aspect index [SW]†
Model $2_{[10m]}$	
	A) Slope ≤ [2.3%]*
	B) Slope > [2.2%]*, Aspect index [NE]*
	C) Slope > [2.3%]*, Aspect index [SW]*
Model $2_{[15m]}$	
	A) Slope ≤ [2.2%]*
	B) Slope > [2.2%]*, Aspect index [NE]*
	C) Slope > [2.2%]*, Aspect index [SW]*, Slope ≤ [2.8%]†
	D) Slope > [2.2%]*, Aspect index [SW]*, Slope > [2.8%]†
Model $2_{[20m]}$	
	A) Slope ≤ [2.2%]†
	B) Slope > [2.2%]†, Aspect index [NE]**
	C) Slope > [2.2%]†, Aspect index [SW]**, Slope ≤ [4.2%]†
	D) Slope > [2.2%]†, Aspect index [SW]**, Slope > [4.2%]†

Note: The resulting mean organic layer thickness (OLT) values were presented in 5-cm classes. But, OLT continuous values were used as explanatory variables.

$_{[5m, 10m, 15m, 20m]}$ refer to the four different resolutions for which each model was used.

NE and SW indicate areas with northeastern- and southwestern-facing slopes, respectively.

** *P-value* < 0.001; * *P-value* < 0.01 and † *P-value* < 0.05.

5.3.3. Forest productivity modelling results

Potential forest productivity across the study area, expressed as site index (SI), was modelled as a function of sets of predictor variables representing organic layer thickness and topography (model 1) and topography only (model 2) at four resolutions (5-, 10-, 15- and 20-m). The results of the regression tree-based models are shown in Figures. 5.5 and 5.6, and Tables 5.4 and 5.5. Table 5.4 summarizes the statistics that were derived during model construction and the regression criteria that were used in predicting forest productivity. Each of the 80 plots was assigned to one of the resulting terminal nodes (A to D for model 1; A to C for model $2_{[5 \text{ and } 10 \text{ m}]}$; A to D for model $2_{[15 \text{ and } 20 \text{ m}]}$). Regression tree model 1 had the highest R^2 and the lowest RMSE (Table 5.5), indicating that organic layer thickness and aspect index were important factors in predicting forest productivity over the study area. Regression tree model 2 was less accurate (lower R^2 and higher RMSE; Table 5.5) than model 1, which was expected since model 2 corresponded to model 1 minus paludification effects. Topographic wetness index, topographic position index, and curvature variables (mean curvature, plan and profile) did not contribute to the form of either regression tree-based model, suggesting that they did not play a role in controlling forest productivity, or at least at the resolutions that were used.

5.3.3.1. Forest productivity modelled using model 1

In model 1, which was based on organic layer thickness and topography, the first node at which the whole dataset was based on mean organic layer thickness data, illustrated that the lowest productivity occurred in areas with very deep organic layers (> 85 cm; terminal node D with mean SI of 9.8 m, $P < 0.001$; Figure 5.5). Plots where the organic layer was < 85 cm thick could be further subdivided based on mean organic layer thickness and aspect index. Within plots where organic layer thickness was ≤ 35 cm, the most productive plots occurred on south-facing slopes (terminal node B, with mean SI of 16.8 m, $P < 0.001$), while plots on north-facing slopes were found to have intermediate mean site index values (terminal node A; mean SI = 14.8 m, $P < 0.05$). The remaining plots had intermediate site index values (Terminal node C, mean SI = 13.7 m, $P < 0.05$), which resulted from higher organic layer thicknesses than those found in the most productive sites. Regression tree models at the four

resolutions had similar predictive quality, with R^2 and RMSE of 0.63 and 1.4 m, respectively (Table 5.5).

Table 5.5. Summary statistics of the regression tree-based models used in this study.

$Model_{[scales]}$	Terminal node splits	n	SI (m)	r	R^2_{adj}	RMSE
$Model\ 1_{[5m, 10m, 15m, 20m]}$				0.79	0.63	1.40
	A	16	14.8			
	B	16	16.8			
	C	41	13.7			
	D	7	9.8			
$Model\ 2_{[5m]}$				0.50	0.25	1.99
	A	56	13.6			
	B	10	14.1			
	C	14	16.6			
$Model\ 2_{[10m]}$				0.51	0.26	1.97
	A	38	13.6			
	B	25	14.0			
	C	17	16.4			
$Model\ 2_{[15m]}$				0.52	0.27	1.96
	A	38	13.4			
	B	19	13.9			
	C	9	14.5			
	D	14	16.6			
$Model\ 2_{[20m]}$				0.56	0.31	1.91
	A	37	13.3			
	B	22	13.8			
	C	13	15.7			
	D	8	17.1			

$_{[5m, 10m, 15m, 20m]}$ refer to the different resolutions for which the model was used.
SI refers to mean site index in metres.
r refers to the Pearson product-moment correlation between measured and predicted values.
NE and SW indicate northeastern- and southwestern-facing slopes, respectively.
RMSE = root mean square error.

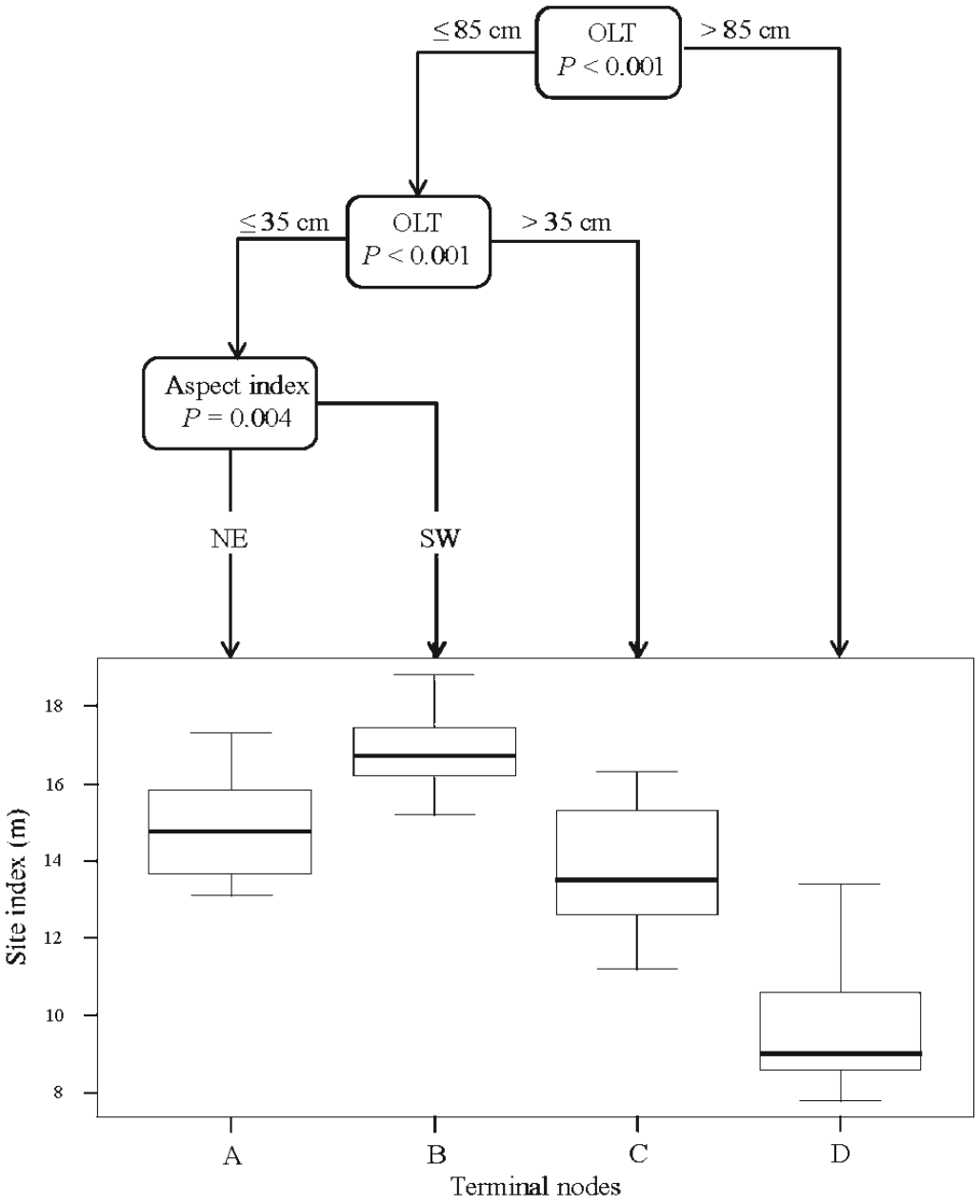

Figure 5.5. Graphical representation of regression tree model 1 at 20-m resolution. The distribution of site indices at the resulting terminal nodes (A to D) is visualized via box-and-whisker plots. The lower and upper edges of the box represent the 25th and 75th percentiles, and the median is represented by the horizontal bar through the middle of the box. The whiskers indicate the 10th and 90th percentiles.

5.3.3.2. Forest productivity modelled using model 2

Model 2 was based only on topographic variables and showed an increase in prediction quality (R^2) with scale increases that ranged from 0.25 to 0.31 for 5- and 10-m resolutions, respectively (Table 5.5). For all resolutions (5- to 20-m), variables that were retained during the model building were slope and aspect index. For model $2_{[5m]}$, plots with slopes greater than 3.7% and southwestern aspects had the highest forest productivity (Terminal node C, mean SI = 16.6 m, $P < 0.5$), while plots with a similar slope threshold and northeast-facing slopes were found in areas with intermediate productivity (terminal node B with SI of 14.1 m, $P < 0.05$). Plots with slopes less than 3.7% also occurred in areas with moderate productivity (terminal node A, mean SI = 13.6, $P < 0.01$; Figure 5.6). Model $2_{[10m]}$ split the data in the same manner, i.e., based on slope and aspect index, but using different slope thresholds (2.3%) and lower *P*-values (all < 0.001). In terms of site index values, Model 2 at 5-m and 10-m resolutions showed the same trend as those at 15-m and 20-m resolutions, but a higher number of terminal nodes were identified (four compared to three for 5- and 10-m resolutions). For 15- and 20-m resolutions, southwest-facing plots were further split, based on respective slope thresholds of 2.8% and 4.2%. Southwest-facing plots with the greater slopes ($2.8\%_{[15m]}$ and $4.2\%_{[20m]}$) had the highest productivity (terminal nodes D with mean SI of 16.6 m and 17.1 m for 5- and 10-m resolutions, respectively).

5.3.4. Construction and validation of predictive site index maps

Predictive spatial forest productivity maps were produced across an area of greater LiDAR coverage (~100 km^2; Figure 5.1B) using the resulting regressions tree-based models 1 and 2 with the highest R^2. Spatial organic layer thickness data were required to map site index, as predicted by our regression tree model 1 across the study area. These data were obtained from a remote sensing-derived map that was created by the Canadian Forest Service (Beaudoin *et al.*, 2013, personal communication), and constitute the only data available for our study area with continuous organic layer thickness values. This map delineated areas (with 25-m pixel resolution) with maximum organic layer thickness values of 65 cm, which limited our use of it to only the highly productive areas (≤ 35 cm, terminal nodes A and B in Figure 5.5). Consequently, a first map showing spatial distribution of site productivity across the study area was produced (Figure 5.7) based on prediction from tree-based regression

model 1. A second site index map was produced using the regression tree rules of model 2, which was based on topographic variables only (Figure 5.8); here, only slope and slope index rasters that had been derived for this study were used. These two maps were validated using an independent randomly chosen dataset (n = 20 plots) from field surveys. The validation aimed to compare spatially mapped site indices of this study with the only exiting coarse productivity map over our study area realized by (Beaudoin *et al.*, 2013, personal communication). Beaudoin's *et al.*,'s (2013) map was generated by combining basal area and organic layer thickness (aforementioned) derived from remote sensing data. This coarse productivity map encompasses three productivity classes, highly productive forest, moderately productive forest, and unproductive forest.

For the purpose of validation, a conventional confusion matrix procedure using overall accuracy and producer accuracy following Congalton (1991) was conducted in this study. The confusion matrix between the coarse productivity map classes and the modelled ones in this study indicated moderate overall accuracies: 50% and 53% for models 1 and 2, respectively. The range of producer's accuracy of model 1 varied between 67%, 55% and 33%, respectively for the highly productive, the moderate productive, and the unproductive forest classes. For model 2, comparisons between the coarse productivity map and the modelled one in this study indicated an overall accuracy of 25% and 64% for the highly productive and moderate classes, respectively; and there was no available data for validating the unproductive forest class. It is important to mention that the validating organic layer thickness and productivity spatial maps that we used here, were compiled at a regional scale (Beaudoin *et al.*, 2013; personal communication), and the coarseness of this data likely affected the overall and producer's accuracies.

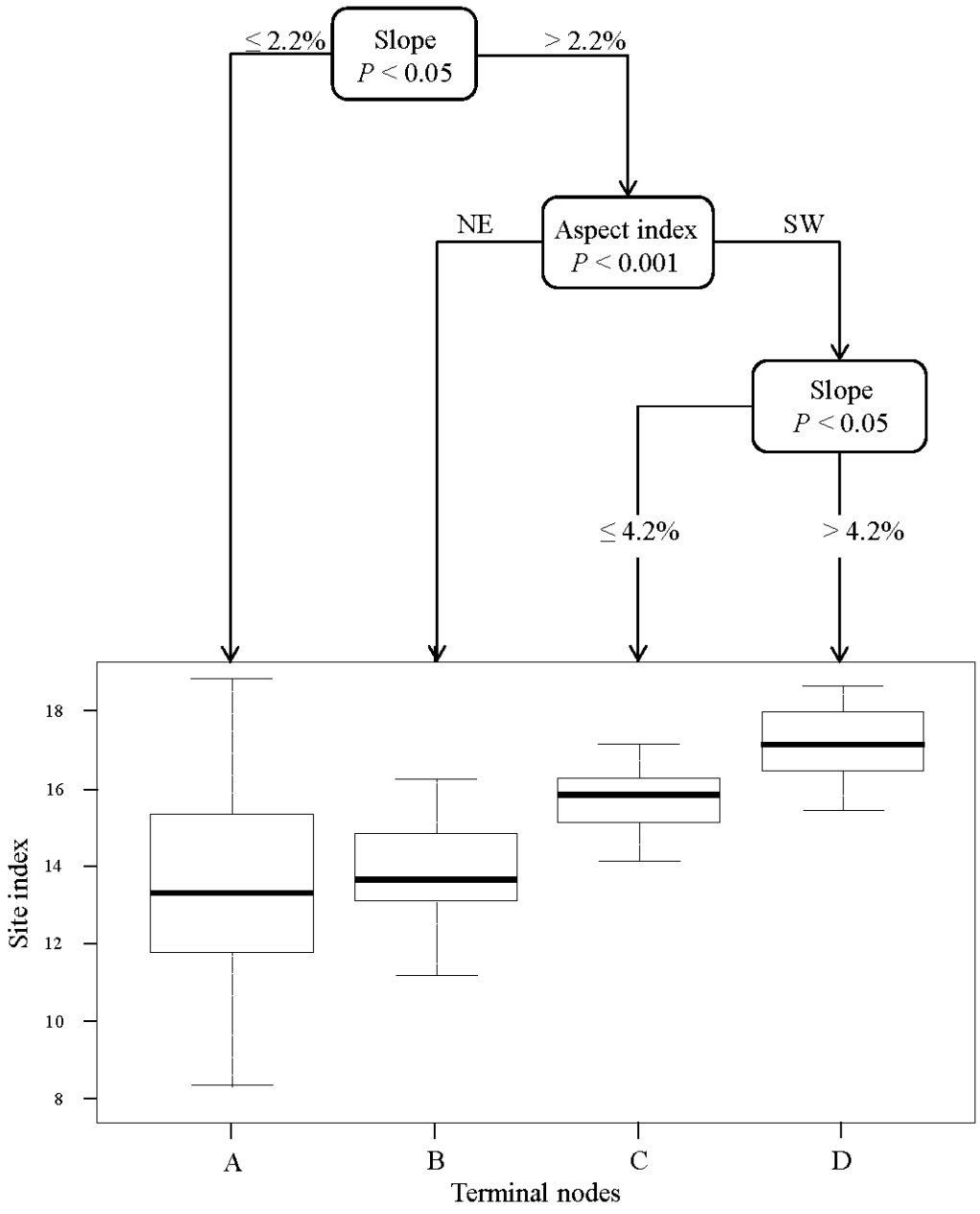

Figure 5.6. Graphical representation of regression tree model 2 at 20-m resolution. The distribution of site indices at the resulting terminal nodes (A to D) is visualized via box-and-whisker plots. The lower and upper edges of the box represent the 25th and 75th percentiles, and the median is represented by the horizontal bar through the middle of the box. The whiskers show the 10th and the 90th percentiles.

5.4. DISCUSSION

5.4.1. Individual relationships between topographic variables and site index

The positive correlation between slope and site index across all resolutions (5- to 20-m) indicated that forest productivity tended to be higher in areas with high slopes and lower in areas with low slopes. This was consistent with other studies that have found similar results in boreal black spruce forests (Simard *et al.*, 2009). Our results also suggested that forest productivity was related to the topographic wetness index, and decreased as values of this index increased. These results have agreed with another study (Emili *et al.*, 2006) in which slope index, which is conceptually similar to the topographic wetness index, was negatively correlated with site index for paludified boreal forest found in British Columbia.

The absence of correlation between elevation and productivity indicated that elevation did not show any obvious trends across the different resolutions and that lower and higher site indices occurred at both high and low elevations within the study area (Figure 5.3c). This result differs from those of other studies conducted within the Canadian boreal zone showing that elevation was a significantly related to forest productivity (Chen *et al.*, 2002; Pinno *et al.*, 2009). In our study, the narrow range of elevations (290-314 m) over the study area could explain the lack of correlation. Thus, it was not surprising that topographic position index was not related to site index across the four resolutions that were employed in our study.

Despite weak correlations between site index and individual topographic variables (Table 5.3), some of these values were statistically significant and provided some insight into which variables influenced the spatial distribution of forest productivity at the landscape-scale. In light of this, forest productivity distribution at the landscape scale clearly could not be explained by simple bivariate relationships between site index and individual predictor variables. The subsequent quantitative subdivision of the landscape into new datasets that were smaller and more homogeneous areas using regression tree-based modelling was a justified choice, which enabled us to incorporate complex interactions among independent variables.

5.4.2. Regression tree model 1

Our results indicated that organic layer thickness was the most important descriptor of forest productivity, with lower forest productivity occurring in plots with deep organic layers. This was consistent with earlier studies across the Clay Belt (Giroux *et al.*, 2001; Lavoie *et al.*, 2005, 2007; Simard *et al.* 2007, 2009). Areas with conditions more favourable for tree growth were encountered in plots with shallow organic layers and southwesterly exposures. Higher forest productivity on southwest-facing slopes could be explained by dry soil conditions, which seem to prevail as result of water movement causing a decrease in organic layer accumulation, combined with growth stimulated by greater solar radiation. In contrast, moderate forest productivity on northeast slopes could be explained by greater moisture storage capacity, combined with lower solar radiation. McCune (2007) found that southwest-facing slopes should have warmer temperatures than southeast-facing slopes, even though they receive equivalent solar radiation inputs. Our study confirmed the importance of an organic layer effect on forest productivity within the Clay Belt, which has been previously reported (Giroux *et al.*, 2001; Laamrani *et al.*, 2014a,b; Simard *et al.*, 2007, 2009), but we also quantified thresholds at which the organic layer could be used to discriminate areas with highest versus lowest forest productivity. Furthermore, organic layer thickness thresholds of 35 cm and 85 cm seemed to represent a breakpoint for discriminating between highly productive and unproductive areas, respectively. The fact that organic layer thickness was used in both the initial split and the terminal splits highlighted the ability of regression tree-based models to detail the effects of a variable, which is generally difficult to achieve with standard regression methods, even with an extensive listing of interaction terms. This is supported by Ryan *et al.*, (2000), who found that regression tree models can be useful in situations where an increasing number of conditional relationships are encountered and when linear models (regressions) lose their benefit under such situations.

Landscape productivity estimates generally are tested only at a single scale (plot-scale in our case), but we demonstrated that the effects of organic layer thickness and topographic variables could operate across multiple scales, since they were both measured at different resolutions scales. The fact that regression tree model 1 at the 5-, 10-, 15- and 20-m resolutions had similar prediction qualities suggested that these four models: (i) operated equally well across scales, suggesting a more general relationship with forest productivity; (ii)

were equally useful for predicting site index; and (iii) the effect of retained variables of model 1 operated similarly at fine and broad scales and were scale-independent.

The site index map that was produced and based on regression tree model 1 was defined only with two classes (highly to moderately productive), given a lack of the full range of organic layer thicknesses that were covered by our models (35-85 cm). However, we believe that regression tree model 1 can be extrapolated to other larger areas that share similar environmental conditions or which have similar LiDAR data availability, especially within the Clay Belt. To do so, more detailed datasets of organic layer thickness that produce the predictive site index map would have to be made available, which would ultimately improve the accuracy of this map. In light of this, the mapping of continuous organic layer thickness over larger areas of the Clay Belt, by using higher resolution satellite imagery and DTMs, is an important and urgent future research topic, given that the predictive capacity of regression tree-based model 1 would likely increase and explain additional variation in the distribution of forest productivity.

5.4.3. Regression tree model 2

Slope and aspect index were the strongest explanatory variables at all resolutions that were studied. As was the case for model 1, more favourable conditions for tree growth were found on southeast-facing-slopes, whereas moderate growth was located in plots on northeast-facing slopes and in areas where lower slope gradients prevailed. Unlike model 1, regression tree-based model 2 did not discriminate areas with conditions that were likely to be less favourable to tree growth because of lower site indices. One finding of our study was that topographic effects were greater for coarser resolutions. Moreover, a slope threshold ranging from 2.2% to 3.7% appeared to represent a cut-off point for separating higher from moderate forest productivity. Even small differences in slope (~ 1.5%) could contribute significantly to variation in forest productivity estimates within the Clay Belt where slope is frequently less than 0.1% (Lavoie *et al.*, 2007). Further, beyond 10-m resolution, initial data splitting was constantly based on a threshold slope value of 2.2%. This was true for coarser resolutions (i.e., 25- and 30-m resolutions, verified but not shown here). Consequently, there is a distinctive scale effect around 10-m resolution (equivalent to 900-m^2 on the ground) that

possibly delineated localized (local) versus landscape (broad) influences on forest productivity.

5.4.4. Model performance

Across all resolutions (5- to 20-m), models 1 and 2 respectively explained 63% and 25-31% of the variation in the dataset. These estimates of model accuracy were comparable to (model 1) or higher than (model 2) other productivity modelling studies reported in the literature (e.g., McKenney and Pedlar, 2003). For most spatial models, $R^2 \leq 0.5$ are common, whereas greater R^2 values (> 0.7) are unusual (Dahlke *et al.*, 2009). For both of our models, aspect index made a significant contribution to estimating forest productivity variability. According to our model 1, slope direction (expressed as the aspect index) was more important than slope gradient in determining forest productivity for the four resolutions that were used, resulting in an unusual relationship. Slope gradient was not retained in model 1, which may be explained by the low slope variability that characterized the study area. A previous study conducted in Swedish boreal forests (Seibert *et al.*, 2007) also found that aspect influence is larger between 40° and 60° latitude, which corresponds to the location of our study area. Both regression tree-based models produced solutions that were easy to understand, represented terminal nodes that were meaningful in terms of the physical processes affecting variability in forest productivity, and consisted of small number of rules.

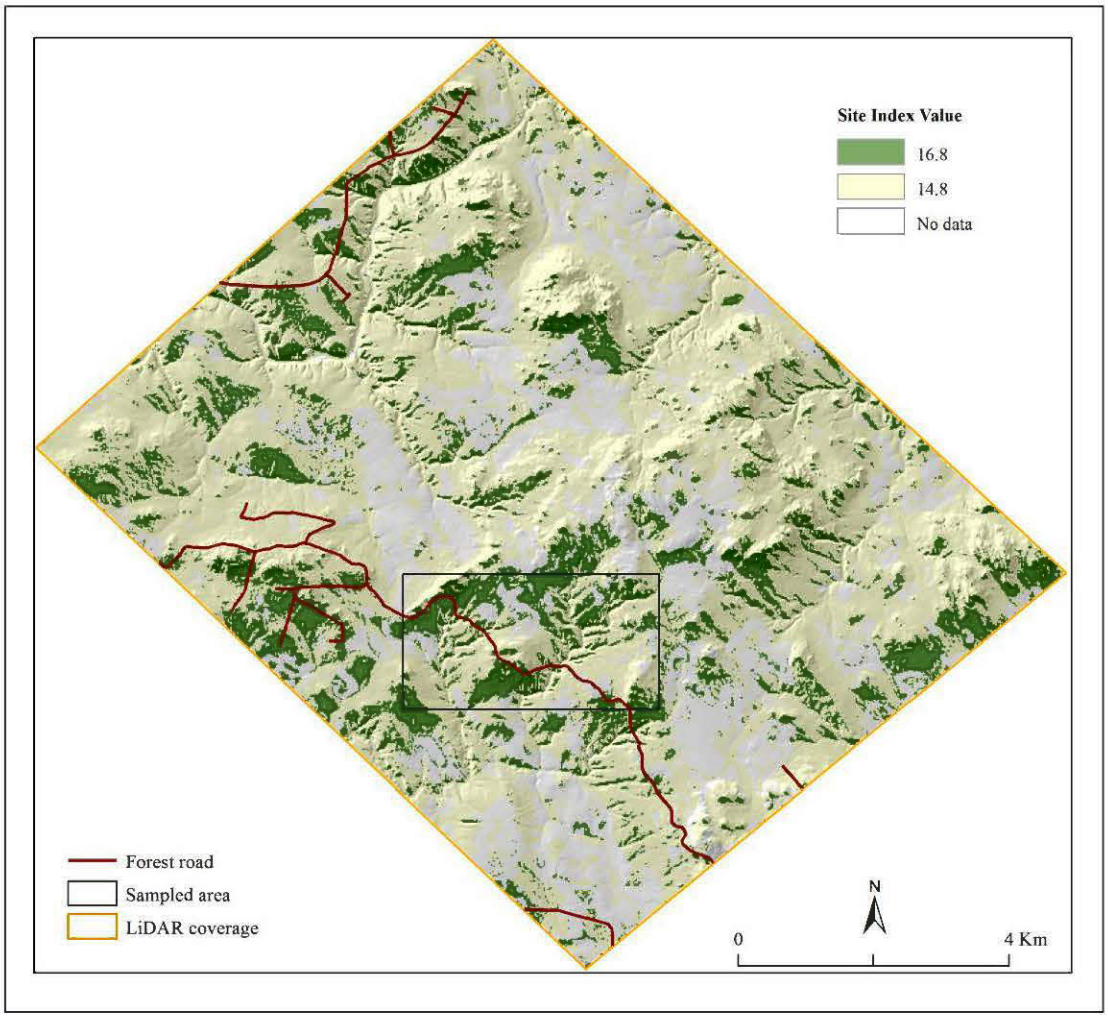

Figure 5.7. Map showing the spatial distribution of site index across the study area as predicted by regression tree model 1.

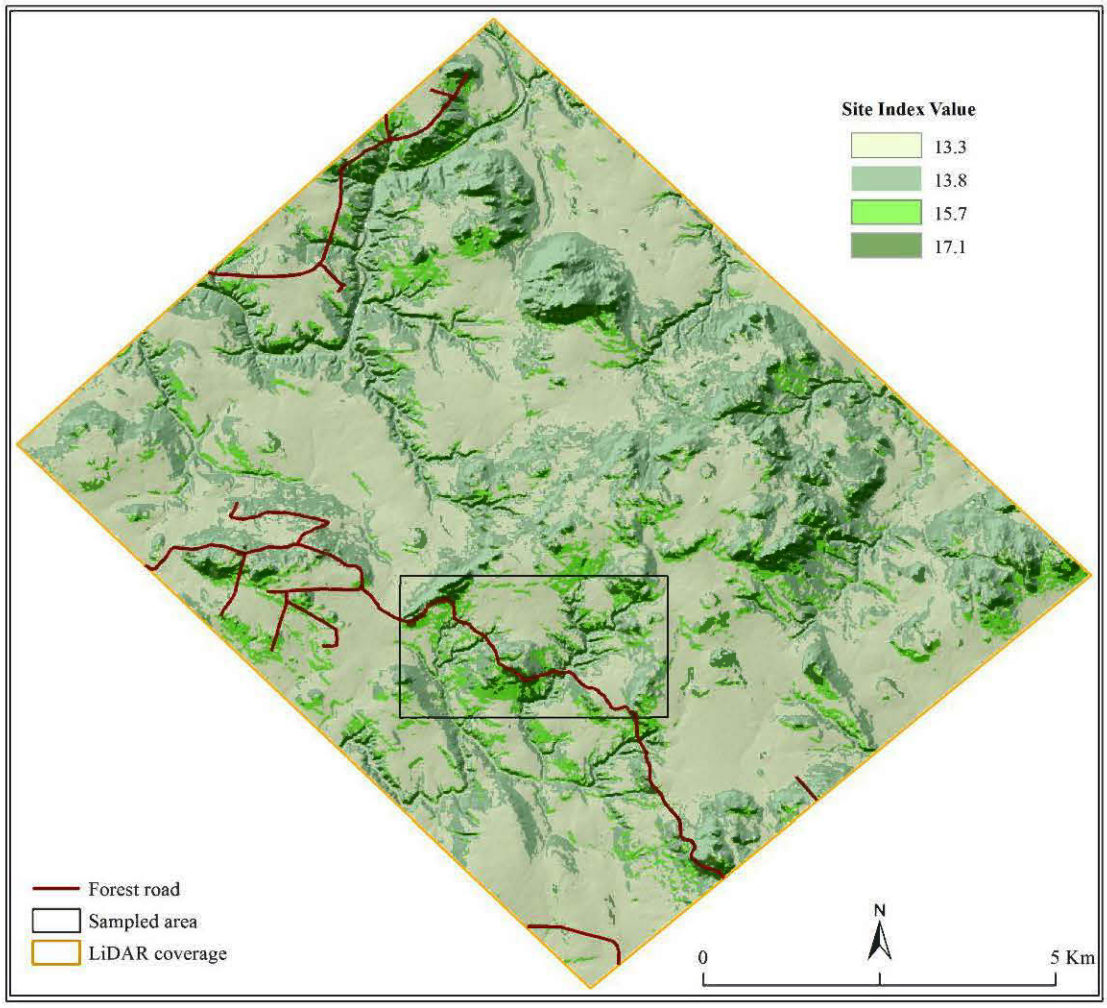

Figure 5.8. Map showing the spatial distribution of site index across study area based on predictions from regression tree model 2.

5.4.5 Management implications

The combination of field measurements with topographic information, which is derived from remotely sensed LiDAR data, has great potential utility for landscape scale management. This approach improved our understanding of how paludification and topography influence tree growth and productivity within the Clay Belt, which constituted a significant first step in predicting and mapping forest productivity across the landscape. Such information could help forest managers predict how forest growth will respond to various harvesting activities. The site index that was used in this study as an estimator of potential productivity is simple in concept, could be easily defined, and provides a quantitative estimator of forest productivity.

Regression tree-based modelling results demonstrated that paludification and topography significantly influence the spatial distribution of productivity. Moreover, these relationships can be used to split the landscape into more homogeneous units in terms of forest productivity; and therefore, could aid in future planning of landscape management. For example, regression tree rules can be used to define both promising areas where efforts and investment should be made to attain higher productivity after logging and planting, and less promising areas where structure and biodiversity of these forests could be preserved.

This study also revealed critical thresholds for forest productivity that should be taken into consideration prior to any management planning. Furthermore, to maintain or improve forest productivity, management should focus on sloping sites (i.e., > 2.2%) with organic layer thicknesses ranging between 35 and 85 cm, rather than on unproductive sites that are associated with low slopes and with deep organic layers (> 85 cm). Southwest-facing sloping were associated with highly productive sites across the investigated areas, and probably a minimum of attention should be given to them since they already constitute the most productive sites. These recommendations were supported by data (Table 5.6), where we found that site indices were related to current productivity (expressed as merchantable volume), which decreased as the volume, basal area and biomass decreased, and increased as they increased. For instance, terminal nodes B and D of Model $1_{[20m]}$ had the highest and lowest average volume of 250 m^3/ha and 25.8 m^3/ha, respectively. Similar trends were recorded for basal area and biomass (Table 5.6) at the various resolutions.

Table 5.6. Summary statistics of the resulting regression tree-based terminal nodes with respect to current productivity.

Model	Terminal node splits	Mean Site index (m)	Volume (m^3/ha)	Basal area (m^2/ha	Biomass (t/ha)
1					
	A	14.8	172.7	31.4	87.9
	B	16.8	250.0	36.6	96.7
	C	13.7	116.0	22.6	66.8
	D	9.8	25.8	6.0	18.6
2					
	A	13.3	101.3	18.5	54.5
	B	13.8	143.0	28.4	81.1
	C	15.7	208.2	33.0	90.7
	D	17.1	262.6	39.6	105.4

Note: 20-m resolution models were used for illustration. Current productivity is expressed as mean values of merchantable volume, basal area, and biomass

Finally, it is worth mentioning that our study sites formed a subset of a larger group of long-term forest growth and yield study plots, which are located in the northwest boreal forest within the Clay Belt region. Our study was conducted prior to the implementation of recent forest management prescriptions (harvesting site preparation and planting). Therefore, results from this study should provide forest managers with an estimate of the original timber volume production, together with site indices prior to logging. They could be used to monitor the effects of forest management practices through time (i.e., forest harvesting, field preparation treatments, and trees replanting) on the original levels of forest productivity.

5.5. CONCLUSIONS

To our knowledge, this study is the first to address the effects of different LiDAR-DTM resolutions on forest productivity, and the relationships between site index and paludification and topography within the boreal forest. We used an unusual approach for assessing productivity at different resolutions. By using a regression tree-based approach, we were able to simultaneously incorporate multi-scale LiDAR-derived topographic variables (elevation, slope, aspect, curvature variables, topographic wetness index, topographic position index,

aspect index) into an explanation of variability in forest productivity within an area of the boreal black spruce forest. Consequently, the two regression tree models at four resolutions (for a total of eight models) that were developed in this study provided insights into which set of predictor variables were the most important for forest productivity, together with the scale at which they operated. Model 1 (based on organic layer thickness and topography) and model 2 (based on topography only) explained up to 63% and 31% of variation in forest productivity, respectively. Both models indicated that higher forest productivity occurred on southeast-facing slopes with shallower organic layers (< 35 cm), where warmer conditions prevailed, while lower productivity sites had very deep organic accumulations (> 85 cm). The most important finding of this study was that paludification operated equally well at both local and landscape scales, whereas the influence of topography on forest productivity increased with increasing slope. Also, there were distinctive scale effects around the 10-m resolution that possibly delineated localized (small) versus landscape (broad) influences on forest productivity. Therefore, the resulting tree models could be applied at finer and operational scales to predict site index at locations for which organic layer thickness information (i.e., permanent plots according to MRNQ) and DTM exist.

B. Conclusion Générale

Approfondir les connaissances sur les relations entre les variables permanentes du site et la productivité forestière de la pessière à épinette noire à l'aide d'approches spatiales est devenue essentielle. Cette thèse a permis d'identifier des relations quantitatives impliquant le degré de paludification, la topographie du sol minéral et de surface et la productivité des forêts à l'échelle locale et du paysage. Les résultats de cette thèse nous ont permis de déterminer différents seuils qui pourraient caractériser, à la fois, des zones paludifiées vs non paludifiés et des zones productives vs improductives. Nous avons été en mesure de cartographier l'étendue spatiale de la paludification (permanente vs réversibles), l'épaisseur de la couche organique (ECO) et la topographie (pente, TWI, TPI etc.) à l'échelle du paysage. Nous avons démontré l'apport significatif de l'utilisation des données terrain et des modèles topographiques multi-résolutions pour quantifier l'effet des échelles sur la productivité forestière. Nos méthodes d'analyse et nos résultats deviennent ainsi un outil essentiel dans la gestion durable des territoires paludifiés. Les aspects innovants de recherche ainsi que les apports scientifiques de chaque chapitre sont détaillés ci-après.

À notre connaissance, la méthode géoradar n'a jamais été utilisée pour documenter la paludification sur la ceinture d'argile. Dans ce contexte, les résultats du premier chapitre de la thèse ont démontré que la méthode géophysique géoradar, ayant une bonne corrélation de ses résultats avec les données du terrain (R^2= 0,87), a permis d'obtenir une cartographie précise, continue et fiable de l'interface couche organique/sol minéral dans des sites faiblement à modérément paludifiés. Par conséquent, le géoradar apparaît comme une méthode efficace pour cartographier l'interface couche organique/sol minéral et sa continuité latérale dans les sites faiblement à modérément paludifiés (ECO = 40 cm). Cependant, en dépit de son incapacité à cartographier l'interface couche organique/sol minéral dans les sites hautement paludifiés (ECO = 95 cm), le recours au géoradar s'est révélé pertinent dans la mise en évidence de l'interface horizon fibrique/couche organique et de sa continuité spatiale dans ces sites. Considérant que l'épaisseur de l'horizon fibrique pourrait être vue comme un indicateur des zones fortement paludifiées (Lafleur *et al.*, 2010), cela rend le géoradar particulièrement intéressant dans la détection des niveaux d'entourbement, ouvrant ainsi la

voie à une utilisation future à l'échelle du paysage. Cette étude a démontré que l'interface sol minéral/couche organique présente une topographie de creux-bosses qui a un effet sur le degré de paludification sur de courtes distances (à l'échelle du site). En effet, les structures en creux correspondant à de petites dépressions (hollows) présentant des taux d'humidité et une accumulation de sphaignes nettement élevés par rapport aux bosses où le sol minéral remonte près de la surface.

En raison de sa capacité de couvrir de larges surfaces à haute résolution et en un court laps de temps, le géoradar pourrait ainsi déterminer d'une manière continue l'interface couche organique/sol minéral et ses variations spatiales dans des milieux peu à moyennement paludifiés de la forêt boréale. Toutefois, avant l'application du géoradar à l'échelle du paysage, des modifications devraient être apportées durant l'acquisition. Pour faciliter une telle acquisition, une couverture de neige sur le sol forestier semble nécessaire, car des mesures géoradar se sont révélées difficiles à réaliser à l'échelle du paysage en présence de débris ligneux grossiers couvrant la surface du sol forestier. De plus, l'utilisation d'antennes à haute fréquence (p. ex., 500, 800 ou 1000 MHz), qui fournissent des résolutions verticales supérieures, pourrait être envisagée afin d'augmenter l'efficacité de la délimitation des différentes interfaces (couche organique/sol minéral; couche organique/horizon fibrique ou sol minéral/socle rocheux) tout en réduisant l'effet des ondes de surface. Pour faire suite au premier chapitre, les relations impliquant la topographie, l'ECO, les types de paludification et la productivité ont été explorées à l'échelle du paysage dans les quatre autres chapitres de la thèse.

Dans le deuxième chapitre de la thèse, nous avons quantifié la topographie de surface par un ensemble de variables prédictives provenant des données LiDAR (p. ex., rasters des pentes, aspect, courbure, etc.) avec différentes résolutions (1, 5, 10, et 20 m). L'analyse par arbre de régression nous a permis de subdiviser le jeu de données en six entités paysagères distinctes, en fonction de la pente, l'exposition, et la courbure totale du terrain. Nous avons utilisé les caractéristiques des six entités résultantes pour délimiter les principaux patrons de l'ECO et pour découvrir des relations spatiales entre l'ECO et les variables topographiques exclusivement à l'échelle du paysage des forêts paludifiées de la ceinture d'argile. Premièrement, la topographie de surface influence l'accumulation de la couche organique à

l'échelle du paysage. Deuxièmement, nous avons déterminé que les zones avec une couche organique épaisse (ECO = 62 cm) avaient des pentes douces (≤ 1,8%), tandis que les zones avec pentes plus raides (> 3,2%) ont été associées à des couches organiques minces (ECO = 27 cm). Troisièmement, les meilleurs résultats ont été obtenus avec des résolutions de 10 et 20 m en comparaison aux deux autres résolutions (1 et 5 m).

En raison de la couche organique relativement épaisse qui caractérise les forêts boréales, la topographie du sol minéral est difficile à déterminer, malgré son importance présumée dans l'accumulation des couches organiques. Dans ce contexte, le troisième chapitre a porté davantage sur le rôle de la topographie du sol minéral dans l'accumulation de couches organiques à l'échelle du paysage. La construction d'un DEM au niveau du sol minéral à l'échelle du paysage a constitué l'élément central de notre démarche et une première dans la caractérisation de la paludification au sein de la pessière à épinette noire. Par la suite, nous avons établi différentes relations quantitatives entre l'ECO et la topographie au niveau du sol minéral grâce à des approches de modélisation par arbre de régression ainsi que par de simples corrélations entre chaque variable topographique et l'ECO. Les modèles développés nous permettent d'affirmer que : (i) la qualité de prédiction du modèle utilisant uniquement les variables topographiques est moins élevée (R^2= 0,34) en comparaison à celle du modèle qui intègre aussi la composition du sol minéral en plus des variables topographiques (R^2= 0,52); (ii) la pente du sol minéral, la composition du sol minéral (argile, till et régolithe), le TWI et l'exposition sont les quatre principales variables influençant l'accumulation de la couche organique; (iii) les valeurs de pente du sol minéral > 3,5% et ≤ 2 % constituent des seuils permettant de distinguer d'une manière respective les zones les plus prometteuses et les plus vulnérables pour l'aménagement forestier; et (iv) les zones avec une exposition nord sont associées à une couche organique plus profonde par rapport à celles exposées vers le sud et l'ouest. Cet effet d'exposition semble être contradictoire aux résultats du chapitre II où les zones avec une association nord-est sont associées à des couches organiques plus faibles par rapport à celles exposées vers le sud-ouest. Cependant, la subdivision de l'exposition en classes plus fines (8 pour le chapitre II *vs* 4 pour le chapitre III) ainsi que l'utilisation de différentes résolutions pourraient expliquer les variations de réponse constatées. Un autre apport majeur de cette étude est le fait que nous avons été en mesure d'établir un seuil de la pente du sol minéral de l'ordre de 3,5% permettant de distinguer les zones paludifiées de

celles non paludifiées. Cette distinction se faisait auparavant en catégorisant les zones paludifiées par des seuils arbitraires. Les modèles utilisés ont réussi à discriminer les entités de paysage hautement paludifiées, sans pour autant être capables de clairement distinguer les deux types de paludification. Cela est probablement dû à la taille réduite de la surface couverte par notre DEM du sol minéral puisque l'effet de certaines variables topographiques (p. ex., TWI) s'exprime mieux sur de grands territoires (nous avons traité de ceci dans le chapitre IV). Les résultats impliquant la topographie au niveau du sol minéral sont en général en accord avec ce qui a été trouvé pour la topographie de surface.

Du point de vue de l'aménagement forestier, les résultats des chapitres II et III nous ont permis: (i) de produire une carte montrant les variations spatiales des épaisseurs de la couche organique à travers le territoire à l'étude; et (ii) de comprendre comment la topographie de surface est liée à l'ECO, ce qui a constitué une première étape dans la prédiction et la cartographie de la productivité forestière à l'échelle du paysage. De telles informations pourraient aider les gestionnaires forestiers à prédire les zones potentielles d'accumulation de couche organique et par conséquent, adopter des pratiques d'aménagement forestier plus adaptées à ces zones. Par exemple, l'indice topographique d'humidité est simple dans son concept, facile à définir, et fournit une notion intuitive d'humidité. Il pourrait donc être utilisé par les gestionnaires forestiers pour mieux gérer les ressources forestières là où l'humidité élevée du sol pourrait affecter la productivité. Pour un maintien, voire une amélioration de la productivité forestière dans la région de la ceinture d'argile, les stratégies de gestion devraient désormais se concentrer sur les sites avec des pentes de surfaces supérieures à 2,3% plutôt que sur des sites plats (pente $\leq$ 1,8%). Ces derniers sont souvent associés à des zones avec une couche organique profonde inappropriée à la plantation d'arbres (Lafleur *et al.*, 2010), offre peu ou pas d'avantages écologiques quant à son aménagement (Simard *et al.*, 2009) et posent des défis énormes pour la machinerie lors des différentes opérations sylvicoles (Lavoie *et al.*, 2007).

Dans le quatrième chapitre, nous avons développé et validé une méthode semi-automatisée de classification des deux types de paludification, réversible et permanente, à l'échelle du paysage. Cette méthode repose sur l'utilisation de la topographie de surface comme support de spatialisation des deux types de paludification. Grâce à cette méthode,

nous avons réussi à subdiviser le terrain à l'étude en des entités paysagères distinctes qui correspondent à des portions de la topographie présentant des propriétés, des formes et des types de paludification relativement homogènes. La délimitation de ces entités spatiales a été réalisée grâce au traitement du MNT dans un environnement SIG (ArcGIS 2011) en utilisant des valeurs seuils de variables topographiques quantitatives. En effet, en combinant des données topographiques, notamment le TPI, le TWI ainsi que la pente de surface, nous avons été en mesure de distinguer et de cartographier pour la première fois la paludification permanente et réversible à l'échelle du paysage dans les forêts paludifiées de la ceinture d'argile. La paludification réversible et permanente sont des concepts considérés jusqu'à dernièrement théoriques que nous avons aussi réussi à discriminer. La méthode de classification s'est avérée efficace pour prédire les conditions morphologiques et d'humidité, tout en fournissant des informations assez précises sur la localisation des zones de paludification permanente et réversible à l'échelle du paysage. Ces zones correspondaient à des entités spatiales distinctes du paysage possédant des caractéristiques géomorphologiques semblables, notamment en termes de tendance à l'accumulation de la couche organique. La cartographie de ces deux types de paludification a exclusivement révélé l'existence des structures en creux (dépressions) souvent linéaires et remplies de tourbes témoignant d'anciens réseaux de drainages (drainage fossilisé). Plusieurs de ces dépressions ont été dévoilées grâce à notre classification et méritent d'être étudiées en profondeur à l'avenir en raison de leur effet négatif sur la productivité. Un autre apport majeur de ce quatrième chapitre est la mise en évidence d'une classification qui a permis de fractionner l'entité morphologique nommée dépression par Weiss (2001) en deux sous-entités statistiquement différentes (le test *HSD* de *Tukey*, $P < 0{,}001$), à savoir des dépressions ouvertes préférentiellement drainées (paludification réversible) et des dépressions fermées potentiellement engorgées (paludification permanente). Ceci contredit la supposition que la paludification permanente est de facto associée à des dépressions naturelles dans le paysage. Dans une optique d'aménagement forestier, la classification proposée offre un outil relativement simple et pratique pour distinguer et cartographier les types de paludification permanente et réversible avec une bonne précision globale. Cette cartographie pourrait être utilisée, à la fois, pour identifier les endroits où des efforts et des investissements devraient se faire pour garantir une productivité égale ou supérieure après la récolte de bois et pour

identifier des zones de rétention dont les attributs, les habitats et la structure sont nécessaires pour la biodiversité. L'outil développé serait particulièrement utile pour la mise en œuvre des stratégies d'aménagement durable dans les régions boréales éloignées où les données de terrain sont particulièrement rares en raison de l'éloignement de ces régions et le manque de structures routières.

Dans le cinquième chapitre nous avons affirmé que l'ECO et sa relation à la topographie sont les deux plus importants facteurs qui influencent la productivité des forêts paludifiées de la ceinture d'argile. Contrairement à un grand nombre d'études qui ont été menées sur une étendue spatiale plus limitée (p. ex., à l'échelle de la placette) dans les forêts paludifiées de la ceinture d'argile, cette thèse a bénéficié de l'utilisation des données LiDAR multi-échelles permettant d'analyser les données à différentes résolutions (5, 10, 15 et 20 m) et sur de larges superficies (~10 000 hectares). Un autre aspect qui distingue ce travail des autres études antérieures sur la productivité forestière de la pessière à épinette noire est l'utilisation d'une variété de variables topographiques, notamment des indices plus complexes tels que le TPI et le TWI, alors que les études antérieures ont utilisé un nombre relativement petit de variables topographiques, calculées sur le terrain (p. ex., la pente).

À notre connaissance, cette thèse est la première à explorer l'effet de différentes résolutions sur la productivité à l'échelle du paysage dans les forêts paludifiées de la ceinture d'argile. En effet, nous visions d'une manière plus spécifique d'acquérir des informations sur la manière dont différentes échelles (résolutions) influencent la productivité forestière à l'échelle du paysage. Pour cela, nous avons combiné des données provenant des MNT et d'autres acquises sur le terrain à différentes résolutions, notamment des données sur le sol et la végétation. Ces dernières ont servi pour le calcul d'indicateurs de productivité potentielle (IQS) et actuelle (volume, surface terrière ou biomasse). Les données de terrain et topographiques recueillies à différentes échelles ont été utilisées pour cartographier spatialement les effets des variables explicatifs (l'ECO et variables topographiques) à différentes résolutions sur la productivité potentielle à l'échelle du paysage. Pour cela, nous avons utilisé une démarche de modélisation basée sur l'application d'arbres de régression. Deux grands modèles ont été utilisés avec quatre résolutions (5, 10, 15 et 20 m) : un premier utilisant toutes les variables explicatives exprimant la paludification et la topographie

(modèle 1), et un deuxième utilisant seulement les variables topographiques issues des différents MNT. D'une façon générale, les résultats de cette modélisation nous ont permis de mettre en valeur notre contribution sous une forme plus appliquée dans laquelle les relations établies nous permettent de prédire et évaluer la productivité forestière. Ils nous ont également permis d'identifier les seuils où certaines résolutions spatiales permettaient de rendre les relations établies significatives à l'échelle du paysage. Plus spécifiquement, les résultats de ce cinquième chapitre ont mis en évidence plusieurs apports majeurs : (i) l'ECO, l'exposition et la pente sont les variables les plus importantes pour expliquer la productivité forestière (63% et 31% de variation expliquée pour les modèles 1 et 2, respectivement) à l'échelle du paysage; (ii) les zones avec un IQS élevé (synonyme de productivité élevée) étaient associées à une couche organique faible (< 35 cm) et à des pentes supérieures à 2,2% orientées sud-ouest, favorisant une plus forte croissance des arbres; (iii) en revanche, les zones avec les plus faibles IQS avaient une couche organique très profonde (> 85 cm). Ces conditions affectent la dynamique de la succession et favorisent l'invasion de mousses et de sphaignes ce qui favorise la progression de la paludification; (iv) le premier modèle semble relativement indépendant de l'échelle (résolutions), alors que la réponse du deuxième modèle augmentait significativement avec la taille du pixel.

Tout comme Simard *et al.*, (2009) et Giroux *et al.*, 2001, cette thèse a confirmé l'importance de l'ECO et la topographie sur la productivité dans les forêts paludifiées de la ceinture d'argile, mais cette fois-ci à l'aide d'une approche paysagère multi-échelles. De plus, les résultats du cinquième chapitre ont permis d'établir des seuils qui pourraient faciliter la distinction entre les zones hautement à moyennement productives des zonnes improductives. Les modèles qui en résultent pourraient être appliqués à des échelles opérationnelles et aux prédictions de la productivité là où des informations sur l'ECO en continu sont disponibles. Parmi celles-ci, on note l'existence d'une tentative de cartographie régionale de cet attribut (ECO) basée sur des données de télédétection par des chercheurs du Centre Forestier des Laurentides (Beaudoin *et al.*, 2013, communication personnelle). La limite de ces données réside cependant dans leur gamme de valeurs (8-65 cm) qui, de ce fait, ne pourrait pas prendre en compte la totalité de variabilité de l'ECO trouvé par notre modèle 1. Toutefois, nous avons utilisé la gamme de valeurs inférieures à 35 cm issus des travaux de Beaudoin *et al.*, (2013, communication personnelle) pour réaliser une cartographie prédictive des deux

classes les plus productives du modèle 1. Une validation de la carte qui en résulte a montré une précision moyenne, fort probablement en raison de la variabilité limitée de ces données. Il est donc important de continuer les recherches afin de doter la région de la ceinture d'argile de données précises, continues et fiables sur la distribution spatiale de l'ECO. De telles données pourraient valoriser davantage l'utilisation des modèles réalisés dans le cadre de cette thèse. Néanmoins, dans une perspective d'aménagement forestier durable, les résultats de ce dernier chapitre ont démontré l'utilité de l'utilisation de données conjointes recueillies sur le terrain et à partir de produit de télédétection (LiDAR) pour l'aménagement forestier à l'échelle du paysage. Cette approche a amélioré notre compréhension de la façon dont la paludification et la topographie influencent la productivité et la croissance des arbres au sein de la ceinture d'argile, ce qui constitue une première étape importante dans la prédiction et la cartographie de la productivité de la forêt à l'échelle du paysage. Les gestionnaires forestiers pourraient ainsi utiliser de telles informations pour prédire comment la croissance de la forêt répondrait à diverses activités de récolte. Par exemple, les résultats de la modélisation basée sur les arbres de régressions ont démontré que les relations entre la paludification, la topographie et la productivité pourraient être utilisées pour séparer le paysage en unités plus homogènes en termes de productivité de la forêt. Rappelons que ce chapitre a également mis en évidence des seuils critiques pour la productivité des forêts qui devraient être pris en considération avant toute planification future de l'aménagement des forêts paludifiées de la ceinture d'argile à l'échelle du paysage. Par exemple, nous recommandons que les activités d'aménagement forestier soient concentrées sur des sites en pente (> 2,2%) avec des épaisseurs de couches organiques comprises entre 35 et 85 cm, plutôt que sur des sites non productifs qui sont associés à des pentes faibles et à des couches organiques profondes (> 85 cm). Les sites en pentes orientées sud-ouest étaient hautement productifs et devraient nécessiter moins d'investissements, car ils constituent déjà les sites les plus productifs dans la zone d'étude. Ces recommandations sont en accord avec les données du Tableau 5.6 montrant la productivité actuelle à l'intérieur de chacune des entités spatiales résultantes des deux modèles sur la productivité.

Il est important de mentionner que les travaux menés au cours de cette thèse font partie d'un projet multidisciplinaire sur la croissance et le rendement à long terme de forêts paludifiées dans la pessière à épinette noire, notamment la région de la ceinture d'argile.

Notre étude a été réalisée avant la mise en œuvre de récents travaux sylvicoles (récolte, préparation de terrain, reboisement). Par conséquent, les résultats de cette étude devraient fournir aux gestionnaires forestiers et aux chercheurs une estimation de la productivité potentielle (IQS) et de la productivité avant coupe (volume de bois d'origine). Ces informations pourraient être ainsi utilisées pour un suivi temporel des effets des pratiques d'aménagement forestier sur les niveaux de productivité d'avant récolte de bois. En définitive, les résultats de cette thèse permettront à l'industrie de mieux planifier les secteurs de remise en production, de diminuer les coûts reliés aux opérations forestières et de mieux prédire les gains en productivité pour l'industrie forestière. À long terme, une telle analyse avec des outils performants permettrait de réduire les coûts liés à l'obtention de cette information sur le terrain. Une autre application des résultats de cette étude serait de démontrer qu'il est possible d'effectuer une cartographie fonctionnelle détaillée de la pente, au lieu d'utiliser des classes de pentes (ex., cartes écoforestières), tout en valorisant l'usage des méthodes à haute résolution comme outils possibles dans la planification et l'aménagement futurs des forêts paludifiées.

En fin, dans une perspective plus globale, à l'ensemble de la ceinture d'argile, les travaux de cette thèse laissent entrevoir une classification des environnements propices à l'identification des foyers de paludification. Les paramètres et les relations identifiés dans cette thèse seront utiles pour une étude plus globale. De plus, les travaux de cette thèse ont clairement souligné le besoin d'integrer aux modèles de terrain (MNT) la connaissance du mode de mise en place et la genèse de ces terrains. À cet effet, la poursuite de ce travail dans une perspective plus globale exigera donc une approche faisant une large place aux facteurs responsables de la topographie du substrat (p. ex., roc). Ces facteurs sont forcément d'ordre géologique et géomorphologique et devront être intégrés à ceux identifiés dans cette étude pour carateriser les foyers de paludification.

C. BIBLIOGRAPHIE

Amato, M., Basso, B., Celano, G., Bitella, G., Morelli, G., and Rossi, R. (2008). In situ detection of tree root distribution and biomass by multi-electrode resistivity imaging. *Tree* Physiology, 28(10), 1441-1448. doi: 10.1093/treephys/28.10.1441.

Annan, A.P. (1999). Ground Penetrating Radar: Survey Design. *Sensors and Software Inc., Mississauga, ON, Canada.*

Anyomi, K.A., Raulier, F., Bergeron, Y., Mailly, D. (2013). The predominance of stand composition and structure over direct climatic and site effects in explaining aspen (*Populus tremuloides* Michaux) site index within boreal and temperate forests of western Quebec, Canada. *Forest Ecology and Management, 302*, 390-403.

Baldwin, D.J.B., Desloges, J.R., and Band, L.E. (2000). Physical Geography of Ontario. In *Ecology of a Managed Terrestrial Landscape: Patterns and Processes of Forest Landscapes in Ontario.* Edited by Perera, A.H., Euler, D.E., and Thompson, I.D. University of British Columbia Press, Vancouver. pp. 141–162.

Bergeron, Y., Gauthier, S., Flannigan, M., Kafka, V., 2004. Fire regimes at the transition between mixedwood and coniferous boreal forest in northwestern Quebec. *Ecology*, *85*(7), 1916-1932.

Bergeron, Y., Gauthier, S., Kafka, V., Lefort, P., and Lesieur, D., 2001. Natural fire frequency for the eastern Canadian boreal forest: Consequences for sustainable forestry. *Canadian Journal Forest Research*, *31*(3), 384-391.

Blyth, E.M., Finch, J., Robinson, M., and Rosier, P. (2004). Can soil moisture be mapped onto the terrain? *Hydrology and Earth System Sciences, 8*(5), 923-930.

Boelter, D. H. (1969). Physical properties of peats as related to degree of decomposition. *Soil Science Society of America Proceedings*, *33*, 606-609

Bolton, D.K., Coops, N.C., and Wulder, M.A. (2013). Measuring forest structure along productivity gradients in the Canadian boreal with small-footprint LiDAR. *Environmental Monitoring and Assessment*, *185*(8), 6617-6634.

Bonan, G.B., and Shugart, H.H., 1989. Environmental factors and ecological processes in boreal forests. *Annual review of ecology and systematics*, *20*, 1-28.

Bou Kheir, R., Bøcher, P.K., Greve, M.B., and Greve, M.H. (2010). The application of GIS based decision-tree models for generating the spatial distribution of hydromorphic organic landscapes in relation to digital terrain data. *Hydrology and Earth System Sciences, 14*(6), 847-857.

Boudreault, C., Bergeron, Y., Gauthier, S., and Drapeau, P. (2002). Bryophyte and lichen communities in mature to old-growth stands in eastern boreal forests of Canada. *Canadian Journal of Forest Research, 32*(6), 1080-1093.

Burrough, P.A., Van Gaans, P.F.M., and MacMillan, R.A. (2000). High-resolution landform classification using fuzzy k -means. *Fuzzy Sets and Systems, 113*(1), 37-52.

Butnor, J.R., Doolittle, J.A., Johnsen, K.H., Samuelson, L., Stokes, T., and Kress, L. (2003). Utility of ground-penetrating radar as a root biomass survey tool in forest systems. *Soil Science Society of America Journal, 67*(5)1607-1615.

Butnor, J.R., Doolittle, J.A., Kress, L., Cohen, S., and Johnsen, K.H. (2001). Use of ground-penetrating radar to study tree roots in the Southeastern United States. *Tree Physiology, 21*(17), 1269-1278.

Catapano, I., Crocco, L., Krellmann, Y., Triltzsch, G., and Soldovieri, F. (2012). A tomographic approach for helicopter-borne ground penetrating radar imaging. *IEEE Geoscience and Remote Sensing Letters, 9*(3), 378-382.

Chen, H.Y.H., Krestov, P.V., and Klinka, K. (2002). Trembling aspen site index in relation to environmental measures of site quality at two spatial scales. *Canadian Journal of Forest Research, 32*(1), 112-119

Clark, R.B., Creed, I.F., and Sass, G.Z. (2009). Mapping hydrologically sensitive areas on the Boreal Plain: A multitemporal analysis of ERS synthetic aperture radar data. *International Journal of Remote Sensing, 30*(10), 2619-2635.

Comas, X., Slater, L., and Reeve, A. (2004). Geophysical evidence for peat basin morphology and stratigraphic controls on vegetation observed in a northern peatland. *Journal of Hydrology, 295*(1-4), 173-184.

Comas, X., Slater, L., and Reeve, A. 2005a. Spatial variability in biogenic gas accumulations in peat soils is revealed by ground-penetrating radar (GPR). *Geophysical Research Letters, 32*(8), 1-4.

Comas, X., Slater, L., and Reeve, A. (2005b). Stratigraphic controls on pool formation in a domed bog inferred from ground penetrating radar (GPR). *Journal of Hydrology, 315*(1-4), 40-51.

Congalton, R. G. (1991). A review of assessing the accuracy of classifications of remotely sensed data. *Remote Sensing of Environment, 37*(1), 35-46.

Crawford, R.M.M., Jeffree, C.E., and Rees, W.G. (2003). Paludification and forest retreat in northern oceanic environments. *Annals of Botany*, 91, 213–226.

Creed, I.F., and Beall, F.D. (2009). Distributed topographic indicators for predicting nitrogen export from headwater catchments. *Water Resources Research, 45*(10), art. No. W10407. Doi: 10.1029/2008WR007285

Creed IF, and Sass GZ. (2011). Digital terrain analysis approaches for tracking hydrological and biogeochemical pathways and processes in forested landscapes, In: Forest hydrology and biogeochemistry: synthesis of past research and future directions. Levia D, Carlyle-Moses D, Tanaka T (eds). Springer-Verlag: New York. pp 69–100

Dahlke, H.E., Behrens, T., Seibert, J., and Andersson, L. (2009). Test of statistical means for the extrapolation of soil depth point information using overlays of spatial environmental data and bootstrapping techniques. *Hydrological Processes, 23*(21), 3017-3029.

Davis, J.L., and Annan, A.P. (1989). Ground penetrating radar for high-resolution mapping of soil and rock stratigraphy. *Geophysical Prospecting*, *37*(5), 531-551.

De Reu, J., Bourgeois, J., Bats, M., Zwertvaegher, A., Gelorini, V., De Smedt, P., Chu, W., Antrop, M., De Maeyer, P., Finke, P., *et al.* (2013). Application of the topographic position index to heterogeneous landscapes. *Geomorphology, 186*, 39-49.

De'Ath, G., and Fabricius, K.E. 2000. Classification and regression trees: A powerful yet simple technique for ecological data analysis. *Ecology*, *81*(11), 3178 –3192.

Deumlich, D., Schmidt, R., and Sommer, M. (2010). A multiscale soil-landform relationship in the glacial-drift area based on digital terrain analysis and soil attributes. *Journal of Plant Nutrition and Soil Science 173*(6), 843-851

Doolittle, J.A., and Collins, M.E. (1995). Use of soil information to determine application of ground-penetrating radar. *Journal of Applied Geophysics*, *33*(1-3), 101-108.

Emili, L.A., Price, J.S., and Fitzgerald, D.F. (2006). Hydrogeological influences on forest community type along forest-peatland complexes in coastal British Columbia. *Canadian Journal of Forest Research*, *36*(8), 2024-2037.

Environment Canada, (2011). Canadian Climate Normals 1971-2000. Matagami weather station. Available online at http://www.ec.gc.ca/. Last accessed January 2014.

ESRI. (2011). ArcGIS Desktop: Release 10. Environmental Systems Research Institute, Redlands, CA, USA. Available online at http://help.arcgis.com/en/arcgisdesktop/10.0/help/; last accessed January 2014.

Everitt, S., and Hothorn, T. (2009). A Handbook of Statistical Analyses Using R, 2nd ed. CRC Press, Francis & Taylor Group.

Fenton, N.J., and Bergeron, Y. (2006). *Sphagnum* spore availability in boreal forests. *Bryologist 109*(2), 173-181.

Fenton, N.J., and Bergeron, Y. (2006). Facilitative succession in a boreal bryophyte community driven by changes in available moisture and light. *Journal of Vegetation Science, 17*(1), 65–76.

Fenton, N., and Bergeron, Y. (2007). Sphagnum community change after partial harvest in black spruce boreal forests. *Forest Ecology and Management, 242*(1), 24 –33.

Fenton, N., Lecomte, N., Légaré, S., and Bergeron, Y. (2005). Paludification in black spruce (*Picea mariana*) forests of eastern Canada: Potential factors and management implications. *Forest Ecology and Management, 213*(1-3), 151-159.

Fenton, N., Légaré, S., Bergeron, Y., and Paré, D. (2006). Soil oxygen within boreal forests across an age gradient. *Canadian Journal of Soil Science, 86*(1), 1-9.

Fenton, N.J., Simard, M., and Bergeron, Y. (2009). Emulating natural disturbances: The role of silviculture in creating even-aged and complex structures in the black spruce boreal forest of eastern North America. *Journal of Forest Research, 14*(5), 258 –267.

Gallant, J.C., and Wilson, J.P. (2000). Primary topographic attributes, in: Wilson, J.P., Gallant, J.C. (Eds.), Terrain Analysis: Principles and Applications. Wiley, New York. pp. 51–85.

Gerber, R., Felix-Henningsen, P., Behrens, T., and Scholten, T. (2010). Applicability of ground-penetrating radar as a tool for nondestructive soil-depth mapping on Pleistocene periglacial slope deposits. *Journal of Plant Nutrition and Soil Science, 173*(2), 173-184.

Gerber, R., Salat, C., Junge, A., Felix-Henningsen, P. (2007). GPR-based detection of Pleistocene periglacial slope deposits at a shallow-depth test site. *Geoderma, 139*(3-4), 346-356

Gessler, P.E., Moore, I.D., McKenzie, N.J., and Ryan, P.J. (1995). Soil-landscape modelling and spatial prediction of soil attributes. *International Journal of Geographical Information Systems, 9*(4), 421–432.

Giroux, J.F., Bergeron, Y., and Veillette, J.J. (2001). Dynamics and morphology of giant circular patterns of low tree density in black spruce stands in northern Quebec. *Canadian Journal of Botany, 79*(4), 420-428

Gómez-Ortiz, D., Martín-Crespo, T., Martín-Velázquez, S., Martínez-Pagán, P., Higueras, H., and Manzano, M. (2010). Application of ground penetrating radar (GPR) to delineate clay layers in wetlands. A case study in the Soto Grande and Soto Chico watercourses, Doñana (SW Spain). *Journal of Applied Geophysics, 72*(2), 107-113.

Gorozhankina, S.M. (1997). Paludification in the Tsentral'no-Sibirskii biosphere reserve (the Yenisei region of Siberia). *Russian Journal of Ecology, 28*(2), 67–72.

Grant, J. A. and P. H. Schultz, (1994). Erosion of ejecta at Meteor Crater: Constraints from ground penetrating radar.. In *Proceedings Fifth International Conference on Ground-Penetrating Radar,* June 12–14, 1994, Kitchener, ON, Canada. Edited by Waterloo Centre for Groundwater Research and the Canadian Geotechnical Society, Waterloo, ON. pp. 789-803.

Grant, R.F. (2004). Modeling topographic effects on net ecosystem productivity of boreal black spruce forests, *Tree Physiology 24*(1), 1–18.

Greve, M.H., Kheir, R.B., Greve, M.B., and Bøcher, P.K. (2012a). Quantifying the ability of environmental parameters to predict soil texture fractions using regression-tree model with GIS and LiDAR data: The case study of Denmark. *Ecological Indicators, 18*, 1-10.

Greve, M.H., Kheir, R.B., Greve, M.B., and Bøcher, P.K. (2012b). Using digital elevation models as an environmental predictor for soil clay contents. *Soil Science Society of America Journal, 76*(6), 2116-2127.

Güntner, A., Seibert, J., and Uhlenbrook, S. (2004). Modeling spatial patterns of saturated areas: An evaluation of different terrain indices. *Water Resources Research, 40*(5),W051141-W0511419.

Hamel, B., Bélanger, N., and Paré, D. (2004). Productivity of black spruce and jack pine stands in Quebec as related to climate, site biological features and soil properties. *Forest Ecology and Management, 191*(1-3), 239-251.

Hänninen, P. (1992). Application of ground penetrating radar to peatland investigations. Fourth international conference on GPR, Rovaniemi, Finland 1992. *Geological Survey of Finland, Special paper, 16*, 217-221.

Häring, T., Dietz, E., Osenstetter, S., Koschitzki, T., and Schröder, B. (2012). Spatial disaggregation of complex soil map units: A decision tree-based approach in Bavarian forest soils. *Geoderma, 185–186*, 37– 47.

Hirano, Y., Dannoura, M., Aono, K., Igarashi, T., Ishii, M., Yamase, K., Makita, N., and Kanazawa, Y. (2009). Limiting factors in the detection of tree roots using ground-penetrating radar. *Plant and Soil, 319*(1-2), 15-24.

Hodgson, M.E., Jensen, J., Raber, G., Tullis, J., and Davis, B.A., Thompson, G., and Schuckman, K. (2005). An evaluation of LiDAR -derived elevation and terrain slope in leaf-off conditions. *Photogrammetric Engineering and Remote Sensing, 71*(7), 817-823.

Hodgson, M.E., Jensen, J.R., Schmidt, L., Schill, S., and Davis, B. (2003). An evaluation of LiDAR - and IFSAR-derived digital elevation models in leaf-on conditions with USGS level 1 and level 2 DEMs. *Remote Sensing of Environment, 84*(2), 295-308.

Holden, J., Burt, T.P., and Vilas, M. (2002). Application of ground-penetrating radar to the identification of subsurface piping in blanket peat. *Earth Surface Processes and Landforms, 27*(3), 235-249

Hollingsworth, T.N., Walker, M.D., and Chapin III, F.S., and Parsons, A.L. (2006). Scale-dependent environmental controls over species composition in Alaskan black spruce communities. *Canadian Journal of Forest Research, 36*(7), 1781-1796.

Horn, B.K.P., 1981. Hill shading and the reflectance map. P IEEE 69, 14-47.

Hothorn, T., Hornik, K., and Zeileis, A. (2006). Unbiased recursive partitioning: A conditional inference framework. *Journal of Computational and Graphical Statistics, 15*(3), 651– 674.

Hruska, J., Cermàk, J., and Sustek, S. (1999). Mapping tree root systems with ground-penetrating radar. *Tree Physiology*, *19*(2), 125-130.

Hyde, P., Dubayah, R., Peterson, B., Blair, J.B., Hofton, M., Hunsaker, C., Knox, R., and Walker, W. (2005). Mapping forest structure for wildlife habitat analysis using waveform LiDAR: Validation of montane ecosystems. *Remote Sensing of Environment, 96*(3-4), 427- 437.

Jenness, J., Majka, D., Beier, P. (2011). Corridor Designer Evaluation Tools: Extension for ArcGIS. Jenness Enterprises. http://www.jennessent.com/arcgis/corridor.htm. Last accessed August 2013.

Johnson, K.D., Scatena, F.N., Johnson, A.H., and Pan, Y. (2009). Controls on soil organic matter content within a northern hardwood forest. *Geoderma, 148*(3-4), 346-356.

Jol, H.M., and Bristow, C.S. (2003). GPR in sediments: Advice on data collection, basic processing and interpretation, a good practice guide. *Geological Society, Special publication*, *211*, 9-27.

Jol, H.M., and Smith, D.G. (1991). Ground penetrating radar of northern lacustrine deltas. *Canadian Journal of Earth Sciences*, Vol. 28, No. 12, pp. 1939-1947.

Kettles, I.M. and Robinson, S.D. (1997). A ground penetrating radar study of peat landforms in the discontinuous permafrost zone near Fort Simpson, Northwest Territories, Canada, in: Northern Forested Wetlands: Ecology and Management. C.C. Trettin, M. F. Jurgensen, D. F. Grigal, M. R. Gale, and J. K. Jeglum (ed.). CRC Lewis Publishers, Boca Raton, FL, USA. pp. 147–160

Kettridge, N., Comas, X., Baird, A., Slater, L., Strack, M., Thompson, D., Jol, H., and Binley, A. (2008). Ecohydrologically important subsurface structures in peatlands revealed by ground-penetrating radar and complex conductivity surveys. *Journal of Geophysical Research G: Biogeosciences*, *113*(4), 1-15.

Kljun, N., Black, T.A., Griffis, T.J., Barr, A.G., Gaumont-Guay, D., Morgenstern, K., McCaughey, J.H., and Nesic, Z. (2006). Response of net ecosystem productivity of three boreal forest stands to drought. *Ecosystems*, *9*(6), 1128-1144.

Laamrani, A., Valeria, O., Cheng, L.Z., Bergeron, Y., and Camerlynck, C. (2013). The use of ground penetrating radar for remote sensing the organic layer-mineral soil interface in paludified boreal forests. *Canadian Journal of Remote Sensing, 39*(1), 74-88.

Laamrani, A., Valeria, O., Fenton, N., Bergeron, Y., and Cheng, L.Z. (2014a). Landscape-scale influence of topography on organic layer accumulation in paludified boreal forests. *Forest Science, 60*(x), xx-xx. Article first published online: 19 September 2013; Doi:10.5849/forsci.13-025.

Laamrani, A., Valeria, O., Fenton, N., Bergeron, Y., and Cheng, L.Z. (2014b). The role of mineral soil topography on the spatial distribution of organic layer thickness in a

paludified boreal landscape. Geoderma. Article first published online: 28 January 2014. http://dx.doi.org/10.1016/j.geoderma.2014.01.003.

Lafleur, B., Fenton, N.J., Paré, D., Simard, M., and Bergeron, Y. (2010). Contrasting effects of season and method of harvest on soil properties and the growth of black spruce regeneration in the boreal forested peatlands of eastern Canada. *Silva Fennica, 44*(5), 799-813.

Lapen, D.R., Moorman, B.J., Price, J.S. 1996. Using ground-penetrating radar to delineate subsurface features along a wetland catena. *Soil Science Society of America Journal, 60*(3), 923-931

Larocque, I., Bergeron, Y., Campbell, I.D., and Bradshaw, R.H.W. (2003). Fire-induced decrease in forest cover on a small rock outcrop in the Abitibi region of Québec, Canada. *Ecoscience, 10*(4), 515–524.

Lavoie, M., Pare, D., Fenton, N., Groot, A., and Taylor, K. (2005). Paludification and management of forested peatlands in Canada: A literature review. *Environmental Reviews, 13*(2), 21-50.

Lavoie, M., Harper, K., Paré, D., and Bergeron, Y. (2007). Spatial pattern in the organic layer and tree growth: A case study from regenerating Picea mariana stands prone to paludification. *Journal of Vegetation Science, 18*(2), 213–222.

Lecomte, N., Simard, M., Bergeron, Y., Larouche, A., Asnong, H., and Richard, P.J.H. (2005). Effects of fire severity and initial tree composition on understorey vegetation dynamics in a boreal landscape inferred from chronosequence and paleoecological data. *Journal of Vegetation Science, 16*(6), 665– 674.

Lindsay, J.B., and Creed, IF. (2005). Removal of artifact depressions from digital elevation models: towards a minimum impact approach. *Hydrological Processes, 19*(16), 3113–3126.

Lowe, D.J. (1985). Application of impulse radar to continuous profiling of tephra-bearing lake sediments and peats: an initial evaluation. *New Zealand Journal of Geology & Geophysics, 28*(4), 667-674.

Lowry, C.S., Fratta, D., and Anderson, M.P. (2009). Ground penetrating radar and spring formation in a groundwater dominated peat wetland. *Journal of Hydrology, 373*(1-2), 68-79.

MacMillan, R., Pettapiece, W., Nolan, S., and Goddard, T. (2000). A generic procedure for automatically segmenting landforms into landform elements using DEMs, heuristic rules and fuzzy logic. *Fuzzy Sets and Systems, 113*(1), 81–109.

MacMillan, R.A., Moon, D.E., and Coupé, R.A. (2007). Automated predictive ecological mapping in a Forest Region of B.C., Canada, 2001-2005. *Geoderma 140*(4), 353-373.

Magnussen, S., and Wulder, M.A. (2012). Post-fire canopy height recovery in Canada's boreal forests using airborne laser scanner (ALS). *Remote Sensing, 4*(6), 1600-1616. doi:10.3390/rs4061600

Mailly, D., Turbis, S., Auger, I., and Pothier, D., 2004. The influence of site tree selection method on site index determination and yield prediction in black spruce stands in northeastern Québec. *Forestry Chronicle, 80*(1), 134-140.

Marchand, W.-D., Killingtveit, Å., Wilén, P., and Wikström, P. (2003). Comparison of ground-based and airborne snow depth measurements with georadar systems, case study. *Nordic Hydrology, 34*(5), 427-448

Martin, W.K.E., and Timmer, V.R. (2006). Capturing spatial variability of soil and litter properties in a forest stand by landform segmentation procedures. *Geoderma 132*(1–2), 169 –181.

McCune, B., 2007. Improved estimates of incident radiation and heat load using non-parametric regression against topographic variables. *Journal of Vegetation Science, 18*(5), 751-754.

McCune, B., and Keon, D., (2002). Equations for potential annual direct incident radiation and heat load. *Journal of Vegetation Science, 13*(4), 603-606.

McKenney, D.W., and Pedlar, J.H. (2003). Spatial models of site index based on climate and soil properties for two boreal tree species in Ontario, Canada. *Forest Ecology and Management, 175*(1-3), 497-507.

McKenzie, N.J. and Ryan, P.J. (1999). Spatial prediction of soil properties using environmental correlation. *Geoderma, 89*(1-2), 67-94.

Moore, I.D., Lewis, A., and Gallant, J.C. (1993). Terrain attributes: estimation methods and scale effects. In: Jakeman, A.J., Beck, M.B. and McAleer, M.J. (Eds.), Modelling Change in Environmental Systems. Wiley London, pp. 189-214.

Moorman, B.J., Robinson, S.D., and Burgess, M.M. (2003). Imaging periglacial conditions with ground-penetrating radar. *Permafrost and Periglacial Processes, 14*(4), 319-329.

Mulder, V.L., de Bruin, S., Schaepman, M.E., and Mayr, T.R. (2011). The use of remote sensing in soil and terrain mapping—A review. *Geoderma, 162*(1–2), 1–19.

Paré, D., Bernier, P., Lafleur, B., Titus, B.D., Thiffault, E., Maynard, D.G., and Guo, X.(2013). Estimating stand-scale biomass, nutrient contents, and associated uncertainties for tree species of Canadian forests. *Canadian Journal of Forest Research, 43*(7), 599-608.

Payette, S. (2001). Les principaux types de tourbières, in: Écologie des tourbières du Québec-Labrador: une perspective nord-américaine, Payette, S., Rochefort. L. (ed.). Presses de l'Université Laval, Québec, QC. pp. 39-89.

Payette S., Rochefort, L. (2001). Écologie des tourbières du Québec-Labrador. S. Payette and L. Rochefort (ed.). Presses de l'Université Laval, Québec, Canada.

Pennock, D.J., and Corre, M.D. (2001). Development and application of landform segmentation procedures. *Soil and Tillage Research, 58*(3– 4), 151-162.

Perron, J.-Y. (1983). Tarif de cubage général-volume marchand brut. Ministère des Ressources naturelles du Québec, Québec, 52 pp.

Peucker, T.K., Fowler, R.J., Little, J.J., and Mark, D.M. (1978). The triangulated irregular network, Proceedings, *Digital Terrain Models (DTM) Symposium, American Society of Photogrammetry*, May 9-11, 1978, St. Louis, Missouri, p. 516-540.

Pierce, A.D., Farris, C.A., and Taylor, A.H. (2012). Use of random forests for modeling and mapping forest canopy fuels for fire behavior analysis in Lassen Volcanic National Park, California, USA. *Forest Ecology and Management, 279*, 77-89.

Pinno, B.D., Paré, D., Guindon, L., and Bélanger, N. (2009). Predicting productivity of trembling aspen in the Boreal Shield ecozone of Quebec using different sources of soil and site information. *Forest Ecology and Management*, *257*(3), 782-789.

Pokharel, B., and Froese, R.E. (2009). Representing site productivity in the basal area increment model for FVS-Ontario. *Forest Ecology and Management*, *258*(5), 657-666.

Pothier, D., and Savard, F. (1998). Actualisation des tables de production pour les principales espèces forestières du Québec. Ministère des Ressources naturelles du Québec. Direction de la recherche forestière, Québec, 183 pp.

Potter, C.S., Coughlan, J.C., and Brooks, V. (1999). Investigations of BOREAS spatial data in support of regional ecosystem modeling. *Journal of Geophysical Research D: Atmospheres, 104*, 27771–27788.

Powers, R.P., Coops, N.C., Morgan, J.L., Wulder, M.A., Nelson, T.A., Drever, C.R., and Cumming, S.G. (2013). A remote sensing approach to biodiversity assessment and regionalization of the Canadian boreal forest. *Progress in Physical Geography, 37*(1), 36-62.

Price, D.T., Alfaro, R.I., Brown, K.J., Flannigan, M.D., Fleming, R.A., Hogg, E.H., Girardin, M.P., Lakusta, T., Johnston, M., McKenney, D.W., Pedlar, J.H., Stratton, T., Sturrock, R.N., Thompson, I.D., Trofymow, J.A., Venier, L.A. (2013). Anticipating the consequences of climate change for Canada's boreal forest ecosystems1. *Environmental Reviews*, *21*, 322-365. dx.doi.org/10.1139/er-2013-0042

R Development Core Team. (2011). R: A language and environment for statistical computing. R Foundation for Statistical Computing, Vienna, Austria. URL http://www.R-project.org/.

Robitaille, A., and Saucier, J.P. (1996). Land district, ecophysiographic units and areas: The landscape mapping of the Ministère des ressources naturelles du Québec. *Environmental Monitoring and Assessment*, *39*(1-3), 127-148.

Robitaille, A., and Saucier, J.-P. (1998). Paysages régionaux du Québec méridional. Les publications du Québec, 213 pp.

Rosa, E., Larocque, M., Pellerin, S., Gagné, S., and Fournier, B. (2009). Determining the number of manual measurements required to improve peat thickness estimations by ground penetrating radar. *Earth Surface Processes and Landforms*, *34*(3), 377-383.

Rothwell, J.J., Futter, M.N., and Dise, N.B. (2008). A classification and regression tree model of controls on dissolved inorganic nitrogen leaching from European forests. *Environmental Pollution, 156*(2), 544-552.

Ryan, P.J., McKenzie, N.J., O'Connell, D., Loughhead, A.N., Leppert, P.M., Jacquier, D., and Ashton, L. (2000). Integrating forest soils information across scales: Spatial prediction of soil properties under Australian forests. Forest Ecology and Management, 138(1-3), 139-157.

Saucier, J.-P., Grondin, P., Robitaille, A., and Bergeron, J.-F. (2003). Zones de végétation et domaines bioclimatiques du Québec. Ministère des Ressources naturelles, de la faune et des parcs du Québec, Québec, QC.

Seibert, J., Stendahl, J., and Sorensen, R. (2007). Topographical influences on soil properties in boreal forests. *Geoderma, 141*(1-2), 139-148.

Simard, M., Bernier, P.Y., Bergeron, Y., Paré, D., and Guérine, L. (2009). Paludification dynamics in the boreal forest of the James Bay Lowlands: Effect of time since fire and topography. *Canadian Journal of Forest Research*, *39*(3), 546-552.

Simard, M., Lecomte, N., Bergeron, Y., Bernier, P.Y., and Pare, D. (2007). Forest productivity decline caused by successional paludification of boreal soils. *Ecological Applications*, *17*(6), 1619-1637.

Simeoni, M.A., Galloway, P.D., O'Neil, A.J., and Gilkes, R.J. (2009). A procedure for mapping the depth to the texture contrast horizon of duplex soils in south-western Australia using ground penetrating radar, GPS and kriging. *Australian Journal of Soil Research*, *47*(6), 613-621.

Skovsgaard, J.P., and Vanclay, J.K. (2008). Forest site productivity: A review of the evolution of dendrometric concepts for even-aged stands. *Forestry, 81*, 13-31. doi:10.1093/forestry/cpm041

Slater, L.D., and Reeve, A. (2002). Investigating peatland stratigraphy and hydrogeology using integrated electrical geophysics. *Geophysics*, *67*(2), 365-378.

Soil Classification Working Group. (1998). The Canadian system of soil classification, 3rd edition. *Agriculture and Agri-Food Canada Publication 1646, Ottawa*, 187 pp.

St-Onge, B., Hu, Y., and Vega, C. (2008). Mapping the height and above-ground biomass of a mixed forest using lidar and stereo Ikonos images. *International Journal of Remote Sensing, 29*(5), 1277-1294.

Sørensen, R., Zinko, U., and Seibert, J. (2006). On the calculation of the topographic wetness index: Evaluation of different methods based on field observations. *Hydrology and Earth System Sciences, 10*(1), 101-112.

Southee, F.M., Treitz, P.M., and Scott, N.A. (2012). Application of LiDAR terrain surfaces for soil moisture modeling. Photogramm. *Photogrammetric Engineering and Remote Sensing, 78*(12), 1241-1251.

Stover, D.B., Day, F.P., Butnor, J.R., and Drake, B.G. (2007). Effect of elevated CO_2 on coarse-root biomass in Florida scrub detected by ground-penetrating radar. *Ecology, 88*(5), 1328-1334.

Sucre, E.B., Tuttle, J.W., and Fox, T.R. (2011). The use of ground-penetrating radar to accurately estimate soil depth in rocky forest soils. *Forest Science, 57*(1), 59-66.

Tagil, S., and Jenness, J.S. (2008). GIS-based automated landform classification and topographic, landcover and geologic attributes of landforms around the Yazoren Polje, Turkey. *Journal of Applied Sciences, 8*(6), 910-921.

Tchir, T.L., Johnson, E.A., and Miyanishi, K. (2004). A model of fragmentation in the Canadian boreal forest. *Canadian Journal of Forest Research, 34*(11), 2248-2262

Theimer, B.D., Nobes, D.C., and Warner, B.G. (1994). A study of the geoelectrical properties of peatlands and their influence on ground-penetrating radar surveying. *Geophysical Prospecting, 42*(3), 179-209.

Thiffault, N., Fenton, N.J., Munson, A.D, Hébert, F., Fournier, R.A, Valeria, O., Bradley, R.L., Bergeron, Y., Grondin, P., Paré, D., and Joanisse, G. (2013). Managing understory vegetation for maintaining productivity in black spruce forests: A synthesis within a multi-scale research model. *Forests 4*, 613-631. Doi:10.3390/f4030613.

Ung, C.H., Bernier, P.Y., Raulier, F., Fournier, R.A., Lambert, M.C., and Régnière, J. (2001). Biophysical site indices for shade tolerant and intolerant boreal species. *Forest Science, 47*(1), 83-95.

Valeria, O., Laamrani, A., and Beaudoin, A. (2012). Monitoring the state of a large boreal forest region in eastern Canada through the use of multi-temporal satellite imagery. *Canadian Journal of Remote Sensing, 38*(1), 91-108.

Veillette, J.J. (1994). Evolution and paleohydrology of glacial Lakes Barlow and Ojibway. *Quaternary Science Reviews, 13*(9-10), 945-971.

Veillette, J.J., Paradis, S.J., Buckle J. (2005). Bedrock and surficial geology of the general area around Rouyn-Noranda, Quebec and Ontario, in: G. Bonham-Carter (Ed.), Metals in the Environment around Smelters at Rouyn-Noranda, Quebec, and Belledune, New Brunswick: Results and Conclusions of the GSC-MITE Point Sources Project. *Geological Survey of Canada, Bulletin, 584*, 1-16.

Veillette, J.J. (2007). Géologie des formations en surface et histoire glaciaire, Rivière Harricana, Québec. Commission Géologique du Canada- Ressources naturelles Canada, Carte 1993A, échelle 1 :100 000. . DOI: 10.4095/224446.

Veillette and Thibaudeau. (2007). Géologie des formations en surface et histoire glaciaire, Rivière Wawagosic, Québec; Commission géologique du Canada-- Ressources naturelles Canada, Carte 1995A, échelle 1 :100 000. DOI:10.4095/224448.

Vepakomma, U., St-Onge, B., and Kneeshaw, D. (2011). Response of a boreal forest to canopy opening: Assessing vertical and lateral tree growth with multi-temporal LiDAR data. *Ecological Applications, 21*(1), 99-121.

von Post, L. & Granlund, E. (1926). Södra Sveriges Torvtillgångar I (Peat resources in southern Sweden I). *Sveriges Geologiska Undersökning, 335*(19), 1–128

Vygodskaya, N.N., Groisman, P.Y., Tchebakova, N.M., Kurbatova, J.A., Panfyorov, O., Parfenova, E.I., and Sogachev, A.F. (2007). Ecosystems and climate interactions in the boreal zone of northern Eurasia. *Environmental Research Letters, 2*(4), 1-7. Doi:10.1088/1748-9326/2/4/045033

Warner, B.G., Nobes, D.C., and Theimer, B.D. (1990). An application of ground penetrating radar to peat stratigraphy of Ellice Swamp, southwestern Ontario. *Canadian Journal of Earth Sciences*, *27*(7), 932-938.

Weber, T.C. (2011). Maximum entropy modeling of mature hardwood forest distribution in four U.S. states. *Forest Ecology and Management, 261*(3), 779-788.

Webster, K.L., Creed, I.F., Beall, F.D., and Bourbonnière, R.A. (2011). A topographic template for estimating soil carbon pools in forested catchments. *Geoderma, 160*(3-4), 457-467.

Weiss, A.D. (2001). Topographic positions and landforms analysis (Conference Poster). ESRI International User Conference, San Diego, CA. Indus Corporation, Seattle, WA.

Wilson, J.P., and Gallant, J.C. (2000). Secondary Topographic Attributes. in: Wilson, J.P., Gallant, J.C. (Eds.), Terrain Analysis: Principles and Applications. Wiley, New York, pp. 87-131.

Woods, M., Pitt, D., Penner, M., Lim, K., Nesbitt, D., Etheridge, D., and Treitz, P. (2011). Operational implementation of a LiDAR inventory in boreal Ontario. *Forestry Chronicle, 87*(4), 512-528.

Work, T.T., St-Onge, B., and Jacobs, J.M. (2011). Response of female beetles to LiDAR derived topographic variables in Eastern boreal mixedwood forests (Coleoptera, Carabidae). *ZooKeys, 147*, 623-639.

Wu, W., Fan, Y., Wang, Z., and Liu, H. (2008). Assessing effects of digital elevation model resolutions on soil-landscape correlations in a hilly area. *Agriculture, Ecosystems and Environment, 126*(3-4), 209-216.

Zenone, T., Morelli, G., Teobaldelli, M., Fischanger, F., Matteucci, M., Sordini, M., Armani, A., Ferrè, C., Chiti, T., and Seufert, G. (2008). Preliminary use of ground-penetrating radar and electrical resistivity tomography to study tree roots in pine forests and poplar plantations. *Functional Plant Biology*, *35*(10), 1047-1058.

Zevenbergen, L.W., Thorne, C.R. (1987). Quantitative analysis of land surface topography. *Earth Surface Processes & Landforms, 12*(1), 47-56.

Zinko, U., Seibert, J., Dynesius, M., and Nilsson, C. (2005). Plant species numbers predicted by a topography-based groundwater flow index. *Ecosystems, 8*(4), 430-441.

D. ANNEXE

GRANDS TRAITS DE LA CEINTURE D'ARGILE

La région naturelle de la ceinture d'argile peut, à première vue, sembler relativement homogène. Toutefois, cette région possède des caractéristiques morphologiques, hydrogéologiques, granulométriques, sédimentologiques, géochimiques et même géotechniques fort variées. Cette section s'inspire du rapport d'évaluation du Dr Jean Veillette (membre externe du jury de la thèse) pour faire une mise en contexte plus détaillée de la ceinture d'argile afin de faire ressortir ses grands traits. La ceinture d'argile est subdivisée en trois zones distinctes selon les cartes du Quaternaire de la Commission Géologique du Canada (CGC). Un bref survol de cette zonation est présenté ci-dessous:

Zone 1: au Québec (comme en Ontario) la très grande partie de la plaine argileuse est à l'extérieur de la zone occupée par les crues de Cochrane et est constituée principalement d'argile varvée, non compacte, facilement érodée et avec des teneurs pratiquement nulles ou faibles en carbonates provenant de la plateforme d'Hudson. À l'ouest d'une droite tracée entre Rouyn-Noranda et Matagami, les teneurs en carbonates provenant de l'argile augmentent graduellement vers le nord-ouest, tandis qu'à l'est de cette droite elles décroissent vers l'est. La zone 1 occupe les parties du bassin glaciolacustre les moins perturbées en surface et renferme par endroits d'épaisses couches d'argile qui masquent les inégalités du substrat. La topographie du sol minéral (MS dans les articles de la thèse) qui se trouve sous la couche organique de ces endroits est généralement peu accidentée. Là où l'épaisseur de l'argile n'excède pas plus que quelques mètres, sa surface moule les formes du substrat glaciaire (till, esker) ou du roc.

Zone 2: partant du sud vers le nord, la deuxième zone en importance est une bande de quelques kilomètres de largeur, parallèle à la marge des crues de Cochrane, qui est constituée principalement d'argile varvée comme la zone au sud, mais qui contient des fragments de matériaux délestés à partir de glaces flottantes dans la partie supérieure (1-2 m) des varves. Cette caractéristique, indiquée par un poncif blanc sur les cartes, donne par endroits une

texture rugueuse à l'argile (gritty clay). Une bonne part de ces matériaux délestés consiste en carbonates provenant de la plateforme d'Hudson au nord-ouest, donnant ainsi des teneurs plus élevées en carbonates que dans la zone 1. En ce qui concerne la productivité forestière, la zone 2 présente des caractéristiques semblables à celles de la zone 1, mais présente certaines perturbations dues aux glaces flottantes. Ces perturbations résultent de dropstones et surtout de sillons d'icebergs qui ont incisé l'argile sur des profondeurs allant jusqu'à 3-4 mètres sous la surface. Les sillons sont massivement concentrés dans des bassins et sont totalement ou partiellement masqués par des dépôts organiques. Ces sillons sont des foyers de paludification n'ayant pas d'expression topographique dans la plupart des cas. Ainsi, on les distingue uniquement par des différences tonales sur photographies aériennes. Il serait intéressant de vérifier si le LiDAR pourrait contribuer à cartographier et discriminer ces sillons. Dans certains cas, ils constituent un réseau de drainage "caché" ou encore fossilisé; alors que dans d'autres cas des ruisseaux, même permanents, empruntent des segments de sillons pour y faire leurs lits. À ce jour, Dr Veillette en a dénombrés plus de 15 000 dans la ceinture d'argile (au Québec et en Ontario). Ces structures constituent donc un agent de perturbation important dans la partie nordique de la ceinture d'argile et devraient vraisemblablement affecter la productivité forestière.

Zone 3: correspondant à la zone la plus nordique, la zone 3 est formée par les dépôts de Cochrane comme tel, donc une argile plus caillouteuse et contenant plus de sable que l'argile des deux autres zones. Cette zone se caractérise aussi par un niveau de compaction plus élevé que les zones 2 et 3, un réseau de drainage chaotique, un substrat minéralogique fort perturbé par plusieurs processus associés aux glaces flottantes et une micro-topographie accidentée. Le secteur à l'étude (Survol LiDAR) s'y trouve et chevauche deux cartes du quaternaire de la CGC (partie sud; Veillette et Thibaudeau (2007) et partie nord; Veillette 2007). La zone 3 est celle qui présente les perturbations les plus importantes, car en plus de celles de la zone 2 on y trouve les rainures résultantes du glissement des glaces sur l'argile (crues de Cochrane) produisant ainsi une surface de planche à laver avec des effets contraignant sur le réseau de drainage mis en place au postglaciaire et aussi sur la paludification des terrains et par conséquent sur la productivité forestière.